The normal distribution of experimental data was assessed using the Kolmogorov-Smirnov normality test. According to the distribution of the data, we performed either parametric or non-parametric tests and p-values < 0.05 were considered significant.

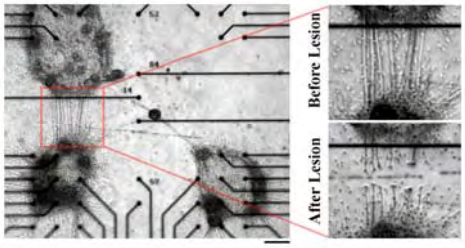

Fig. 1. Optical micrograph of a patterned culture (hippocampal neurons, 20 DIV), composed of 3 cell clusters (or modules) over a 4Q MEA. The same culture was monitored before (left) and after (right) the optical lesion. It is visible that neural connections between the upper left cluster and all the others were cut by the laser. Screen bar 200 μm.

3 Results

Depending on the distance between modules, the module networks are able or not to establish spontaneous neuronal connections among them. Fig. 1 reports optical images of a representative culture before (left) and after the optical lesion (right).

We analysed both spontaneous and evoked activity of modular networks before and after lesion. Regarding spontaneous dynamics, the strong synchronization of activity observed among the clusters before the lesion (Fig. 2A), disappears almost completely after it (Fig. 2B). Moreover, a global decrease in the network mean firing rate is observed after the lesion, both inside the isolated cluster, and in all the other clusters that were previously connected to the isolated one. Before performing the lesion, electrical stimulation was able to evoke activity both within the cluster hosting the stimulating channel and in the connected modules (Fig. 2C, black profiles). After laser dissection, the evoked activity remains confined within the isolated cluster without spreading towards the other ones (Fig. 2C, red profiles). Figure 2D shows that a global decrease in the evoked activity after the laser cut is present in both local and distal responses. Since lesion is aimed at reducing the amount of connections among clusters, inter-cluster responses are more affected than intra-cluster ones.

4 Summary

We showed that selective laser dissection of interconnections among neural assemblies affects both spontaneous and evoked activity of modular networks, by inducing de-synchronization between the different modules during spontaneous activity, and preventing propagation of evoked responses among modules. Those preliminary results present a reproducible experimental model, which can be used as a test-bed for the design and development of innovative neuro-prostheses aimed at restoring lost neuronal functionality between distinct brain areas, at the level of the central nervous system.

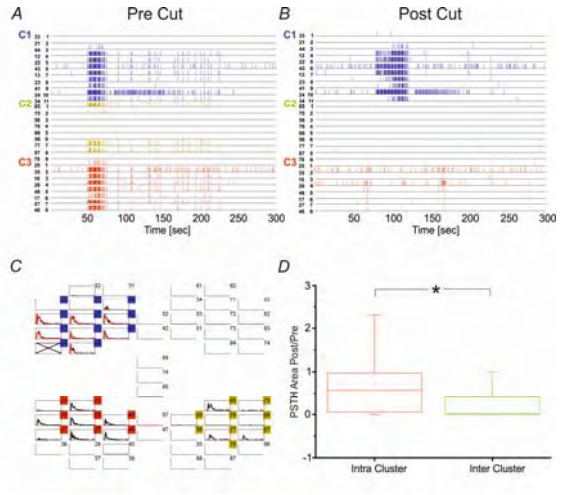

Fig. 2. Comparison of spontaneous and evoked activity of healthy and damaged modular cultures. A, B. 5-minute raster plot of spontaneous activity of a representative patterned network before (A) and after (B) lesion. The activity of different clusters (i.e. C1, C2 and C3) has been highlighted in different colors. The blue one (C1) is the isolated cluster. C. Post-stimulus time histograms (PSTH) obtained when stimulating a channel belonging to the isolated cluster. The electrodes labelled in blue belong to the isolated cluster, while the black cross indicates the stimulated channel. Black curves report the evoked activity before the lesion, while the red ones refer to the evoked activity after it. D. Comparison between the statistical distributions of normalized PSTH areas (i.e. ratio between post-lesion PSTH areas over pre-lesion ones), either within the stimulated cluster (Intra Cluster) or in all the other ones (Inter Cluster). Statistical analysis has been performed by using the Mann-Whitney test [*p<0.05]).

Acknowledgement

The research leading to these results has received funding from the European Union's Seventh Framework Programme (ICT-FET FP7/2007-2013, FET Young Explorers scheme) under grant agreement n° 284772 BRAINBOW (www.brainbowproject.eu).

References

[1] Berger, T. W., Hampson, R. E., Song, D., Goonawardena, A., Marmarelis, V. Z., and Deadwyler, S. A. (2011): A cortical neural prosthesis for restoring and enhancing memory. J Neural Eng, 8, 046017.

[2] Guggenmos, D. J., Azin, M., Barbay, S., Mahnken, J. D., Dunham, C., Mohseni, P., and Nudo, R. J. (2013): Restoration of function after brain damage using a neural prosthesis. Proc Natl Acad Sci U S A, 110, 21177-82.

[3] Bonifazi, P., Difato, F., Massobrio, P., Breschi, G. L., Pasquale, V., Levi, T., Goldin, M., Bornat, Y., Tedesco, M., Bisio, M., Kanner, S., Galron, R., Tessadori, J., Taverna, S., and Chiappalone, M. (2013): In vitro large-scale experimental and theoretical studies for the realization of bi-directional brain-prostheses. Front Neural Circuits, 7, 40.

[4] Difato, F., Dal Maschio, M., Marconi, E., Ronzitti, G., Maccionel A., Fellin, T., Berdondini, L., Chieregatti, E., Benfenati, F. and Blau, A. (2011): Combined optical tweezers and laser dissector for controlled ablation of functional connections in neural networks. J Biomed Opt, 16(5), 051306.

[5] Shein Idelson, M., Ben-Jacob, E., and Hanein, Y. (2010): Innate synchronous oscillations in freely-organized small neuronal circuits. PLoS One, 5, e14443.

Simulation of hPSC Derived Neuronal Networks with Short and Long Reaching Axons

Kerstin Lenk[1*], Laura Ylä-Outinen[2], Lukas H B Tietz[1], Susanna Narkilahti[2], Jari A K Hyttinen[1]

1 BioMediTech and Department of Electronics and Communications Engineering, Tampere University of Technology, Tampere, Finland
2 NeuroGroup, BioMediTech, University of Tampere, Tampere, Finland
* Corresponding author. E-mail address: kerstin.lenk@tut.fi

Abstract
In the past, we developed a simple model which simulates neuronal activity as observed in a neuronal network cultivated on a multielectrode array (MEA). The model is based on an inhomogeneous Poisson process to simulate neurons which are active without external input or stimulus as observed in MEA experiments. In the previous version of the model, the time slice for the occurrence of one spike was 5 milliseconds. In the present work, we added topology by defining the connection from one neuron to another neuron with short or long reaching axons. For each of the two emerging subpopulations we added a different time delay for communication. We compared the simulated spike trains with different delays to experimental data of neuronal cell network derived from human pluripotent stem cells (hPSC-NN). These hPSC-NNs exhibit highly variable network structure and time-varying dynamics. To explore and validate the developing burst and spike activities of such network simulations we applied spike train statistics. The results indicate that by introducing delays we could enhance the biological plausibility of the INEX model.

1 Introduction

Neuronal networks can be simulated on different abstract levels representing different specificity of the underlying biological systems. In the past, we have built a phenomenological model called INEX (INhibitory-EXcitatory) that was used to simulate neuronal activity recorded from frontal cortex tissue of embryonic mice using *in vitro* 2D microelectrode arrays (MEAs) [1] and maturating neuronal cell networks derived from human pluripotent stem cells (hPSC-NN; unpublished data). So far, a spike was only generated within a 5 millisecond time slice including also the refractory period. Further, each action potential needed the same time from one neuron to another. The aim of this presented work is to explore the effect changing the topologically invariant INEX into a network with network topology by adding a distance dependent delay after the occurrence of a spike to simulate short and long reaching axons. Here the network is tuned to properties of those derived by hPSC-NN measured by MEAs and we study the effect of this simple topology on the network parameters.

2 Methods

2.1 MEA recordings and Spike sorting

Six-well MEA recordings from human embryonic stem cells derived neuronal cultures [2,3] were done for approximately 300 seconds on 30-50 days of culturing. Each MEA has 1-3 bursting wells, so that we analyzed in total 15 wells. Signals were sampled at 20 kHz or 50 kHz, and stored to a standard PC using the MC Rack software (MCS). The culture temperature was maintained at +37°C using a TC02 temperature controller (MCS) during the measurements. Recordings were visually inspected for artifacts and the measurements or channels likely to contain artifacts were excluded from the further analysis.

Channels were considered as inactive when less than 20 spikes per minute [4] were recorded. Additionally, if less than two channels per well were active, the well data was excluded from further analysis. We performed spike sorting with wave_clus [5].

To get a reference for the simulation, we calculated the medians and lower and upper quartiles of spike rate and burst rate separately for all electrodes. Briefly, the burst analysis algorithm, which was used to examine the intrinsic bursting, relies on the cumulative moving average (CMA) and the skewness (α) of the interspike interval (ISI) histogram. For bursting, the ISI threshold was found at the ISI closest to the value of $\alpha \cdot CMA_m$ where CMA_m is the average of CMA. Additionally, three or more spikes had to be in a row. Kapucu et al. [4] has demonstrated the functionality of the tool for highly variable network structures and time-varying dynamics as in hPSC-NNs.

2.2 INEX model

The INEX model is based on an inhomogeneous Poisson process [6] to simulate neurons which are active without external input or stimulus as observed in MEA experiments. The momentary firing rate λ_i of neuron i in time slice t_k is calculated by $\lambda_i(t_k) = c_i + \sum_j y_{ji} s_j(t_{k-1})$ if $c_i + \sum_j y_{ji} s_j(t_{k-1}) > 0$,

otherwise $\lambda_i(t_k) = 0$. The parameter c_i denotes the basic activity, y_{ji} the synaptic strength of all neurons j connected to neuron i and s_j the particular spike of the previous time slice of all neurons j (1 for a spike and 0 for no spike).

We divided the population in neurons with short- or long reaching axons. For each of the two emerging subpopulations we added a different time delay to the neurons. The time delay σ is randomly set between 0.5 and 1 for long reaching axons and it is randomly set between 0 and 0.5 for short reaching axons. If s=1, σ is reduced by 0.1 in every following time slice. If σ=0, an action potential occurs and σ is set to its original value.

The parameters of the INEX model are chosen in such a way that the resulting spike trains resemble spike trains of 2D MEA experiments with hPSC-NNs with respect to spike and burst rate [1]. A network with 1,000 neurons with ten percent of all possible connections was simulated. We ran the simulations without delays [1] and with a network where 20 per cent of all neurons, which were randomly chosen, had short or long reaching axons. For both simulation types the other parameters were the same. The resulting spike trains had a length of 300 seconds. The simulation tool was run with these constrains twenty times to get statistically significant data.

For validation, we calculated four features [spike rate (spikes/minute), burst rate (bursts/minute), burst duration (in milliseconds) and the spike number per burst] for each of the simulated spike trains using the above mentioned burst analysis tool by Kapucu et al. [4] and compared them with the same features obtained from the above mentioned MEA experiments with hPSC-NNs.

3 Results and Discussion

The simulated activity with and without delay exhibits typical spike and burst patterns as known from MEA experiments with maturated hPSC-NNs [3]. The spike rate, burst rate and number spikes per burst are slightly lower in the networks with delays than without delays. The burst duration was for both simulation types the same. The variation of inhibitory and excitatory parameters as well as the addition of time delays was able to produce similar spiking characteristics as measured.

4 Conclusions

Introducing the delays we could enhance the biological plausibility of the INEX model. To conclude, the calculated features adapted from spikes and bursts as well as the spike train statistics show that the activity of hPSC-NNs as observed in MEA experiments can be modeled by the INEX model including time delays.

Acknowledgement

This research has been supported by the 3DNeuroN project in the European Union's Seventh Framework Programme, Future and Emerging Technologies, grant agreement n°296590. Furthermore, the authors thank Inkeri Vornanen for her support.

References

[1] Lenk, K. (2011): A Simple Phenomenological Neuronal Model with Inhibitory and Excitatory Synapses. *Springer Lecture Notes in Computer Science, 7015, 232-238*.

[2] Ylä-Outinen, L., Heikkilä, J., Skottman, H., Suuronen, R., Äänismaa, R., Narkilahti, S. (2010): Human cell-based micro electrode array platform for studying neurotoxicity. *Front. Neuroengineering, 3.*

[3] Heikkilä, T., Ylä-Outinen, L., Tanskanen, J.M.A., Lappalainen, R., Skottman, H., Suuronen, R., Hyttinen, J., Narkilahti, S. (2009): Human embryonic stem cell-derived neuronal cells form spontaneously active neuronal networks in vitro. *Exp. Neurol., 218(1), 109-116.*

[4] Kapucu, F. E., Tanskanen, J.M.A., Mikkonen, J.E., Ylä-Outinen, L., Narkilahti, S., Hyttinen, J.A.K (2012): Burst analysis tool for developing neuronal networks exhibiting highly varying action potential dynamics. *Front. Comput. Neurosci., 6.*

[5] Quiroga, R.Q., Nadasdy, Z., Ben-Shaul, Y. (2004). Unsupervised spike detection and sorting with wavelets and superparamagnetic clustering. *Neural Comput., 8,1661-1687*.

[6] Heeger, D. (2000): Poisson model of spike generation.

Simplicial Complex and Betti Numbers to Characterize Co-Activation Patterns in Cortical Cultures

Virginia Pirino[1]*, Paolo Massobrio[1], Eva Riccomagno[2], Sergio Martinoia[1]

1 Neuroengineering and Bio-nano Technology Group (NBT), Department of Informatics Bioengineering Robotics and System Engineering, University o Genova, Genova, Italy
2 Department of Mathematics, University of Genova, Genoa, Italy
* Corresponding author. E-mail address: virginia.pirino@edu.unige.it

Abstract
Simplicial complex and Betti numbers provide new methods to investigate and analyse complex/high dimensional networks. In this study, such an approach has been applied to cortical networks coupled to Micro-Electrode Arrays (MEAs) in order to extract sub-networks characterized by a repetitive synchronous activity. Moreover, the proposed algorithm allows also to compare the spontaneous and stimulus-evoked activity of the neural cultures and to describe some topological features of the detected sub-networks.

1 Background / Aims

Recently, statistics and topology have offered their tools to biologists and engineers to develop novel techniques for exploratory data analysis and modelling [1-5]. In this work, we propose a specific technique based on simplicial complexes and Betti numbers to investigate different resolution levels of co-activity (defined as a period of synchronous firing of a group of neurons) of neuronal networks coupled to Micro-Electrode Arrays (MEAs), during spontaneous and stimulus-evoked activity conditions.

2 Methods / Statistics

We analysed electrophysiological activity of cortical cultures coupled to MEAs composed by 60 TiN/SiN planar round electrodes organized in a 8 × 8 square grid (excluded corners). After 1200× amplification, signals were sampled at 10 kHz and acquired through the data acquisition card and MC_Rack software (Multi Channel Systems, MCS, Reutlingen, Germany). Electrical stimuli were delivered by using a commercial general-purpose stimulus generator (STG 1008, MCS), which allowed to apply current and voltage pulses to selected electrodes of the MEA. Stimuli were sent sequentially to the selected electrode at a frequency of 0.2 Hz for five minutes. Probe pulse amplitude was fixed at 1.5V peak-to-peak. The stimulus pulse was biphasic (positive phase first) and lasted for 500μs with a 50% duty cycle.

The results presented in this work came from eight cortical cultures recorded during the fourth week *in vitro*. Each experiment consists of six spontaneous phases and eight stimulus-evoked phases lasting five minutes each.

Data were aggregated by grouping the electrodes in clusters, named meta-neurons, of different sizes. In this way, we analysed the networks activity on different resolution levels: from a macro to a micro point of view. Specifically, *a meta-neuron* is a representative of a collection of electrodes: it carries on the information of that group in a sort of mean behavior.

To reduce the data space without losing fundamental system characteristics, each clustered recording has been binned and then a binary matrix was obtained by applying a threshold evaluated on the basis of the mean firing rate of each meta-neuron. The columns of the binary matrix contain the co-activity patterns of the network. The most recursive ones were plotted into a weighted simplicial complex (the weights are representative of their occurrences). Finally, the sequence of Betti numbers associated to each simplicial complex has been computed to derive information on the clusters connectivity.

3 Results

The presence of sub-networks of repetitive co-activation patterns is evident in all the choice of meta-neuron size (i.e. resolution level). Fig.1 shows a representative recording of spontaneous (Fig. 1A) and stimulus-evoked activity (Fig. 1B) of one representative experiment. The raster plots correspondent to the two recordings (Fig 1C and D respectively) emphasize that the involved meta-neurons in the clusters (red bars) have a less homogeneous firing activity than the not-involved ones.

By comparing the results of spontaneous and stimulus-evoked activity, it emerges that the evoked activity resembles the spontaneous one. Specifically, the delivery of electrical stimulation excited the network by increasing its own activity. Moreover, this result is evident by comparing the occurrences of each meta-neuron appearing in the two depicted sub-networks (Fig.1 A and B). The bar plot in Fig.1E

compares the occurrences of each meta-neurons involved in the sub-networks.
By varying the size of meta-neurons, the percentage of the detected sites in both conditions results on average 78%.

Finally, the sequence of Betti numbers gives information on the cluster connectivity of the sub-network represented by the simplicial complex. In our study, only the two first Betti numbers take values different from zero. Specifically, the first Betti number (i.e., β_0) gives the number of connected components and the second one (i.e., β_1) gives the number of one-dimensional holes. In our experiments, we found that β_0 varies from 1 to 6 and on average is equal to 1.49; while β_1 is 1 or 2 and on average is equal to 0.05. This means that the sub-networks are mainly composed by one or two clusters, and each of them is almost always fully connected. By comparing the sequence of Betti numbers relative to the spontaneous and the stimulus-evoked recordings, no difference emerges, suggesting that the network behaviour is quite similar.

A further analysis was done by focusing on the variation of the meta-neurons size from 14 to 30 to 60 sites. In Fig.2, the filtration along the three different resolution levels of a specific recording is shown. The sub-network depicted in panel C is almost completely contained in the sub-network of panel B that is completely contained in the one of panel A.

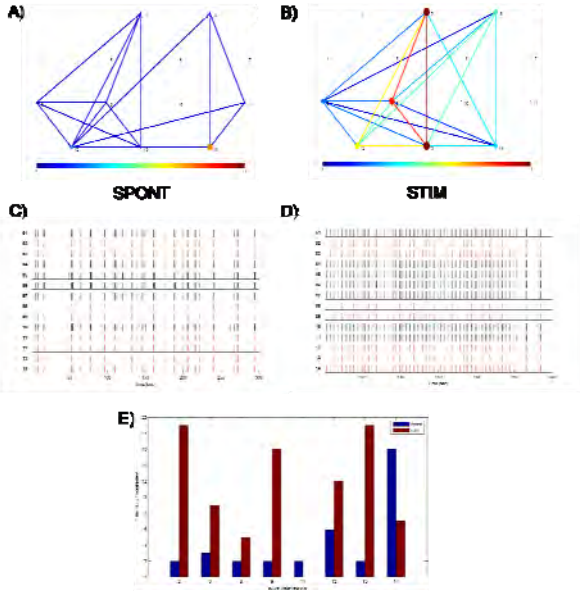

Fig. 1. Sub-networks of a spontaneous (A) and stimulus-evoked recording (B) of a representative experiment, (C-D) correspondent raster plots and the bar plot (E) relative to the occurrences of each meta-neuron involved in the sub-networks. The red spike trains in C and D correspond to the activity of the meta-neurons involved in the sub-networks.

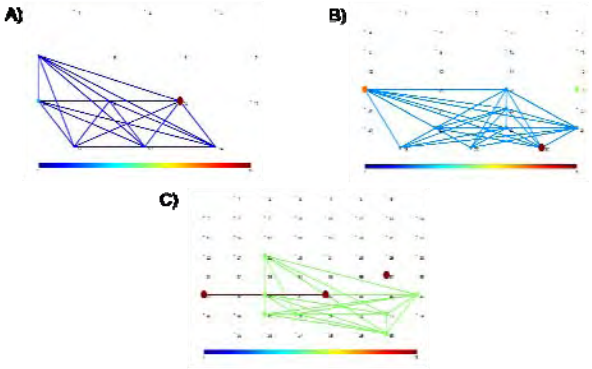

Fig. 2. Filtration of a representative recording along three different resolution levels: from 14 (A) to 30 (B) up to 60 meta-neurons (C).

4 Conclusion/Summary

Simplicial complexes and Betti numbers give a topological and algebraic characterization of the repetitive co-activation patterns. The analysis of the network firing activity highlights that our algorithm selects a sub-population of neurons that fires differently from the rest of the network. Moreover, there are few differences in the components and in the topology of the detected sub-networks both in spontaneous and in stimulus-evoked activity.

The strength of this method is its capacity to reduce the network size maintaining its intrinsic characteristics. As shown in Fig.2, the reduction of the network size does not affect the result. The filtration gives a good analysis of the main features of the network from a macro to a micro point of view without losing important information.

Furthermore, the algorithm allows to investigate the network connectivity in a different way from the classical algorithms based on cross-correlation and information theory [6]. These methods are pairwise and mainly focused on the time factor of spikes series. On the contrary, the presented method works on the entire network and puts the emphasis on the firing behaviour of each meta-neuron.

References

[1] Carlsson (2009) : Topology and data. *Bull. Amer. Math. Soc., 46(2), 255-308.*
[2] Curto and Itskov (2008): Cell Groups Reveal Real Structure of Stimulus Space. *PLoS Comput Biol, 4(10) : e1000205.*
[3] Dabaghian, Memoli, Frank and Carlsson (2012): A Topological Paradigm for Hippocampal Spatial Map Formation Using Persistent Homology. *PLoS Comput Biol 8(8): e1002581.*
[4] Petri, Scolamiero, Donato and Vaccarino (2013): Topological Strata of weighted Complex Networks. *PLoS ONE 8(6): e66506.*
[5] Singh, Memoli, Sapiro, Carlsson and Ringach (2010): Topological Analysis of Population Activity in Visual Cortex. *Journal of Vision, 8(8):11, 1-18.*
[6] Garofalo, Nieus, Massobrio and Martinoia (2009): Evaluation of the Performance of Information Theory-Based Methods and Cross-Correlation to Estimate the Functional Connectivity in Cortical Networks. *PLoS ONE 4(8): e6482.*

Investigation of Neuronal Activity Recorded with Multi-Electrode Arrays Using Principal Component Analysis

Patrick Schuller[1], Johann K. Mika[1], Heinz Wanzenböck[1*], Petra Scholze[2], Emmerich Bertagnolli[1]

1 Institute of Solid State Electronics, Vienna University of Technology, Vienna, Austria
2 Center for Brain Research, Medical University of Vienna, Vienna, Austria
* Corresponding author. E-mail address: heinz.wanzenboeck@tuwien.ac.at

Abstract
Analyzing neuronal activity recorded with Microelectrode Arrays (MEAs) can be a tricky task especially with a high amount of electrodes coupled with a high sampling rate. There are several methods to identify single neurites in the recorded data, each dependent on the scientific question. To investigate the influence of neurotrophins on the growth and activity of neurites we developed a specific MEA with an upper compartment where the electrical activity of neurites in microchannels is recorded. The unknown number of these neurites in the microchannels provides a huge challenge in data analysis. We developed an analyzing software using principal component analysis to detect the neuronal activity in each microchannel, to quantify the number of neurites per channel and to correlate the identified neurites. The developed software can be easily adapted to different MEA designs and several parameters can be adjusted to fit the requirements of the experiment. Using optical microscopy we further correlated the number of neurites in the channels with the analyzed data.

1 Introduction

In the last years MEAs emerged to a standardized method to record neuronal activity from in-vitro cultures. Nevertheless, many scientific questions require an individual design of the MEA. To investigate the influence of neurotrophins on the growth and activity of neurites individual MEAs were developed at the Institute of Solid State Electronics to separate neurites from their somata using artificial microchannels (Figure 1). Neuronal activity was recorded using microelectrodes below these microchannels. The identification of single neurites out of the recorded data in a single channel is a tricky task. There are several methods to identify neuronal activity in the recorded data e.g. threshold-, matched-filter-, or wavelet detection [1-3].

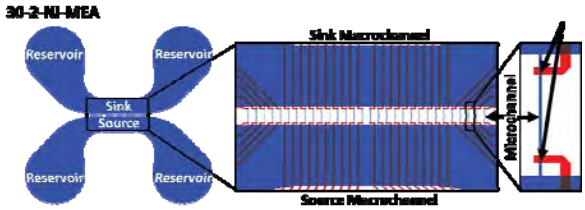

Fig. 1. Neurite Isolation-Multi Electrode Array microchannel/microelectrode setup

In order to identify single neurites we used principal component analysis (PCA) with clustering. Using MATLAB we developed a new analysis software called SpikeControl to detect the neuronal activity in each microchannel, quantify the number of neurites per channel and correlate the identified neurites with each other. We also correlated the analyzed data with optical investigations of the microchannels resulting in similar numbers of neurites.

2 Materials and Methods

Figure 2 shows the data flow of the recorded neuronal activity. Using the individual designed MEA electrical signals were recorded using the MEA1060 Amplifier and MC_Rack v4.5.3 software. The recorded data was then processed using our software SpikeControl (SC) with graphical user interface, developed in MATLAB. Because of the long analyzing time due to a high sampling rate and a high number of electrodes we divided SpikeControl in two parts (Figure 2).

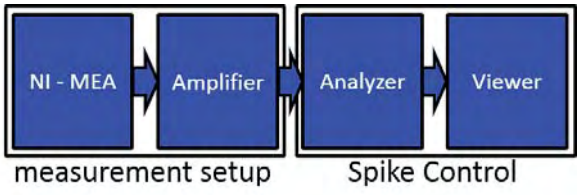

Fig.2. Data flow diagram of the developed SpikeControl software

The SC Analyzer performs the main analysis independent from user interaction, using the SC Viewer the processed data can be viewed and post analyzed.

SC Analyzer

The SC Analyzer applies a filter followed by threshold detection to a set of data. The filter can be modified in several ways e.g. filter type, cut-off frequencies and order of the filter or a custom filter can be chosen. The optimal parameters for the threshold analysis can also be determined [4]. Afterwards a threshold analysis with user adaptable threshold values is performed and the analyzed data can be saved.

SC Viewer

The analyzed data can be reopened and viewed with the SC Viewer. Using PCA and clustering the number of neurites per channel can be determined. Neighboring spike activity can be correlated and a spike-timeline of all microelectrodes can be displayed.

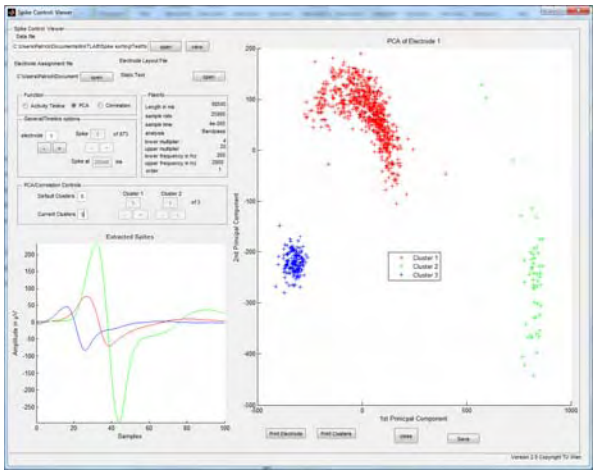

Fig.3. SpikeControl Viewer PCA Mode

3 Results

SpikeControl dramatically reduced the analysis time to identify neuronal activity of isolated neurites.

We tested the software with different designs of MEAs and neurite isolation chambers. With the SC Analyzer the best parameters for further analysis can be evaluated using different filter settings. Depending on the file size (related to sampling time, number of channels et cetera) and the overall number of files the filtering and threshold detection took minutes to hours. We compared the results manually with several tests to ensure the correct function. Using the SC Viewer it was possible to identify different neurites inside a microchannel using principal component analysis. Figure 3 shows the different shapes of the action potentials and their associated clusters. In Figure 4 an overview of the clusters of all 60 channels is presented. Each channel shows individual numbers of clusters which are dedicated to specific individual neurites. The number of neurites per microchannel can be verified by optical microscopy. Using cross- and autocorrelation of the spikes also gives more information about the type of neuron and their environment.

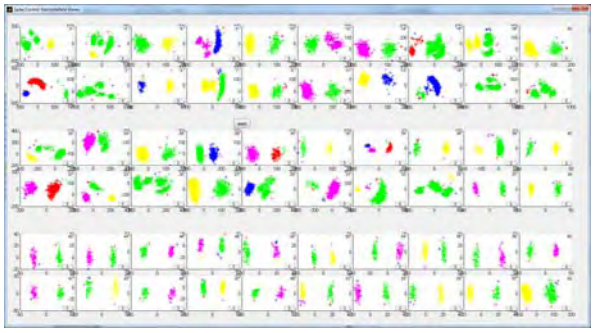

Fig.4. SpikeControl Viewer -overview of the PCA of all electrodes

4 Conclusion and discussion

A software tool for the analysis of signals recorded with MEAs was developed. A suitable approach using a combination of threshold detection and principal component analysis was chosen and implemented with a graphical user interface. The analysis of data recorded with MEAs showed that the implemented methods can be used to detect neuronal activity, another result was the correspondence of clusters, created from the data of the principal component analysis, with single neurites. The results indicate that SpikeControl is a versatile tool for spatiotemporal mapping of growing neurites on NI-MEA's.

References

[1] Lewicki, M.S. (1998): A review of methods for spike sorting: the detection and classification of neural action potentials. *Network, Vol 9, Issue 4, R56 – R68.*

[2] Nenadic, Z.,Burdick, J. W. (2005): Spike detection using the continuous wavelet transform. *IEEE Trans Biomed Eng, Vol 52, Issue 1, 75-81.*

[3] Obeid, I.,Wolf, P. D. (2004): Evaluation of spike-detection algorithms for a brain-machine interface application. *IEEE Trans Biomed Eng, Vol 51, Issue 6, 905-11.*

[4] Kim, S., McNames, J. (2007): Automatic spike detection based on adaptive template matching for extracellular neural recordings. *J. Neurosci Methods, Vol 165, Issue 2, 165-174.*

Modelling Seizure-Like Superburst Activity of Dissociated Neuronal Cultures

Simonov Alexander[1*], Esir Pavel[1], Mukhina Irina[1,2], Kazantsev Victor[1,3]

1 Lobachevsky State University of Nizhny Novgorod, Russia
2 Nizhny Novgorod State Medical Academy, Nizhny Novgorod, Russia
3 Institute of Applied Physics RAS, Nizhny Novgorod, Russia
* Corresponding author. E-mail address: simonov@neuro.nnov.ru

Abstract
A simple spiking neuronal network model describing signaling in dissociated hippocampal cultures is proposed. The model reproduces essential patterns of population activity experimentally observed. Using mathemathical modeling and computer simulatoins the network level dynamical principles of bursting to superbursting mode switch driven by modification of key model parameters were revealed. Our results indicate that the time decay of excitatory postsynaptic currents, the balance between excitation and inhibition and short-term plasticity kinetics are the most crucial factors underlying superbursting phenomenon in cultured neuronal networks.

1 Introduction

Dissociated cultures of neuronal networks grown on multielectrode arrays (MEA) are known to generate wide range of population activity patterns. During development after asynchronous spikes population bursts appear and become more complex with the culture maturation. Among them several types of so-called superbursts have been observed and classified [1]. It has been recently proposed that enzymatic digestion of the brain extracellular matrix molecules evokes such superburst activity which can be used as an experimental model of epileptic sezure-like discharges [2]. Epileptiform superbursts contain several subbursts either with relatively short intervals between them filled with low level of asynchronous activity, or coupled to each other with smooth transition between them. To reveal network level dynamical mechanisms of such superburst discharge generation we propose a spiking neuronal network model reproducing seizure-like superburst activity of dissociated neuronal cultures.

2 Model

The model was composed of single spiking units modelled by Izhikevich neurons [3] interconnected via Tsodyks-Uziel-Markram model [4] phenomenologically implementing short-term plasticity mechanisms. Depending on time constsnts of synaptic resource depletion and recovery the model exhibits either depression or fascillitation Postsynaptic currents were simulated to mimic kinetics of four different receptor types, i.e. AMPA, NMDA, GABAA and GABAB receptors. The neuronal network contained three neuronal populations: two types of excitatory pyramidal neurons found in CA1 and CA3 areas and fast-spiking inhibitory interneurons, fine-tuned to reproduce spiking patterns of hippocampal neurons. We used the following sizes of the populations: 350 CA1 pyramidal neurons, 290 CA3 pyramidal neurons and 70 fast-spiking interneurons providing the ratio between excitatory and inhibitory populations approximately 9:1.

To mimic a network of neurons cultured on MEA all the units were distributed on a probe of 1100*1100 um. Velocity of action potential propagating was taken 50 mm/s, axonal conduction delays were proportional to the distances between pairs of connected neurons. Most of the connections were local with small fraction of distant connections. We took gaussian probability of connection between 2 cells depending on the distance with p_{center} — 0.5, σ — 200 um. In average there were about 55 connections per neuron or ~13% from all the possible connections The simulations were performed using NEST simulator [5].

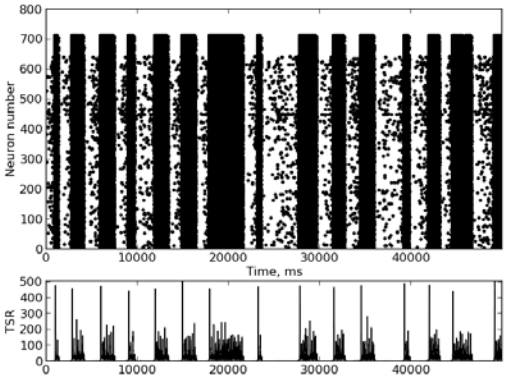

Fig. 1. An example of seizure-like superburst activity in the model.

3 Results

The model is capable to generate population bursts found in dissociated cultures in normal conditions. According to experimental observations digestion of the extracellular matrix leads to breaking the balance between excitation and inhibition engaging the network to the regime of hyperexcitability. In phenomenological modelling of spiking neuronal networks this balance shift was achieved by altering synaptic efficacies. We found that increasing weights of excitatory synapses evoked seizure-like superbursts generation. An example of superbursting activity is shown in fig.1.

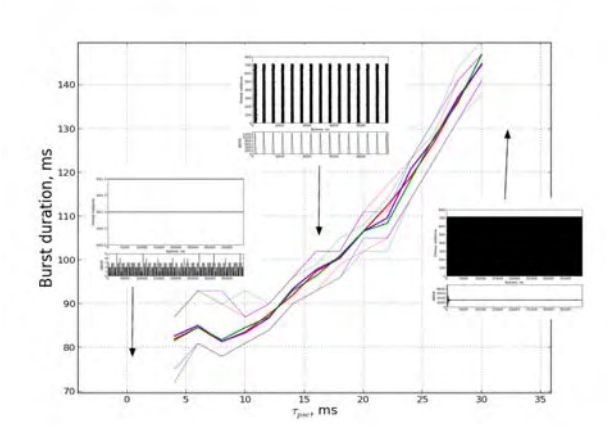

Fig. 2. Average burst duration depending on time constant of postsynaptic currents (τ_{psc}) in the model.

Another parameter playing a key role in generating superburst discharges is time of excitatory postsynaptic current decay τ_{psc}. Increasing this time significantly expanded the parameter range of the stable suberbursting mode. When the weight values were taken for obtaining normal bursting activity, increasing τ_{psc} slightly affects to average burst duration, as it is showt in fig.2. Here different colors correspond to different ratios between τ_{psc} for excitatory and inhibitory currents. The blue curve represents the same values of time decay, the green one shows the dependence for inhibitory time being two times greater than the excitatory one, and the red curve is for inhibitory time constant being two times smaller than the excitatory one. The thin curves show standard deviations. Insets depict examples of population activity rasters.

Finally we proposed simple characteristics reflecting the level of whole network depolarization and average synaptic excitatory conductancies to show the role of the found network parameters in the epileptiform activity formation. Fig.3 shows the characteristics for a single superburst. Here the averaged membrane potential of the excitatory neurons is shown in blue. The green and red colours represent traces of the average AMPA and NMDA synaptic conductancies respectively.

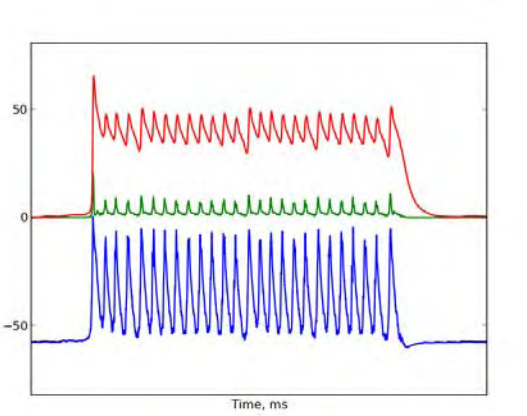

Fig. 3. Averaged network depolarization and excitatory AMPA and NMDA synaptic conductancies during a single epileptiform superburst.

4 Conclusion

The mathematical modelling study allowed finding the mechanisms of seizure-like superburst epileptiform activity generation in dissociated cultures of neuronal networks. The main findings indicate that such activity occurs due to an interplay between different time scales of the local elements dynamics, i.e. refractory period, short-term depression, postsynaptic potentials decay and spike-frequency adaptation, and requires activation of NMDA receptors.

Acknowledgement

The research was supported by The Ministry of Education and Science of Russia, Grant for Leading Scientists (No11.G34.31.0012), by the Russian President Grant No MK-4602.2013.4 and by the Russian President Scholarship No. SP-991.2012.4 and by the Russian Foundation for Basic Research grants # 13-02-01223, 13-04-12041.

References

[1] D. A. Wagenaar, J. Pine, and S. M. Potter, BMC Neurosci., vol. 7, p. 11, Jan. 2006.
[2] M. Vedunova, et. al, Front. Cell. Neurosci., vol. 7, p. Article 149, 10 p., 2013.
[3] E. M. Izhikevich, “Dynamical systems in neuroscience: the geometry of excitability and bursting,” Dyn. Syst., 2007.
[4] M. Tsodyks, A. Uziel, and H. Markram, J. Neurosci., vol. 20, no. 1, p. RC50, Jan. 2000.
[5] M.-O. Gewaltig and M. Diesmann, Scholarpedia, vol. 2, no. 4, p. 1430, 2007.

Cross-Correlation of Neural Culture Spiking Activity on Multielectrode Arrays is Strongly Dependent on Bursting Activity Pattern

Pimashkin Alexey[1,2*], Gladkov Arseniy[1,3], Lepina Anastasia[1,3], Mukhina Irina[1,2,3], Kazantsev Victor[1,2]

1 Neuroscience Center, N.I. Lobachevsky State University of Nizhny Novgorod, Nizhny Novgorod, Russia
2 Department of Nonlinear Dynamics, Institute of Applied Physics RAS, Nizhny Novgorod, Russia
3 Normal Physiology Department, Nizhny Novgorod State Medical Academy, Nizhny Novgorod, Russia
* Corresponding author. E-mail address: pimashkin@neuro.nnov.ru

Abstract

Network spiking activity patterns formed in neuronal cultures can be monitored using multielectrode arrays (MEA). It has been demonstrated in many studies that spontaneous and stimulus evoked spike sequences in population bursts recorded from different electrodes display significant cross-correlation which can be interpreted as a connectivity or spike transfer through neural network. We have shown that high cross-correlation in the network can be explained by specific features of the bursting pattern.

1 Introduction

Spontaneous and evoked spiking activity in dissociated cultures has the form of population bursts (100-400 ms) generated by significant number of neurons in the network. Recent studies have shown that during burst initiation the spiking times occur with high repeatability (Pimashkin et al., 2011).It has been also reported on local signal propagation between nearby electrodes in the burst initiation stage (Gandolfo et al., 2010). However, many other works use cross-correlation analysis applied to the whole burst as a measure to estimate spike propagation delay and connectivity strength. In this study we show that the cross-correlation can strongly depend on the time profile of spiking rate in the bursts.

2 Methods

Dissociated hippocampal cells were grown on microelectrode arrays (MEA, Multichannel Systems, Germany). 60 microelectrodes with 30 µm in diameter and 200 µm interelectrode spacing were used for recording electrophysiological signals. Cell plating procedure and activity analysis methods can be found in Pimashkin et al. (2013). For the analysis we recorded 1 hour of the spontaneous activity. All experiments were performed with cultures on 21-45 DIV. For the spiking activity from each electrode we defined a *spike rate profile* as average number of spikes found from a burst onset in every millisecond (Fig. 1 A, C). Next, for each pair of electrode activity we defined the following characteristics. A time delay of a maximum cross-correlation of the spike-rate profiles was defined as a *pair profile correlation*. A time difference of the first spikes in the burst was defined as *activation time delta*. A time difference of maxima in the *spike-rate profiles* in each electrode was defined as a *peak spike-rate delta*. Spike transfer measure for each electrode pair (i,j) was defined as percentage of spikes from i-th electrode found on j-th electrode with various time delay (Fig. 1 B). Time delay value corresponding to the peak of this measure was considered as a *spike transfer delay*.

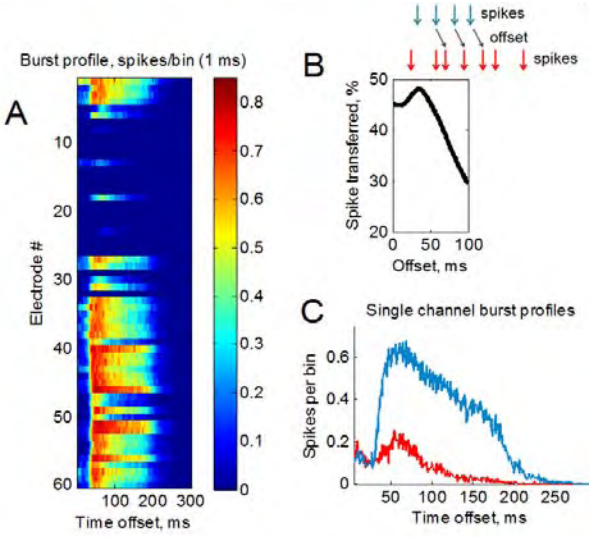

Fig. 1. Spike-rate profile of spontaneous bursts and channel pair activity relations. (**A**) Average spike number on each electrode every millisecond with various time offsets of burst initiation (spike-rate profile). (**B**) *Top* – schematic representation of spike transfer estimation. *Bottom* - Example of cross-correlation (*spike transfer* measure) between activity in a pair of electrodes 42 and 3. (**C**) Examples of spike-rate profiles (spikes per 1 ms time bin) for electrodes 42 and 3.

3 Results

To explore spike transfer characteristics we calculated *spike rate profile* (see Methods) for each electrode (Fig. 1 A). Then we calculated *pair profile correlation*, which represented maximal likehood between burst profiles recorded from different electrodes (Fig. 1 C). Figure 2 A shows the dependence of *pair profile correlation* on *spike transfer delay* for each electrode pairs in one culture. Figure 2 B shows the dependence of the *activation time delta* on the *spike transfer delay* for the same data. A linear relation of the characteristic can be clearly seen in (A) in contrast to (B).

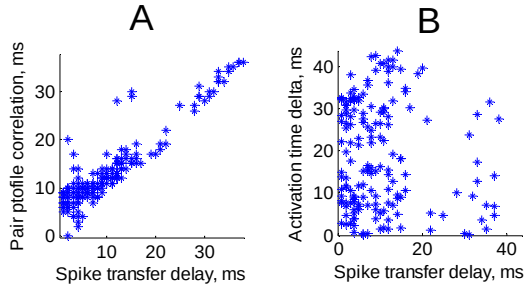

Fig. 2. Cross-correlation between pairs spiking activity from different electrodes. (**A**) Dependence of the *spike transfer* measure on the *pair profile correlation*. Each point - comparison of electrode activity pair. (**B**) Dependence of the *activation time delta* on the *pair profile correlation*

Next we investigated the relations between these characteristics. The set of points was approximated by line function, and then the coefficient of determination R_2 was calculated to estimate the quality of the approximation, and hence their linear dependence. We found that R_2 for the dependence of the *pair profile correlation* on the *spike transfer delay* (Fig. 3 A) was equal to R=0.4703 (n=8 cultures, 12 recordings). Also we estimated R_2 for the other characteristics of bursting activity. Figure 3 B shows the dependence of the *activation time delta* on *the spike transfer delay* (R_2=0.0816). Figure 3 B shows the dependence of the *pair profile correlation* on *the spike transfer delay* (R_2=0.0996). The results indicate the presence of high linear dependence of the two pairwise correlation characteristics of the bursts. Oppositely, pairwise electrode-to-electrode comparison of the activation time and the maximum spiking rate time displayed to be uncorrelated.

4 Conclusions

We found that the spike transfer characteristics taken here as cross-correlation measure which should represent functional connectivity indicator revealed only the dependence between spiking rate profiles of non-stationarity spiking sequence in the bursts. The results showed that the spike transfer is linearly dependent on the spike rate cross-correlation measure. It suggests that both methods effectively reflects correlations in the spiking rate dynamics. The result also suggests that the connectivity measure in the cultured network should be independent to instantaneous frequency of the spikes within the bursts.

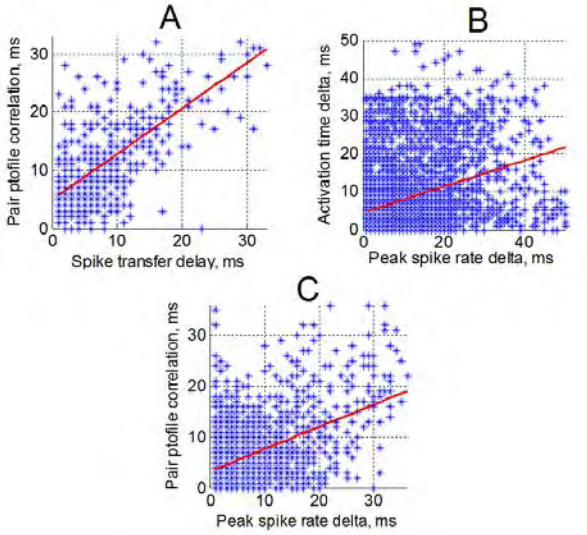

Fig. 3. (**A**) *The spike transfer* measure versus the spike rate profile, coefficient of determination R=0.4703. (**B**) Electrode pairwise difference of activation time (*activation time delta*) and peaks of spike-rate profile (*peak spike rate delta*), R=0.0816. (**C**) The *peak spike rate delta* and the *pair profile correlation*, R=0.0996.

Acknowledgement

This research was supported by Russian Foundation for basic research (№13-02-01223/13, №13-04-12041/13), Grant for Leading Scientists (11.G34.31.0012), Russian President Grant № MK-4602.2013.4.

References

[1] Pimashkin A., Gladkov A., Mukhina I. and Kazantsev V. (2013) Adaptive enhancement of learning protocol in hippocampal cultured networks grown on multielectrode arrays. *Front. Neural Circuits* 7:87.

[2] Pimashkin A., Kastalskiy I., Simonov A., Koryagina E., Mukhina I. and Kazantsev V. (2011) Spiking signatures of spontaneous activity bursts in hippocampal cultures. *Front. Comput. Neurosci*. 5:46

[3] Gandolfo, M., Maccione, a, Tedesco, M., Martinoia, S., & Berdondini, L. (2010). Tracking burst patterns in hippocampal cultures with high-density CMOS-MEAs. *Journal of Neural Engineering*, 7(5)

[4] Le Feber, J., Rutten, W. L. C., Stegenga, J., Wolters, P. S., Ramakers, G. J. a, & Van Pelt, J. (2007). Conditional firing probabilities in cultured neuronal networks: a stable underlying structure in widely varying spontaneous activity patterns. Journal of neural engineering, 4(2), 54–67

Spontaneous and Stimulus Induced Connectivity Changes in Cultured Neural Network

Arseniy Gladkov[1,3*], Alexey Pimashkin[1,2], Anastasia Lepina[1,3], Victor Kazantsev[1,2], Irina Mukhina[1,3]

1 Neuroscience Center, N.I. Lobachevsky State University of Nizhny Novgorod, Nizhny Novgorod, Russia
2 Department of Nonlinear Dynamics, Institute of Applied Physics RAS, Nizhny Novgorod, Russia
3 Normal Physiology Department, Nizhny Novgorod State Medical Academy, Nizhny Novgorod, Russia
* Corresponding author. E-mail address: gladkov@neuro.nnov.ru

Abstract

Cultured neural networks grown on multielectrode arrays are convenient model to investigate learning and memory at cellular and network level. Spontaneous bioelectrical activity in such networks demonstrated quite high variability in mature culture (more than 30 DIV). It can be also associated with changes associated with synaptic plasticity in network functioning. In particular, we have shown that changes in connectivity can be induced by electrical stimulation and can be preserved up to 10-20 minutes. We also noted that the induced changes in connectivity can effectively interfere with changes due to spontaneous activity appeared at time scale of hours.

1 Methods

1.1 Network Stimulation

Hippocampal neural cells from mice embryos at 18-th prenatal day were plated on 60-electrode arrays (Multichannel systems, Germany). Cell plating procedure and activity analysis methods were explained in Pimashkin et al., 2013. Low frequency stimulation (30 pulses per each of 12 selected electrodes with 5 s interval) was imposed to induce changes of network connectivity, e.g. network plasticity. Experimental protocol included 3 hours of spontaneous activity recorded before and after stimulation. These 3 hour recordings were devided on 60 and 20 minute intervals for analysis.

1.2 Cross-correlation analysis

Cross-correlation of activity observed from each electrode pair (i,j) was calculated as percentage of spikes from i-th electrode found on j-th electrode with various time delay. A strength of connection was estimated as the percent of spikes found on the recording electrode. A time delay with corresponding to maximum of the spike-transfer function was treated as connectivity delay. If the connectivity delay was greater than 3 ms (Fig.1), then the pair was considered as synaptically connected (Le Feber et al., 2007). Connectivity change was estimated for sequential segments of the recordings relative to initial segment. Coefficient of connectivity change was defined as the percent of appeared and disappeared connections comparing to the initial segment. We also introduced coefficient of *stable connection strength changes* defined as the average strength change only for connections found in the both segments.

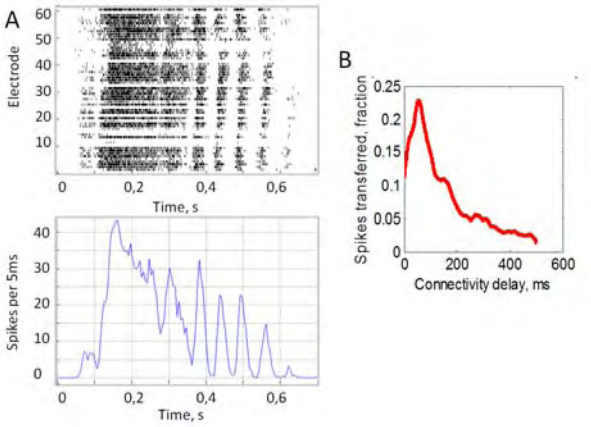

Fig. 1. A. Raster of the network burst. B. Connectivity estimation measure based on cross-correlation of activity on 2 sites of network (see Methods).

2 Results

We found that the electrical stimulation induced changes in functional network connectivity (e.g. the network plasticity) which can be reliably detected at the that on time scale of 10-20 minutes. After this interval the spontaneous activity of the network may affect these changes leading to spontaneous changes in the connectivity. It appeared at time scale of 12-18 hours. Note, that at minutes time scale the strength connectivity changes by spontaneous dynamics is much less than stimulus induced effect. Total number of connections in 20 and 60 min time scales was preserved after stimulation. It indicated that connectivity was reorganized only, but not expanded or decreased.

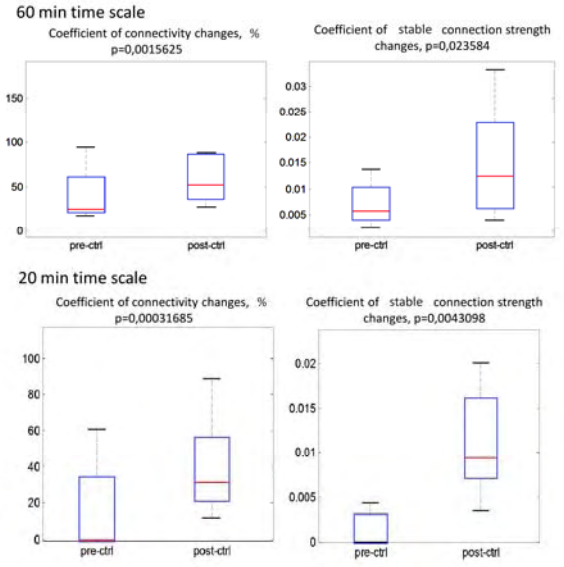

Fig. 2. Network connectivity changes on 20 min and 60 min time scales after low-frequency stimulation. Pre-ctrl – comparison of the network connectivity between initial recording (first 20 or 60 minutes) and recording before stimulation. Post-ctrl – comparison of the networks state between initial recording and first recording after stimulation. Box: central mark is the median, the edges of the box are the 25th and 75th percentiles. P-value was estimated using Mann-Whitney test.

3 Conclusion

We have shown that electrical stimulation of cultured neural network can be effective tool to induced changes in synaptic connectivity at network level at minutes time scale. Long term effect of the plasticity was hardly detect because of significant impact of spontaneous dynamics.

Acknowledgement

This research was supported by Russian Foundation for basic research (№13-02-01223/13, №13-04-12041/13), Grant for Leading Scientists (11.G34.31.0012), Russian President Grant № MK-4602.2013.4

References

[1] Pimashkin A., Gladkov A., Mukhina I. and Kazantsev V. (2013) Adaptive enhancement of learning protocol in hippocampal cultured networks grown on multielectrode arrays. *Front. Neural Circuits* 7:87.

[2] Le Feber, J., Rutten, W. L. C., Stegenga, J., Wolters, P. S., Ramakers, G. J. a, & Van Pelt, J. (2007). Conditional firing probabilities in cultured neuronal networks: a stable underlying structure in widely varying spontaneous activity patterns. *Journal of neural engineering*, 4(2), 54–67

Short ISI stimulation modifies firing property of a cultured neuronal network

Hidekatsu Ito[1], Suguru N. Kudoh[1]

1 School of Science and Technology, Kwansei Gakuin University, 2-1 Gakuen, Sanda, Japan

Abstract

Memory in our brain was generated by complex network activity. To elucidate relationship between activity of neuronal network and spatiotemporal pattern of evoked spikes, using multi-electrode array (MEA) dish, measuring extracellular potentials. Temporal activity pattern is changed according to inter-spike-interval (ISI) of electrical conditioning stimulus. In other words, dissociated neuronal network memorizes timing of stimulation in temporal pattern of spontaneous activity. In this report, we show that relationship between spontaneous neuronal activity and patterns of sequential electrical stimuli.

1 Introduction

Cultured neurons reorganized complex networks on a multi-electrodes array dish, and spontaneous electrical activity was observed [1, 2]. Spontaneous activity pattern changes depending on the culture days, and the synchronized electrical activity comes to be confirmed in cortical dissociated culture [3, 4]. When sequential electrical stimuli from two electrodes were applied to neuronal network, firing property of neuronal network was changed [5]. We focused on the relationship between the spontaneous activity and conditioning sequential stimuli in cultured neuronal network, and found that the temporal pattern of spontaneous activity was modified according to ISI of electrical conditioning stimulus.

2 Materials and methods

Dissociated rat hippocampal neurons were placed in an arranged cloning ring with a diameter of 7 mm at the center of a MED probe. The density of seeded cells was 7800 cells/mm^2. Culture medium consisted of 45% Ham's F12, 45% Dulbecco's modified minimum essential medium, 5% horse serum, and 5% fetal calf serum, 100 U/ml penicillin, 100 μ g/ml streptomycin, and 5 μg/ml insulin. To elucidate response against an electrical input, we applied single stimulus and paired stimuli to the neuronal network. Recordings electrical spike activity were performed before and after electrical stimulus. We estimated intervals between the major peaks of spontaneous activity. The intervals were compared among 4 different conditions, (1)before single stimulus, (2)after single stimulus, (3)after paired stimuli and (4)after single stimulus.

3 Result and Discussions

The mean spike intervals in an example single neuronal network are 405.5±67.6 ms (mean±SE) before single stimulus, 713.7±92.5ms after single stimulus, 864.8±94.8 ms after paired stimuli, 745.7±75.7 ms after single stimulus, respectively. The mean intervals between the major peaks of the activity tended to increase after both of single stimulus and paired stimuli. The mean intervals after paired stimuli were increased to approximately 800 - 900 ms. This value was close to the ISI of paired stimuli. The modified intervals between the peaks in spontaneous activity depended on the ISI of applied paired stimuli. In addition, the mean intervals after single stimulus in Fig.2 (2) and (4) were resembled each other. The spike interval in spontaneous activity is able to be controlled by stimulation procedure. These results indicated that dissociated neuronal network memorizes timing of stimulation in temporal pattern of spontaneous activity.

4 Conclusion

The spike intervals in spontaneous activity is able to be controlled by ISI of sequential conditioning stimuli. A livingneuronal network memorizes timing of stimulation in temporal pattern of spontaneous activity, even in their semi-artificial environments.

5 References

[1] Gross GW, Rieske E, Kreutzberg GW and Meyer A, (1977) A new fixed-array multimicroelectrode system designed for long-term recording., Neurosci Lett 6, pp:101-105

[2] Pine J, (1980) Recording action potentials from cultured neurons with extracellular microcircuit electrodes., J Neurosci Methods, pp:19-31

[3] Eytan D, Marom S, (2006) Dynamics and effective topology underlying synchronization in networks of cortical neurons., J of Neurosci, 26, pp:8465-8476

[4] Wagenaar DA, Pine J, Potter SM, (2006) An extremely rich repertorie of bursting patterns during the development of cortical cultures. BMC Neurosci 7:11

[5] Shahaf G, Marom S, (2001) Learning in networks of cortical neurons, J. Neurosci., Vol.21, No.22, pp.8782-8788

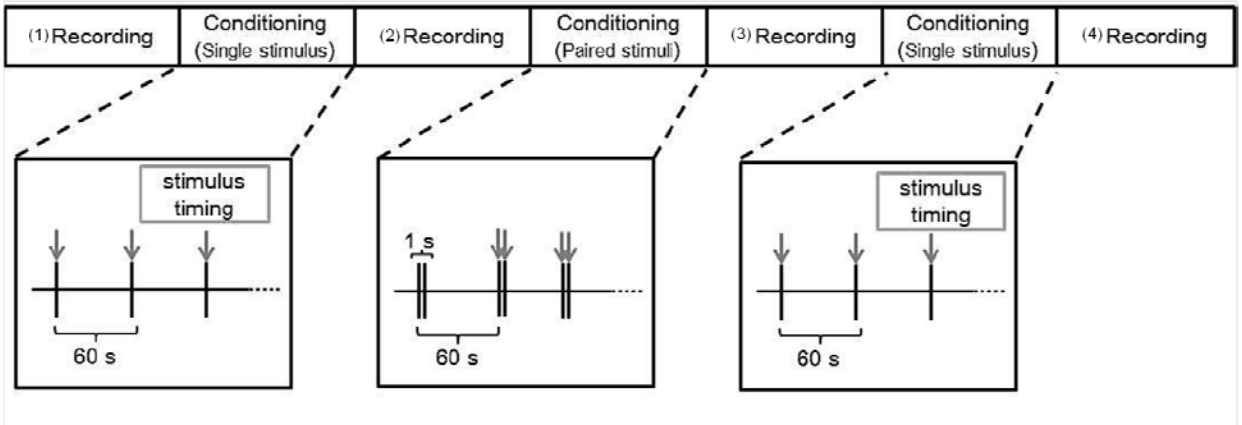

Fig.1 Experimental procedure.
Single stimulus and Paired stimuli are applied to neuronal network. Recordings of electrical activities were performed before and after the conditoning.

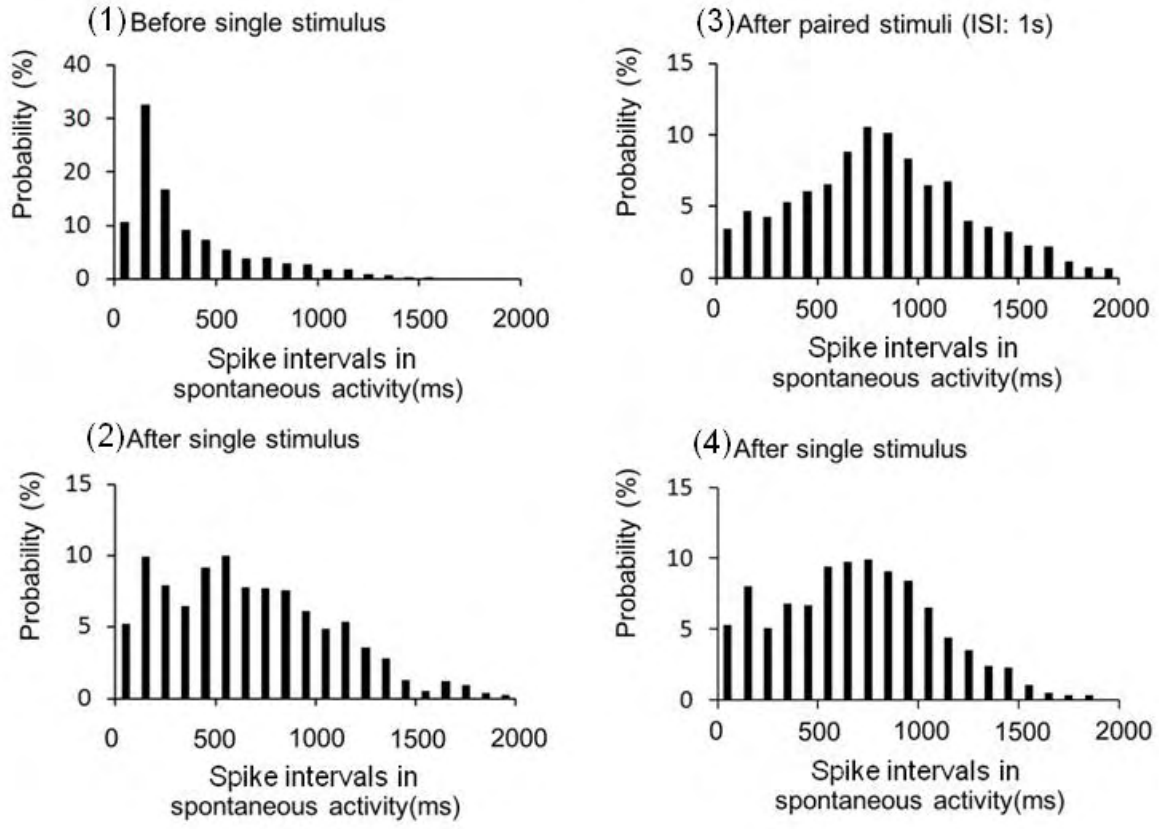

Fig.2 Different firing properties of spontaneous activity are induced by each stimulus procedure.

In Vivo Recordings and Stimulation

Skin-like Neuroprosthesis Based on Elastomeric Composites for Chronic Epidural Electrical Stimulation of Paralyzed Rats

Alexandre Larmagnac[1*], Niko Wenger[2], Pavel Musienko[2], Janos Vörös[1], Grégoire Courtine[2]

1 Laboratory of Biosensors and Bioelectronics, ETH Zurich, Switzerland
2 International Paraplegic Foundation Chair in Spinal Cord Repair, Center for Neuroprosthetics, EPFL, Switzerland
* Corresponding author. E-mail address: larmagnac@biomed.ee.ethz.ch

Abstract
We previously reported the design of an all-elastomeric stretchable multi-electrode array (sMEA) to electrically interface soft and moving tissue of the body such as the spinal cord. Here, we will show some results of chronic *in vivo* studies in rodents that demonstrate the superiority of skin-like sMEAs based on poly(dimethylsiloxane) (PDMS) over standard polyimide MEAs when interfaced to the spinal cord and especially in the subdural space.

1 Backround / Aims

There is growing evidence that electrical spinal cord stimulation may contribute to improving motor execution and recovery after spinal cord injury (SCI), Parkinson's disease, multiple sclerosis and possibly other neurological disorders affecting descending control systems. Epidural electrical stimulation (EES) applied on the dorsal aspect of the spinal cord facilitates motor execution through the recruitment of afferent fibers that activates segmental reflex circuits and propriospinal neuronal networks [1]. Accordingly, EES applied at specific locations over the lumbosacral spinal cord engages specific subsets of neuronal circuits, thus leading to distinct patterns of limb movements [2]. These results open the intriguing possibility to design multi-site EES strategies to enable a finer control of locomotion than currently possible with existing stimulation paradigms. However, no systematic studies on the potential benefit of multi-site EES have been conducted so far, largely because of the lack of interfaces for simultaneously delivering stimulation at multiple spinal cord locations in freely behaving subjects. Here, we present a novel neuroprosthetic multi-electrode array (MEA) for multi-site EES *in vivo*.

2 Methods / Statistics

Our MEAs have been designed in soft material, which enables chronic implantation of the interface not only epidurally (see Fig. 1) but also subdurally without damage of the surrounding neural structures. The MEA acts as a second biocompatible skin that bends and moves with the spinal cord. For chronic applications involving rehabilitation, MEAs have to survive large, chronic mechanical stresses caused by the relative movements between the spine and the vertebrae, as well as the contraction of powerful trunk muscles (see Fig. 2). We developed and optimized stretchable conductive leads that can survive such high mechanical stress for extended durations. PDMS was chosen as substrate material because of its mechanical properties similar to that of the dura mater. Thus it is possible to produce a second-skin that does not harm the underlying cord and roots on which stretchable leads can be integrated. Stretchable tracks of silver-filled PDMS (Ag-PDMS) were screen-printed on this PDMS substrate and insulated by a second layer of PDMS. Electrodes of 350 µm were made by exposing the Ag-PDMS and coating it with Pt-Ir. CT scans of implanted rats (see Fig. 1) were also done to control the integrity and better visualize the sMEA *in vivo* and possibly find unwanted extreme stress regions. All these mechanical deformations should be reduced by designing the MEAs and implanting them adequately.

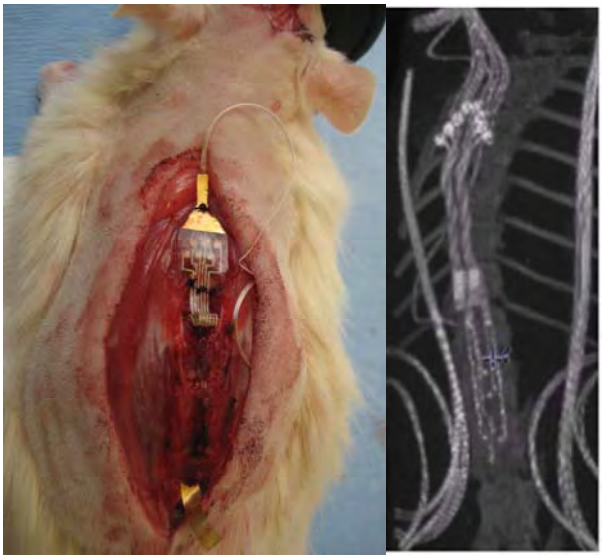

Fig. 1. Pictures of our MEA taken during implantation (left) and by a CT scanner few months after implantation (right).

3 Results

The elastic properties of our elastomeric composites conferred stretchability to the implant. Samples loaded with 23% vol. of Ag remained conductive at strains > 100%. Stimulation sites remained fully functional during stretching as large as 60% of the total length. Testing in rats with MEA chronically implanted over epidural lumbosacral segments showed no sign of inflammation and preserved implant integrity several months after surgery. As early as 1 week after a complete SCI, each electrode of the MEA was able to elicit locomotion on a treadmill with site-specific features in paralyzed rats.

4 Conclusion/Summary

Our novel MEA and implantation technique provide the technological framework to develop advanced multisite EES algorithms that increase the facilitation of specific locomotor patterns and enhance gait improvement with rehabilitation.

Fig. 2. Pictures of a freely moving rat implanted with our sMEA in a turning position with the spine making a closed circle. Local strains as high as 70% were measured where the implant enters the spinal canal.

Acknowledgement

This project was financed by the ETH Zurich, the international paraplegic foundation, the ERC Walk Again, and the “NEUWalk” project of the European Union FP7 program.

References

[1] Courtine et al. (2009). Transformation of nonfunctional spinal circuits into functional states after the loss of brain input. *Nature Neuroscience*, 12, 10, 1333-U167.

[2] Musienko et al. (2009). Combinatory Electrical and Pharmacological Neuroprosthetic Interfaces to Regain Motor Function After Spinal Cord Injury. *IEEE Transactions on Biomedical Engineering*, 56, 11, 2707-2711.

Electrical Stimulation of the Auditory Brainstem with a Flexible Polyimide Microelectrode Array

Amélie Guex[1*], Rohit U. Verma [2], Ariel E. Hight [2], M. Christian Brown[2], Philippe Renaud [3], Daniel J. Lee [2], Stéphanie P. Lacour [1]

1 LSBI, Center for neuroprosthetics, EPFL, Lausanne, Switzerland
2 Eaton-Peabody Laboratories, Massachusetts Eye and Ear Infirmary, Boston, USA
3 LMIS4, STI, EPFL, Lausanne, Switzerland
* Corresponding author. E-mail address: amelie.guex@epfl.ch

Abstract
In an attempt to improve the auditory brainstem implant (ABI), an alternative hearing strategy for patients that cannot benefit from a cochlear implant, a flexible 5-channel polyimide implant was designed and fabricated with standard microfabrication processes. Devices were implanted on the dorsal cochlear nucleus surface of Sprague-Dawley rats and the effect of electrode diameter and inter-electrode distance during bipolar stimulation was studied. Results show a successful stimulation of the auditory system with the 5-channel electrode array. An effect of the electrode diameter and inter-electrode distance was also identified from the auditory brainstem responses (ABR) and multiunit recordings form the inferior colliculus (IC). These results show the possibility of improving the spatial specificity by optimizing the design and flexibility of the electrode array.

1 Background/Aims

Auditory brainstem implants (ABI) are an alternative hearing strategy for patients that cannot benefit from a cochlear implant (CI) because of a disconnection between the peripheral and central auditory systems. ABI users speech recognition scores are however very variable and on average poorer than CI users. Only a limited range of distinct frequencies can be accessed and current spreads to neighbouring non-auditory structures, causing extra-auditory sensations[1]. This might be due to the rigid electrode design of the current ABI that requires high current levels. In this study, a new design of ABI based on flexible polyimide substrate is proposed and tested. The flexible substrate associated to an optimization of the electrodes geometry and location might increase the spatial selectivity of stimulation by better conforming to the curvilinear structure of the cochlear nucleus.

2 Methods

Fabrication

Microelectrode arrays (MEAs) consist of a layer of 350 nm thick platinum film located between two 22 µm thick polyimide layers and are fabricated using standard microfabrication processes[2]. 5 electrode sites are located on a single line with inter-electrode distances of 400 µm and designed to match the tonotopically organised mediolateral axis of the dorsal cochlear nucleus (DCN) during in vivo experiments. Implants with 3 different electrode diameters are designed (100 µm, 150 µm and 200 µm). A PEDOT:PSS conducting polymer coating is electropolymerized on the electrode sites and results in a decrease of impedance and increase of charge injection capacity of more than one order of magnitude.

In vivo tests

In vivo experiments are performed on Sprague-Dawley rats (350-500 g) anesthetized with ketamine and xylazine. The dorsal cochlear nucleus (DCN) surface is exposed by suctioning part of the cerebellum to allow placement of the MEA and bipolar stimulation is induced (symmetric biphasic, 0.2 ms per phase, 23Hz). Auditory brainstem responses (ABR) are recorded with subcutaneous wire electrodes placed on the vertex, behind the ipsilateral ear and on the back of the animal. Multi-unit recordings are obtained from the inferior colliculus (IC) with a 16-channel electrode array (Neuronexus Technologies, Inc.) placed along the tonotopic axis of the IC central nucleus.

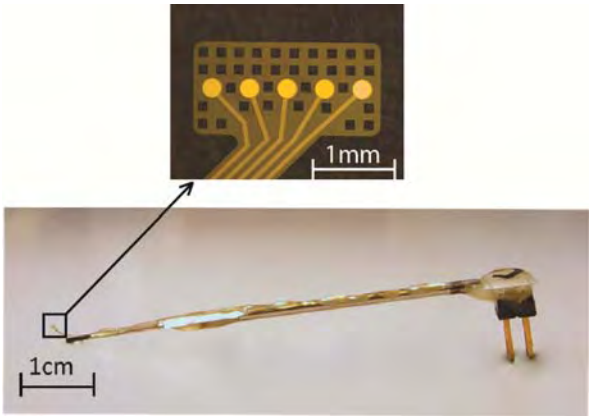

Fig. 1. Picture of the 5-electrode array and packaging

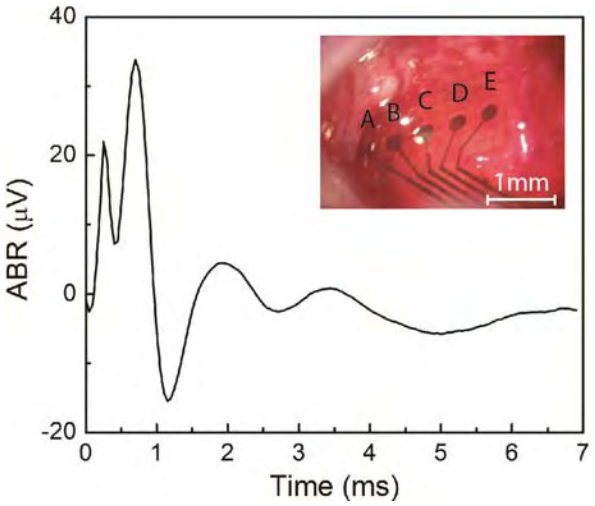

Fig. 2. Example of an auditory brainstem response (ABR) obtained following stimulation with the MEA placed at the surface of the dorsal cochlear nucleus. (Biphasic symmetric stimulation pulses, 0.2 mA, 0.2ms/phase at 23Hz)

3 Results

Activation of the auditory system was successfully recorded with electrodes of different diameters: large-amplitude ABRs and robust neural firing rates in the IC were evoked. Auditory brainstem responses (ABRs) were found to be on average smaller at identical current level for small electrode sites (<150 µm) and inter-electrode distances (<800 µm), indicating an increase in spatial selectivity of stimulation in these conditions. Recordings from the inferior colliculus showed a high variability in frequency specificity. A high frequency specificity was observed in some cases, whereas other experiments showed broad frequency activation in all conditions. This suggests the possibility to access different frequency channels with an optimized design.

Thresholds of activation were on average higher after bipolar stimulation with channels AB (as defined in Figure 2), which reflects a poor contact of the lateral part of the implant on the DCN surface. Further flexibility of the polyimide substrate might then be needed in order to optimise the contact over the whole surface of the DCN and minimize stimulation thresholds.

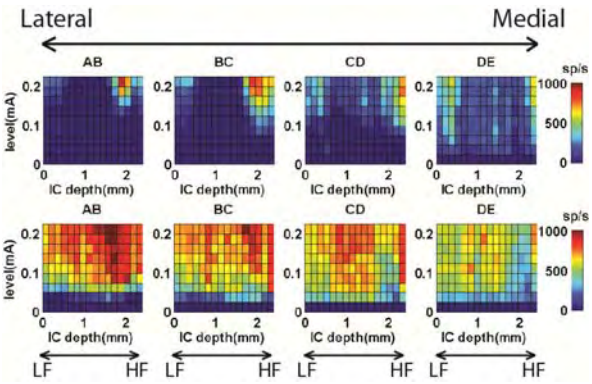

Fig. 3. Examples of spike rates recorded in the inferior colliculus (IC) following bipolar stimulation (400 µm inter-electrodes distances) at different locations on the CN surface..

4 Conclusion

Our results show that the auditory system can be successfully stimulated with a flexible microfabricated electrode array placed at the surface of the DCN. Far-field as well as direct multi-unit recording data can provide some guidelines for the optimization of the pad geometry, density and conformability to the DCN surface in order to further enhance the spatial selectivity of stimulation. By using small electrode sites (<150 µm) and further decreasing inter-electrode distances (<800 µm) on a thinner thus more compliant polyimide substrate, a higher spatial specificity of stimulation might be achieved, allowing for both access to more independent frequency channels and decrease of the non-auditory side-effects (due to spread of current to neighbouring non-auditory structures).

Further work involves optimization of the selectivity of stimulation as well as scaling up this design for use in larger animal models.

Acknowledgement

This work is funded by Fondation Bertarelli.

References

[1] Coletti et al., “Progress in restoration of hearing with the auditory brainstem implant”, *Progress in Brain Research*, Volume 175, 2009, pp333-345

[2] Mercanzini et al., “Demonstration of cortical recording using novel flexible neural probes”, Sensors and Actuators A: Physical, Volume 143, Issue 1, May 2008, pp90-96.

PDMS Based µ-ECoG

Arthur Hirsch[1*], Ivan Minev[1], Natalia Pavlova[2], Léonie Asboth[2], Grégoire Courtine[2], Stéphanie P. Lacour[1]

1 Laboratory for Soft Bioelectronic Interfaces, Centre for Neuroprosthetics, EPFL, Switzerland
2 UPCOURTINE, Brain Mind Institute, EPFL, Switzerland
* Corresponding author. E-mail address: arthur.hirsch@epfl.ch, stephanie.lacour@epfl.ch

Abstract
Micron scale ECoGs, termed µ-ECoGs, are miniaturized array prepared with microfabrication techniques and implemented on thin polymer films. We introduce an innovative design where the electrode array is made of ultrathin and elastic metal film embedded in a soft, elastic silicone. The soft µ-ECoG array hosts 3x3 electrodes distributed over 2.25mm^2. The transparency of the substrate allows us to combine recordings of cortex signals in mouse expressing Channelrhodopsin-2 with localised light stimulation, making this technology especially promising for the future developments of optoelectronic implants.

1 Background

Electrocorticography (ECoG) is clinically used for brain mapping and pre-surgical localization of epileptic seizure. It has also gained some interest for brain machine interface (BMI) as it offers an interesting trade-off between highly invasive intracortical electrode array and low-resolution electroencephalography (EEG). With the rapid development of optogenetics as an alternative neuromodulation tool, ECoG recordings are now combined with optical stimulation of neurons for bidirectional optogenetics BMI [1] [2]. We propose a soft micro-ECoG technology compatible with light stimulation using transparent, stretchable silicone elastomer as a substrate.

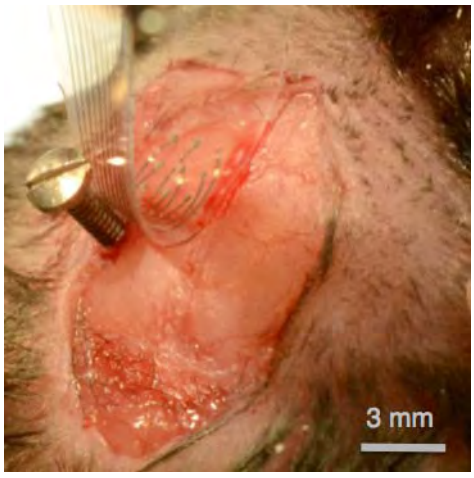

Fig. 1. Micro-ECoG on mouse cortex

2 Methods

2.1 Electrode fabrication

The micro-ECoG array is prepared using standard microfabrication adapted to the use of an elastomeric carrier substrate. A thin gold film (5 nm Cr, 35 nm Au) deposited on a polydimethylsiloxane (PDMS) substrate is patterned in interconnects and electrode contacts, and encapsulated with another membrane of PDMS. The electrode sites are further coated with a soft conducting composite. The electrode (ø150 µm) matrix has a 3x3 layout designed to cover about 1.5mm x 1.5mm of the mouse cortex.

2.2 Electrode characterization

Electrochemical characterization of the electrodes was conducted using a potentiostat (Gamry inc.) with the electrodes immersed in a phosphate buffered saline (PBS) solution, at room temperature. A platinum wire and Ag/AgCl electrode are selected for as counter and reference electrodes, respectively.

2.3 Acute recordings

Acute epidural recordings of evoked brain potentials were obtained with the soft micro-ECoG in mouse expressing Channelrhodopsin-2, and under ketamine anaesthesia. Series of photostimuli (4Hz) were applied by shining a laser (150mW.mm^{-2}, 472 nm, 9 ms pulse) coupled to an optical fiber through the transparent PDMS substrate; using a micromanipulator holder, the optical fiber was scanned at different locations across the mouse cortex. Resulting potentials and trigger signals were acquired using a TDT neurophysiology workstation (Tucker Davies Technologies Inc.) and sampled at 24,414 Hz. One of the nine electrodes was used as the reference.

3 Results

The micro-ECoG array features 9 electrodes(ø150 µm) spaced by 750 µm on a 2.25 mm2 recording area. Electrochemical characterization of the array revealed low impedance moduli of 4.1 kΩ ± 2.3 kΩ and phase of -15o ± 3o at 1kHz. The built-in microstructure of gold thin film on PDMS allows for the implant to flex, twist and stretch without causing electrical failure of the device [3]. Signals recorded during an acute in vivo experiment displayed low background noise of 60µV peak-to-peak, and negative potentials of up to 2mV were evoked. Spatially defined potentials could be observed with multiple negative and positive potential peaks (fig.2) in accordance with the literature [1].Figure 2 displays an overlay of evoked potentials recorded by one electrode in response to light stimulation (150mW.mm-2, 472 nm, 9 ms pulse). Figure 2 displays an overlay of evoked potentials recorded by one electrode in response to light stimulation (150mW.mm-2, 472 nm, 9 ms pulse).

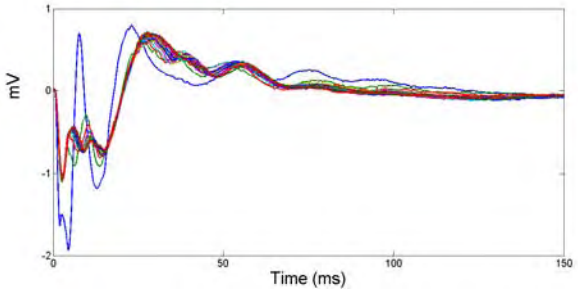

Fig. 2. Overlay of the evoked potentials of a single electrode in response of a series of stimuli

Averaged evoked potentials over the series of light stimuli (in an animal under anaesthesia) for each electrode and stimulation sites are presented Figure 3. The optical fiber is apposed on the surface of the PDMS array in positions A (top left corner) or B (bottom right corner). Apart from electrode 6, which displays much lower signal amplitude, all electrodes monitor the ECoG signals. For a given stimulation location, the overall shape of the signals recorded on each electrode is the same but its amplitude is correlated to the optical fiber proximity: the closer the stimulation, the larger the amplitude (peak-to-peak) of the signal.

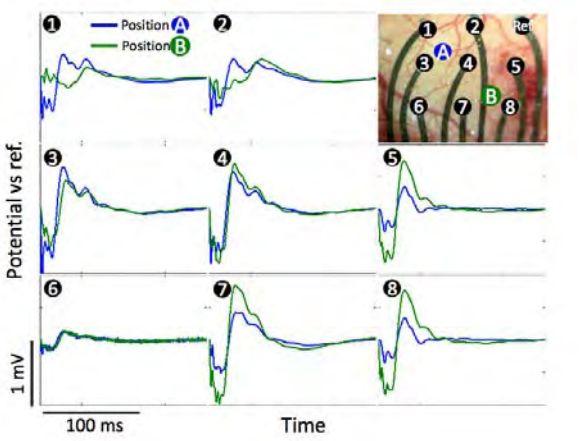

Fig. 3. Average evoked potentials of the different electrodes for two different stimulation posiitons

4 Conclusion

We have developed a soft microelectrode array for electrocorticography, fabricated on a 140µm thick transparent PDMS membrane. As a proof-of-concept acute experiment, this shows that soft electrode arrays integrated in elastomeric substrate can be successfully implemented in epidural micro-ECoG arrays. PDMS transparency and compatibility with micro/ nanofabrication make PDMS particularly suitable for the design and development of a range of optoelectronic implants. The microfabrication approach also allows the implant design to be customized and scaled up to larger surface areas.

Acknowledgement

This work is supported by the Fondation Bertarelli and FNS nano-tera.ch .

References

[1] Richner, Thomas J., et al. "Optogenetic micro-electrocorticography for modulating and localizing cerebral cortex activity." Journal of neural engineering 11.1 (2014): 016010.

[2] Kwon, Ki Yong, et al. "Opto-µECoG array: Transparent µECoG electrode array and integrated LEDs for optogenetics." Biomedical Circuits and Systems Conference (BioCAS), 2012 IEEE. IEEE, 2012.

[3] Minev, I. R., & Lacour, S. P. "Impedance spectroscopy on stretchable microelectrode arrays. Applied Physics Letters, 2010 , 97(4), 043707.

MEA Technology

Oral Presentations

Conducting Polymer Devices for *In Vivo* Electrophysiology.

George G. Malliaras

Department of Bioelectronics, Ecole Nationale Supérieure des Mines, Gardanne, France
E-mail address: malliaras@emse.fr

Abstract
A visible trend over the past few years involves the application of conducting polymer devices to the interface with biology, with applications both in sensing and actuation. Examples include biosensors, artificial muscles and neural interface devices. The latter are of particular interest, as conducting polymers offer several distinct advantages compared to incumbent technologies and lead to better quality recordings. As such, they promise to yield new tools for neuroscience and enhance our understanding on how the brain works. We review a few examples of electrodes and transistors for applications ranging from recording neural activity on the surface of the brain to cutaneous recordings of electroencephalograms.

1 Introduction

In this extended abstract we review our work on conducting polymer electrodes for *in vivo* electrophysiology. Our interest in these materials stems mostly from the 3D nature of the interaction between a conducting polymer such as poly(3,4-ethylenedioxythiophene) doped with poly(styrene sulfonate) (PEDOT:PSS), and biological media [1]. As shown in Fig. 1, ions can be exchanged between a PEDOT:PSS film and an electrolyte, and this can be used to alter the conductivity of the polymer (for biosensing), or to deliver ions in an electrolyte (for bioactuation).

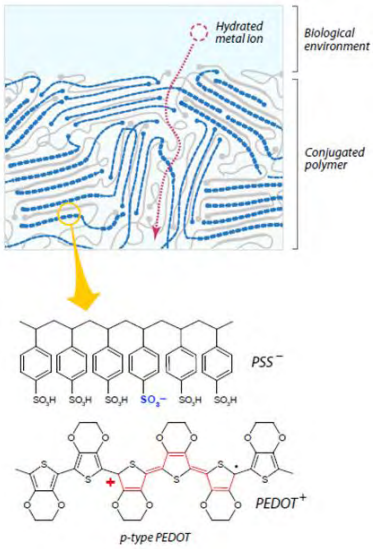

Fig. 1. Schematics of the organic conductor PEDOT:PSS at the interface with an electrolyte.

2 Electrodes

Conducting polymer films coated on top of traditional electrodes such as Au or Pt are known to decrease electrochemical impedance. We have exploited this phenomenon both *in vitro* [2] and *in vivo* [3] in order to demonstrate microelectrode arrays that record signals from tissue slices and rat brains, respectively, with high signal-to-noise ratios (SNR). Of particular interest is the finding that electrocorticography (ECoG) arrays using PEDOT:PSS electrodes can record brain activity in rats with a spatial resolution of the order of 60 microns.

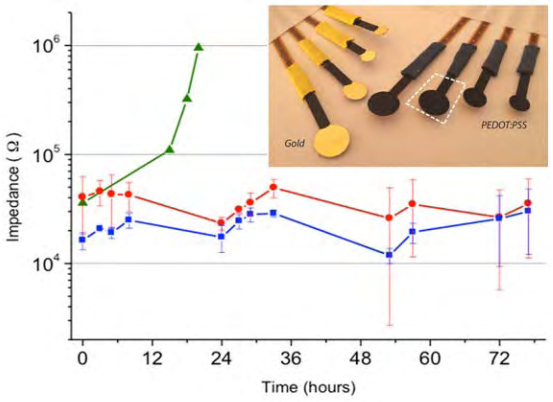

Fig. 2. Electrode/skin impedance at 1 kHz for IL gel-assisted Au and PEDOT:PSS electrodes and commercial Ag/AgCl electrode with an aqueous gel. Insert shows electrode structure.

The same impedance lowering phenomenon can be exploited in macro-scale electrodes such as the ones used for cutaneous recordings. One of the main issues with conventional electroencephalography (EEG) electrodes is that they utilize an aqueous gel that dries after a few hours and prohibits long term recordings. Our first attempt to overcome this problem was by using dry conducting polymer electrodes,

which were shown to record EEG spectra as well as gel-assisted commercial electrodes [4]. Even better performance was achieved using conducting polymer electrodes coated with an ionic liquid (IL) gel [5]. The latter shows negligible vapour pressure (does not dry out) and enables long term recordings (Fig. 2).

3 Transistors

A step up in terms of sophistication and performance can be achieved when using a transistor as the recording device. We develop organic electrochemical transistors (OECTs), in which the polymer channel, made of PEDOT:PSS, is in direct contact with the electrolyte (cerebrospinal fluid in the case of ECoG). The local field potential at the conducting polymer/electrolyte interface changes the conductivity of the PEDOT:PSS film by driving the exchange of ions between the film and the electrolyte. This leads to transistors that show exceptionally high transconductance (Fig. 3) [6].

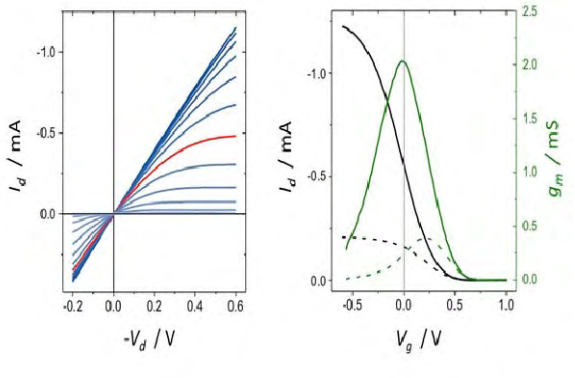

Fig. 3. Electrical characteristics of a microfabricated organic electrochemical transistor. The red output curve is at zero gate voltage, while the green curve shows the transconductance.

OECTs act as amplifying transducers and are ideal for biomedical applications [7] due to a combination of properties such as low voltage operation, compatibility with many substrates, including mechanically flexible ones, and high gain and stability.

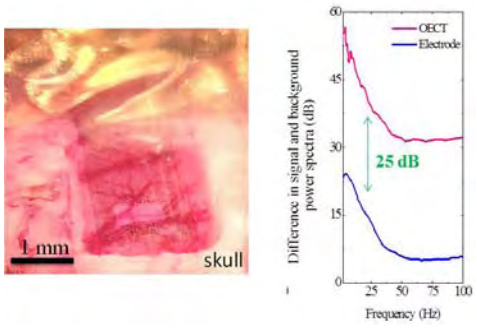

Fig. 4. Flexible array of electrodes and transistors placed on the cortex of a rat. Power spectra plot showing SNR of recordings obtained with electrodes and transistors.

We integrated OECTs and conducting polymer electrodes on mechanically flexible parylene films and used them to record electrocorticograms in rats (Fig. 4). We found that the OECTs record with a higher signal-to-noise ratio than electrodes as a result of their inherent (power) amplification [8].

4 Conclusions

Conducting polymers have the potential to lead to the development of new tools for neuroscience. This stems from a combination of properties, with the most important one being their 3D interaction with ions in electrolytes. We leveraged this property to develop electrodes and transistors that record brain activity with high signal-to-noise ratio.

Acknowledgement

All work discussed in this abstract was performed within a collaboration of the Department of Bioelectronics of the Ecole des Mines and the Systems Neuroscience Institute of the INSERM/Aix Marseille University in the Provence region of France. People who participated in this research are Dion Khodagholy, Pierre Leleux, Thomas Doublet, Marc Ferro, Michele Sessolo, Jonathan Rivnay, Esma Ismailova, Pascale Quilichini, Antoine Ghestem, Christian Benar, Jean-Michel Badier, and Christophe Bernard.

References

[1] J. Rivnay, R.M. Owens, and G.G. Malliaras, "The rise of organic bioelectronics", Chem. Mater. 26, 679 (2014).
[2] M. Sessolo, D. Khodagholy, J. Rivnay, F. Maddalena, M. Gleyzes, E. Steidl, B. Buisson, and G.G. Malliaras, "Easy-to-fabricate conducting polymer microelectrode arrays", Adv. Mater. 25, 2135 (2013).
[3] D. Khodagholy, T. Doublet, M. Gurfinkel, P. Quilichini, E. Ismailova, P. Leleux, T. Herve, S. Sanaur, C. Bernard, and G.G. Malliaras, “Highly conformable conducting polymer electrodes for in vivo recordings”, Adv. Mater. 36, H268 (2011).
[4] P. Leleux, J.-M. Badier, J. Rivnay, C. Bénar, T. Hervé, P. Chauvel, and G.G. Malliaras, "Conducting polymer electrodes for electroencephalography", Adv. Healthcare Mater. 3, 490 (2014).
[5] P. Leleux, C. Johnson, X. Strakosas, J. Rivnay, T. Hervé, R.M. Owens and G.G. Malliaras, "Ionic liquid gel-assisted electrodes for long-term cutaneous recordings", Adv. Healthcare Mater., in press (2014).
[6] D. Khodagholy, J. Rivnay, M. Sessolo, M. Gurfinkel, P. Leleux, L.H. Jimison, E. Stavrinidou, T. Herve, S. Sanaur, R.M. Owens, and G.G. Malliaras, "High Transconductance Organic Electrochemical Transistors", Nature Comm. 4, 2133 (2013).
[7] J. Rivnay, P. Leleux, M. Sessolo, D. Khodagholy, T. Hervé, M. Fiocchi, and G.G. Malliaras, "Organic electrochemical transistors with maximum transconductance at zero gate bias", Adv. Mater. 25, 7010 (2013).
[8] D. Khodagholy, T. Doublet, P. Quilichini, M. Gurfinkel, P. Leleux, A. Ghestem, E. Ismailova, T. Herve, S. Sanaur, C. Bernard, and G.G. Malliaras, "In vivo recordings of brain activity using organic transistors" Nature Comm. 4, 1575 (2013).

In-vitro Recordings of Electrogenic Cells Activity with Organic Field Effect Transistors

A. Spanu[1,2]*, S. Lai[1], P. Cosseddu[1], M. Tedesco[2], A.Bonfiglio[1,3], and S. Martinoia[2]

1 University of Cagliari – Dept. of Electrical and Electronic Engineering, Piazza d'Armi, 09123 Cagliari, Italy
2 University of Genova – Dept. of Informatics, Bioengineering, Robotics and System Engineering, Via Opera Pia 13, 16145 Genova, Italy
3 CNR – Institute of Nanoscience, Via Campi 213/A, 41125 Modena, Italy
* Corresponding author. E-mail address: andrea.spanu@edu.unige.it

Abstract
A novel, reference-less platform for the electrophysiological monitoring of excitable cells is here presented. The system is based on the use of an Organic Thin Film Transistor (OTFT) specifically tailored in order to host a sensing area where living electrogenic cells are cultured. Their electrical activity is monitored by means of the variations of the device threshold voltage induced by the small charge quantities displaced across the cell membrane during the occurrence of an action potential. The designed organic transistors were able to monitor reliably and with a good level of sensitivity the culture's electrical activity. Moreover, the mechanically flexible and transparent substrate, the low cost of the employed technology, and the fact that the proposed system does not need a reference electrode for the measurements, make this novel platform extremely promising for cellular electrophysiology and, particularly, as basic structure for the development of a next generation of *in-vivo* bio-electronic interface.

1 Background / Aims

Devices based on organic semiconductors offer the possibility of implementing innovative applications using low-cost processing techniques. In particular, organic chemo and bio-sensors have been recently developed with good performances in terms of sensitivity [*1, 2*]. Because of these results and because of the many interesting materials' properties (such as flexibility, transparency and biocompatibility), these devices seem very promising for monitoring electrical phenomena occurring at the bio-electronic interface. Though organic electro-chemical transistors (OECTs) have been successfully employed for electrophysiological applications both in-vivo and in-vitro [*3, 4*], Organic Thin Film Transistors (OTFTs) have not yet been employed so far to this aim mainly because of the high operating voltages and the low charge carriers mobility that puts a serious limit on the frequency range of the signals that might be applied as input. The aim of this work is to merge electrophysiology and organic electronics by exploiting the very interesting properties of a particular OTFT called Organic Charge Modulated Field Effect Transistor (OCMFET).

2 Methods

The OCMFET [*5, 6*] is a low-voltage floating gate OTFT with a control gate to set its working point and a sensing area (represented by the final part of the elongated floating gate) upon which the cells are cultured (fig. 1A). The cells' activity determines a modulation of the threshold voltage of the transistor causing a variation of the output current (fig. 1B).

The peculiar structure of the OCMFET allows keeping the sensing and the active area separated, thus preventing the organic semiconductor from getting in contact with the culture's liquid environment. Moreover, thanks to the presence of the control gate, the system does not require any external reference electrode. To broaden the bandwidth of the transistor we introduced a self-alignment process in order to reduce the parasitic capacitances and compensate for the low carriers mobility (*7*). The proposed system consists of an organic sensor (an array of up to 16 OCMFET with common control gate and source) and a front-end electronics for the signal conditioning.

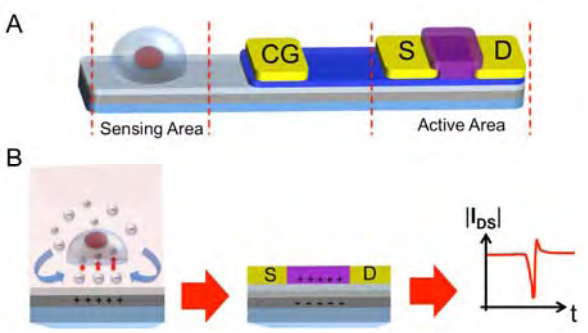

Fig. 1. Cross section of the OCMFET. (A) The device is a floating gate OTFT with a sensing area and a control gate through which the working point is set. (B) The charge displacement across the cell membrane induces a fluctuation of charges inside the floating gate; the subsequent modulation of the field effect leads to a variation of the I_{DS} current of the organic transistor.

3 Results

The system has been successfully tested with cardiac rat myocyte cultures. In fig. 2 one minute of spontaneous electrical activity of an embryonic rat cardiomyocytes culture (8 days in vitro - DIV) mantained at a contant temperature of 37 °C in a controlled atmosphere (5 % of CO_2, 95 % of humidity) is shown. The cultures showed a tipical periodic activity of about 0.8 Hz. During the experimental sessione, the devices were operated with a control gate voltage and a source-drain voltage of -1 V (a typical value for the threshold voltage of such a device is 0 V).

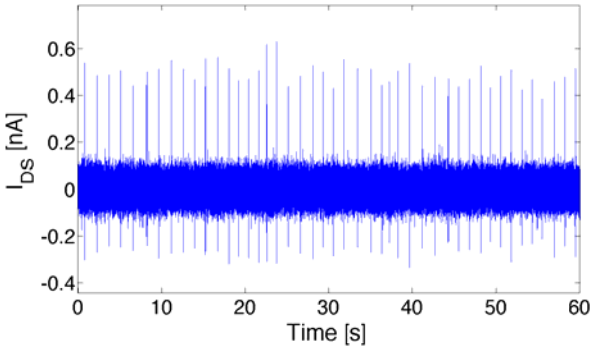

Fig. 2. OFET recording of the spontaneous activity of an embryonic rat cardiomyocytes culture (8 Days In Vitro - DIV).

4 Conclusion/Summary

We have presented an innovative, reference-less device, based on a particular organic field effect transistor called OCMFET, which is able to record and amplify the signals produced by the spontaneous electrical activity of living cells. The proposed system (consisting of 16 identical OCMFETs and a dedicated readout electronics) has been successfully tested with cardiac rat myocytes cultures, and it showed interesting performances in terms of signal to noise ratio and reliability. The OCMFET is reference-less, flexible, transparent and it is make with low cost techniques and these features make this device a novel powerful tool for realizing active substrates for cell cultures at low cost, thus opening a perspective for the fabrication of disposable, active substrates for cell monitoring both *in-vitro* and *in-vivo*.

References

[1] M. Berggren, A. Richter-Dahlfors. Organic Bioelectronics. *Adv. Mat.*, **19**, 3201–3213 (2007).

[2] D. T. Simon, S. Kurup, K. C. Larsson, R. Hori, K. Tybrandt, *et al*. Organic electronics for precise delivery of neurotransmitters to modulate mammalian sensory function. Nature Materials, **8**, 742-746 (2009).

[3] D. A. Bernards, G. G. Malliaras. Steady-State and Transient Behavior of Organic Electrochemical Transistors. *Adv. Fun. Mater.*, **17**, 3538–3544 (2007).

[4] D. Khodagholy, T. Doublet, P. Quilichini, M. Gurfinkel, P. Leleux, et al.. In vivo recordings of brain activity using organic transistors. Nature Comm., 4, Article Number1575 (2013).

[5] M. Barbaro, A. Bonfiglio, L. Raffo. A charge-modulated FET for detection of biomolecular processes: conception, modeling, and simulation. IEEE Trans. El. Dev., 53(1), 158–166 (2006).

[6] A. Caboni, E. Orgiu, E. Scavetta, M. Barbaro, A. Bonfiglio. Organic-based sensor for chemical detection in aqueous solution. Appl. Phys. Lett., 95(12) (2009).

[7] S. Lai, P. Cosseddu, G. C. Gazzadi, M. Barbaro, A. Bonfiglio. Towards high frequency performances of ultra-low voltage OTFTs: Combining self-alignment and hybrid, nanosized dielectrics. Organic Electronics, 14(3), 754-761 (2013).

High-Density CMOS-based Microelectrode Array Platform for Large-Scale Neuronal Network Analysis

Jan Müller[1*], Marco Ballini[1], Yihui Chen[1], Paolo Livi[1], Milos Radivojevic[1], Urs Frey[2], Douglas Bakkum[1] and Andreas Hierlemann[1]

1 ETH Zurich, Department of Biosystems Science and Engineering, Basel, Switzerland.
2 RIKEN Quantitative Biology Center, Kobe, Japan.
* Corresponding author. E-mail address: jan.mueller@bsse.ethz.ch

Abstract
We present a high-density CMOS-based microelectrode array featuring 26,400 bidirectional Pt microelectrodes and 1024 parallel readout channels. Enabled through a flexible scheme of selecting the most appropriate recording and stimulation sites, activity of neuronal networks with hundreds of cells can be recorded for hours. By using only the electrodes for recordings that pick up neuronal activity, best use of available resources can be made. We demonstrate how the high density of recording electrodes (17.5 µm pitch) together with the low-noise readout amplifiers increases spike-sorting yield and thus allows for more accurate inferences of network topologies.

1 Introduction

Neurons connect to each other through thousands of synapses to form large networks. In order to better understand how signals propagate through such networks and how information processing is performed, it is desirable to know the functional connectivity of such networks and to track its evolution over time. As opposed to many imaging techniques, extracellular action potential recordings are a non-lethal means to infer such connectivity. Previous attempts to record from neuronal networks either failed to reliably resolve individual cells, or they recorded from individual cells but only very few at the same time [1]. Here, we try to overcome these limitations by employing a high-density microelectrode array (HD-MEA) [2,3,4,5] with a large number of parallel readout channels. Our aim is to record from a medium-size population (>1000) of individually resolved neurons and to infer their functional relation. By being able to record from potentially every neuron in a culture, more accurate connectivity estimates will be possible as opposed to recording from an under-sampled population [6].

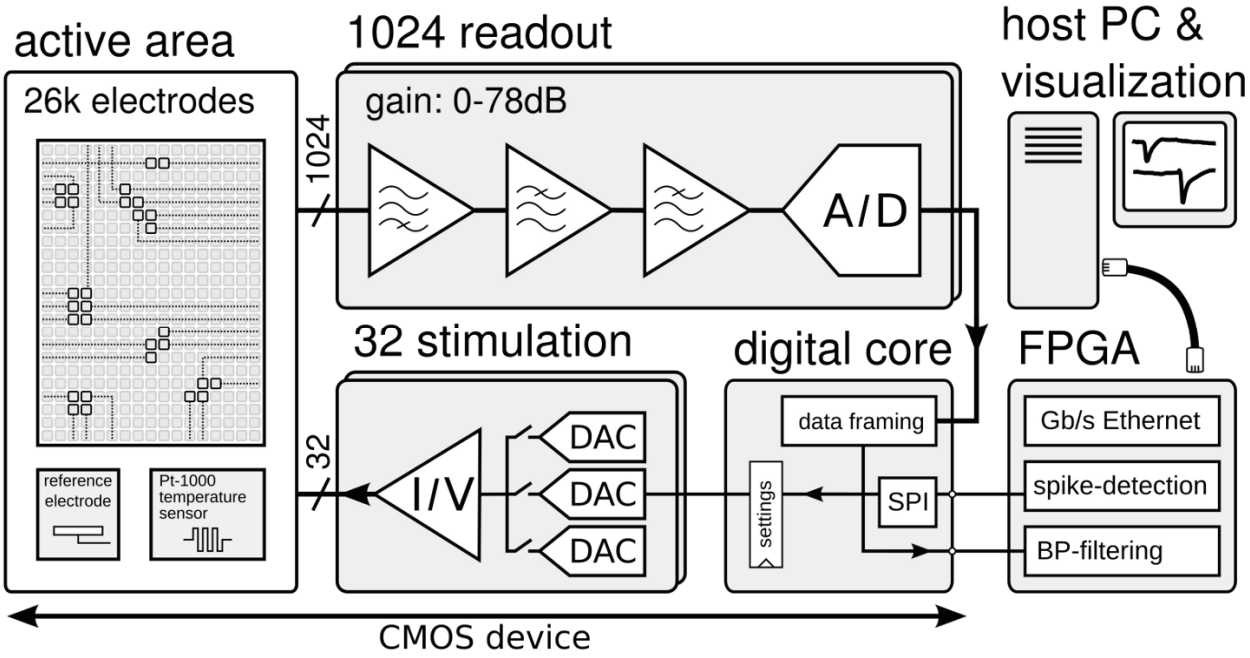

Fig. 1. Block diagram of the CMOS-MEA system. The 1024 readout channels and the 32 stimulation units are connected through a set of switches to a subset of the 26,400 Pt microelectrodes. An FPGA is used to communicate with the CMOS HD-MEA and to pre-process the data before streaming it through Ethernet to a host PC for data visualization and storage.

2 Methods

We developed a complementary metal-oxide-semiconductor (CMOS)-based high-density microelectrode array (HD-MEA) featuring 26,400 bidirectional Pt microelectrodes with a center-to-center pitch of 17.5 µm [7]. Enabled through a versatile matrix of switches and wires, residing below the electrodes, 1024 low-noise voltage recording units (2.4 μV_{rms} in the action-potential signal band, 300 Hz – 10 kHz), as well as 32 current and voltage stimulation units can be connected to an almost arbitrary subset of these electrodes (Figure 1 and 2) [8]. Cortical neurons have been cultured on the chip according to protocols described in [9], and recordings were performed after 30 DIV. By first scanning through all electrodes, individual neurons could be localized. Multiple electrodes usually record the extracellular action potential of one neuron, and groups of cells aggregate into clusters. Therefore, locally dense and globally sparse patches of electrodes providing good cell separability can be identified and used for further recordings. Employing a dense electrode selection only where many cells reside, allows for economic usage of scarce recording units. After spike sorting the recorded data, spike trains are obtained for all recorded neurons, and the cross-correlation between pairs of cells can be computed to reveal parts of the network structure.

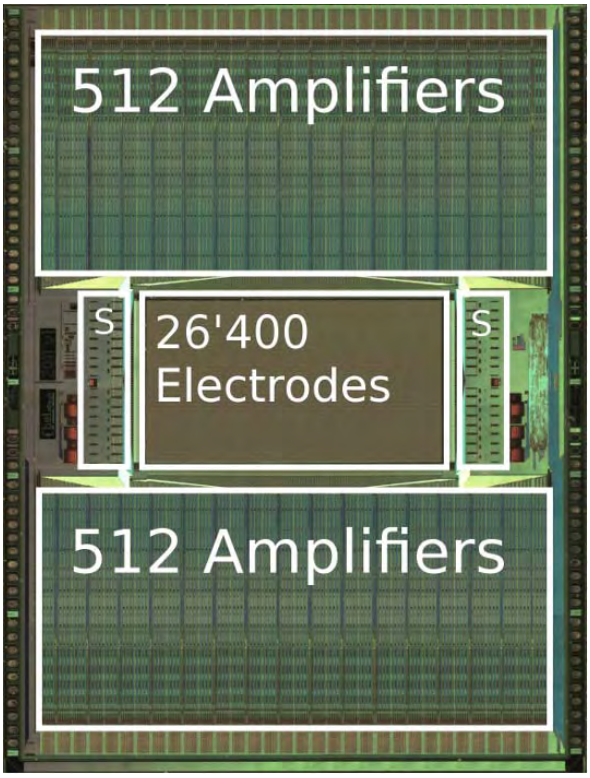

Fig. 2. Micrograph of the fabricated CMOS device. The array with the 26,400 Pt microelectrodes is surrounded by 1024 readout channels residing at the top and bottom, as well as 32 stimulation units located to the left and right of the chip.

3 Results

First, different electrode-to-readout configurations were scanned through the array, and recordings from all electrodes were analyzed for neuronal activity. Once spots with high activity were identified, electrodes in these areas were selected for further experiments. Recordings from these electrode clusters were performed for 2.5 hours. Figure 3 shows such a cluster of electrodes, which allows for separating four distinct waveforms. Figure 4 shows the localization of the electrode cluster (red arrow) with respect to the full array.

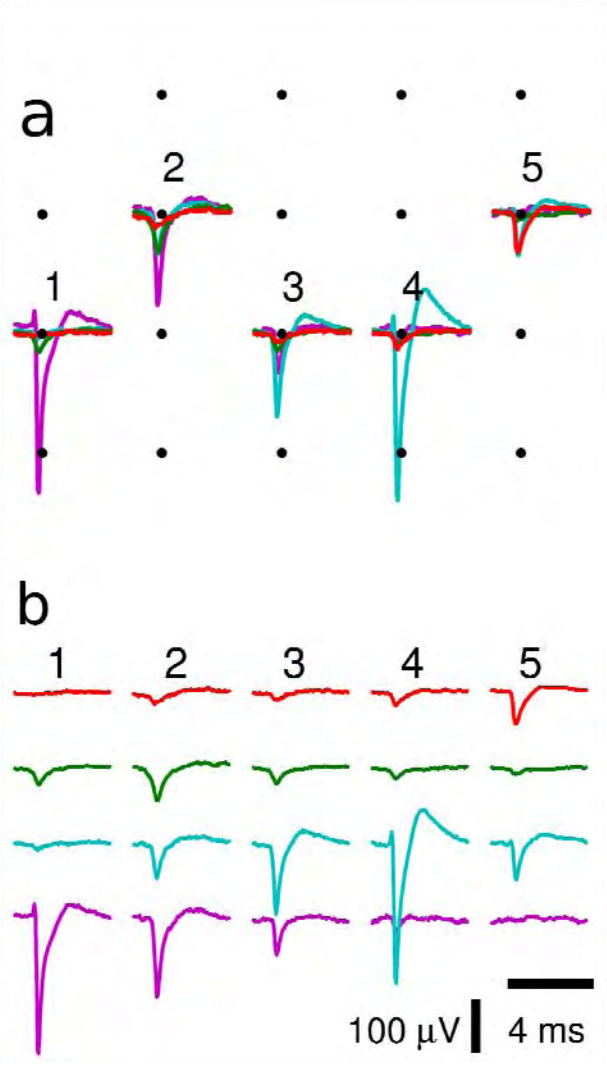

Fig. 3. Spike-triggered-average waveforms of action potentials. a) Example of five electrodes (1-5) providing a locally dense cluster of recording sites. By using only the electrodes that convey the most information, redundant recordings are avoided. b) The five electrodes from a) reveal four distinct clusters of events. The clusters are color-coded, and it is shown how the amplitude for each cluster varies across the five electrodes.

.

Through these clusters, 1105 individual cells could be identified. Computing the cross-correlation between pairs of cells revealed elevated probability of correlated firing within milliseconds for a few pairs [10]. Figure 5 shows the cross-correlation curves for four neurons. Their approximate location is indicated with a green arrow.

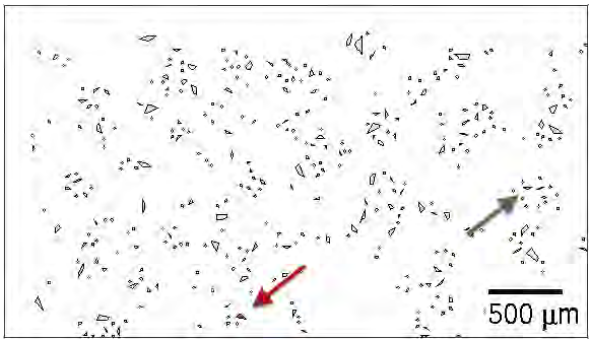

Fig. 4. Location of the selected electrode clusters on the 3.85 × 2.10 mm^2 array. By recording from these spots, a total of 1105 neurons could be identified and their network-wide interaction was analyzed.

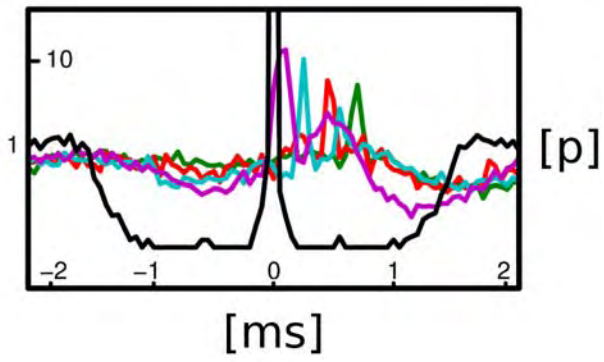

Fig. 5. Auto-correlation (black) and cross-correlation curves for four neurons originating from the same electrode cluster. These neurons seem to have elevated spiking activity immediately after each other indicating a causal link.

4 Conclusion

Owing to the large amount of high-spatial-resolution recording sites and the excellent signal-to-noise ratio of the recording units, our presented setup allows for identifying and tracking large networks of neuronal cells (>1000) over long timescales (hours to days). The cross correlation between cell pairs provides a first-order approximation of the network structure. Tracing how connections change due to electrical stimulation protocols and over time provides a powerful tool to study synaptic plasticity in such networks.

Acknowledgement

We would like to thank Alexander Stettler, Jörg Rothe and Marta Lewandowska for their help with the experimental setup and cell culture preparations. This work was supported by the ERC Advanced Grant "NeuroCMOS" under contract number AdG 267351. Milos Radivojevic and Douglas J. Bakkum received funding support from the Swiss National Foundation through an Ambizione Grant (PZ00P3_132245).

References

[1] Gerhard, F., Kispersky, T., Gutierrez, G. J., Marder, E., Kramer, M., & Eden, U. (2013). Successful reconstruction of a physiological circuit with known connectivity from spiking activity alone. *PLoS computational biology*, *9*(7), e1003138.

[2] Hierlemann, A., Frey, U., Hafizovic, S., & Heer, F. (2011). Growing Cells Atop Microelectronic Chips: Interfacing Electrogenic Cells In Vitro With CMOS-Based Microelectrode Arrays. *Proceedings of the Ieee*, *99*(2), 252-284. doi: 10.1109/jproc.2010.2066532

[3] B. Eversmann et al., "A 128 x 128 CMOS Biosensor Array for Extracellular Recording of Neural Activity," *IEEE J. Solid-State Circuits*, pp. 2306-2317, Dec., 2003.

[4] L. Berdondini et al., "High-density Electrode Array for Imaging in Vitro Electrophysiological Activity," *Biosensors and Bioelectronics*, vol. 21, Issue 1, pp. 167-174, 2005.

[5] U. Frey, J. Sedivy, F. Heer, R. Pedron, M. Ballini, J. Mueller, D. Bakkum, S. Hafizovic, F. D. Faraci, F. Greve, K.-U. Kirstein, and A. Hierlemann, "Switch-Matrix-Based High-Density Microelectrode Array in CMOS Technology," *Solid-State Circuits, IEEE Journal of*, vol. 45, no. 2, pp. 467–482, 2010.

[6] Stevenson, I. H., & Koerding, K. (2011). *Inferring spike-timing-dependent plasticity from spike train data.* Paper presented at the NIPS.

[7] Ballini, M., Muller, J., Livi, P., Chen, Y., Frey, U., Shadmani, A., Hierlemann, A. (2013). A 1024-channel CMOS microelectrode-array system with 26'400 electrodes for recording and stimulation of electro-active cells in-vitro. *2013 Symposium on VLSI Circuits*, C54-C55.

[8] Müller, J. et al. (2013). *Conferring flexibility and reconfigurability to a 26,400 microelectrode CMOS array for high throughput neural recordings.* Paper presented at the Solid-State Sensors, Actuators and Microsystems (TRANSDUCERS & EUROSENSORS XXVII), 2013 Transducers & Eurosensors XXVII: The 17th International Conference on.

[9] D. J. Bakkum, U. Frey, M. Radivojevic, T. L. Russell, J. Müller, M. Fiscella, H. Takahashi, and A. Hierlemann, "Tracking axonal action potential propagation on a high-density microelectrode array across hundreds of sites.," *Nature communications*, vol. 4, p. 2181, 2013.

[10] Fujisawa, S., Amarasingham, A., Harrison, M. T., & Buzsáki, G. (2008). Behavior-dependent short-term assembly dynamics in the medial prefrontal cortex. *Nature neuroscience*, *11*(7), 823-833.

A Capacitively-Coupled CMOS-MEA with 4225 Recording Sites and 1024 Stimulation Sites

Gabriel Bertotti[1*], Norman Dodel[1], Stefan Keil[1], Dirk Wolansky[2], Bernd Tillak[2], Matthias Schreiter[3], Max Eickenscheidt[4], Günther Zeck[4], Alfred Stett[4], Andreas Möller[5], Karl-Heinz Boven[5], and Roland Thewes[1]

1 TU Berlin, Faculty of EECS, Chair of Sensor and Actuator Systems, Berlin, Germany
2 IHP GmbH, Technology/Process Research, Frankfurt/Oder, Germany
3 Siemens AG, Corporate Technology, Research & Technology Center, Munich, Germany
4 Natural and Medical Sciences Institute at the University Tübingen, Neurochip Research Group, Reutlingen, Germany
5 Multi Channel Systems GmbH, Reutlingen, Germany
* Corresponding author. E-mail address: gabriel.bertotti@tu-berlin.de

Abstract
A CMOS-based MEA with 4225 recording sites and 1024 stimulation sites is used to achieve high spatiotemporal resolution in in-vitro neural tissue interfacing experiments. Active area is 1 mm × 1 mm or 2 mm × 2 mm, respectively. A thin high-k dielectric serves as sensor interface between solid-state chip and biology.

1 Introduction

During the last decade, CMOS-based MEAs [1-6] have attracted huge attention, since they promise increased spatiotemporal resolution in extracellular interfacing with neural tissue and cultivated neural networks compared to their classical passive counterparts.

Different approaches have been published concerning the interfacing technique as such, namely to use noble metal electrodes [2-4, 6] or purely capacitive recording / stimulation sites utilizing a high-k dielectric covering the respective interfacing electrodes [1, 5]. Moreover, also different readout techniques are in use, focusing on entire area imaging [1, 2, 5] or high spatial selectability concerning the positions in space to be monitored [3, 6].

In this paper, we present a CMOS chip using a purely capacitive recording/stimulation approach aiming for full chip or selected (entire) area neural tissue activity imaging.

2 Methods and System Setup

A schematic cross section of the extended CMOS process used, a photo of the chip surface, and an assembled chip are shown in Fig. 1.

We use a 6 metal standard 1.8 V 180 nm CMOS process with 3.3 V devices for analog and I/O purposes. A thin TiN electrode covered by a 30 nm Ti-Zr high-k oxide [7] is then fabricated on top of the CMOS wafer. The recording electrodes are connected to the gates of related sensor transistors.

The layout of the various metal layers used for the electrical interconnects on the chip is configured such that these layers also provide an efficient light shield for the active CMOS devices in the silicon substrate,

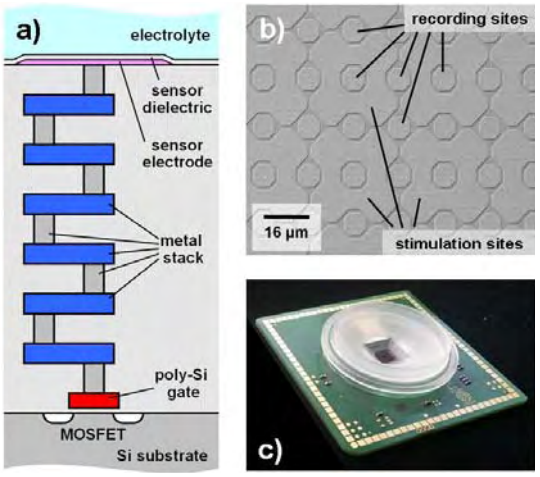

Figure 1: a) Schematic technology cross section. b) Photo of the chip surface (chip with 16 µm recording site pitch and 32 µm stimulation site pitch. c) Assembled chip.

allowing operation of the chips under illumination or in combination with light-based stimulation of the biological content.

The chips provide 4225 recording sites and 1024 stimulation sites, recording site diameter is approximately 8 µm, recording site pitch is 16 µm (design A) or 32 µm (design B). The stimulation sites have a far larger area and are arranged in between the recording sites as shown in the chip surface photo in Fig. 1b).

The chips are assembled on a 5.5 cm x 5.5 cm carrier PCB (Fig. 1c)) which also provides the electrical contacts to the reader unit (Fig. 2). That unit consists of further gain stages, A/D converts the signals, and further processes the sampled signals. The output is connected to a standard PC workstation equipped with custom data-management software.

Figure 2: Chip operating unit and data acquisition system

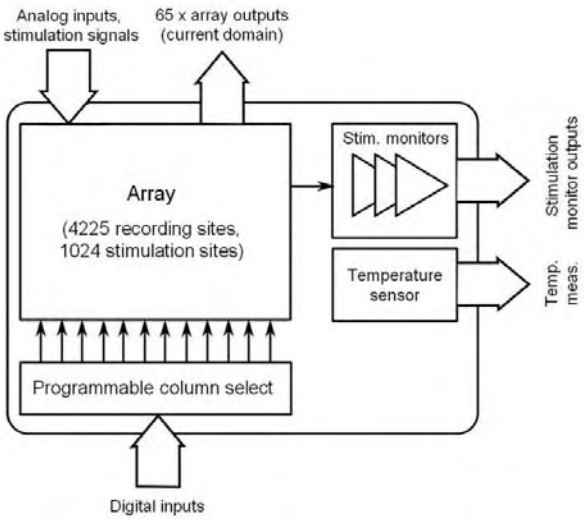

Figure 3: Block diagram of the entire chip.

Fig. 3 shows a simplified block diagram of the chip. The array of sensor transistors is organized in 65 columns and 65 rows. Only one column per time is read out through the row connections. By means of the programmable column select circuit readout can be directed to the entire array or to a subset of columns in a time multiplexed-manner. A 3-bit parallel digital
interface is used to program the respective block.

The monitor amplifiers depicted in the upper right corner of the figure can optionally be used to monitor the stimulation signals applied to the array. Moreover, a simple temperature sensor is implemented to provide information about on-die temperature thus allowing optimization of the measurement setup concerning biological boundary conditions.

3 Design Issues

In Figs. 4 and 5 the concepts of stimulation and recording circuitry are depicted.

Each stimulation site can be connected to three different stimulation signals (whereas in practice frequently one of the related signal lines is held at GND potential), that can be defined by software and are generated by the chip operating unit, or left floating. For that purpose a 2048 bit signal (2 bit for

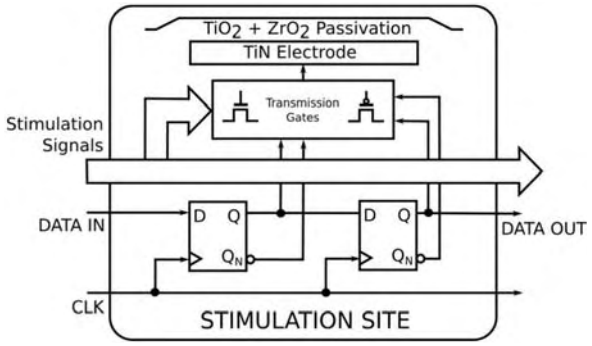

Figure 4: Stimulation circuitry block diagram.

each stimulation site, cf. Fig. 4) is serially transmitted to the chip and stored in a related shift register which meanders through the entire array. For each stimulation site a simple decoder circuit controls switches operated as 1-to-4 multiplexer. In the transistor level realization, the decoding functionality is directly realized by the transmission gate arrangement used as switches. The stimulation circuitry can handle signals with 3.3 V peak-to-peak amplitude.

The basic recording technique is schematically sketched in Fig. 5. The recording electrodes are directly capacitively coupled to one recording transistor per site and sense the local variation of the electric potential in the electrolyte near the electrode. The induced voltage variation on the gate of sensor transistors causes a variation in their drain-to-source current similar as in [1, 5].

Every 200 ns a column of 65 transistors, which share a common source connected to the column line, is activated by lowering the column voltage by the column select circuit. Every transistor of the array has its drain terminal connected to a corresponding row line, so that the 65 drain currents of the active column are fed out separately to the off-chip acquisition unit. Transistors of non-active columns do not conduct any current so that they do not contribute to the current of the row lines. The acquisition unit converts the current signals into voltage signals, removes transistor operating-point related offsets, digitizes and eventually transmits the data to the PC.

The gates of the recording transistors are biased (not shown in the figure for simplicity) with the biasing branch being in a high-ohmic state during regular recording operation. For this reason a second device operated as switch is implemented within each sensing site. After having assigned a voltage to all gates of the recording devices by closing these switches, they are opened and the recording gate nodes become sensitive to potential changes in the electrolyte. The opened switches formally modify the transfer function of the recording sites into a high-pass filter function. However, the time constant is far below the minimum frequency of all signals of interest.

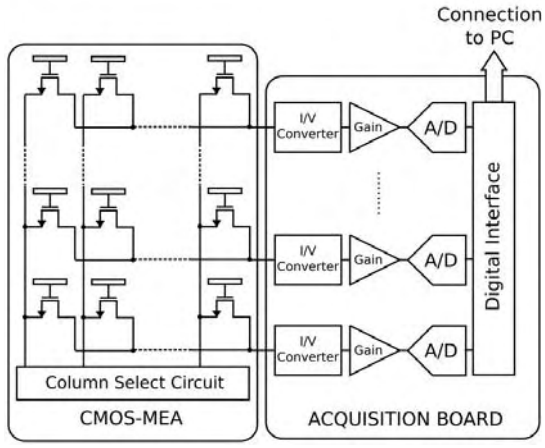

Figure 5: Simplified schematic of the recording concept

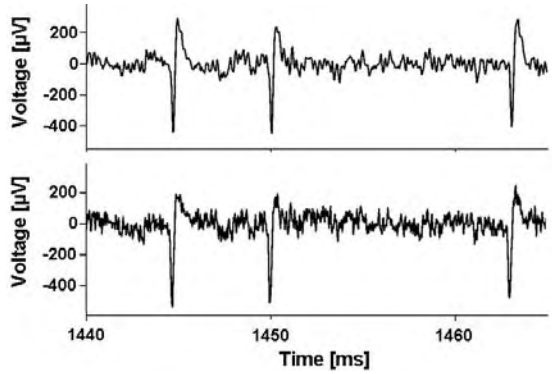

Figure 6: Spontaneous activity of a guinea pig. Results depicted with and without digital low-pass filtering.

The maximum acquisition full frame rate of 77 kHz allows consideration of frequency components above 30 kHz. Of course, the operating frequency can also be scaled down resulting in a reduced noise floor. Imaging of only a portion of the entire array allows for further SNR improvement.

Last but not least it should be mentioned that the system also provides the possibility to calibrate each one of the 4225 sensor sites.

4 Measured Results

Fig. 6 shows exemplary measurements of spontaneous activity of a guinea pig retina measured by a chip with and without digital post processing (low-pass filtering): a signal-to-noise ratio of approximately 10 V/V is obtained.

Further exemplary results from guinea pig retina are shown in Fig. 7. There, a chip with 16 µm recording site pitch and 32 µm stimulation site pitch is used. The position of the recording sites depicted in rectangles in the different plots is counted from the left side and from the top of the array. Extracellular voltage traces are plotted for nine neighbouring recording sites. After an electrical stimulus, which is also captured by the sensors and is responsible for the first negative peak visible in every trace, a passive tissue response is recorded on all electrodes. For stimulation three columns of stimulation sites are used at the right border of the chip. Stimulus induced neural activity is detected by the subset of four electrodes underneath a retinal neuron (top-right plots). A blanking circuit, typical solution for commercial available MEAs based on metal electrodes [8], is not needed.

Further details with emphasis on biological aspects are provided elsewhere [9].

5 Summary

In conclusion, a CMOS-based MEA with 4225 capacitively coupled recording sites and 1024 capacitively coupled stimulation sites has been demonstrated. Measurements with biological contents reveal proper functionality.

References

[1] Eversmann, B., Jenkner, M., Hofmann, F., Paulus, C., Brederlow, R., Holzapfl, B., Fromherz, P., Merz, M., Brenner, M., Schreiter, M., Gabl, R., Plehnert, K., Steinhauser, M., Eckstein, G., Schmitt-Landsiedel, D., Thewes, R. (2004): A 128 × 128 CMOS biosensor array for extracellular recording of neural activity. *IEEE Journal of Solid-State Circuits*, Vol. 38, Issue 12, 2306-2317.

[2] Imfeld, K., Neukom, S., Maccione, A., Bornat, Y., Martinoia, S., Farine, P.-A., Koudelka-Hep, M., Berdondini, L. (2008): Large-Scale, High-Resolution Data Acquisition System for Extracellular Recording of Electrophysiological Activity. *IEEE Transactions on Biomedical Engineering*, Vol. 55, Issue 8, 2064–2073.

[3] Frey, U., Sedivy, J., Heer, F., Pedron, R., Ballini, M., Mueller, J., Bakkum, D., Hafizovic, S., Faraci, F.D., Greve, F., Kirstein, K.-U., Hierlemann, A. (2010): Switch-Matrix-Based High-Density Microelectrode Array in CMOS Technology. *IEEE Journal of Solid-State Circuits*, Vol. 45, Issue 2, 467-482.

[4] Huys, R., Braeken, D., Wouters, J., Loo, J., Severi, S., Vleugels, F., Bartic, C., Borghs, G., Eberle, W. (2010): A novel 16k micro-nail CMOS-chip for in-vitro single-cell recording, stimulation and impedance measurements. *IEEE Engineering in Medicine and Biology Society*, 2726-2729.

[5] Eversmann, B., Lambacher, A., Gerling, T., Kunze, A., Fromherz, P., Thewes, R. (2011): A neural tissue interfacing chip for in-vitro applications with 32k recording / stimulation channels on an active area of 2.6 mm^2. *Proc. European Solid-State Circuits Conference (ESSCIRC)*, 211-214.

[6] Ballini, M., Muller, J., Livi, P., Chen, Y., Frey, U., Shadmani, A., Jones, I.L., Gong, W., Fiscella, M., Radivojevic, M., Bakkum, D., Stettler, A., Heer, F., Hierlemann, A. (2013): A 1024-channel CMOS microelectrode-array system with 26'400 electrodes for recording and stimulation of electro-active cells in-vitro. *Proc. Symposium on VLSI Circuits*, C54-C55.

[7] Wallrap, F. and Fromherz, P. (2006): TiO2 and HfO2 in electrolyte-oxide-silicon configuration for applications in bioelectronics. *Journal of Applied Physics*, 99, 114103.

[8] Taketani, M., Baudry, M. (2006): Advances in Network Electrophysiology. Using Multi-Electrode Arrays. *Springer*.

[9] Velychko, D., Eickenscheidt, M., Thewes, R., Zeck, G. (2014): Simultaneous Stimulation and Recording of Retinal Action Potentials Using Capacitively Coupled High-Density CMOS-based MEAs. *Proc. 9th Int. Meeting on Substrate-Integrated Microelectrodes*

.

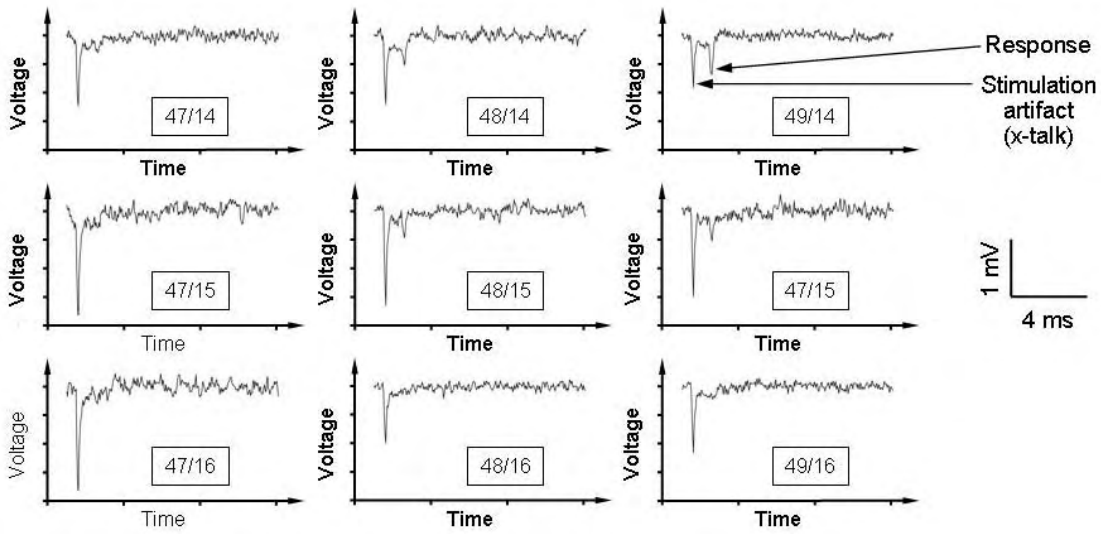

Figure 7: Neural activity measured from a guinea pig retina at nine adjacent positions. Chip with 16 µm recording site pitch and 32 µm stimulation site pitch. The position of the recording sites depicted in rectangles in the different plots is counted from the left side and from the top. The activity is triggered by electrical stimulation using 3 columns of stimulation sites at the right border of the chip. A sawtooth pulse with 1 V amplitude, 500 ms rising edge, and 100 µs falling edge is used. Stimulus induced neural activity is visible in the top-right pixels.

Acknowledgement

Support and funding of this project by the German Ministry of Education and Research, Projektträger Jülich and Projektträger VDI is gratefully acknowledged (references 0315636A and 1312038).

Electronic Motion Tracking of Single Migrating T Cells Using Field-Effect Transistor Arrays

Jessica Ka-Yan Law[1]*, Xuan-Thang Vu[1], Xiao Zhou[2], Saya Ri Heidingsfelder[1], Bin Qu[2], Markus Hoth[2], Sven Ingebrandt[1]

1 Department of Informatics & Microsystem Technology, University of Applied Sciences Kaiserslautern, Zweibrücken, Germany
2 Department of Biophysics, Saarland University, Homburg, Germany
* Corresponding author: jessica.law@fh-kl.de

Abstract
Motion tracking of migrating cell is usually performed with the help of high-end microscopy. In the present study, we propose an alternative, label-free, electronic platform to detect the migration of individual cells. Field-effect transistor arrays with flat topography and the transistor size compared to a single cell were fabricated. By monitoring the impedimetric changes of the transistor input, we can identify the migration of the cells electronically.

1 Introduction

Cytotoxic T cells play an important role in the immune system by migrating throughout the whole body, recognising, and then eliminating specific pathogens [1]. In order to monitor the migration process, real-time motion tracking with microscopic imaging has been used to analyse the cell movement over time. Traditionally, cells need to be labelled for automatic cell tracking. However, the staining can be invasive and causing cell death. Label-free cell tracking is possible but involves tedious single cell identification under conventional phase contrast microscope [2]. We aim to provide an innovative and non-invasive way to study T cell migration by means of electronic signals.

In the present study, the migration of single T cells on field-effect transistor (FET) arrays was measured using impedance spectroscopy. Non-invasive and real-time motion tracking of a single migrating T cell can be reflected by the changes of transistor-transfer function (TTF).

2 Methods

2.1 Cell culture protocol

Peripheral blood mononuclear lymphocytes (PBML) were isolated and purified from human donor blood samples. In the present study, $CD8^+$ T cells were negatively isolated with CD3/CD28 bead activators. PBML were cultured in a mixture of CD3/CD8 bead activators for 3 days. $CD3^+$ and $CD28^+$ T cells with the beads were removed by a magnet on day 3. The remaining $CD8^+$ T cells were then re-suspended in complete medium (AIMV medium supplemented with 10 % FCS and 100U/ml IL-2).

2.2 Sensor devices

P-type open-gate FETs were fabricated in the cleanroom at the University of Applied Sciences Kaiserslautern, Zweibrücken. 12 transistor gates (width 12 µm and length 5 µm) were fabricated at the centre of a 5×5 mm^2 silicon substrate. FET sensors were fabricated having almost flat topography except for transistor gate openings according to the fabrication protocol shown in figure 1 [3].

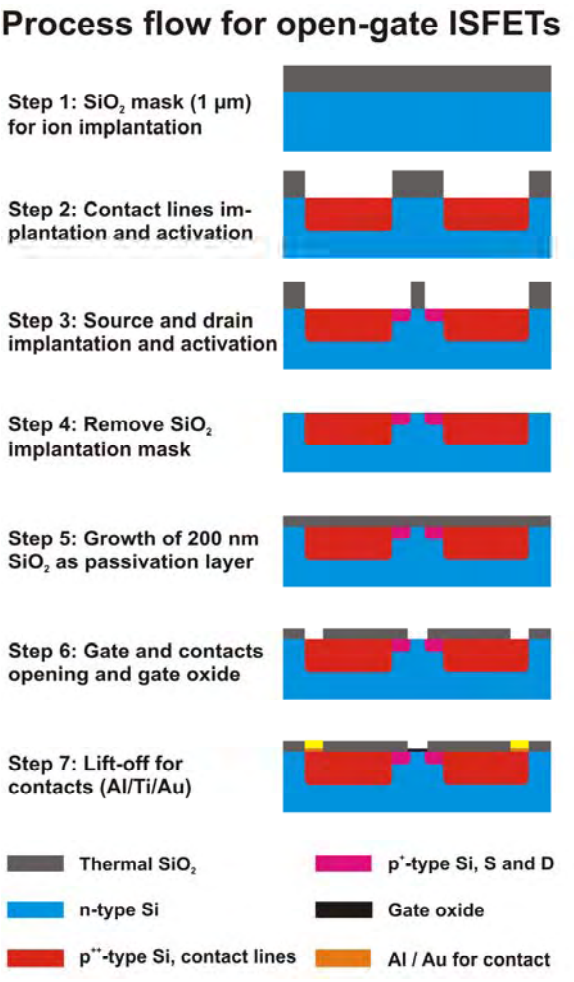

Fig. 2. The fabrication process flow of the quasi-planar FETs for cell migration measurements [3].

The FETs were encapsulated with a biocompatible polymer and a glass ring forming a cell culture chamber for impedance experiments.

2.3 Experiments

Impedimetric changes of the fibronectin-coated (0.1 mg/ml) transistors caused by the T cells were measured by a portable 16 channel amplifier system. Two measurement modes were used: (a) range of frequencies (1 kHz to 1 MHz) and (b) a fixed frequency (300 kHz) were applied to the FETs and the transfer functions were measured. Static adhesion of T cells on the transistor gates was measured primarily for identifying the optimum frequency, which will later be used for the real-time measurement (Fig. 2). Transfer functions of the transistors were measured as a value indicating the impedance changes in response to the appearance of the cells. Out of these spectra, we can extract cell-related parameters like seal resistance (R_{seal}) of the cell membrane with the transistor and the cell membrane capacitance (C_m) [4].

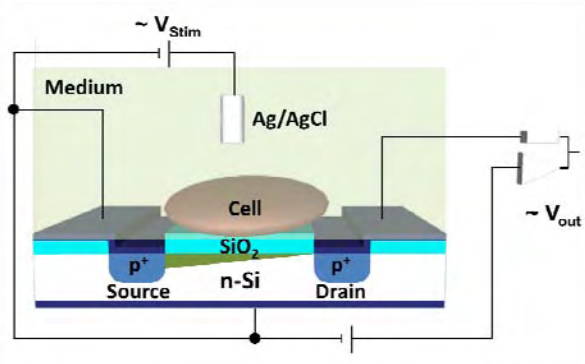

Fig. 2. Schematic of a cell covered field-effect transistor to explain the configuration for transistor transfer-function measurements [6].

In order to restrict the movement of the migrating T cells, the adhesion area on the FET surface was controlled by aligned micro-contact printing [5]. In the present study, we used this micro-contact printing (µCP) technique in small dimensions. We designed a silicon mask with a pattern of 15 µm wide lines with 50 µm gaps in between and used it as a mold to produce PDMS stamps of this pattern. The PDMS stamp was firstly pre-incubated with 0.1 mg/ml fibronectin. Afterwards, the stamp was aligned on top of the FET device using reflection microscopy. The 15 µm wide lines were aligned on top of the transistors. Then the PDMS stamp was pressed against the FET device and allowed the fibronectin molecules to be transferred from the stamp to the FET surface. Afterwards, the uncovered areas of the FET surface were blocked by poly-L-lysine-g-poly(ethylene glycol) (PLL-g-PEG). The polycationic backbone absorbs electrostatically on the uncovered area, rendering repulsive surfaces which are resistant to protein and cell adsorption.

3 Results

In order to study the locomotion of a single migrating T cell, 4×4 arrays of transistors (width: 12 µm; length 5 µm) with flat topography were fabricated. The size of a transistor gate area of our devices is in comparison to the size of an attached single T cell (Fig. 3). The new design minimise the height of the edges between the contact lines and the surfaces, which allows the T cells to migrate almost unaffected by topographical obstacles. With the fibronectin lines, however, we restricted the migration by chemical guiding cues.

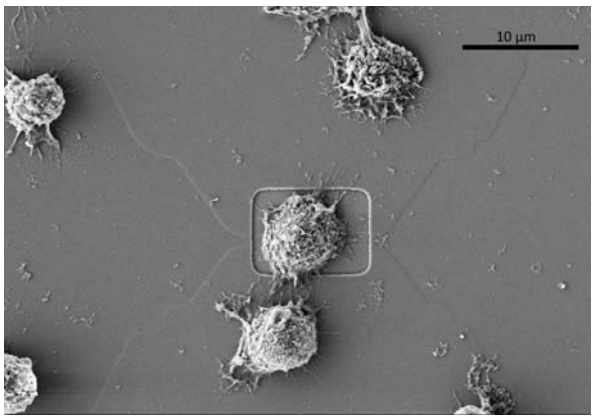

Fig. 3. A cytotoxic T cell adheres on top of a field-effect transistor gate with a dimension of 12×5 µm^2.

At first we performed static adhesion measurements recording full TTF spectra in order to study the sensitivity of the FET devices and the cell-related parameters of the T cells. A comparison was made in between cell-free transistors and cell-attached transistors. Significant differences in TTF spectra were observed between 100 kHz and 500 kHz (Fig. 4). The result is in line with our previously published data, where we used similar FET devices having a slightly different topography [3].

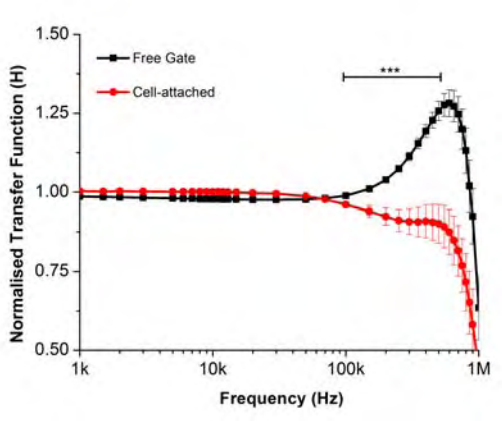

Fig. 4. Significant TTF differences between free transistors and cell-attached transistors can be detected at the frequencies ranging from 100 kHz to 500 kHz (***p < 0.001).

In order to capture individual dynamic motion of the T cells, time-dependent measurements of a transistor gate with freely-migrating T cell on top were

measured as previously described [3, 6, 7]. A fixed frequency of 300 kHz was chosen since the TTF values between cell-covered and cell-free transistor had the most significance differences there (Fig. 4).

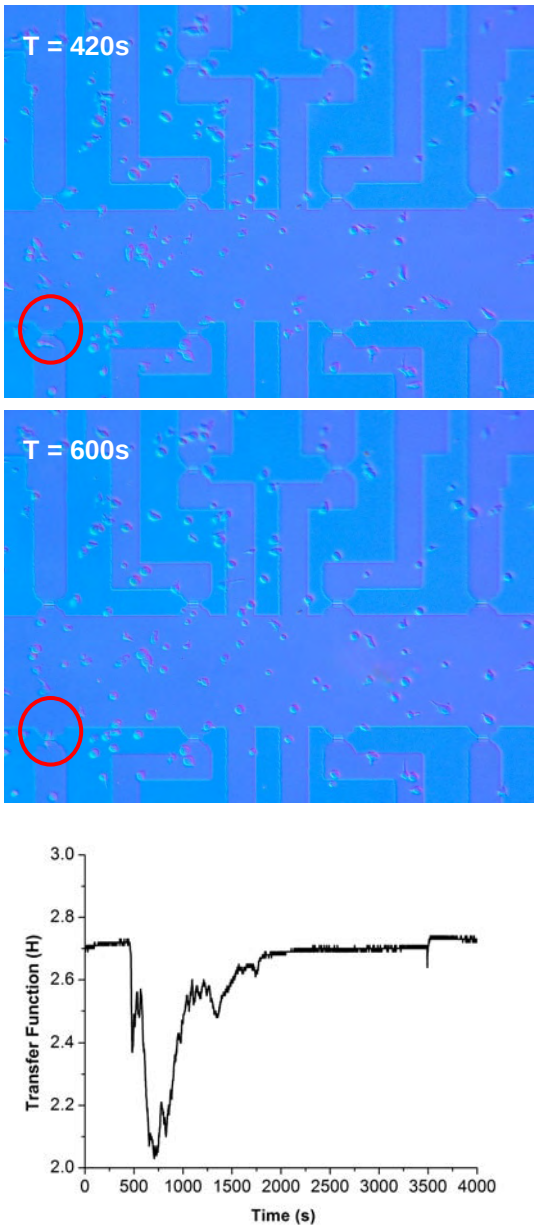

Fig. 5. Transistor-transfer function changes when a migrating T cell adheres on top of a transistor gate. When the transistor is free, the transfer function remains constant. However, when the cell starts migrating towards the transistor, changes in TTF can be observed. The interferences observed during the process are mainly due to the micro-motion of cell membrane on top of the transistor during the migration.

In first experiments we used a high density culture of T cells and allowed the cells to migrate freely over the surface of the sensor chip. Since the current chip design only hold 16 transistors with spacing of 200 µm, just a few events can be recorded out of one culture. When a T cell was migrating on top of a transistor gate partially or completely covering it, the amplitude of the signal was changing accordingly (Fig. 5).

Since T cells preferably migrate on fibronectin-coated surface only, we limited in the next experiments the movement of the T cells by aligned µCP. We aligned the fibronectin lines on the FET device surface along the transistors. Migration of the T cells was clearly observed along these fibronectin lines (Fig. 6) instead of the random migration in the previous experiments. However, the distance in between the transistors is still too far in the current design. The T cells were not able to migrate from one transistor to another within our measurement time.

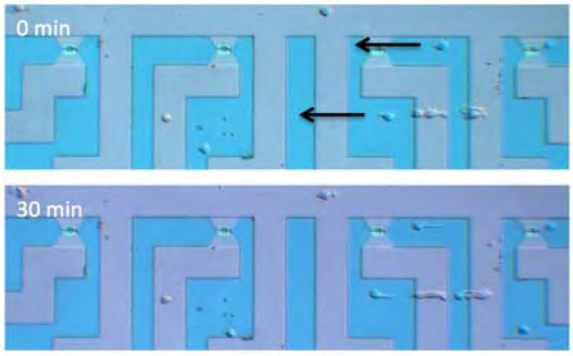

Fig. 6. Two time points of the migration assay on fibronectin lines: 0 min (beginning) and 30 min (end) are shown. Arrows correlate with the printed fibronectin lines and indicate the direction of cell movement during the migration assay.

4 Conclusions and Outlook

In the present study, we were able to detect single cell movements using our field-effect transistor arrays. Due to the flat topography of the devices, cells can move freely on the sensor surface without topographic obstacles. In addition, aligned micro-contact printing can be easily applied on our devices using a home-made alignment setup. Our measurement technique can be used down to single cell resolution, which is important for studies of individual cell responses rather than a collective response from a population of cells. Compared to the common migration assays using optical microscopy, this label-free platform offers a simple and low-cost alternative for tracking single cell migration. However, in its current design the sensor devices contain not enough sensor spots to follow the cells electronically. In future we aim to a higher integration of sensors in order to realize a novel electronic platform for motion tracking in parallel to adhesion strength sensing using our method.

Acknowledgements

This work was supported by the Federal Ministry of Education and Research in Germany under projects 17008X10 and 17042X11. The authors thank Mr. Rainer Lilischkis (University of Applied Sciences Kaiserslautern) for his support with SEM imaging.

References

[1] Huppa, J. B. and Davis, M. M. (2003). T-cell-antigen recognition and the immunological synapse. *Nature Reviews Immunology, 3, 973-983.*

[2] J. B. Beltman, A. F. M. Marée, and R. J. de Boer (2009): Analysing immune cell migration. *Nature Reviews Immunology, 9, 789-798.*

[3] A. Susloparova, X. T. Vu, D. Koppenhöfer, J. K. Y. Law, S. Ingebrandt (2014): Investigation of ISFET device parameters to optimize for impedimetric sensing of cellular adhesion. *physica status solidi (a), 1–9 / DOI 10.1002/pssa.201330636.*

[4] A. Susloparova, D. Koppenhöfer, J.K.Y. Law, X.T. Vu, S. Ingebrandt (2014): Electrical cell-substrate impedance sensing with field-effect transistors is able to unravel cellular adhesion and detachment processes on a single cell level. *Submitted*

[5] L. Lauer, S. Ingebrandt, M. Scholl, A. Offenhäusser (2001): Aligned microcontact printing of biomolecules on microelectronic device surfaces. *IEEE Transactions on Biomedical Engineering*, 48, 838-842.

[6] D. Koppenhöfer, A. Susloparova, D. Docter, R.H. Stauber, S. Ingebrandt (2013): Monitoring nanoparticle induced cell death in H441 cells using field-effect transistors. *Biosensors and Bioelectronics, 40, 89-95.*

[7] S. Schäfer, S. Eick, B. Hofmann, T. Dufaux, R. Stockmann, G. Wrobel, A. Offenhäusser, S. Ingebrandt (2009): Time-dependent observation of individual cellular binding events to field-effect transistors, *Biosensors and Bioelectronics, 24, 1201-1208.*

Nano-Needle Gated Field Effect Transistor (NGFET) Array for Intracellular Recording and Stimulation of Neurons

Rao Rashmi B.[1*], Singh Katyayani[1], Sikdar Sujit K.[2] and Bhat Navakanta[3]

1 Centre for Nano Science and Engineering
2 Molecular Biophysics Unit
3 Centre for Nano Science and Engineering & Electrical Communication Engineering, Indian Institute of Science, Bangalore, INDIA-560012
* Corresponding author. E-mail address: rashmi@cense.iisc.ernet.in

Abstract
The endeavour to understand the neural articulation in a network has given rise to a vast paradigm of micro- and nano-engineered electrode arrays. Due to the intrinsic impedance associated with such miniaturized electrodes, which decreases the SNR, researchers have started to explore the possibility of using impedance – independent Field Effect Transistors (FETs) for cellular recording. In this study, we report the fabrication of nano-needle gated FETs (NGFETs), which can be used for intracellular neuronal recording using a top-down approach. Dissociated hippocampal culture was grown on the NGFET devices to verify the biocompatibility and mechanical stability of the nano-needles.

1 Introduction

A major part of neuro-electronics based research today, focuses on micro/nano semiconductor- and polymer- devices for stimulating/recording neuronal networks. Other than the patch clamping technique, which was invented almost 40 years ago, by Sakmann & Neher [1,2], very few alternative techniques have been reported for recording intracellular potentials, of such electrically active cells. On the other hand, planar micro-electrode arrays (MEAs) are widely used for recording extracellular field potential of neural networks. Electrophysiologists prefer that the interface between such electrodes/pipettes and the cell is small, in order to improve the spatio - temporal resolution, and, minimize cell invasiveness. However, this tends to increase the impedance during signal recording. Modifications in the MEA technology, including, gold- mushroom shaped micro- electrodes[3,4], localized electroporation[4,5], vertical nano-wire[6] and nano-pillar[7] electrode arrays which have been used to obtain transient / continuous, long –term intracellular recording do not provide a significant improvement in the SNR, owing to their intrinsically high impedance. Alternatively, impedance independent Field-Effect-Transistors (FETs) have been reported to give good SNR, despite their reduced size[4, 8, 9].

Recently, Duan *et.al*[10] have reported the fabrication of a bottom-up technique to grow branched, nano-wire FETs for intracellular recording in cardiomycetes, wherein, a phospo-lipid coated nano-tube was selectively integrated atop the channel of a Si-Nanowire-FET. The nano-tube lures the cytoplasmic contents into it, which gates the FET channel. Therefore, any change in the trans-membrane voltage of the cell varies the conductance of the FET. The same device structure could be used to study the cross-talk of neurons in a network. However, for multi-site recordings (from hundreds of neurons), with a single neuron resolution, it is inapt to use randomly oriented nano-wire devices grown using bottom up – technique. Here, we report the fabrication of NGFET array using standard lithography-top down approach, by decorating nano-needles on top of FET channel, to have a better control over spatial resolution and study neuronal network properties.

2 Methods

2.1 Device fabrication:

Si - FET array was patterned in the device layer (200 nm) of a p- type SOI wafer, having buried oxide thickness of 1 µm. The FET area was defined by E-beam lithography (EBL), followed by Si – reactive ion etching (RIE) in a plasma of SF_6 (20 sccm) and C_4F_8 (30 sccm) at 6 mTorr, with RF and ICP power of 30 W and 1200 W respectively. The source/drain-contacts were formed by the lift – off technique, after EBL and metal deposition by sputtering Ti/Au (10/70 nm). The metal tracks were passivated with SiO_2 (500 nm) deposited by Plasma-enhanced chemical vapour deposition (PECVD) using SiH_4 (8.5 sccm), N_2O (710 sccm), N_2 (161 sccm) at 350 °C, 10 W and 1000mT pressure. The oxide at the FET gate region, (Fig 1, e) (i.e. the site of nano-tube integration), was selectively etched in BHF after EBL patterning.

The nano-needle was patterned atop the FET-channel according to the process described in Fig 1 and Fig 2. A resist stack of PMMA -950-C6 and HSQ was spin coated on the FET patterned wafer. Nano-

circles were patterned on the HSQ layer by EBL and developed in 0.26 N TMAH solution.

The needles were formed by ashing the PMMA resist using HSQ as a mask, in oxygen plasma (O_2 flow-rate -10 sccm, RF power – 50W, ICP power – 300W at 10 mTorr), followed by the conformal deposition of a thin film (100nm) of SiO_2 by PECVD as described above, at 140 ^{0}C. The needle tips, containing the HSQ mask and SiO_2 film, was then selectively etched by directional RIE, similar to the spacer etch technique, in a plasma of O_2 (4 sccm) and C_4F_8 (50 sccm) with RF power - 50W, ICP power - 1500W at 10 mTorr. Finally, the PMMA sacrificial layer was removed by dipping the chip in acetone for 15 mins.

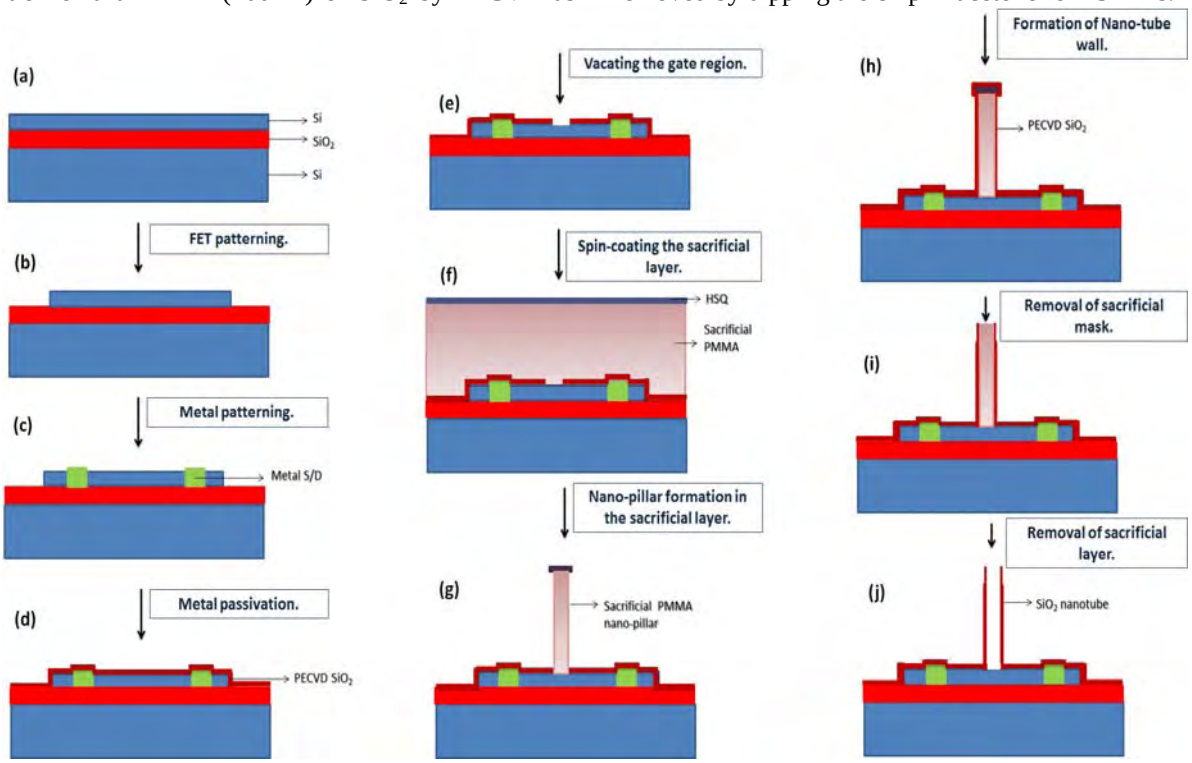

Fig 1 : Fabrication of NGFETs : (a) SOI wafer with device layer 200 nm. (b) Si etching to form the FET base. (c) Patterning of metal S/D and contacts by lift off after sputtering Ti/Au. (d) Passivating metal lines by deposition of PECVD SiO_2 (500 nm). (e) Removal of SiO_2 in the gate region using EBL patterning, followed by SiO_2 etching in BHF. (f) Spin-coating the sacrificial layer stack of PMMA-950-C6 and HSQ. (g) Formation of nano-pillar by ashing PMMA in oxygen plasma. (h) Forming the nano-tube walls by depositing PECVD SiO_2 (100 nm) at 140 °C. (i) Removal of sacrificial mask, now containing SiO_2 and HSQ, by RIE. (j) Removal of sacrificial PMMA layer by acetone dip.

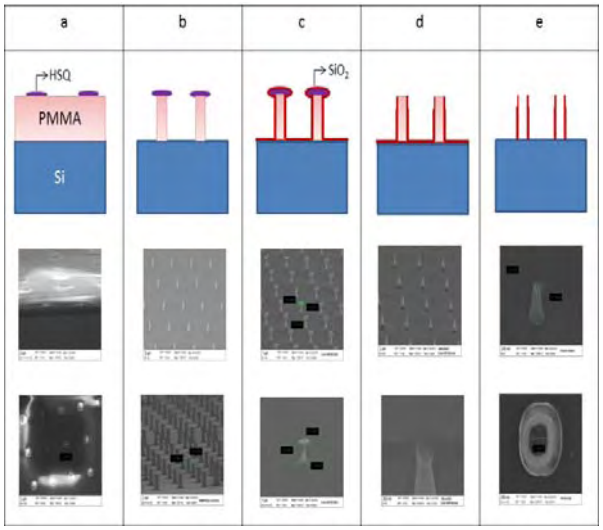

Fig 2: Fabrication of Nano-needles : (a) Patterning of HSQ on PMMA. (b) Ashing of PMMA using O2. (c) PECVD deposition of SiO2. (d) Removal of SiO2 + HSQ by RIE. (e) Removal of PMMA by acetone

2.2 Sample preparation before culturing:

The NGFET chips were exposed to oxygen plasma for one minute followed by incubation in 70% ethanol for 20 mins and washing with sterile Milli-Q water for 3-4 times. The samples were then air dried UV treated for 20 mins. Then, 10µg/ml PEI in borate buffer was added on the chip and incubated for one hour , followed by washing, drying and UV treatment as above. Prior to culturing, the chips were incubated with 1 mg/ml laminin diluted in 1 ml of culture medium, for 20 mins, and washed with media, 3-4 times. The culture medium used was Dulbecco's modified Eagle's medium F12 HAM supplemented with N1, FBS (10%) and antibiotic antimycotic (1%).

2.3 Neuronal Culture:

Primary rat hippocampal neuronal culture was prepared as described previously[11,12]. Hippocampi dissected from male/female Wistar rats (P_0-P_2) were dissociated in papain (20 U/ml at 37 °C), followed by gentle trituration. The dissociated cells were plated onto the PEI + laminin coated NGFET chip for 45 mins. The cells were further replenished by flooding 1

ml media and incubated. The neurons were fed twice a week. To prevent glial cell overgrowth, 20 µM cytosine-b-D- arabinofuranoside was included in the medium after 3-4 days. Experiments were performed with the approval of the Indian Institute of Science Ethical Committee, according to CPSCEA guidelines, India. Animals (Wistar rats) were bred and maintained in the Central Animal Facility of IISc.

3 Results and Discussion

To have a better control over simulataneous, multiplexed recordings in a neuronal network, we have adopted a top-down approach to create the NGFET array as shown in Fig 1. The crucial step in the process is the alignment of the nano-needles atop the FET channel. Use of a thick sacrificial film in a top-down process reduces the alignment accuracy during the EBL overlay. Therefore, the success of the process depends on the crafty selection of the sacrificial layer for nano-needle formation. Here, in our process, we used a sacrificial resist stack of PMMA- 950-C6 and HSQ, from which we fabricated hollow nano-needles with tip – ID ~ 400 nm and length ~ 1.5 µm. Fig 3 shows SEM micrograph of a single NGFET. The top – view of the image clearly indicates that the nano-needles are hollow. The ID of the nano- needles can be decreased by reducing the size of the nano-dots patterned on the HSQ layer during EBL.

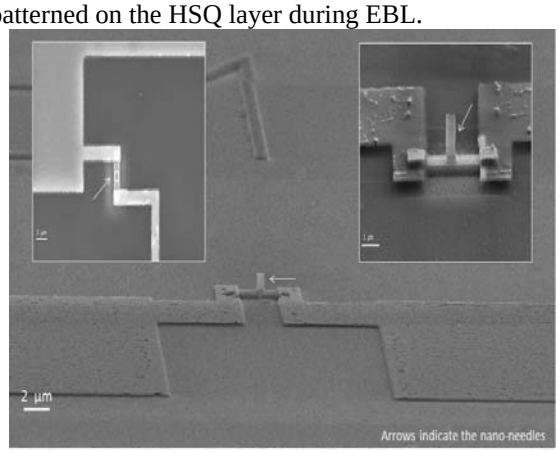

Fig. 3: SEM micrograph showing the top- view and cross -sectional view of a single NGFET.

To obtain simultaneous recording from multiple neurons, the inter-connects were patterned to suit the foot-print of the Multi-channel systems® - MEA recording setup. The final device layout, integrating over 100 NGFET `devices is shown in Fig.- 4.

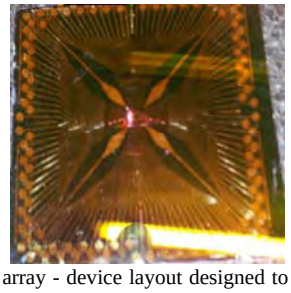

Fig. 4: NGFET array - device layout designed to suit the footprint of MEA recording system.

Dissociated hippocampal neurons were cultured on the NGFETs to check for the bio-compatibility of the devices. On comparision of DIC microscopic images of the hippocampal neuronal culture grown on a control SOI wafer (Fig. 5a, without any nano-needles, processed under similar conditions as the NGFETs) and a NGFET chip (Fig. 5b), it was seen that that the presence of nano-needles did not dramatically vary the cell density.

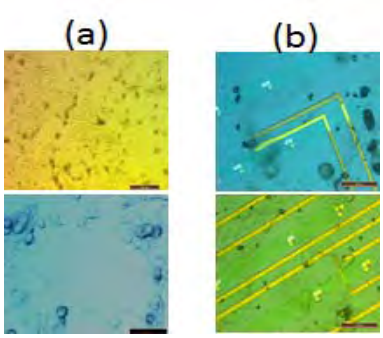

Fig. 5: DIC images of dissociated, 10 day- old , hippocampal cultures grown on (a) SOI wafer(control) and (b) NGFET chip.

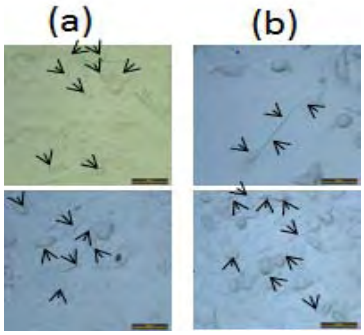

Fig. 6: DIC images of dissociated hippocampal culture (8 day old) grown on nano-needles with tip inner diameters (a) 700 nm and (b) 300 nm. Arrows indicate contacts between neurons and nano-needles.

To further check for the effect of their presence, cultures were grown on nano-needles with different diameters (<1 µm). Fig. 6 shows neurons on top of nano-needles with two different dimensions. It was seen that the nano-needles are not deleterious to the network formation, and , also makes contact with the cells.

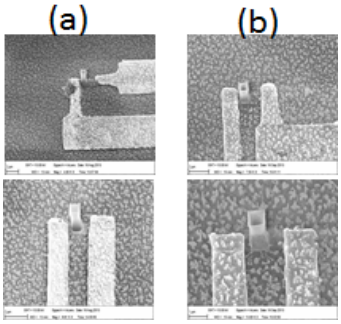

Fig. 7: SEM micrograph of NGFET after (a) first and (b) second culture on same device, indicating the mechanical stability of the devices

To check if the NGFETs can withstand the harsh culture conditions and the cleaning steps before re-use, SEM imaging was done after each culture. Fig. 7 shows that the NGFET devices are robust, based on the fact that the devices were intact after multiple neuronal cultures on the same chip.

4 Conclusion

Till now, we have been successful in device fabrication, and, establishing the bio-compatibility and robustness of the NGFET devices. Further experiments will focus on the electrical characterization of the NGFETs and recording from dissociated neuronal cultures.

Acknowledgement

This work was carried out at the National Nano Fabrication Centre and the Neuro-electronics Lab at CeNSE, IISc, Bangalore, funded by MCIT and DST, Govt. of India.

References

[1] Sakmann B. & Neher E. (1984). Patch clamp techniques for studying ionic channels in excitable membranes. *Annu. Rev. Physiol*., 46, 455–472.

[2] Zhao Y., Inayat S., Dikin D.A., Singer J.H., Ruoff R.S, Troy J.B., (2009). *Proc. IMechE: J. Nanoengineering and Nanosystems*, 222.

[3] Hai A. and Spira. (2012). On-chip electroporation, membrane repair dynamics and transient in-cell recordings by arrays of gold mushroom-shaped microelectrodes. *Lab Chip.*, 12, 2865–2873.

[4] Fendyur A. and Spira. (2012). Toward on-chip, in-cell recordings from cultured cardiomyocytes by arrays of gold mushroom-shaped microelectrode. *Frontiers in Neuroengineering*, 5,21, 1-10.

[5] Robinson J.T., Jorgolli M., Shaek A.K., Yoon M.H., Gertner R.S., Park H. (2012).Vertical nanowire electrode arrays as a scalable platform for intracellular interfacing to neuronal circuits. *Nat. Nanotechnol.* 7, 180–184.

[6] Xie,C., Lin,Z., Hanson,L., Cui,Y., Cui,B. (2012). Intracellular recording of action potentials by nanopillar electroporation. *Nat. Nanotechnol.*, 7, 185–190.

[7] Tian B., Cohen-Karni T., Qing Q., Duan X., Xie P., Lieber C. M. (2010). Three-dimensional,flexible nanoscale field-effect transistors as localized bioprobes. *Science*, 329, 830–834.

[8] Patolsky F., Timko B.P., Yu G., Fang Y., Greytak A.B., Zheng G., Lieber C.M. (2006). Detection, Stimulation, and Inhibition of Neuronal Signals with High-Density Nanowire Transistor Arrays, *Science*, 313, 1100-1104.

[9] Fu T.M., Duan X., Jiang Z., Dai X., Xie P., Cheng Z., Lieber C.M. (2014). Sub-10-nm intracellular bioelectronic probes from nanowire–nanotube heterostructures. *PNAS*, 111,4, 1259-1264.

[10] Duan X., Gao R., Xie P., Cohen- Karni T., Qing Q., Choe H.S., Tian B., Jiang X., Lieber C. M. (2012). Intracellular recordings of action potentials by an extracellular nanoscale field-effect transistor. *Nat. Nanotechnol.*, 7, 174–179.

[11] Potter S.M. and DeMarse T.B. (2001). A new approach to neural cell culture for long-term studies. *J. Neurosci. Meth.*, 110, 17–24.

[12] Rao S.P. and Sikdar S.K. (2004). Estradiol-induced changes in the activity of hippocampal neurons in network culture are suppressed by co-incubation with gabapentin. *Brain Res*., 1022, 126–136.

Two-Chamber MEA to Unidirectionally Connect Neuronal Cultures

Joost le Feber[1,2*], Wybren Postma[1], Wim Rutten[3], Eddy de Weerd[3], and Marcel Weusthof[1]

1 Biomedical Signals and Systems, University of Twente, Enschede, the Netherlands
2 Clinical Neurophysiology, University of Twente, Enschede, the Netherlands
3 Neural Engineering Dept./Biomedical Signals and Systems, University of Twente, Enschede , the Netherlands
4 BIOs-Lab on a Chip Group, University of Twente, Enschede, the Netherlands
* Corresponding/ presenting author. E-mail address: j.lefeber@utwente.nl

Abstract
We designed a two chamber MEA aiming to create a unidirectional connection between the networks in both chambers (source and target). To achieve this unidirectionality, all interconnecting channels contained barbs that hindered axon growth in the opposite direction (from target to source). Visual inspection showed that axons predominantly grew through the channels from source to target. This observation was confirmed by spontaneous activity recordings. Cross-correlation between the signals from two electrodes inside the channels suggested signal propagation at ~2 m/s from source to target. Cross-correlation between the firing patterns in both chambers indicated that most correlated activity was initiated in the source chamber, which was also reflected in a significantly lower fraction of partial bursts in the source chamber. Finally, electrical stimulation in the source chamber induced a fast response in the source chamber, and a slower response in the target chamber. Stimulation in the target chamber evoked a fast response in the target chamber, but no response in the source. These results confirm the achievement of a predominantly unidirectional connection from source to target.

1 Introduction

Although many aspects of network functioning of neuronal tissue can be investigated using commercially available MEAs, some applications may require additional structure. Typically, such additional structure involves unidirectional connectivity between two networks, to avoid that the cells in both chambers eventually form one large, oddly shaped network. Pan et al. [1] achieved unidirectional growth by sequential plating; the second culture was plated 10 days later, after axons of the first culture had completely occupied the channels. A possible disadvantage of this method is the limited time window for experiments due to this additional delay. Several studies require mature connectivity (> 3 weeks old [2]), and cultures often start to deteriorate or detach from the glass surface after ~4 weeks. We designed and validated a custom made MEA with two culture chambers (source and target) for simultaneous plating and interconnecting channels designed to support axon growth in one direction only.

2 Methods

2.1 Construction

We designed a glass ground plate to have electrodes in both chambers and in the connecting channels (black dots and vertical lines in Fig1B). Gold electrodes (thickness 400 nm) were deposited on a four inch Pyrex glass wafer, by sputtering on an intermediate titanium layer (sputtered first) that constituted the electrode leads. A 0.5 µm layer of Silicon Nitride was deposited using lowressure chemical vapour deposition (LPCVD) over the Pyrex wafer for electrical insulation. Electrode contact areas were opened by etching through the nitride layer in a reactive ion etch (RIE) step, using CHF_3.

A second layer that contained the structures of the chambers and channels was mounted on the glass. This second layer was constructed in silicon or polydimethylsiloxaan (PDMS). All channels had a 20 (width) x 5 µm (height) cross sectional area, and contained barbs that narrowed the channel width down to ~7 µm, as shown in Fig 1C.

The silicon top layer was constructed using a 500 µm SOI wafer, which contained a buried insulating layer (0.5 µm SiO_2), 50 µm below the surface. This enabled us to etch the entrances of the channels on both sides (5 µm deep), the central part of the channels (50 µm deep), and the bottom of the chambers (50 µm deep) from the shallow side, and to completely open the chambers and the area above the central part of the channels from the other side without destroying the fragile channel structures.

To construct the PDMS layers, we used a silicon mould with the same layout as the silicon top layers. PDMS easily adhered to the glass, for the silicon devices, we used anodic bonding. Therefore, the two contacted wafers were heated to 250–400 °C to mobilize the ions while a voltage of 1000-1500 V was applied.

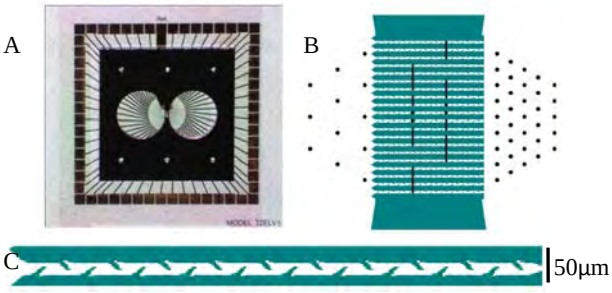

Fig. 1. The silicon-glass device. **A**) shows the complete device, **B**) depicts the layout of electrodes (black) and channels (green). **C**) Close-up of a channel (10 barbs per side, length:800 µm).

2.2 Validation

Visually

We stained axons with cell tracker green (5-Chloromethylfluorescein Diacetate; Invitrogen) and counted the number of barbs (on one side of the channels) that the axons in the channels passed in either direction, at different ages.

Spontaneous activity

Several channels contained two electrodes (see Fig 1). We cross-correlated the signals (expressed as point processes) in those channels where both electrodes picked up activity, to determine the latency with maximum correlation. Because the amplitude of action potentials vastly exceeded the RMS noise level, this latency was largely determined by the timing of action potentials at both electrodes.

Secondly, we cross-correlated the summed activity (predominantly burst envelopes) recorded in both chambers to determine the latency with maximum correlation.

Finally, we calculated the fraction of partial bursts (bursts that occurred only in one of the two chambers) in both chambers. Assuming that bursts may be intrinsic or ignited by a burst in the other chamber, this fraction is inversely related to the probability that a burst is propagated to the other chamber.

Stimulus responses

We electrically stimulated all electrodes, and calculated the mean post-stimulus time histogram (PSTH) in both chambers. To avoid a strong bias by spontaneously occurring bursts, only those responses were taken into account, where the summed PSTH of multiple stimuli at that electrode was larger than all individual PSTHs. This approach ignored outlying PSTHs that possibly resulted from a spontaneous network burst shortly after a stimulus. Average PSTHs were considered to show a significant response if the mean ± SEM did not overlap zero.

3 Results

We plated 20 times on glass-silicon devices (two cultures each), and 20 times on glass-PDMS devices. Remarkably, most cultures on glass-PDMS became active, but none on the glass-silicon devices. Consequently, all results were obtained with the glass-PDMS devices, from cultures being at least 19 days old.

In total we labeled seventeen different cultures with cell tracker green. Until the axons reached the other side of the channel, it was possible to determine the direction of growth. We observed axon growth from source to target chamber passing multiple barbs (see Figure 2), whereas axons growing in the other direction never passed more than two barbs.

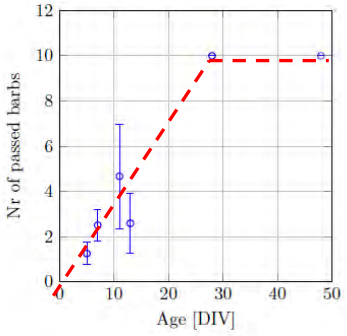

Fig. 2. The number of barbs (on one side) passing in the foreseen direction as a function of age. We never saw axons passing more than two barbs in the opposite direction.

In fourteen channels (six different experiments) we measured action potentials at both electrodes We found peaks in the cross correlation curves at a positive latency in seven channels and at a negative latency in one channel. In the other channels the cross correlation curve did not show a significant peak. Overall mean latency was 0.12 ms, suggesting a propagation speed of 2±1.7m/s from source to target.

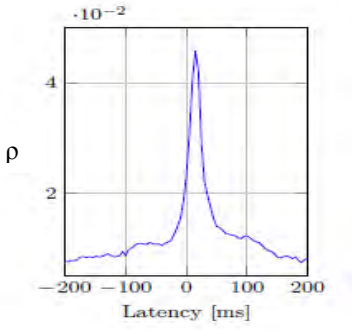

Fig. 3. Example of cross-correlation (ρ) between summed activity in source and target chambers.

In fourteen experiments we recorded spontaneous activity in both chambers. In ten experiments we found a clear peak in the cross-correlation curve between the
activity patterns in both chambers. Maximum cross-correlation was found at a mean latency of 7±19ms,

indicating a tendency that activity in the target was preceded by activity in the source.

In all 14 experiments we calculated the fraction of partial bursts (see methods) in both chambers. In the source chamber the fraction of partial bursts (47±30%) was significantly lower than that in the target chamber (70±16%), t-test: p=0.02.

Finally, we determined the mean PSTH in both chambers after stimulation in either chamber. Stimulation in the source chamber yielded a significant response in that chamber at 0-40ms, and in that target chamber at 40-80ms. Target chamber stimulation induced a significant response in the target chamber at 0-70 ms, and no response in the source chamber (see Fig 4).

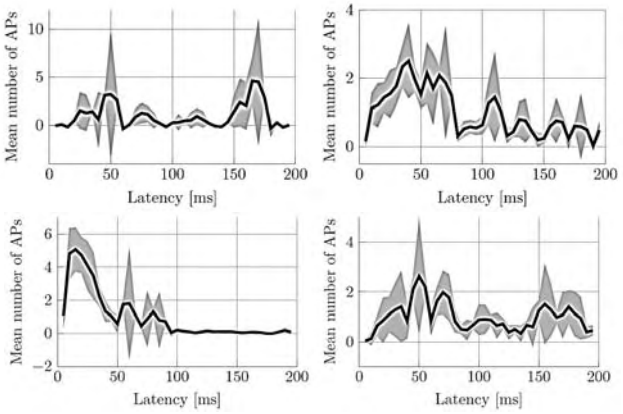

Fig. 4. Average response in source chamber (left column) and target chamber (right column) to electrical stimulation in source chamber (top row), or target chamber (bottom row). Grey zones indicate SEM.

4 Discussion

The activity patterns of cultured dissociated cortical neurons are usually dominated by network bursts. These bursts often hamper plasticity studies, and have been hypothesized to result from the lack of input to the cultures [3]. Electrical [4] or pharmacological stimulation [3,5] have been shown to reduce burstiness, and may facilitate plasticity studies. Here we developed a system where the main culture continuously receives spontaneous or stimulated activity from an auxiliary culture.

We used a newly designed MEA to achieve dual cultures that were coupled in one direction, that is, the culture in the source chamber provided input to the culture in the target chamber, but not vice versa. We validated the unidirectionality of the connections in several ways.

Visual inspection had the possible disadvantage that the direction of growth could no longer be determined after the axon had reached the other side of the channels. However, observations during growth show that axons initially grew through the channels from source to target. It is possible that, once the first axons found their way through the channels, others followed their path, possibly also in the opposite direction. Pan et al used slightly lower tunnels, and claim that growth in the opposite direction was largely impeded because the tunnels were already full [1].

Nine of the twenty channels contained two electrodes (see Fig 1), but it appeared quite difficult to record activity from both electrodes inside a channel. Possibly the design of the electrodes, some of which covered multiple (up to four) channels, introduced too much shunt to ground, if the electrodes were not sufficiently covered by axons in one or more of the channels. Nevertheless, we recorded activity from both electrodes in 14 channels. In 50% of those channels cross-correlation indicated signal propagation from source to target, 43% was indecisive. One experiment (7%) suggested signal propagation in the opposite direction. This experiment was also deviant in the other analyses. Possibly, we erroneously rotated the PDMS top layer 180 degrees in this experiment.

Cross correlation of the summed activity in both chambers included predominantly burst envelopes, and indicated that bursts in the source chamber tended to precede bursts in the target chamber. In theory, it is possible that a burst started in one chamber, and then very rapidly propagated to the other one, even before a clear network burst became visible in the first chamber. Such a scenario might be the major cause of the relatively high standard deviation of the mean latency, and might mask the actual direction of signal propagation. However, it seems very improbable that this happened in the majority of network bursts, and therefore the latency with maximum cross-correlation is presumed to be a good indicator of the direction of signal propagation and therefore of the direction of axon growth.

In general, all results supported the conclusion that the achieved connectivity between the two chambers is predominantly unidirectional.

The advantage of our approach is that we could already start recording from mature cultures after 19 days. However, Fig 2 shows that it took considerably longer than in [1] for the axons to grow completely through the channels, which largely reduced the gained time window for experimenting. Our channels were twice as long as those in [1] and contained 10 barbs per side, which appeared to be far more than necessary to impede axon growth in the opposite direction. Thus, we may further improve the design by shortening the channels to 300-400 μm, containing 3-4 barbs per side. Further improvement may come from the silicon devices, which offer superior visibility inside the channels and additional options for perfusion. Their failure to record activity so far, may be related to problems during the bonding process. In particular we found carbon and oxygen contamination on the electrodes of the glass silicon devices, which may be due to the high temperature during the anodic bonding process.

References

[1] Pan, L., et al., *Propagation of action potential activity in a predefined microtunnel neural network* J Neural Eng, 2011. **8**(4): p. 1-12.
[2] le Feber, J., et al., *Conditional firing probabilities in cultured neuronal networks: a stable underlying structure in widely varying spontaneous activity patterns.* J. Neural Eng., 2007. **4**: p. 54-67.
[3] Le Feber, J., I.I. Stoyanova, and M. Chiappalone, *Connectivity, excitability and activity patterns in neuronal networks.* Phys. Biol., 2014: p. accepted for publication.
[4] Wagenaar, D.A., et al., *Controlling bursting in cortical cultures with closed-loop multi-electrode stimulation.* J Neurosci, 2005. **25**(3): p. 680-8.
[5] Corner, M., *Spontaneous neuronal burst discharges as dependent and independent variables in the maturation of cerebral cortex tissue cultured in vivo: a review of activity-dependent studies in live 'model' systems for the development of intrinsically generated bioelectric slow-wave sleep patterns.* Brain res rev, 2008. **59**: p. 221-244.

MEA Technology

New Materials and Designs

Effect of Ion Sensitivity on Extracellular Recordings with Graphene Transistors

Lucas Hess, Martin Lottner*, Michael Sejer Wismer, Jose A. Garrido

Walter Schottky Institut, Physik-Department, Technische Universität München, Germany
* Corresponding author. E-Mail address: martin.lottner@wsi.tum.de

Abstract
In this contribution, we show that non-saturating behaviour of extracellular recordings with graphene transistors of voltage-clamp stimulated modified HEK-293 cells can be explained using an electrodiffusive point-contact model that includes the ion sensitivity of graphene.

1 Introduction

Graphene solution gated field effect transistors (G-SGFETs) have been shown to exhibit high transconductance and low noise characteristics enabling the measurement of cellular electrical activity [1, 2]. However, the details of electrical coupling between cells and graphene transistors have not been fully understood. For instance, the influence of ion sensitivity of graphene transistors [3] on extracellular recordings has not yet been explored. Previously, the dynamics of ion concentrations in the cell-transistor cleft were discussed for Si transistors using an electrodiffusive point-contact model [4]. In this work we extend this study to the case of G-SGFETs.

2 Materials & Methods

Chips: We used arrays of 64, 10µm x 20µm, G-SGFETs, produced as previously described [1].

Cell measurements: HEK-293 cells, expressing the Shaker B potassium ion channel were cultured as previously described [5] and plated onto coated (Fibronectin, Sigma) transistor chips at 1000cells/mm2, two hours before experiments were performed. Transistor currents were recorded using an in-house built amplification system. A commercial patch clamp amplifier (EPC10, HEKA, Germany) was used.

3 Results & Discussion

Figure 1a shows cell-transistor cleft potential recordings of a voltage-clamped HEK-293 cell on top of a G-SGFET. The cell was depolarized using rectangular voltage pulses with a duration of 10ms and different amplitudes (indicated in the figure). After the characteristic capacitive currents, a gradual increase of the membrane current, due to opening dynamics of the Shaker K_+ channels, can be observed (Fig.1a). Interestingly, while the pipette current saturates after a few milliseconds, the cleft potential does not (Fig.1b), contrary to the expected transistor response considering a standard point-contact model. We have used an extended point-contact model to consider electrodiffusion and the ion sensitivity of our graphene transistors. As shown, such a model is in good agreement with the experimental results (Fig.1c).

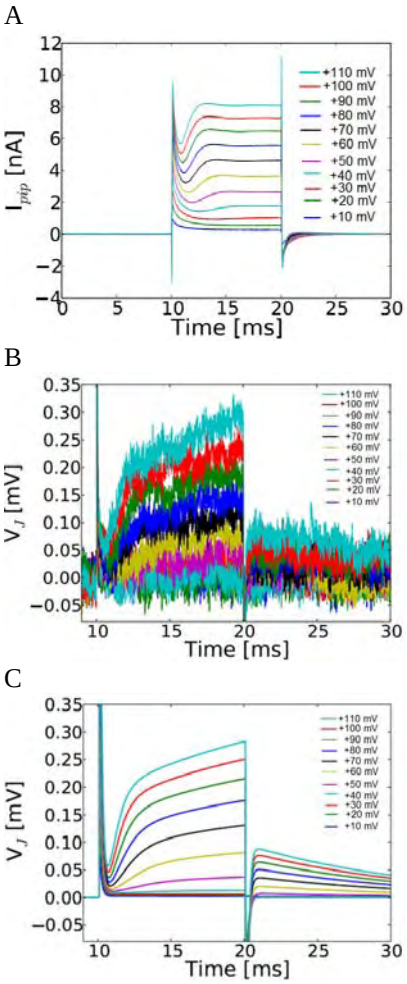

Fig 1: Membrane currents and cell-transistor cleft potential of a HEK-293 cell expressing Shaker B Potassium Channels under stimulation with rectangular voltage-clamp pulses. (a) Voltage-clamp current recording. (b) Corresponding G-SGFET extracellular cleft voltage recordings. (c) Simulated extracellular potential using a modified point-contact model that includes electrodiffusion in the cleft.

4 Conclusion

Consideration of the varying ion concentration in the cell-transistor cleft and the ion sensitivity of graphene transistors can satisfactorily explain the non-saturating behaviour of extracellular recordings of HEK-293 cells with graphene transistors.

References

[1] Hess, L. H., et al. (2011): Graphene Transistor Arrays for Recording Action Potentials from Electrogenic Cells. Advanced Materials, 23, 5045-5049.

[2] Hess, L. H., et al. (2013): Graphene Transistors for Bioelectronics. Proceedings of the Ieee, 101, 1780-1792.

[3] Wangyang, F., et al. (2012): Sensing with liquid-gated graphene field-effect transistors. 1-2.

[4] Brittinger, M. and Fromherz, P. (2005): Field-effect transistor with recombinant potassium channels: fast and slow response by electrical and chemical interactions. Applied Physics A, 81, 439-447.

[5] Becker-Freyseng, C. and Fromherz, P. (2011): Quantised transistor response to ion channels revealed by nonstationary noise analysis. EPL (Europhysics Letters), 96, 38005.

Boron Doped Diamond for Neural Stimulation or Recording

Fabien Sauter-Starace[1],Jean-Louis Divoux[2], Clément Herbert[3], Hugues Girard[3],Christine Mer[3], Philippe Bergonzo[3]

1 CEA LETI CLINATEC, Minatec Campus, 38054 Grenoble France;
2 MXM Group, 2720 Ch. St Bernard 06220 VALLAURIS France;
3 CEA-LIST, Diamond Sensors Laboratory, Gif-sur-Yvette 91191, France

Background/Aims
The number of available materials for electrodes is quite limited for in-vitro and in-vivo recordings. Several problems must be tackled: (a) the biocompatibility of the material itself, (b) the response of the living cells or tissue – glial scar must be avoided, (c) the charge injection and charge density limit.
For point (a) there are numerous normalized controls to assess the biocompatibility the ISO10993. The main drawback of these tests would be the similitude with a real living tissue with the mechanical constraints of a real implant. For point (b), either for recording where the signal to noise ratio is very important to discriminate signal of single or multiunit activity or for stimulation where selectivity is crucial to optimize the stimulation field and thus avoid side effects. Schwartz[i] described to glial scar process for intracortical brain machine interface. Eventually for point (c), the charge injections are recalled by Stieglitz[ii], these limits are ruled by the potential of the electrode during stimulation for metals. Platinum is much better than gold (75µC/cm2 versus 20µC/cm2) but still too weak for high stimulation with small electrodes which is the harshest condition for the charge density parameter. Thus to address these three conditions, we investigated the properties of boron doped diamond for recording or stimulation multi-electrode array or active implantable medical devices.

1 Methods/Statistics

Nanocristalline diamond is grown at high temperature after nanoseeding. The coated substrates are placed in hot plasma conditions. So as to obtain a conductive layer boron simultaneously injected. These atoms have the ability to penetrate the carbon lattice in substitution. Eventually the boron doping is in the range of 10^{23} atoms/cm^3. The substrates are disks or cylinders made of platinum iridium (90/10) which is classically used for cochlear or deep brain stimulation electrodes. Thus we should be able to compare our new electrodes to the gold standard of implantable devices.

2 Results

The electrodes were cut from a thick platinum iridium foil using a specific process which gives to the electrodes a roughness in the range of 1.6µm RMS. In former experiments (on platinum foils) we had to use a tungsten adhesion layer but thanks to the roughness given by the machining process the adhesion of nanocristalline diamond is promoted, see Fig. 1.

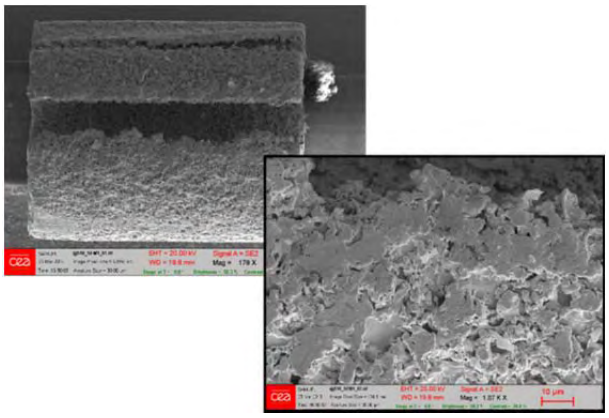

Cochlear electrodes raw from machining -before coating

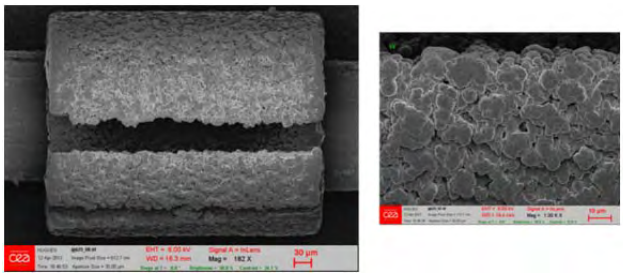

Cochlear electrodes coated and diamond growth

Fig. 1: preliminary tests of diamond growth on implantable electrodes

Meanwhile another batch of electrodes dedicated to cochlear implants were then electrically welded and integrated in an insulation silicone rubber, which proves the compatibility of diamond coating with processes of implantable medical devices, see Fig. 2a.

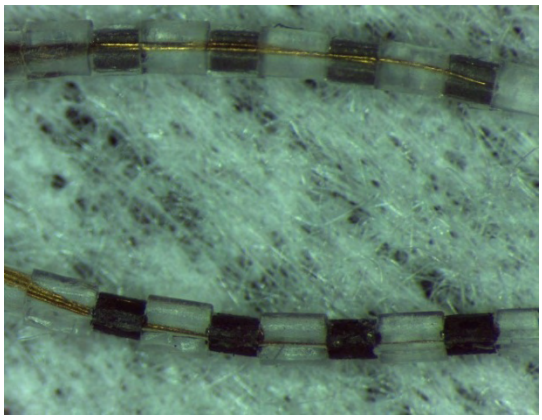

(a) full integration of the diamond coating in an industrial process

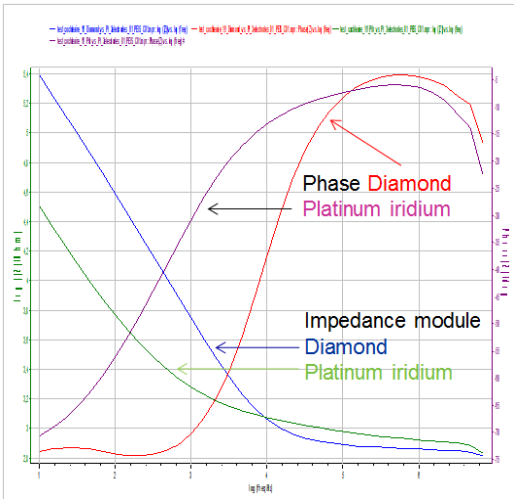

(b) impedance spectroscopy

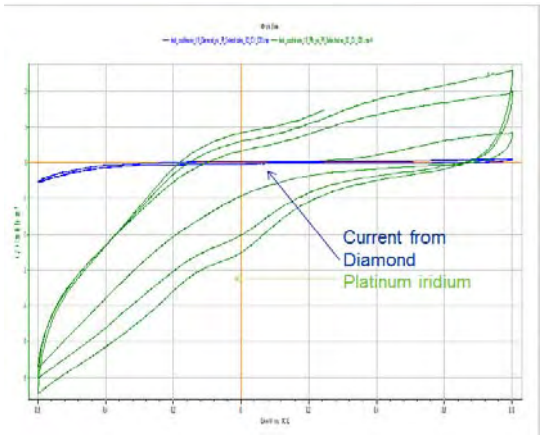

(c) cyclic voltammetry

Fig. 2: Integration and characterization of the diamond coated cochlear electrode

In the set-up the diamond coating was too thick and this deposition tends to smooth the platinum iridium hence the effective surface is reduced by the deposition, which is consistent with the EIS of Fig. 2b. Consequently even if the potential water window is higher than platinum, the CSC (cathodic storage capacity) is weaker than rough platinum (338 vs 4810µC/cm^2 see Fig. 2c). The effective surface of the diamond electrodes must be drastically increased. This was recently achieved by our group using carbon nanotubes as scaffold for boron doped diamond[iii]. Such process was applied on cortical disks. We demonstrated the feasibility of the carbon nanotubes growth on platinum iridium disks and the coverage of nanocristalline diamond, see Fig. 3. With this final adaptation we will take advantage of a large water window of the diamond and an incredibly high effective surface.

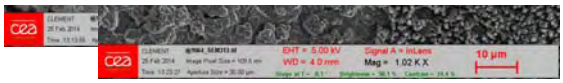

Fig. 3: carbon nanotubes grown on nanocristalline diamond and coated by nanocristalline diamond

3 Conclusion/Summary

The first comparison of boron doped diamond with platinum iridium based on the impedance spectroscopy and cyclic voltammetry is not favorable to diamond. Nevertheless, we already demonstrated the feasibility of the integration of diamond electrodes with an industrial process. Moreover, technical developments on electrodes are under progress to drastically increase to effective surface.

Acknowledgement

This work is part of the NEUROCARE project supported by the European commission in the FP7/NMP program n° 280433

References

[1] A.B. Schwartz, X.T. Cui, D.J. Weber, D.W. Moran. Brain controlled interfaces: Movement Restoration with Neural Prosthetics, Neuron 52, 205–220, October 5, 2006

[2] T. Stieglitz, Neuroprothetics, Theory and practice, Electrode material for recording and stimulation, vol. 2, 2004

[3] C. Hebert, J.P. Mazellier, E. Scorsone, M. Mermoux, P. Bergonzo, Boosting the electrochemical properties of diamond electrodes using carbon nanotube scaffolds, Carbon, Volume 71, May 2014, Pages 27–33

Impedance Considerations on MEA – the Effect of Electrode Materials and Coatings

Tomi Ryynänen[1*], Manoj Sivasubramaniapandian[1], Marja Peltola[2], Susanna Narkilahti[2], Jukka Lekkala[1]

1 Department of Automation Science and Engineering and BioMediTech, Tampere University of Technology, Tampere, Finland
2 NeuroGroup, BioMediTech, University of Tampere, Tampere, Finland
* Corresponding author. E-mail address: tomi.ryynanen@tut.fi

Abstract
We have evaluated how different electrode materials and coatings used to improve cell attachment affect on impedance and noise levels of microelectrodes on MEAs. Titanium nitride (TiN), titanium, and atomic layer deposited iridium oxide (IrOx) were experimentally studied as electrode materials and, in addition, several other materials were reviewed from the literature. From MEA coatings polyethylenimine (PEI) and laminin, gelatin, and Matrigel™ were studied. The results support titanium nitride's and platinum black's position as the most commonly used low impedance electrode materials on MEAs, whereas IrOx and carbon nano tube based materials are promising alternatives as the microelectrode materials. PEI and laminin, and gelatin coatings did not cause any significant change in the overall performance of the MEAs, but a substantial increase in impedance was observed with Matrigel™, especially when applied as thick layer.

1 Background

Probably the most common technical parameter to compare the performance of a microelectrode array (MEA) is its impedance, commonly given at 1 kHz. Typically lower impedance means lower signal-to-noise ratio, which is favored when the signals measured from MEA need to be analyzed. In addition, the large impedances can drastically affect the charge transfer capacity at the electrode vs. medium/tissue interface. Thus, throughout the history of MEAs, researchers have tried to develop low impedance electrode materials, or at least have tried to find good compromise between the costs and performance of the microelectrodes.

As the top surface, i.e. the insulator layer of MEAs is typically made of silicon nitride or some other material that does not promote attachment and growth of cells or tissue slices, biologists are forced to apply protein or other additional coating on MEAs. The coating not covering only the insulator layer but also the electrodes undoubtedly changes the electrode vs. medium/tissue interface, even if the coating may in the best case be only one or few monolayers thick. Because of the changes, it is obvious that the technical specifications given for MEA do not apply as such anymore after the coating. As far as we know, the effect of coatings on MEA performance, namely on impedance and noise level, has not been widely studied and thus we wanted to find out if the biologists should pay more attention on their coating selections in order to maintain the high signal quality and whether the race towards lower impedance electrode materials makes any sense if at the end the coating has major effect on the total impedance.

2 Methods

200/30iR-Ti MEAs from Multichannel Systems (Reutlingen, Germany) were used as TiN MEAs in electrode material studies and also as the MEAs in all the coating studies. Fabrication of atomic layer deposited iridium oxide (ALD IrOx) and titanium MEAs followed the guidelines described in more detail in [1]. For other electrode materials the impedance values were found from the literature and normalized to 30 µm electrode size.

The impedance measurements were performed with a 60 channel impedance testing device MEA-IT from Multichannel Systems. In-house made PDMS rings [2] were used to form culture chamber to hold liquids around the electrodes. The culture chambers were filled with buffer solution 24 hours before every measurement. In case of coating experiments the same MEA was measured at first without coating, then coated with the material under study, and finally re-measured after coating removal.

Noise measurements were done at 50 kHz measurement frequency with USB-MEA 1060 (electrode materials) and MEA-2100 (coatings) systems from Multichannel Systems and RMS noise voltage was calculated as described in [1]. All the measurements were performed at room temperature.

Detailed description of coating protocols used in this study is given in [3]. But shortly, 1 ml of 0.05 % (w/v) PEI, was added to the MEA and incubated for two hours. Unbound PEI was aspirated; the wells were rinsed with sterile water, and dried. 1 ml of murine laminin, diluted to 20 µg/ml with Dulbecco's phosphate buffered saline was added thereafter and incubated for two hours. In case of gelatin, 1 ml of 0.1 % Type A porcine gelatin was added and incubated for an

hour. Two different procedures were adopted for Matrigel™ with reduced growth factor. Thick layer, where 50 µl/cm^2 of Matrigel™ was added, and thin layer where Matrigel™ in one-tenth of concentration diluted using Dulbecco's modified eagle medium was added in sufficient quantities, and incubated for 30 minutes. The incubator was maintained at 37 °C and a water bath was used to prevent evaporation. Unbound material was aspirated thereafter.

3 Results

3.1 Electrode materials

The impedance and noise results both from our experiments and literature are summarized in table 1. TiN, Pt black, activated sputtered IrOx and novel Pedot-CNT electrodes have comparable impedances around 20-50 kΩ. Unactivated sputtered and ALD IrOx have ten times higher impedance, which raises interest to try electrochemical activation on ALD IrOx in further studies, especially because of highly competitive noise results achieved already without activation. However, the electrode material noise results should be compared with caution as the sampling period was only a few seconds. Bare metal electrodes, on the contrary, are not competitive when only impedance in considered, but depending on application the performance may still be sufficient and shorter fabrication times and cost issues cannot be ignored either.

Table 1. Typical average impedance and noise values for 30 µm microelectrodes made of different materials.

Material	Impedance @1kHz (kΩ)	RMS noise (µV)	Reference
Ti	>1800	9.1	This study and [1]
Sputtered TiN	30-50	1.65-5.5	This study, [1], and Multichannel Systems
Unactivated ALD IrOx	165-450	4.6	This study and [1]
Unactivated sputtered IrOx	~450		[4]
Activated sputtered IrOx	~23		[4]
Pt black	25		Axion Biosystems
Pt	800-1100		Qwane Biosciences
Au	1000-1300		Qwane Biosciences
Pedot-CNT	~20		Multichannel Systems

3.2 Coatings

Independent of coating material or its thickness, the change caused on RMS noise was found to be negligible, as shown in table 2. The same applies on impedance results of PEI and laminin, and Gelatin. On the contrary, Matrigel™ clearly increases the impedance and the increase is proportional to the layer thickness.

Table 2. Difference of average impedance and RMS noise between uncoated and coated MEA for different coating materials.

Material	Increase of impedance @1kHz (kΩ)	Increase of RMS noise (µV)
PEI and laminin	2.4	0.04
Gelatin	2.7	-0.01
Matrigel™ (0.25 µm)	5.8	0.06
Matrigel™ (4.5 µm)	10.1	0.08

4 Conclusions

Based on the impedance and noise results it is well understandable why TiN and Pt black have been the most popular electrode materials on MEAs. However, iridium oxide and CNT based electrodes are promising candidates requiring some more studies and acceptance from the end-users. Polyethyleneimine (PEI) and laminin, and gelatin coatings are safe choices as MEA coatings as they do not cause any significant change in the overall performance of the MEAs. On the contrary, Matrigel™ users must accept higher impedance caused by the coating.

Acknowledgement

Authors want to thank Joose Kreutzer from TUT MST-group for providing PDMS rings, Juha Heikkilä from UTA NeuroGroup for aiding in measurements, Janne Koivisto and Dr. Katriina Aalto-Setälä from UTA HeartGroup for consultation in Matrigel™ issues, and Dr. Jani Hämäläinen and professor Markku Leskelä from University of Helsinki for ALD IrOx depositions. This work was supported by Tekes (decision numbers 40346/11 and 40345/11) and Council of Tampere Region.

References

[1] T. Ryynänen et al., 2012. *Journal of Vacuum Science & Technology A*, vol. 30, num. 4.
[2] J. Kreutzer et al., 2012. *Journal of Bionic Engineering*, vol. 9, issue 1.
[3] M. Sivasubramaniapandian, 2014. Master's thesis, Tampere University of Technology.
[4] S. Gawad et al. 2009, *Frontiers in Neuroengineering*, 2, 1.

Carbon Nanotube Multi-Electrode Array Chips for Noninvasive Real-Time Measurement of Dopamine, Action Potentials, and Postsynaptic Potentials

Mao Fukuda[1], Keiichi Shirakawa[1], Hideyasu Jiko[1], Ikuro Suzuki[2*]

1 Alpha MED Scientific Inc., 209 Saito-incubator, 7-7-15 Saito-asagi, Ibaraki, Osaka 567-0085, Japan
2 Graduate School of Bionics, Tokyo University of Technology, 1404-1 Katakura, Hachioji, Tokyo 192-0982, Japan
*Corresponding author E-mail address: isuzuki@stf.teu.ac.jp, s.ikurou@gmail.com

1 Background/Aim

Microelectrode array technologies allow analysis of neural function at both the single cell and network levels and permit stable long-term recordings from cultures and isolated tissues. Current applications include monitoring changes in the transmitter or electrophysiological phenotype in cultured or acute samples, and studies of synaptic plasticity.

Although MEAs have been used widely for measuring action potentials (AP) and field postsynaptic potentials (fPSPs), it is still difficult to measure presynaptic activity such as neurotransmitter release from the presynaptic bouton. The pathogenesis and symptoms of many neurological diseases stem from dysregulation of neurotransmitters; hence the simultaneous measurement of transmitter release and postsynaptic response could provide further insight into these diseases.

The traditional technology for measuring many electrochemically active neurotransmitters involves oxidation-reduction reactions at the electrode surface. Dopamine has been measured using carbon fibers, glassy carbon, or carbon nanotube (CNT) electrodes, and several reports have shown CNTs' high sensitivity to electrochemically active species such as dopamine.

The most widely used methods for modifying CNTs on the electrode surface are immersion drying and direct chemical deposition (CVD). However, immersion drying field CNT coatings with limited durability, while direct CVD requires

expensive technology. Thus, we aim at developing a novel CMT-MEA to be used for both electrophysiology and highly sensitive detection of dopamine using simple electroplating technologies.

2 Methods/Statistics

2.1 Fabrication of CNT-MEA

CNTs are electroplated on the surface of indium-tin-oxide (ITO).

Planar ITO-MEAs containing 64 electrodes on a glass substrate is used. To insulate each electrode, acrylic imide insulating film was coated on the entire glass surface and the electrodes were exposed to chemical etching. MWCNTs were electroplated onto the surface of the ITO electrode. The dispersed MWCNT solution was dripped onto ITO-MEA and electroplated using an electrochemical analyser in a two electrode mode using a Pt reference electrode. Electroplating as well as all electrochemical experiments were performed with an ALS1140A electrochemical analyser.

2.2 Evaluation for the CNT-MEA

Electrochemical measurements of dopamine were performed using the CNT-MEA with an Ag/AgCl reference electrode and a Pt counter electrode. Ag/AgCl and Pt electrodes were inserted into the chamber on the CNT-MEA and fixed at the ring cap. The amperometric response of dopamine was recorded at +0.3V.

Electrophysiological recording were performed both with neuron cultures and hippocampal slices. For neuron cultures, hippocampi from E18 rat were removed and trypsinized at 37 degree for 15 min and dissociated by trituration in Hank's balanced salt solution. The cell suspension was briefly centrifuged and the pellet resuspended in 5 ml neurobasal medium containing 2% B27 serum-free supplement and 1% penicillin-streptomycin. A droplet of cell suspension was loaded onto poly-d-lysine-coated CNT-MEA at 130 cells/mm2 and maintained in culture under a 5%Co2 atmosphere at 37 degree.

Hippocampus slices were prepared from 4-weeks-old male mouse. Slices of 300 um thickness were maintained at room temperature in a holding chamber containing oxygenated artificial cerebrospinal fluid (aCSF) and allowed to equilibrate for at least one hour prior to physiological measurements. All electrophysiological recordings were performed using the CNT-MEA connected to the MED64 micro electrode array system.

For real-time measurement of synaptic dopamine release, striatal regions of coronal or saggital brain slices were used. Slices were obtained and maintained with same procedure to

above. The CNT-MEA containing the slice wase connected to a 30 degree heating plate and chamber was continuously perfused with oxygenated ACSF at 29-30 degree. An Ag/AgCL wire and a Pt wire in the superfusion chamber acted as reference and counter electrode, respectively. To detect dopamine, the amperometric response was recorded at +0.3V and an acquisition rate of 100 Hz.

3 Results

The CNTs plated onto the surface of ITO electrodes formed particles or retained their tubular shape (Fig.1), and gaps between the particles increased the electrode surface area. The CNTs remained on the MEAs even after more than 3min ultrasonic cleaning,that highlight their durability.

High sensitivity amperometric responses to dopamine is observed as the current rises with applications of dopamine solution compared to with PBS which does not show any changes, and the results were repeated three times. Dopamine release was exhibited with striatal slices as changes of amperometric current-time responses (Fig.2).

The capability of the CNT-MEA for electrophysiological recording of APs and fPSPs were assessed. Neurons cultured on the CNT-MEAs for over 1 month exhibit spontaneous APs occurred in synchronized bursts at many of the electrodes, which underscores their high-durability and non-invasive natures. fPSPs were also tested. Detections of fPSPs were measured using mouse hippocampal slices plated in a superfusion chamber with the CNT-MEA. Spontaneous activities from the CA1 stratum radium were obtained before and after 30 mM high K; perfusion.

4 Conclusion/Summary

We fabricated a novel MEA by electroplating carbon nanotubes onto ITO MEAs. These CNT-MEA exhibited high current densities and high sensitivity to dopamine as indicated by the detection of nanomolar dopamine concentrations. We have successfully measured dopamine release as well as APs and fPSPs from brain slices and cultured neurons. These results suggest that our CNT-MEA has broad applicability in both basic neuroscience research and preclinical studies of neural diseases, including studies of network properties in epilepsy and the screening of neuroprotective drugs against different pathological conditions.

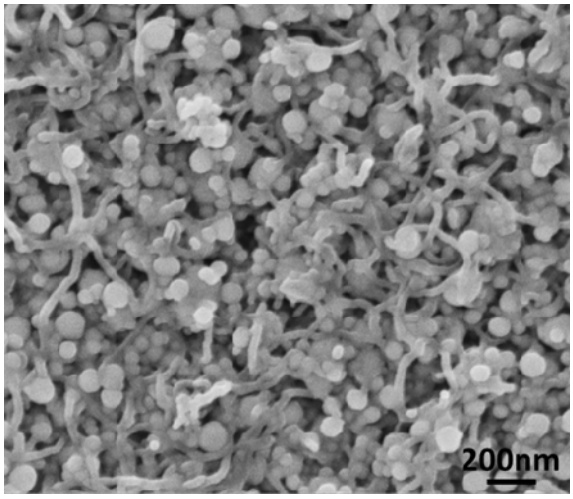

Fig 1. Structure of CNT-MEA

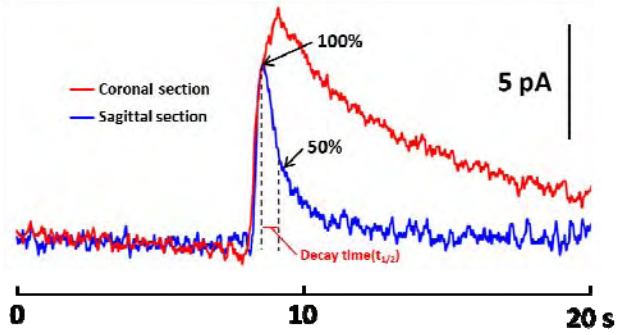

Fig.2 Real-time measurements of dopamine release

Evaluation of Materials and Fabrication Techniques for Capacitive Electrodes

Sebastian Röhler[1*], Claus J. Burkhardt[1], Dieter P. Kern[2], Alfred Stett[1]

1 NMI Natural and Medical Sciences Institute, Reutlingen
2 Institute of Applied Physics, University of Tübingen, Tübingen
* Corresponding author. E-mail address: sebastian.roehler@nmi.de

Abstract
In order to achieve long-term stability of microelectrodes for *in-vitro* and *in-vivo* applications it is appropriate to use electrodes with purely capacitive behaviour. Different materials were investigated regarding their possible use as dielectrics of capacitive microelectrodes. The relative permittivity (i.e. capacitance per area), the breakdown voltage, the leakage current and the electrical noise generated by the dielectric were measured. The tested materials include dielectrics with high permittivities (barium titanate, titanium oxide), high band gap (hafnium oxide) and combinations of these properties (mixed oxide of titanium and zirconium).

1 Long-term stable microelectrodes

Implantable neural prostheses are being used to target different diseases like deafness [1], blindness [2], foot drop [3], loss of bladder control [4] and Parkinson's disease [5]. One crucial point with these implants is long-term stability. For reasonable applications not only the encapsulation must withstand degradation for several years but also the electrodes used for tissue stimulation must not corrode within this time span. One approach is the use of electrodes with purely capacitive behaviour, were electrically induced degradation processes are completely blocked [6]. Besides these applications electrodes of this type can be used for capacitive *in-vitro* stimulation [7] and for coupling of extracellular signals to substrate integrated transistors for signal amplification [8].

2 Fabrication Process

We fabricated capacitive electrodes by depositing different dielectrics on metal electrodes. On dedicated test samples (fig. 1) the electric properties of these dielectrics were tested in the metal-insulator-electrolyte (MIE) configuration (fig. 2).

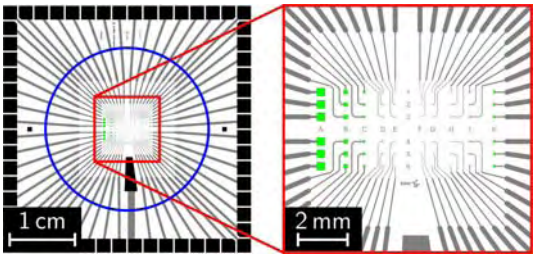

Fig. 1. Design of the test samples (green: active area, blue: area covered with electrolyte).

The investigated dielectrics were titanium oxide (TiO_2) and hafnium oxide (HfO_2) fabricated by atomic layer deposition (ALD) and a mixed oxide of titanium and zirconium ($Ti_xZr_{1-x}O_2$) and barium titanate ($BaTiO_3$) fabricated by physical vapour deposition (PVD).

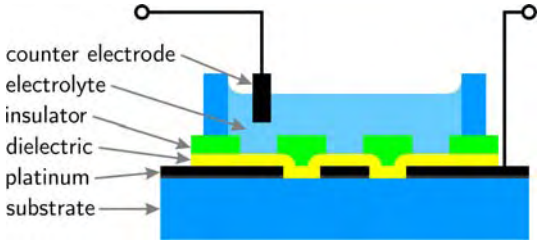

Fig. 2. Schematic cross section of the test samples used for electrical characterisation.

3 Measurement setup

The capacitances were measured using voltage ramps (fig. 3).

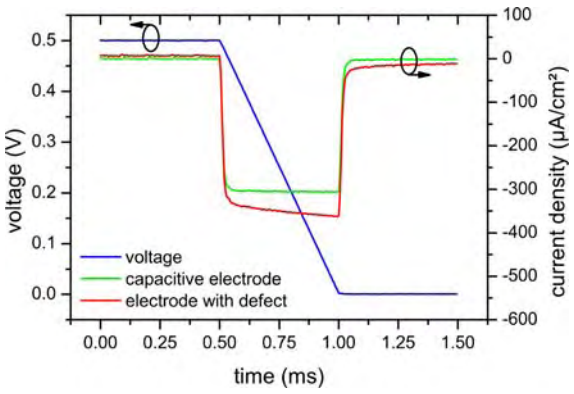

Fig. 3. Capacitance measurement with voltage ramps. The green graph shows the current response of an electrode with purely capacitive behaviour. The red graph shows a superimposed faradaic current.

This method was suitable to distinguish electrodes with purely capacitive behaviour (green graph) from electrodes with superimposing faradaic currents

due to defects in the dielectric (red graph).

The breakdown voltage and the leakage current were determined in DC measurements. Furthermore the electrical noise generated by the electrode was measured.

4 Results

With sputtered oxides a capacitance of up to 3 µF/cm^2 can be reached (fig. 4). The permittivities amount to 95 for $Ti_xZr_{1-x}O_2$ and 170 for $BaTiO_3$. The permittivities of the ALD layers are lower (TiO_2: 30, HfO_2: 16) but due to their good coverage and homogeneity they still show capacitive behaviour even for thicknesses down to 10 nm.

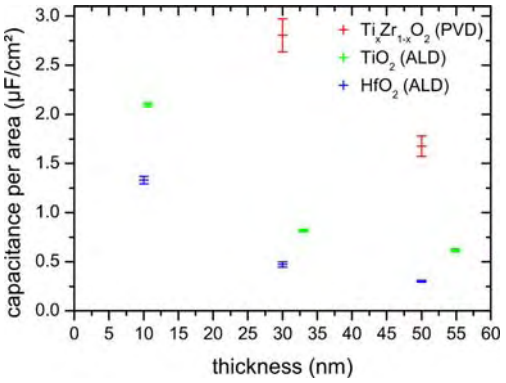

Fig. 4. Capacitance per area of different dielectrics.

The ALD layers show lower leakage currents and higher breakdown voltages (2.7 MV/cm for HfO_2 compared to 540 kV/cm for $Ti_xZr_{1-x}O_2$). The permittivity of $BaTiO_3$ depends on the temperature of the annealing step performed after deposition and can be adjusted between 10 and 170 (fig. 5).

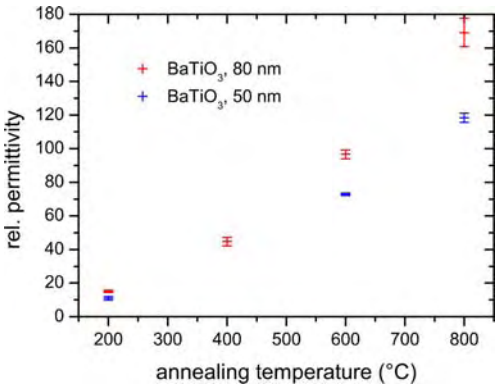

Fig. 5. Permittivity of $BaTiO_3$ annealed at different temperatures.

It is understood that the increase of permittivity is caused by a growth of the grain size during annealing. This has been confirmed by AFM and TEM analysis (fig. 6).

The results of the noise measurements are given in table 1. The main contribution to the electrical noise can be identified as k_BT/C-noise and therefore depends mainly on the capacitance of the electrode (the higher the capacitance, the lower the noise).

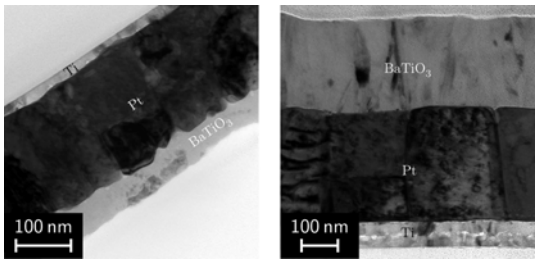

Fig. 6. TEM images of cross sections of Ti-Pt-$BaTiO_3$ stacks after annealing at 800°C.

	Capacitance	Noise
HfO_2, 30 nm	0.47 µF/cm^2	10.4 µV
TiO_2, 33 nm	0.82 µF/cm^2	9.7 µV
$Ti_xZr_{1-x}O_2$, 30 nm	2.80 µF/cm^2	3.9 µV
bare Platinum	-	2.6 µV

Table 1. Specific capacitance of different dielectrics and electrical noise (RMS, 5 Hz…10 kHz) generated by round electrodes with a diameter of 30 µm.

5 Summary

For the fabrication of capacitive electrodes dielectrics with high permittivity ($BaTiO_3$, TiO_2), high band gap (HfO_2), and materials combining these two properties ($Ti_xZr_{1-x}O_2$) were investigated. The capacitance per area, the leakage current, the electrical breakdown and the electrical noise were measured. The sputtered dielectrics show high permittivities whereas the ALD layers exhibit higher breakdown voltage and lower leakage currents. Depending on the specific application and the corresponding requirements concerning the electrodes the acquired data can be used for the development of future stimulation devices.

Acknowledgement

This work was supported by the Federal Ministry of Education and Research (BMBF), grant 01GQ0834 (Bernsteinfocus Neurotechnology: Hybrid brain). The support by Birgit Schröppel and the clean room staff at the NMI is kindly acknowledged.

References

[1] B. S. Wilson, and M. F. Dorman, *Hearing Research* 242, 3 (2008).
[2] E. Zrenner, *Science Translational Medicine* 5, 210ps16 (2013).
[3] R. van Swigchem et al., *Physical Therapy* 92, 398 (2012).
[4] N. J. M. Rijkhoff et al., *Neurourology and Urodynamics* 16, 39 (1997).
[5] H. C. Walker et al., *J. Neurophysiol.* 105, 1112 (2011).
[6] D. R. Merrill, M. Bikson, and J. G. R. Jefferys, *J. Neurosci. Meth.* 141, 171 (2005).
[7] M. Eickenscheidt et al., *J. Neurophysiol.* 107, 2742 (2012).
[8] A. Lambacher et al., *Appl. Phys. A* 102, 1 (2011).

Chemical Vapor Deposition Grown Carbon Nanotubes on Recessed Contacts of Flexible Polyimide MEAs

Kerstin Schneider[1*], Boris Stamm[2], Katja Gutöhrlein[2], Claus Burkhardt[2], Alfred Stett[2] and Dieter P. Kern[1]

1 Insitute for Applied Physics, University of Tübingen, Auf der Morgenstelle 10, 72076 Tübingen
2 NMI Natural and Medical Sciences Institute at the University of Tübingen, Markwiesenstraße 55, 72770 Reutlingen
*Corresponding author. E-mail address: kerstin.schneider@uni-tuebingen.de

Abstract
Since the first report on CNTs by Iijima in 1991, CNTs are becoming more and more important for applications, e.g. as electrode materials, in field emitter devices or in sensors. Carbon is also an inert material, so it is an ideal candidate for implant technology, e. g. for neuronal stimulation. Such implants are normally out of a flexible and insulating material, like polyimide, which carbonizes at temperatures higher than 400°C. On the other hand CNTs are often grown by CVD or plasma enhanced CVD (PECVD) processes, which require typically temperatures around 700 °C. So it is necessary first to find an adequate growing process for temperatures around 350°C-400°C and second to test their adhesion onto the substrate.

1 Background/Aims

Carbon nanotubes (CNTs) are ideal candidates as electrode materials for neuronal stimulation and monitoring devices such as microelectrode arrays (MEA). They provide a high charge injection limit without significant Faradic reactions [1] and CNT electrodes have a high surface area to volume ratio.
Flexible MEAs [2] typically consist of thin conductors buried in a flexible insulator such as polyimide, with the contact areas opened e.g. by dry etching of the polyimide. It is the objective of this work to fabricate CNT carpets on the contact areas of polyimide MEAs.

2 Methods

Chemical vapour deposition (CVD) on patterned catalysts is a convenient way of producing CNTs at
desired locations. However, this process typically requires temperatures in the 600°C to 800°C range.
A carbon containing gas e.g. acetylene is dissociating at a transition metal catalyst, fullerene like carbon caps are forming, from which the CNTs will grow. Amorphous carbon has to be etched away by a hydrogen containing gas, e. g. ammonia [3]. Proper selection of the catalyst material, its thickness, the precursor (an acetylene/ammonia mixture), the pressure and growth time enable growth at temperatures as low as 350°C. A standard polyimide MEA is made by a first layer of polyimide, imidized between 330°C and 350°C, on which the conduction paths and the electrodes are structured. A second layer of polyimide is insulating the different electrodes. The electrodes are then opened via an argon plasma. Complete MEAs as well as 1cm*1cm test samples were investigated in this study. In our CNT process had the samples are heated up to 350°C or 400°C, which leads to an catalyst poisoning by outgasing from the polyimide [4]. This can be prevented by growth temperature pre-treatment in ammonia. In order to test whether a higher imidization temperature reduces outgasing at growth temperature, CNT growth on MEAs which were imidized at 400°C is compared with growth on standard polyimide MEAs.
CNT-adhesion is tested by determining maximum allowable shear forces. For this purpose the test samples with an area of 1cm*1cm are pushed with a defined force against an Agar-Agar surface and then pulled sideways while the required shear force is measured (see Fig. 1). The integrity of the CNT carpets is checked by optical and scanning electron microscopy.

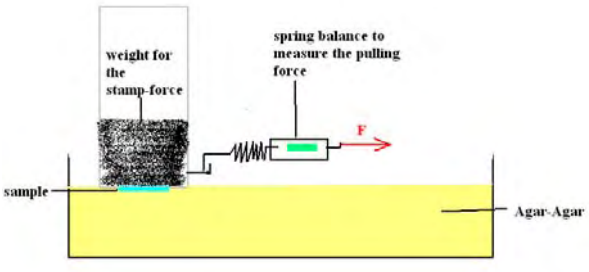

Fig. 1. The adhesion test set up.

3 Results

With a gas mixture of 1:1, a growth pressure of 5mbar, a growth time of 5 min, a 2 nm thick Ni catalyst and pre-treatment with ammonia at 60 mbar, at 400°C for 15 min for test samples or 150 min for polyimide standard MEAs, it was possible to grow CNTs with a total height of about 2 µm. At 350°C it is necessary to pretreat the samples at 60 mbar for 60 min and standard polyimide MEAs for 5 h in order to grow CNTs with an total height of about 1 µm. For standard polyimide MEAs we were not able to reduce the pretreatment time by increasing the pretreatment pressure even further.

The only difference between test samples and polyimide MEAs is their size.Therefore simply too much total outgasing may be the problem with the MEAs.

The tests on MEAs with an increased imidization temperature (400°C instead of 350°C) showed that with this polyimide it was possible to reduce the pretreatment time for 400°C growth from 150 min down to 15 min, for 350°C growth from 5h down to 3h. The total height of these CNTs was between 1 µm up to 2 µm (see Fig. 2). It appears that the polyimide which is imidized at 400°C is less carbonizing at 400°C or 350°C growth temperature. Since in our experience 350°C is essentially a lower limit for CVD growth of CNTs and obviously then the catalyst has to be in perfect condition, even the lower outgasing is still affecting the process.

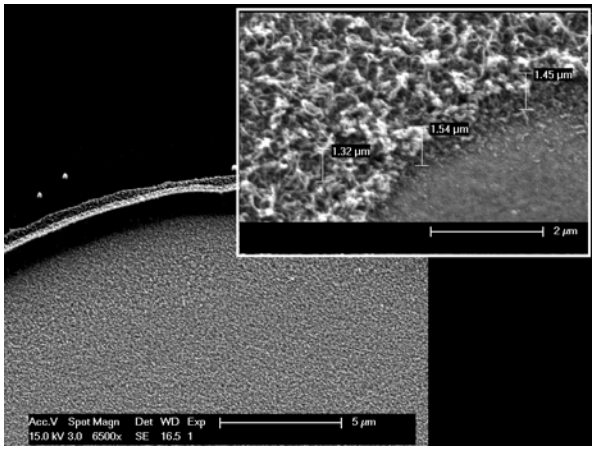

Fig. 2.CNTs grown onto an electrode at 350°C with a pretreatment of 3 h in NH_3 at 60 mbar. The inset shows a higher magnification image of an area from a different electrode on the same sample.

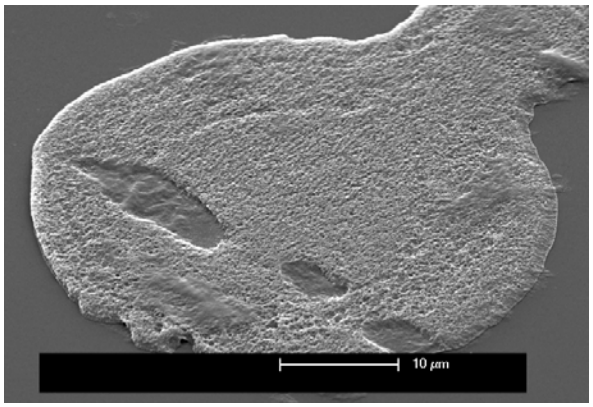

Fig. 3. A CNTs covered electrode after applying a shear force of 7,2 N. These CNTs were lying on the substrate, so the Agar-Agar was not able to remove them.

Adhesion was tested for samples with CNTs grown on planar polyimide and for such with the CNTs in a recess. On planar polyimide CNTs can tolerate shear forces between 2.4 N and up to 7.2 N, dependent on their morphology, i.e. whether they are standing up vertically or lying mostly flat on the surface (see Fig. 3). A few of the samples with vertically aligned CNTs were damaged at even lower forces. When the CNTs are grown in a recess they can tolerate shear forces in excess of 15 N (see Fig. 4).

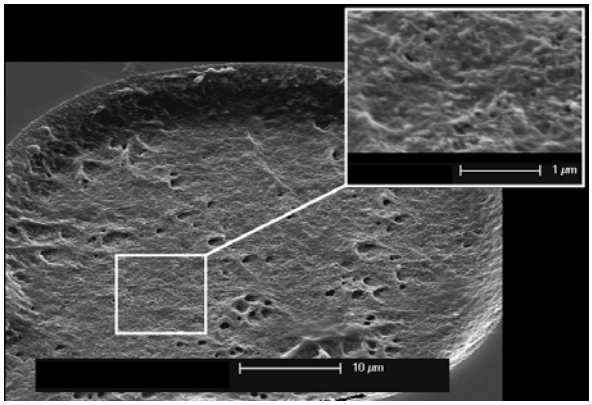

Fig. 4: CNTs grown in a trench after the adhesion test with 15 N. The inset shows the marked area at higher magnification and it is seen that the CNTs are still there, covered with Agar-Agar.

4 Conclusion/Summary

With a pre-treatment in ammonia at growth temperature and high pressure CNT forests can be grown on the recessed contacts of polyimide MEAs at polyimide-compatible temperatures between 350°C and 400°C. The preteatment time can be reduced by imidizing the polyimide at 400°C instead of 350°C. Shear tests indicate that on planar surfaces the maximum tolerable shear forces are lower for vertically oriented CNTs than for those oriented parallel to the surface. This may be due to an easier access of the lateral forces from the side of the tubes. The tolerable forces are even higher when the CNTs are grown in a trench deeper than the tube height. In this case no direct access from the side of the tubes is possible.

Acknowledgement

We thank the BW-Stiftung and the Federal Ministry for Education and Research for partial funding.

References

[1] Wang K., Fishman H.A., Dai H., Harris J.S. Neural Stimulation with a Carbon Nanotube Microelectrode Array,Nano Lett., **6** (9), p. 2043–2048 (2006).

[2] Molina-Luna K., Buitrago M.M., et al. Cortical stimulation mapping using epidurally implanted thinfilm microelectrode arrays. J. Neuroscience Methods, **161** p. 118–125 (2007).

[3] S. Hofmann, R. Sharma, et al. In situ observation of catalyst dynamics during surface-bound carbon nantube nucleation, Nano letters, vol. 7 no. 3, p. 602-608 (2007)

[4] Hatori H., Yamada Y., et al. The mechanism of polyimide pyrolysis in the early stage. Carbon, 34 (2) p. 201–208 (1996).

Diamond-Based Platforms for Long-Term Growth and Investigation of Neurons

Alexandra Voss[1], Hongying Wei[2], Maria Giese[2], Monika Stengl[2], Johann Peter Reithmaier[1], Cyril Popov[1*]

1 Institute of Nanostructure Technologies and Analytics, CINSAT, University of Kassel, Germany
2 Department of Animal Physiology, CINSAT, University of Kassel, Germany
* Corresponding author. E-mail address: popov@ina.uni-kassel.de

Abstract
The suitability of integration of ultrananocrystalline diamond (UNCD) films into the fabrication of platforms for neuronal investigation was determined. This includes the adaption of the deposition process on new substrates, like glasses and metal layers, as well as the structuring techniques for the diamond films. Additionally new possibilities for cell culture preparation were investigated exploiting the advantageous properties of UNCD layer systems.

1 Introduction

The high chemical stability and biocompatibility make all types of diamond films well suited substrates for cell growth. Accompanied with exceptional mechanical properties and easily tuneable electrical behaviour combined with a broad electrochemical window they are ideal platforms for diverse biotechnological applications. The current work is dedicated to the use of ultrananocrystalline/amorphous carbon (UNCD/a-C) films as insulating layer in passive multielectrode arrays (MEA). The nanostructured surface topography (Fig. 1) of these films provides enhanced cell adhesion especially after hydrophilic surface modification without compromising their viability [1].

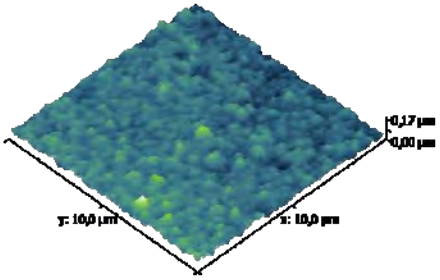

Fig. 1. 3D AFM image of UNCD/a-C surface showing grain-like nanoscopic features.

2 Methods

2.1 Deposition

The diamond films were deposited by microwave plasma assisted chemical vapour deposition (MW-CVD) from a precursor mixture of 17% methane in nitrogen. The substrates used were (100) Si and different thermostable glasses ultrasonically pre-treated with diamond powder suspensions to enhance the diamond nucleation density. The films were characterized regarding their morphology, crystallinity, topography and thickness depending on the deposition time. In a second series of experiments different metals (Au, Ti and Pt) were deposited by e-beam evaporation before the pre-treatment and diamond growth. The resulting film quality was observed by optical microscopy and scanning electron microscopy (SEM).

To alter the surface chemistry and introduce hydrophilic behaviour oxidation via UV/O_3 treatment or O_2 plasma, and amination by exposure to NH_3/N_2 plasma were performed. The efficiency of these techniques and stability of the achieved modifications have already been shown[1,2].

2.2 Cell Cultures

The obtained diamond layers were used as substrates for plating of cultures of pacemaker neurons from the cockroach *R. maderae*. The tissue was excised and enzymatically dissociated into single cells (collagenase and dispase). The cell suspension in the enzyme solution was plated on UNCD surfaces in sterile plastic cell culture dishes. The cells were settled for only 5 minutes and washed with culture medium. The primary cell cultures were kept in a dark humidified incubator. The cell adhesion and physiological responses to the neurotransmitter acetylcholine were examined with calcium imaging experiments. The improved cell adhesion on hydrophilic UNCD/a-C surfaces was used to establish a shortened culture preparation protocol without centrifugal sedimentation.

3 Results

3.1 Deposition and properties of UNCD films

The resulting UNCD/a-C coatings were composed of diamond nanocrystallites (below 10 nm in a diameter) embedded in a matrix of amorphous carbon. The nanostructured surface typical for UNCD as shown by atomic force microscopy (AFM, Fig. 1) and

SEM enhances the available contact area and could be advantageous for cell adhesion.

The wettability of as-grown and modified samples was studied by contact angle measurements, their surface composition by X-ray photoelectron spectroscopy (XPS). The contact angle of the as-grown UNCD/a-C surface against water was about 70° and decreased to values below 10° after the modifications revealing an successful change of the surface termination with replacement of the surface H atoms by O-, OH- and NH_2-groups rendering the modified surfaces hydrophilic. XPS measurements showed that the as-grown surfaces were very clean. After the modifications the surface concentrations of oxygen and nitrogen increased indicating an oxidation or amination of the surface, respectively (Fig. 2).

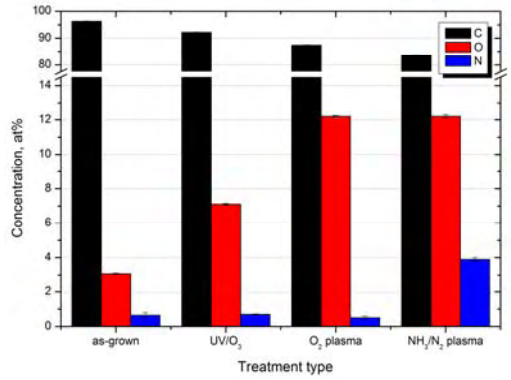

Fig. 2. Surface composition of as-grown and modified UNCD/a-C surfaces determined by XPS.

To enable the observation with fluorescence microscopy simultaneously to the electrical measurements UNCD/a-C films were deposited on glass substrates. Due to the high deposition temperature (600 °C) during the MW-CVD process only few types of glasses were suitable (e.g. Vycor F 1737, Corning Eagle 2000, fused silica). Plating and optical microscopy of neurons cultured on top of the emerging layers was possible on all three glasses.

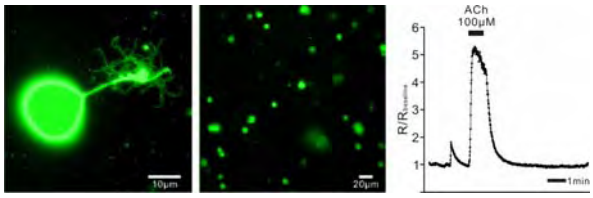

Fig. 3. Cultures of pacemaker neurons from *R. maderae* on fused silica/UNCD layer system; fura-2 fluorescence imaging [1] and physiological responses to neurotransmitter acetycholine (right panel).

In order to further increase the light transmittance the UNCD film thickness was reduced by enhancing the primary nucleation density achieved during the pre-treatment and decreasing the deposition time at the same process parameters. Pre-treatment with Opal Seeds (Adàmas Nano) resulted in very high nucleation densities (>10^{10} cm^{-2}) and later deposition achieved completely closed and uniform layers after less than 15 min. After 45 min of deposition the UNCD layer thickness was ca. 200 nm. The deposition speed was around 5.5 nm/min.

Deposition of UNCD films on different metal layers showed good adhesion and uniform layer properties on titanium and platinum. On gold films the UNCD layer delaminated. This could be decreased by using a titanium interlayer but still the layer quality on gold was not sufficient.

3.2 Neuron cultures

In previous experiments the improved adhesion of pacemaker neurons of *R. maderae* was confirmed on UNCD layers with different surface terminations [1]. These data were used to improve the cell culture preparation technique. During common preparation protocols centrifugation is applied to extract protease enzymes added in a previous step. This harsh handling could cause major damage to the cells. The stronger attachment on the UNCD platforms now allowed the neurons to adhere within 5 min. Therefore, the centrifugation step could be avoided. The application of acetylcholine triggered a strong and large increase in the intracellular calcium concentration, indicating that the neurons are not depolarized and healthy (Fig.3). Therefore the improved cell culture protocol with UNCD surfaces did not interfere with neuronal physiological responses.

Acknowledgement

The authors would like to acknowledge the Deutsche Forschungsgemeinschaft (DFG) for the financial support under the project PO 789/3-1.

References

[1] A. Voss, H. Wei, C. Müller, C. Popov, G. Ceccone, C. Ziegler, M. Stengl, J.P. Reithmaier (2012): Influence of the surface termination of ultrananocrystalline diamond/amorphous carbon composite films on their interaction with neurons. *Diamond and Related Materials, 26, 60-65.*

[2] A. Voss, M. Mozafari, C. Popov, G. Ceccone, W. Kulisch, and J. Reithmaier (2012): Stability of the surface termination of differently modified ultrananocrystalline diamond/amorphous carbon composite films. *Surface and Coatings Technology, 209, 184–189*

Cost-Effective Technique to Create CNTs Layers Enhancing Neuronal Network Development and Activity

Amélie Béduer[1*], Arushi Varshney[1], Emmanuel Flahaut[2], Marc Heuschkel[3], Philippe Renaud[1]

1 Microsystems Laboratory, Ecole Polytechnique Fédérale de Lausanne (EPFL), CH-1015 Lausanne, Switzerland
2 University of Toulouse; UPS, INP; Institut Carnot Cirimat, F-31062 Toulouse cedex 9, France
3 Qwane Biosciences SA, EPFL Innovation Park, Lausanne, Switzerland
* Corresponding author. E-mail address: amelie.beduer@epfl.ch

Abstract
We demonstrate that dense and homogeneous DWNT layers can be easily created on existing MEA-chips using cost-effective spray coating technique and present significant advantages of DWNT layers for neuronal network development regarding morphology and spontaneous activity.

1 Introduction

Carbon Nanotubes (CNT) have different properties, such as extraordinary strength, toughness, electrical conductivity, and specific surface area, which make them excellent candidates for interfacing with neural tissues [1], [2]. From several studies involving cell culture on CNT layers, it is becoming clear that nanotopography exhibited by CNT layers stimulates behavioral changes in cells and plays a critical role in modifying cell development and proliferation, as well as the strength of adhesion to substrates [3], [4]. In this work, we demonstrate the use of CNTs layers to enhance neural networks spontaneous activity. We use a cost-effective methodology to create dense and homogeneous CNTs layers directly on surfaces of commercially available MEA chips. In particular, we focused on the use of transparent ITO electrodes coated with double-walled CNTs (DWNTs) allowing direct observation of cells during culture time.

2 Materials and Methods

2.1 Carbon nanotubes layer fabrication

CNTs were prepared in-house by catalytic chemical vapor deposition (CCVD) of CH_4 at 1000°C(H_2:CH_4 atmosphere), as reported earlier [5]. After catalyst removal by dissolution with a concentrated aqueous HCl solution, CNTs were filtered and washed with deionised water until neutral. The sample contained approximately 80% of the double-walled nanotubes (DWNTs), the rest being mainly single-walled nanotubes (~15%) and triple-walled nanotubes. In order to obtain a stable CNT suspension and to avoid nanotubes agglomeration, we added a non-cytotoxic dispersing agent, the caraboxymethylcellulose (CMC). DWNTs and CMC were mixed with ultrapure water with a mass ratio of 1:10 (CNTs: 0.1% and CMC: 1%). The CNT concentration of this suspension corresponds to 1µg/mL.

In order to generate dense and homogeneous layers of DWNTs on the MEA-chip surface, a spray-coating technique was used. This technique is cost-effective and scalable to a large areas. Used spray coater device is presented in Figure 1a. Before spray coating, MEA chips surfaces were made hydrophilic by applying an oxygen plasma treatment (0.6mbar O_2, 20s). Spray-coating was carried out for 3min to cover a MEA-chip and obtain a dense CNT layer, 100±20 nm in thickness. Using shadow masks, it was also possible to deposit DWNT layers on specific areas of the chip.

2.2 Primary mouse cortical neurons culture and analysis

All experimental procedures were carried out according to the Swiss federation rules for animal experiments. Mouse primary cortical neurons were prepared from embryonic day 17 Of1 fetal mouse brains. Cortices were digested in medium containing papain (20 U/ml) and dissociated by mechanical trituration. Cells were plated in neurobasal medium supplemented with 2% B27 and 2 mM Glutamax. Prior to neuronal cell culture, MEA chips were coated with polyethylene imine (0.01%w/v) and laminin (20µg/mL). Cortical neurons were seeded at different densities and maintained during 23 days on MEA chips (Qwane Biosciences SA, Switzerland) and on MEA chips equipped with a thin DWNT layer.

Images of at least 200 cells on four randomly chosen observation fields were captured and analyzed for each experimental condition and for each experiment. Experiments were repeated at least three times. Cell density was quantified as the number of cell nuclei on a given surface. Neural network morphology was evaluated using actin cytoskeleton staining and immune staining of the synapses. Spontaneous activity of neural networks was recorded each 2 or 3 days and quantified.

3 Results

Electrically conductive thin DWNTs films increased electrodes sensitivity and reduced significantly background signals without creating short-cuts between electrodes or shunting electrodes.

Figure 2 presents typical neuronal networks obtained for cultures performed on a classical MEA-chip (Ctrl) and on a MEA-chip equipped with a layer of DWNTs. On control chips, neurons tend to assemble and neurite bundles are observed. On the contrary, neurite networks are more homogeneously developed on DWNT-chip and further demonstrate that thin layers of DWNTs can serve as effective substrates for neural cell culture. Growing neurons sense the physical and chemical properties of the local substrate in a contact-dependent manner and retrieve essential guidance cues. DWNT homogeneous films have also been shown to influence neurite branching and density.

Spontaneous activity was found higher on DWNT-chips. Reported number of bursts per minute was three times higher on DWNT chips and due to lower electrode impedance, bursts amplitude was also higher. Furthermore, we demonstrate that activity appears earlier on DWNT-chips, certainly due to better network sprouting and development.

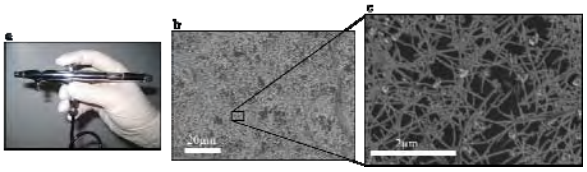

Fig. 1. a . Spray-coating device used to create CNT layers. b-c : SEM images of CNTs layers.

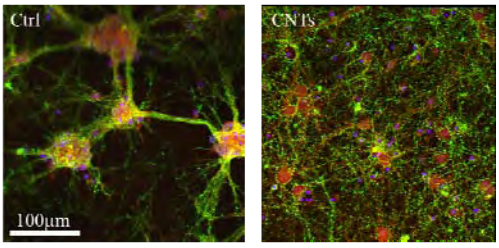

Fig. 2. Mouse cortical neurons cultured on MEA-chips without (ctrl) and with CNTs thin layers. Staining: red: actin cytoskeleton, green: synapses, blue: cell nuclei.

We demonstrate that dense and homogeneous DWNT layers can be easily created on existing MEA-chips using cost-effective spray coating technique and present significant advantages of DWNT layers for neuronal network development regarding morphology and spontaneous activity.

References

[1] Kotov N. A., Winter J. O., Clements I. P., Jan E., Timko B. P., Campidelli S., Pathak S., Mazzatenta A., Lieber C. M., Prato M., Bellamkonda R. V., Silva G. A., Kam N. W. S., Patolsky F., and Ballerini L. (2009), Nanomaterials for Neural Interfaces, *Adv. Mater., 1, 3970–4004*

[2] Ben-Jacob E. and Hanein Y. (2008), Carbon nanotube microelectrodes for neuronal interfacing, *J. Mater. Chem., 18, 5181-5186*

[3] Lee W. and Parpura V. (2009), Chapter 6 - Carbon nanotubes as substrates/scaffolds for neural cell growth, *Progress in Brain Research, Hari Shanker Sharma, Ed. Elsevier, 180,110–125*

[4] Keefer E. W., Botterman B. R., Romero M. I., Rossi A. F., and Gross G. W. (2008), Carbon nanotube coating improves neuronal recordings, *Nat. Nanotechnol., 3,. 434–439*

[5] Flahaut E., Bacsa R., Peigney A., and Laurent C. (2003), Gram-scale CCVD synthesis of double-walled carbon nanotubes, *Chem. Commun., 12, 1442-1443*

A Novel 3D Microelectrode Array for Extracellular Signal Recording of Acute Brain Slices

Carolin K. Kleber[1], Manuel Martina[1], Claus J. Burkhardt[1*], Elke Guenther[1], Udo Kraushaar[1]

1 NMI Natural and Medical Sciences Institute at the University of Tübingen, Reutlingen, Germany
* Corresponding author. E-mail address: claus.burkhardt@nmi.de

Abstract
The MEA system is a powerful tool to observe cell communication and network activity within acute brain slices. Typically, preparation procedures cause a layer of dead cells at the surface of the acute slice, which results in reduced electrical recording performance. A MEA with 3D electrodes is supposed to enhance the recorded signals by penetrating this dead cell layer. In our work, we present a new design and fabrication process for a 3D electrode array that is based on micro-needle electrodes and show the first results for its applicability to the extracellular recording of rat hippocampal slices.

1 Introduction

Microelectrode Arrays (MEAs) present the state of the art technology to study noninvasively the neuronal network activity within acute brain slices. Depending on the slicing procedure, a layer of dead cells on the surface of the brain slice is unavoidable. This layer has a negative influence on the signal quality, i.e. both amplitude and kinetics, depending on the thickness of the layer. To overcome this limitation, MEAs with three-dimensional electrodes are used, which penetrate this layer and thus allow to reduce the distance between the electrodes and the electrophysiologically active cells [1]. We utilized a novel design for a 3D MEA which was developed at the NMI and is based on stable micro-needle electrodes fabricated by standard photolithography techniques [2, 3, 4]. This work presents first results on the applicability of the new 3D MEA to the extracellular recording of acute rat hippocampal slices.

2 Materials and Methods

The 3D MEAs were composed of 59 micro-needle electrodes aligned in a 8 x 8 pattern on a standard glass substrate. The 50 µm high micro-needles consisted of metallised glass bodies that were coated with an insulation layer (silicon nitride). The non-insulated tip of the needles (10 µm height), combined with an additional layer of titanium nitride, defined the active conducting area of the electrode, Fig. 1 & 2. The electrodes were mechanically stable and displayed low impedance (131.7 ± 3) kOhm at 1kHz and low noise characteristics (5.6 ± 0.3) µV. Rat hippocampal slices were prepared from young Sprague – Dawley rats (postnatal day 17-27). The slices were stimulated with a biphasic pulse in the hippocampal CA1 region and recorded with the remaining electrodes. A MEA1060-BC amplifier (MultiChannelSystems) was used for the experiments.

3 Results

Field excitatory postsynaptic potentials (fEPSP) of hippocampal slices could be recorded with both standard and 3D MEAs, Fig. 3 & 4. The signals recorded with the 3D MEAs displayed similar characteristics with significantly higher amlitudes (2.5 times) when compared to standard MEAs. On the other hand, the time from the initial placement of the brain slice until reaching stable recording conditions was similar in both cases. Pharmacological modulation of the signals confirmed that the recorded signals were of synaptic origin.

Consistently good signals from up to 20 individual tissue slices and a REM analysis afterwards confirmed the mechanical stability of the MEA's 3D electrodes and its applicability for prolonged experiments as well as its reusability.

4 Conclusions and Outlook

We present the proof of concept for a new 3D MEA. In comparison to recordings with standard MEAs we were able to obtain significantly higher signal amplitudes with overall stable signal characteristics. With its mechanically stable micro-needle electrodes, the new 3D MEA presents a promising product with the perspective for a wide field of applications including tissue slices (e.g. from brain and heart, respectively) and wholemount retina.

Additional 3D MEA designs with even sharper and higher tips, as well as smaller and better localized electrode areas are planned.

References

[1] M.O. Heuschkel et al., *Journal of Neuroscience Methods* **114** (2), 135-148, 2002.
[2] M.O. Heuschkel, *Series in Microsystems* **13,** 2001.
[3] S. Röhler et al., *Microelectronic Engineering* **98**, 453-457, 2012.
[4] M. Martina et al., *HARMNST BoA 2013*, 208-209, 2013.

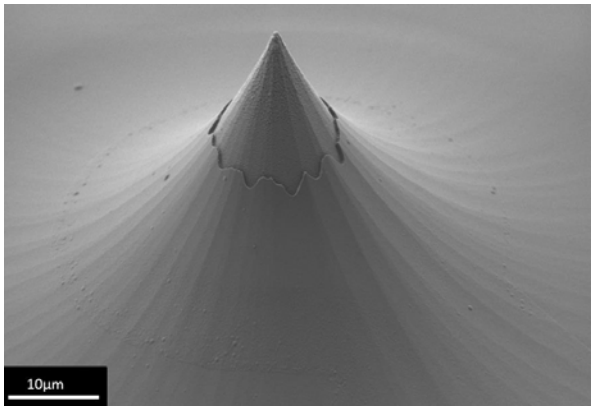

Fig.1. Tilted SEM image of the electrode array. Shown is one micro-needle electrode located on the electrode field that consists of a total number of 59 electrodes.

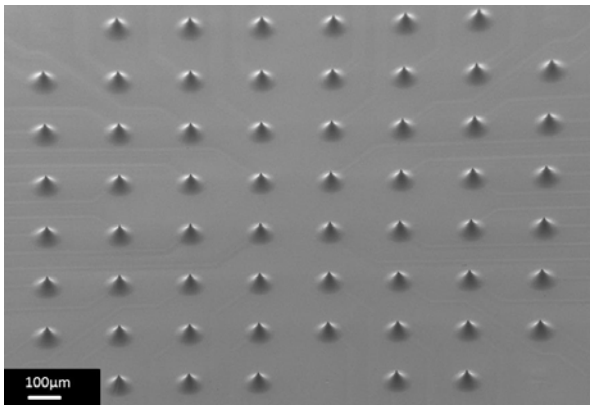

Fig.2. Tilted SEM image of the electrode array. Shown is the electrode field located in the center of the 3D MEA.

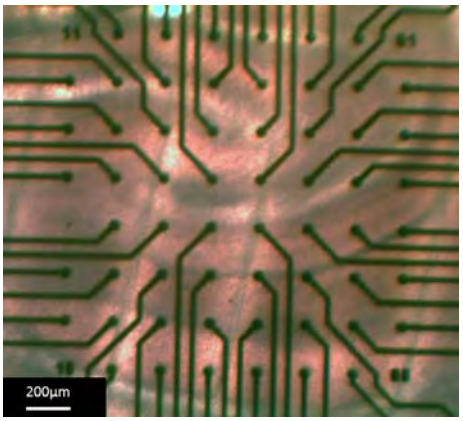

Fig.3. Picture of extracellular recordings with the 3D MEA. The prepared rat hippocampal slice is placed on the MEA and stimulated in the CA1 region with a bi-phasic pulse.

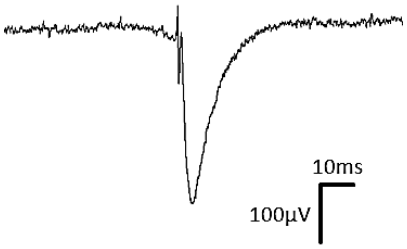

Fig.4. An exemplary postsynaptic field potential recorded in the near proximity to the stimulating electrode.

Realisation of Co-Culture MEA Biochips Using a Novel SU-8 Fabrication Process for Applications in Axonal and Synaptic Biology

Marc Heuschkel[1*], Nader Jedidi[1], Solomzi Makohliso[1]

1 Qwane Biosciences SA, EPFL Innovation Park, Building C, CH-1015 Lausanne, Switzerland
* Corresponding author. E-mail address: marc.heuschkel@qwane.com

Abstract
The use of dissociated neuronal cultures on MEAs is valuable in neuroscience and synaptic biology. However, the process of obtaining these dissociated cultures involves a complete disruption of the native neuro-circuitry. Towards improving and controlling the organisation of dissociated neuronal cultures, various studies have been working on multi-chamber MEAs that are connected to each other via micro-tunnels in order to guide axonal outgrowth and the final neural architecture. Here, we present a novel micro-fabrication procedure that facilitates the realisation of co-culture MEA chips with micro-tunnels, as well as the integration of microfluidic channels to enable simplified culture perfusion during experiments.

1 Backround / Aims

MEA platforms to investigate axonal biology have been described previously by several research groups [1-5]. It is based on micro-tunnel structures connecting two culture chambers within same MEA biochip. The obtained co-culture devices are made of a MEA substrate covered with a moulded polydimethylsiloxane (PDMS) part that defines the micro-tunnels and the two culture chambers.

This manufacturing principle is simple and low-cost. However, alignment of the PDMS part on the conventional MEA is not easy and the MEA electrode shapes and locations are not optimized for the given application. Furthermore, the current devices do not allow easy perfusion of the culture chambers as the PDMS/substrate bonding is not strong enough to allow the application of liquid pressure within the assembly without pressing permanently the PDMS part on the MEA substrate.

In order to overcome these drawbacks, a novel fabrication technology has been developed allowing generation of micro-tunnels and culture chambers made only of SU-8 epoxy directly on the MEA biochip.

2 Methods

The developed technology is based on a lamination process of SU-8 epoxy dry films. A broad range of thicknesses of SU-8 epoxy dry films (1µm to 500µm) can be obtained in a single step on plastic sheets and can be transferred onto the MEA substrates by a lamination process, which generates SU-8 multilayer structures, including cavities (e.g. embedded micro-tunnels and chambers). Figure 1 shows the manufacturing principle of the novel MEA biochips (centre and right schematics). The definition of the micro-tunnels by photolithography on the MEA allows improved alignment with the embedded electrodes. The closed SU-8 cavities allow perfusion of the culture chambers.

3 Results

The authors designed several MEA layouts similar to already existing devices [1-3] (see Figure 2), but manufactured the MEA culture chambers using only SU-8 epoxy. Figure 3 shows the resulting micro-tunnels on the MEA biochips. The platinum recording electrodes were coated subsequently either with platinum black or PEDOT coating, in order to optimize electrode characteristics.

4 Conclusion/Summary

Novel MEA biochips incorporating well-defined micro-tunnels and culture chambers have been successfully designed and realized using a new SU-8 dry film lamination process.

Acknowledgement

This research was supported via a grant from the European Community's Seventh Framework Program FP7-NMP-2011-SMALL-5 under Grant Agreement n°280433 - NEUROCARE.

References

[1] A.M. Taylor et al, Nat Methods 2(8), 599-605, 2005.
[2] A.M. Taylor et al, Neuron 66, 57-68, 2010.
[3] T. T Kanagasabapathi et al, Frontiers in Neuroengineering, 10.3389/fneng.2011.0013, 2011.
[4] L. Pan et al, J. Neural Eng. 8 (046031), 2011.
[5] Y. Takayama et al., Biosystems 107, 1-8, 2012.

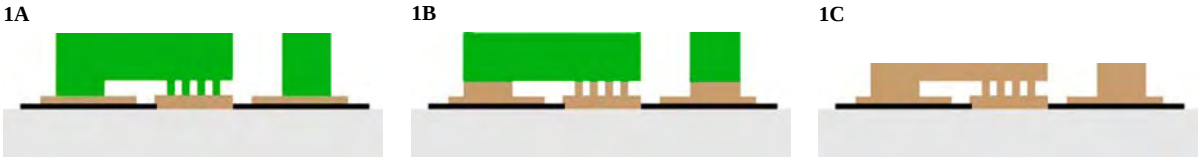

Fig. 1. Figure 1A shows the schematic of previously reported co-culture MEA devices [1-5] based on PDMS structures bonded onto the MEA biochip. Figure 1B shows the configuration of MEA device where the micro-tunnels are well defined by micro-fabrication of SU-8 epoxy and are eventually covered with PDMS. Figure 1C displays the configuration of MEA device where the micro-tunnels are made entirely from SU-8 epoxy material. Colour code: grey = glass, black = electrodes, brown = SU8 epoxy, green = PDMS.

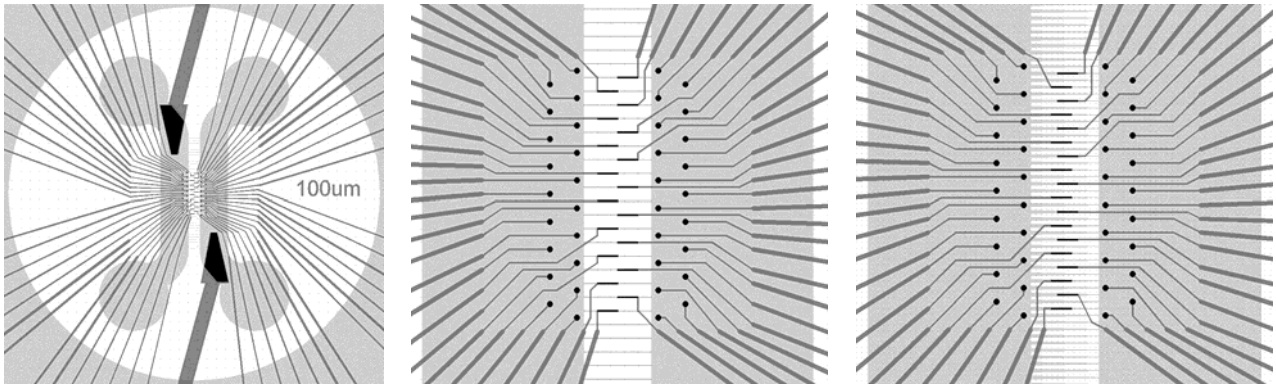

Fig. 2. The left picture presents the MEA layout overview. In the centre, it includes two culture chambers of 1.2mm x 6mm x100µm with a fluidic inlet and outlet of diameter 3mm diameter (light grey) connected together by small micro-tunnels of 500µm length, 5µm height and 5-25µm width. It incorporates 56 recording/stimulation electrodes (19 in each culture chambers and 18 within the micro-tunnels) and 2 large reference electrodes. The electrode wires are represented in in dark grey and the effective electrodes in black. Centre and right pictures represent higher magnification views showing the centre of two different MEA layout including different micro-tunnel designs.

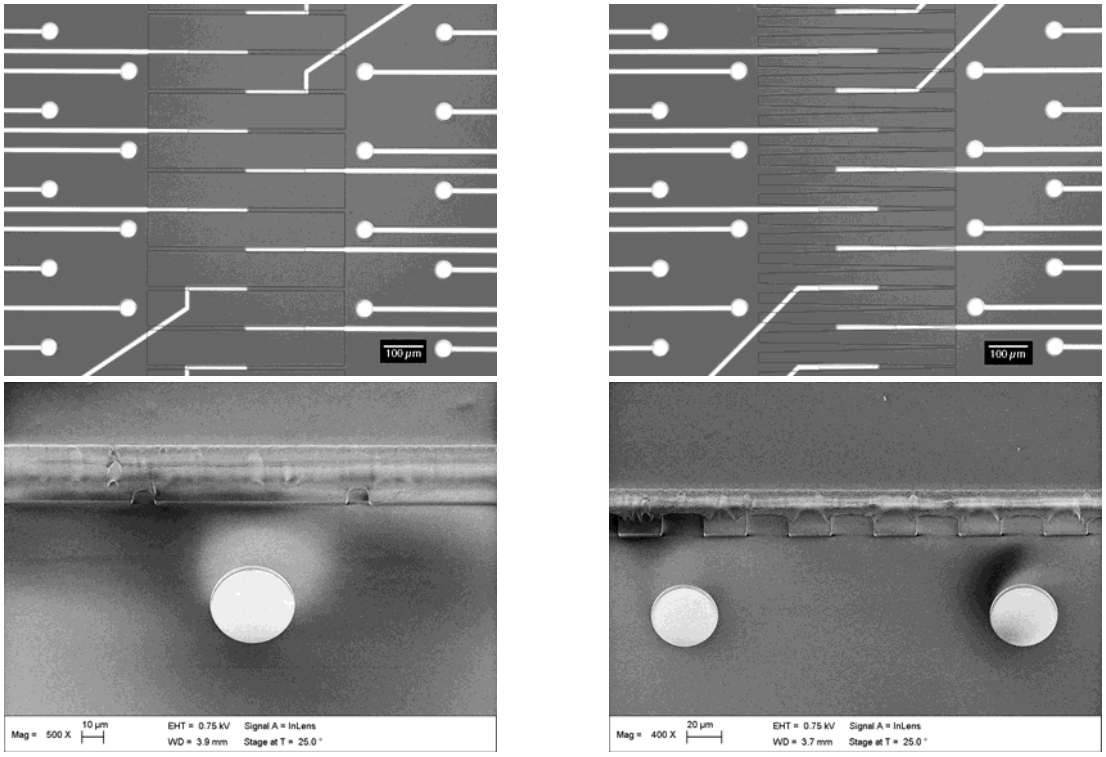

Fig. 3. Top, pictures of the defined SU-8 micro-tunnels before closing the channels. Electrodes are mainly located inside the micro-tunnels as well as closely to the micro-tunnel entrances. Bottom, SEM pictures of the closed SU-8 micro-tunnels. The circular light-grey structures are platinum recording/stimulation electrodes of diameter 30µm.

Advances in Diamond Microelectrode Arrays

T. Conte[1,2], Z. Gao[1], J.B. Destro-Filho[2], V. Carabelli[3], E. Carbone[3] and A. Pasquarelli[1*]

1 Institute of Electron Devices and Circuit, Ulm University, 89069 Ulm, Germany
2 School of Electrical Engineering, Federal University of Uberlandia, Brazil
3 Department of Drug Science, NIS Centre, CNISM, University of Torino, 10125 Torino, Italy
* Corresponding author. E-mail address: alberto.pasquarelli@uni-ulm.de

Abstract
This paper presents our latest development regarding multi-electrodes arrays in boron-doped nanocrystalline diamond technology. Thanks to the significant improvements in pattern complexity, spatial resolution, material transparency and target application as reported here, this can be considered a completely new device generation.

1 Introduction

1.1 Background/Aims

Boron-doped nanocrystalline diamond (NCD) MEAs can provide excellent performances by measuring cell activity in amperometric and potentiometric applications. Results obtained with 9-channel devices for high spatial resolution with single cells, and 16-channel devices for multicellular samples, demonstrated that diamond MEAs deliver the same signal quality of the best competing technologies [1 - 3].

At the same time, the two designs showed inherent limitations: 1) the localization of the release site requires a complex mathematical modelling of the MEA9 device, and 2) the MEA16 has a limited detection area. To address both issues we developed a completely new generation of devices: a 12-channel array for high spatial resolution, having identical electrodes on a regular grid, and a 64-channel array for widening the multicellular samples. Special attention was paid on transparency enhancement and use of thinner substrates, to permit confocal and TIRF microscopy.

2 Materials and Methods

2.1 Technology

For these new devices, we first improved the thin-film NCD-on-Sapphire technology [4] by replacing silicon-based interlayer and bias-enhanced nucleation (BEN) with seeding with a nanodiamond colloidal suspension [5]. In this way, a transparency in excess of 50 % could be extended up to the near-UV spectral region, thus permitting even the use of the fluorescent marker Fura2 for the ratiometric detection of free intracellular calcium (Fig. 1).

A significant second improvement addressed the problem of the stress caused by the thermal mismatch between the NCD-film and the carrier (Fig. 2), and consisted in replacing the sapphire substrate with a high-temperature glass having the same thermal expansion behaviour of silicon, as carrier material.

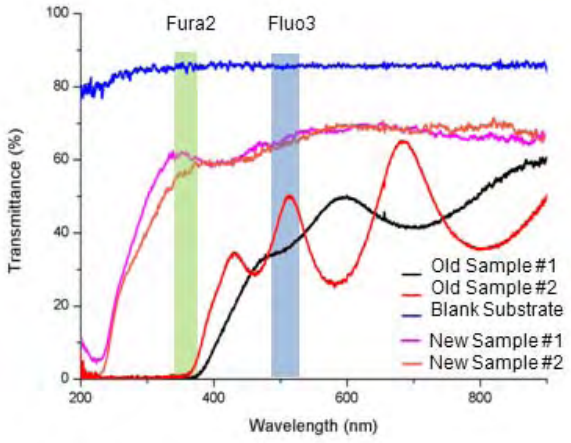

Fig. 1. Transmittance spectrum in the UV-VIS range for previous and new samples.

In fact sapphire shows a thermal expansion which is ~ three-fold the one of diamond, leading to a strong compressive stress in the diamond thin-film when cooling down to room temperature after the growth process run at 700~800 °C.

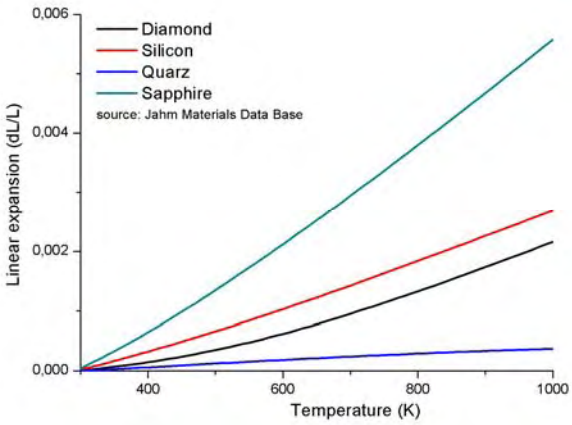

Fig. 2. Linear thermal expansion of diamond, silicon, quartz and sapphire substrate materials.

This stress is still acceptable on samples up to 1 cm side length, but it undermines quite severely the adhesion of the NCD-films on larger samples, like the 20x20 mm one used in the new 64-Ch MEA. Quartz, on its side, shows the opposite phenomenon having a

very little thermal expansion, which leads to a strong tensile stress in the brittle NCD-film after cooling, with the consequence of multiple fractures. The selected glass is specifically developed by SCHOTT AG (Mainz, Germany) for compatibility with the semiconductor technology and can be processed at temperatures of up to ~700 °C, thus allowing the growth of boron-doped NCD-films of good quality.

2.2 Design and Fabrication

All NCD-films are ~200 nm thick. The thickness of the glass substrate is only 200 µm, thus allowing the use of oil immersion objectives required for confocal and TIRF microscopy.

The MEA64 design (Fig. 3) resembles the widely used MCS-layout, with electrodes of 20 µm diameter arranged on a completely filled 8x8 square grid with 200 µm pitch, as shown in Fig.3b. Its fabrication is based on standard optical lithography, wet and dry etching processes.

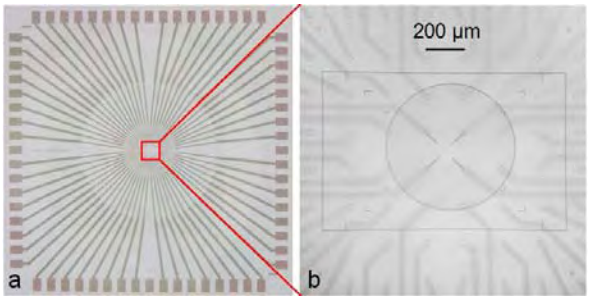

Fig. 3. MEA64: a) whole chip, b) electrodes detail

The MEA12 is a completely new design with 12 electrodes of 2 µm in diameter placed on a 4x4 grid with 5 µm pitch, whereas the outer corners of the grid are occupied by the wires connecting the inner electrodes of the array. Details of this device are illustrated in Fig 4. In order to reach the precision needed for both the electrodes pattern and the successive alignment of the passivation, we adopted for this device the electron beam lithography (EBL).

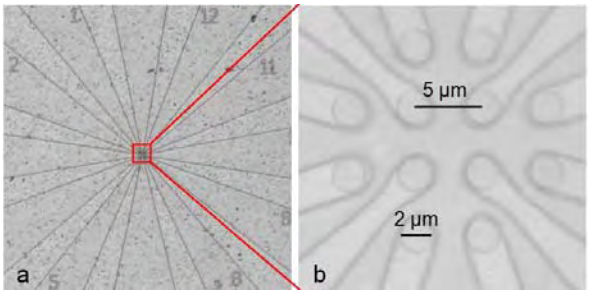

Fig. 4. MEA12: a) mid-region, b) electrodes detail.

2.3 Characterization

The optical transmittance spectrum of the samples was performed with a spectrophotometer (Ocean Optics HR2000+ES) and a dual light source (halogen and deuterium lamps) which covers a UV-VIS-NIR range from 200 to 1100 nm. All samples were measured after the growth of the NCD-film, i.e. before the lithographic pattern transfer. This is due to the spot size (400 µm) of the light beam used for the measurement. The characteristics of the new NCD-MEA64 where measured channel by channel, since the read-out electronics is still under development, following a test protocol which includes cyclic-voltammetry and impedance spectroscopy carried out with a potentiostat (Princeton Applied Research PARSTAT 2273). The MEA12 fits the already available electronics of the old MEA16, and this setup allows simultaneous measurements on all channels.

3 Results

Both devices (MEA64 and MEA12) show the typical characteristics of NCD-microelectrodes: series resistances in the lower tens of kΩ range, specific capacity of ~20 µF/cm² and water-splitting potential window larger than 2.5 Volts. The significantly improved transparency, compared with the previous device generation, is shown in Fig. 1.

Experiments with biological samples will be carried out and reported in future works.

4 Conclusion/Summary

This work describes the latest technological advances achieved by our group in design, fabrication and characterization of diamond MEAs. These electrodes have already proven in the previous layouts to be excellent in amperometry and very good in potentiometry. With the latest improvements, the devices can be adopted in a wider choice of applications ranging from the study of single cells secretory areas with high spatial resolution to complex multicellular samples. Furthermore, the enhanced transparency and the thin substrate material allow confocal and TIRF microscopy measurements.

Acknowledgement

Special thanks to Thomas Hantschel (IMEC, Belgium) for helpful discussion on the seeding technique and to Stefan Jenisch (Ulm) for the EBL processes.

References

[1] Carabelli et al., Biosens & Bioelectr, 2010
[2] Colombo et al., Diam. & Rel. Mat., 2011
[3] Gosso et al., The Journal of Physiology (in press), 2014
[4] Gao et al., Diam. & Rel. Mat., 2010
[5] Tsigkourakos et al, Phys. Status Solidi, 2012

Towards Stretchable High-Density Multielectrode Arrays

Flurin Stauffer[1*], Vincent Martinez[1], Mohammed Adagunodo[2], Janos Vörös[1], Alexandre Larmagnac[1]

1 Laboratory of Biosensors and Bioelectronics, ETH Zurich, Switzerland
2 Faculty of Medicine, Biomedical Engineering, University of Bern, Switzerland
* Corresponding author. E-mail address: stauffer@biomed.ee.ethz.ch

Abstract
We present a method to produce stretchable high-density leads based on silver nanowires (AgNW) in polydimethylsiloxane (PDMS). We fabricated leads with widths as small as 20 µm with an initial sheet resistance of ~2 Ω/□ that can be stretched thousands of cycles at 20% strain with a resistance increase of about 70%. This method can potentially increase our multielectrode array (MEA) density by a factor of 3 to 5 compared to our current implants.

1 Introduction

Epidural spinal cord stimulation in combination with chemical stimulation and rehabilitation training can restore voluntary locomotor movements in spinalised rats [1]. Stretchable high-density multielectrode arrays (MEAs) are desired because they allow compensating relative movements between the electrodes and the specific stimulation sites on the spinal cord by switching to the electrodes that evoke motor-like movement patterns. Stretchable MEAs based on conductive PDMS have been successfully implanted in spinalised rats for epidural spinal cord stimulation [2]. They withstand the mechanical stress during implantation and subsequent rat movements. However, the electrode density in these implants is limited by the fabrication method (minimal 150 µm tracks and 100 µm gaps using stencil printing). Additionally, these implants do not withstand local shear stress induced when the vertebrae are crushing the stretchable leads. Feng Xu and Yong Zhu reported the use of AgNW networks in PDMS as elastic conductors [3]. AgNW thin films can maintain their conductivity under high strains due to the sliding of the nanowire in the network. We focus on our recent effort in patterning AgNW thin film tracks with high aspect ratio and their potential use as stretchable high-density leads.

2 Materials & Methods

The presented work focuses on patterned AgNW thin films in PDMS and investigates their electrical responses under mechanical stress. We conduct uniaxial tensile testing and fatigue testing and we examine the effect of local shear stress on the conductivity of the leads. Additionally, we currently investigate the stability of AgNW-PDMS in saline.

3 Results

We demonstrate the feasibility of patterning AgNW tracks with high aspect ratio embedded in PMDS. Stretchable conductive leads 20 µm wide and several centimetres long exhibit a sheet resistance of ~2 Ω/□ and can be stretched thousands of cycles at 20% strain without loosing electrical conductivity. These results support the idea of using patterned AgNW-PDMS for stretchable high-density leads.

4 Conclusion

We now can potentially increase the MEA density by a factor of 3 to 5 compared to our current implants. Since implants based on conductive PDMS have been shown to be stable and biocompatible in vivo in rats [2], we are confident to use our fabrication technique to produce stretchable high-density MEAs for epidural spinal cord stimulation.

Acknowledgement

Thanks to Stephen Wheeler & Martin Lanz for their help in the workshop and cleanroom and to ETH Zurich, EU Neuwalk project, Nano-Tera.ch and SNFS for funding.

References

[1] Van den Brand, R. et al., 2012. Restoring voluntary control of locomotion after paralyzing spinal cord injury. *Science (New York, N.Y.)*, 336(6085), pp.1182–5.
[2] Larmagnac, A. et al., 2012. Skin-Like PDMS-Based Multielectrode Array for Epidural Electrical Stimulation to Promote Locomotion in Paralyzed Rats, in IFMBE Proceedings: *5th European Conference of the International Federation for Medical and Biological Engineering*, ed, Ákos Jobbágy, vol. 37, pp. 1180-81
[3] Xu, F. & Zhu, Y., 2012. Highly conductive and stretchable silver nanowire conductors. *Advanced materials (Deerfield Beach, Fla.)*, 24(37), pp.5117–22.

Towards Local Chemical Stimulation Through a Nanopore Array on a Microelectrode Array

Peter D. Jones, Paolo Cesare, and Martin Stelzle*

NMI Natural and Medical Sciences Institute at the University of Tuebingen, Germany
* Corresponding author. E-mail address: martin.stelzle@nmi.de

Abstract
We present here a new concept for local chemical stimulation of cells, by integrating an array of nanopore chemical release sites on a microelectrode array (MEA). Microfluidic channels address individual nanopores with chemical and electrical control. Integration of hydrophobically-gated nanopores will eliminate diffusive leakage, which is a primary challenge of chemical stimulation devices. Results of proof-of-concept experiments to demonstrate neuronal response to a chemical stimulus are forthcoming.

1 Background and aims

Electrophysiology reveals a limited view of cellular communication, as it can only indirectly address the intricate chemical signalling pathways of neurons. Electrical stimulation, for example, is nonspecific and limited in resolution, and exclusively excitatory. Artificial interfacing with chemical neurotransmitters would enable more natural interaction with cells and could improve the capabilities of neuroprosthetics [1]. However, recording or producing localized chemical signals remains challenging.

This work focuses on the need for novel tools for biologically relevant artificial chemical stimulation. Existing methods have low throughput, are technically challenging, have low resolution, or are limited by diffusive leakage [2–7].

Our new method uses an array of nanopores for local and selective chemical release (Fig. 1). Hydrophobic gating will prevent undesirable diffusive leakage (Fig. 2) [8]. Precise chemical release will selectively stimulate subpopulations of neurons in a cell culture, in a format compatible with standard MEA methods, including electrophysiology and microscopy.

2 Methods

Nanopores were fabricated by focused ion beam milling (Zeiss Auriga) in freestanding SiN_x or SiN_x/Ti/Au membranes. Pore behaviour depends on control of dimensions and surface properties. Hydrophobicity was imbued by silane modification of silicon nitride surfaces or by gold–thiol chemistry. Microfluidic channels were integrated by SU-8 photolithography on MEAs (MCS Multi Channel Systems, Reutlingen, Germany). Nanopore membranes were bonded to the microfluidic channels for individual addressing.

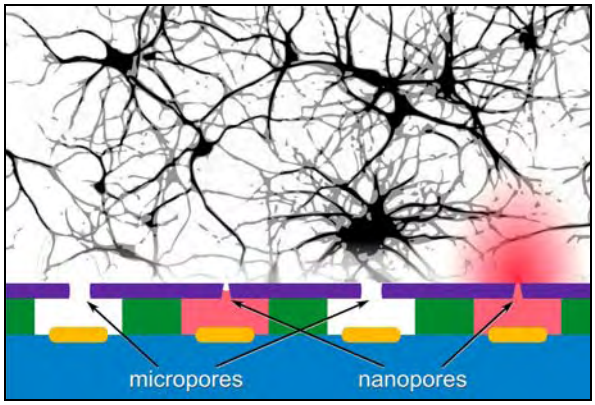

Fig. 1. Schematic cross-section of a chemical stimulation MEA. The MEA (blue with gold electrodes) has integrated microfluidics (green structure filled with pink solution) and a nanopore membrane (purple) for chemical stimulation of electroactive cells (black). Hydrophobic gating will control chemical release without diffusion. The right nanopore shows chemical release while the left is blocked. Electrodes will address cells through micropores, to enable simultaneous chemical stimulation and electrical recording.

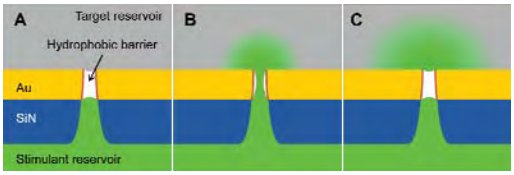

Fig. 2. Schematic cross-section of hydrophobic gating in a nanopore. (A) A water vapour barrier in a hydrophobic nanopore separates liquids on opposite sides of a membrane. (B) An applied voltage wets the pore, enabling chemical release. (C) Restoration of the barrier stops release.

Each microfluidic channel is fluidically and electrically isolated, and release from nanopores can be controlled electrically or by replacing the solution in the microfluidic channel. Half of the electrodes remain available for electrophysiological measurements through micropores in the bonded membrane [10].

Single nanopores were also fabricated in discrete chips. By mounting the chips in a custom microfluidic apparatus, transport properties of the nanopores were

investigated by measurements of ionic current, impedance spectroscopy, and fluorescence microscopy.

Electrical measurements of nanopores were performed with Ag/AgCl electrodes in a two-electrode configuration. Fluorescence microscopy observed the release of a carboxyfluorescein tracer from individual nanopores.

3 Results and discussion

We have developed a chemical stimulation MEA (Fig. 3), comprising an array of thirty nanopores addressed by individual microfluidic channels integrated on a 60 electrode MEA. The remaining electrodes are exposed through the microfluidic layer for electrical interfacing with cells. Localized chemical release from individual hydrophilic nanopores has been observed by fluorescence microscopy (Fig. 4).

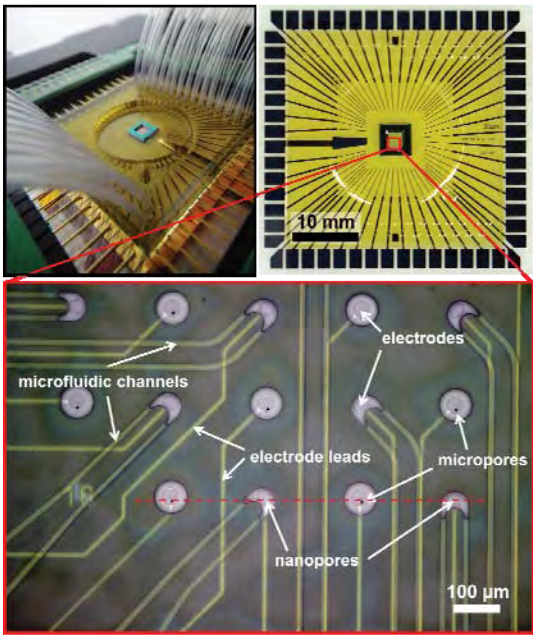

Fig. 3. A modified MEA with an integrated nanopore array and microfluidic network. (top left) The chemical stimulation MEA showing electrical and fluidic connection. (top right) The yellow area of the MEA contains microfluidic channels to address the nanopore array at the centre. (bottom) A detailed view of the microelectrode array shows the integrated microfluidic channels. The bright regions are a suspended nanomembrane, containing nanopores for chemical release and micropores for electrical recording. A schematic cross-section of the dashed red line is in Fig. 1.

Fig. 4. Fluorescent release from a single nanopore, controlled by filling the microchannel with a tracer. Contrast adjusted for clarity.

Nanopores have been fabricated with minimum diameters of approximately 30 nm in membranes thinner than 1 µm. Investigations with single hydrophobic nanopores have electrically actuated the hydrophobic barrier (Fig. 5). Presently, only limited reversibility of gating has been observed. Work is continuing to develop a reproducible dewetting mechanism.

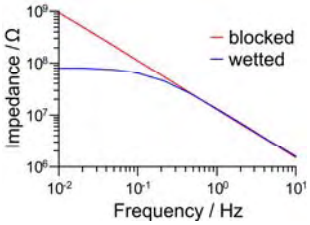

Fig. 5. Impedance spectra of a single nanopore. The blocked spectrum was recorded first, and shows only the capacitance of the nanomembrane. An applied voltage wetted the pore, after which the impedance spectrum shows the resistive pore conductance.

Forthcoming proof-of-concept experiments will measure the electrophysiological response of cultured dorsal root ganglion neurons to chemical stimulation of local subpopulations. This device will be broadly applicable to investigations of chemical signalling pathways.

Acknowledgement

Assistance from Sebastian Röhler, Angelika Stumpf, Dr. Gerhard Heusel, and Dr. Claus Burkhardt from the NMI Microsystems and Nanotechnology group is gratefully acknowledged. We would like to thank Dr. Elke Guenther for insightful discussions. This work is supported by the European Commission (7th Framework Programme, Marie Curie Initial systems Training Network "NAMASEN", contract n. 264872).

References

[1] P. G. Finlayson, R. Iezzi, Invest. Ophthalmol. Vis. Sci. 2010, 51, 3619.
[2] M. C. Peterman, J. Noolandi, M. S. Blumenkranz, H. A. Fishman, Proc. Natl. Acad. Sci. U. S. A. 2004, 101, 9951.
[3] D. Ghezzi, A. Menegon, A. Pedrocchi, F. Valtorta, G. Ferrigno, J. Neurosci. Methods 2008, 175, 70.
[4] R. W. Invernizzi, E. Esposito, Microiontophoresis and Related Methods. Encycl. Psychopharmacol. 2010, 775–781.
[5] A. Scott, K. Weir, C. Easton, W. Huynh, W. J. Moody, A. Folch, Lab Chip 2012.
[6] J. F. S. Cogollo, H. Dermutz, T. Zambelli, J. Vörös, In 8th Int. Meeting on Substrate-Integrated Microelectrode Arrays; Stett, A.; Zeck, G., Eds.; NMI Natural and Medical Sciences Institute at the University of Tuebingen: Reutlingen, 2012.
[7] O. Frey, T. Holtzman, R. M. McNamara, D. E. H. Theobald, P. D. van der Wal, N. F. de Rooij, J. W. Dalley, M. Koudelka-Hep, Sensors Actuators B Chem. 2011, 154, 96.
[8] P. D. Jones, B. Schroeppel, R. Roth, D. P. Kern, M. Stelzle, In Proceedings of the 39th International Conference on Micro and Nano Engineering; London, UK, 2013.
[9] J. M. Karlsson, F. Carlborg, F. Saharil, F. Forsberg, F. Niklaus, W. van der Wijngaart, T. Haraldsson, In Proceedings Micro Total Analysis Systems (microTAS) 2012; Okinawa, Japan, 2012; Vol. 1600, pp. 225–227.
[10] B. Hofmann, E. Kätelhön, M. Schottdorf, A. Offenhäusser, B. Wolfrum, Lab Chip 2011, 11, 1054.

Polymer-Based *In Vivo* Transducers with Conductive Polymer Mixture Polydimethylsiloxane Composite Electrodes

Asiyeh Golabchi[1*], Rouhollah Habibey[1], Marina Nanni[1], Francesca Succol[1], Axel Blau[1]

1 Fondazione Istituto Italiano di Tecnologia (IIT), Dept. of Neuroscience and Brain Technologies (NBT), Neurotechnologies (NTech), Via Morego 30, 16163 Genoa, Italy, www.iit.it
* Corresponding author. E-mail address: Asiyeh.golabchi@iit.it

Abstract
There is an emerging demand for flexible, tissue-conformable microelectrode implants that can follow the curvature and topography of the brain. This includes the optimization of electrode geometries and their electrical properties for the recording of individual spikes at cellular resolution. Currently, the integration of electrical components into flexible electronics and the generation of durable conductors is still challenging. Here we present a second generation of flexible, PDMS-based MEAs designed for recording within the media-longitudinal fissure in the prefrontal cortex (PFC) of rodents.

1 Methods

1.1 Design

The electrode-, track- and connection pad-patterns were sketched out with standard layout software (Expert, Silvaco), transferred into high-aspect ratio negative photoresist and molded into PDMS by soft lithography. The fabrication steps have been explained before [1]. Here, a polymer MEA (*polyMEA*) composed of 18 electrodes with diameters ranging from 50 µm to 130 µm in 10 µm increments was designed for recording from different brain layers (Fig. 1).

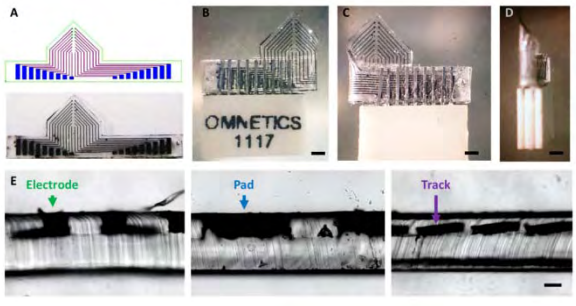

Fig. 1. Overall layout and connecting scheme for the presented *in vivo polyMEA*. A) CAD design and resulting *polyMEA*; pad width: 414 µm. B-D) *polyMEA* squeeze-clamped between an Omnetics strip connector (A79006-001) 0.757 mm pitch, double-row pin connector (front, back and side). E) Cross section views of the *polyMEA* electrodes (left), pads (middle) and buried tracks (right). Scale bars: 1 mm (B-D), 100 µm (E).

1.2 Material Selection

PDMS (Sylgard 184, Dow Corning) was selected as the insulator substrate due to its flexibility and closer Young's modulus to that of brain tissue. It is supplied as a two-component system being composed of a base and a curing agent (10:1 ratio (v/v)). As conductive material we chose a mixture of PEDOT:PSS (P Jet 700, Heareus) with additives (2.5% DMSO, 2.5% sorbitol) and carbon and graphite in PDMS to form a conductive composite. These were mixed until the DC resistance dropped below 10 kΩ per 1 cm distance.

1.3 Fabrication

After filling the cavities of the PDMS scaffold with the conductive material and curing it, the probe backside was insulated with a thin layer of PDMS. The probe was then folded along the shaft edge and a transparency temporarily slid between them to push its pads against the pins of an Omnetics nano-connector. The impedance characteristics of the electrodes were evaluated before and after connecting to the connector. For ensuring that the materials were biocompatible, we cultured neurons on *in vitro* probes made from the same materials and compared them with neurons on commercial MEAs (Multi Channel Systems) as controls.

2 Results

Biocompatibility was confirmed *in vitro* with cortical neurons on flexible MEAs (Fig. 2). Over a recording period of 40 days, the signal-to-noise ratio was about five, indicating that the probes and materials are sufficiently stable to be used in long-term recordings (Fig. 3).

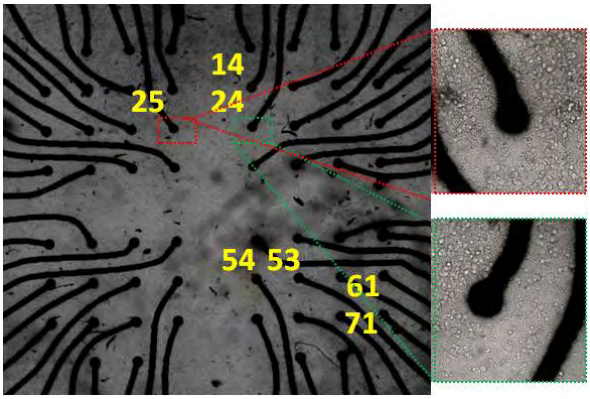

Fig. 2. Absence of cytotoxicity as validated *in vitro* for a cortical network (40 DIV) (electrode pitch: 400 µm)

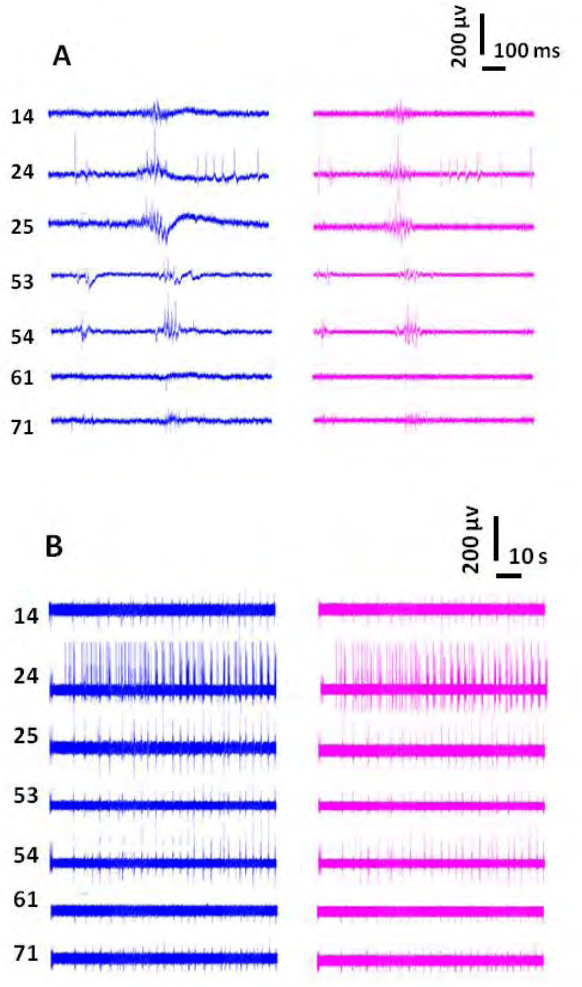

Fig. 3. High signal-to-noise ratio in exemplary *in vitro* recordings (40 DIV). A) Short-term recording window with individual spikes, B) Long-term recording window. The low frequency noise was removed by a Bessel 2nd order, high-pass filtered (cut-off at 50 Hz).

The impedance measurements before and after connecting the probes to the connectors also confirmed a reliable squeeze-clamping interconnection and the functionality of all 18 micro-electrodes (Fig. 4).

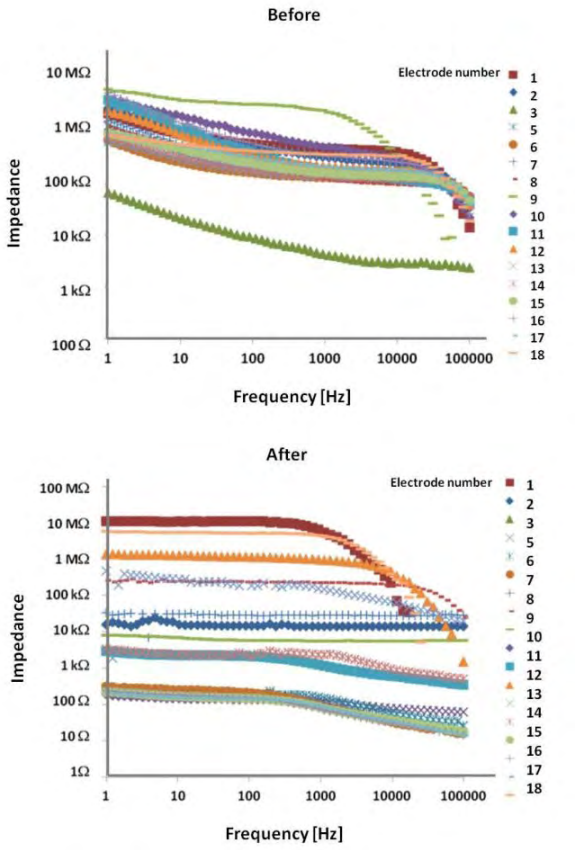

Fig. 4. *polyMEA* impedance characteristics before and after connecting the probe to the Omnetics connector.

3 Conclusion

We developed a flexible MEA with 18 electrodes suitable for being implanted into the brain. We successfully evaluated the connection between the individual probe pads and their corresponding connector pins. The impedance of most recording sites in this *in vivo polyMEA* is below 1 MΩ at 1 kHz. This probe will be considered for chronic recordings.

Acknowledgement

We thank the Fondazione Istituto Italiano di Tecnologia for supporting this study.

References

[1] Blau, A., ET AL. (2011). Flaxible all-polymer microelectrode arrays for the capture of cardiac and neuronal signals. *Biomaterials, 32(7)*, 1778-86.

Nanostructured Diamond Microelectrode Arrays for Neural Recording and Stimulation

Gaëlle Piret[1,2*], Clément Hébert[3], Lionel Rousseau[4], Emmanuel Scorsone[3], Raphaël Kiran[3], Myline Cottance[4], Gaëlle Lissorgues[4], Marc Heuschkel[5] , Serge Picaud[6] , Blaise Yvert[1,2], Philippe Bergonzo[3]

1 INSERM, Clinatec, U1167, F-38 000 Grenoble, France.
2 CEA-Léti, Clinatec, U1167, F-38 000 Grenoble, France.
3 CEA LIST, Diamond Sensors Laboratory, F-91191 Gif-sur-Yvette, France
4 Université Paris-Est, ESYCOM, ESIEE Paris, 2 boulevard Blaise Pascal, 93162 Noisy le Grand, France
5 Qwane Biosciences SA, EPFL Innovation Park, CH-1015 Lausanne, Switzerland
6 Institut de la Vision, UMRS 968 Inserm/UPMC, UMR7210 CNRS, 17 Rue Moreau, 75012 Paris, France
* Corresponding author. E-mail address: gaelle.offrancpiret@cea.fr

Abstract
The development of stimulation implant and neuronal recording system currently needs highly stable and biocompatible microelectrode arrays (MEAs) offering large number of electrodes. However, high density integration requires small diameter electrodes leading to both a low signal to noise ratio (due to high impedance) and a small charge injection capacity. These issues could be overcome by nanostructuration of the electrode surface. In this context, we developed MEAs made of nano-structured diamond, which is known to be biocompatible and chemically stable.

1 MEA fabrication

Two types of MEAs were fabricated on glass substrates using micro-fabrication steps as shown in figure 1. One includes the growth of nanocrystalline boron-doped diamond (BDD), and the other a combination of BDD and Carbon Nanotubes (CNTs) growth.

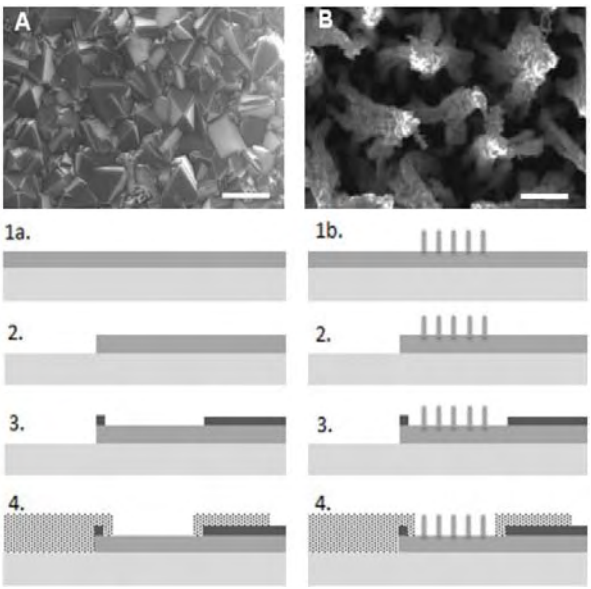

Fig. 1. Scanning Electron Microscopy (SEM) images of A) a BDD electrode, and B) a BDD/CNTs electrode, and MEAs fabrication steps: 1. BDD growth (1a) or both CNTs and BDD growth (1b), 2. BDD etching, 3. Metal deposition, 4. Passivation (SU8 or Si_3N_4). Scale bar, 600nm.

The first BDD MEA has BDD electrodes exhibiting a macro-structured surface (figure 1. A) [1] and the second CNTs/BDD MEA has nanostructured electrodes covered with 3 µm long CNTs coated by 30nm of BDD, resulting in a high-aspect ratio nanostructured surface and a very large surface area (figure 1. B).

2 MEA characterization

MEA types can be assembled on a printed circuit board, compatible with the data acquisition system from MultiChannelSystems (MCS) as shown in figure 2.

MEAs were characterized by cyclic voltammetry (CV), electrochemical impedance spectroscopy, and their noise level was measured with the MCS set up used for neural recording. CV measurements show a wide potential window that is about 3.1 V for BDD electrodes, due to the typical BDD reduction and oxidation of water occurring at -1.5 V and 1.9 V. The potential window of the nanostructured CNTs/BDD electrodes is rather between 2.4 and 2.6 V but the double layer capacitance is increased by a factor of 184 compared to the BDD ones. The impedance is divided by a factor 84 for the nanostructured CNTs/BDD MEA compared to the BDD MEA [2], and the noise level is decreased as well.

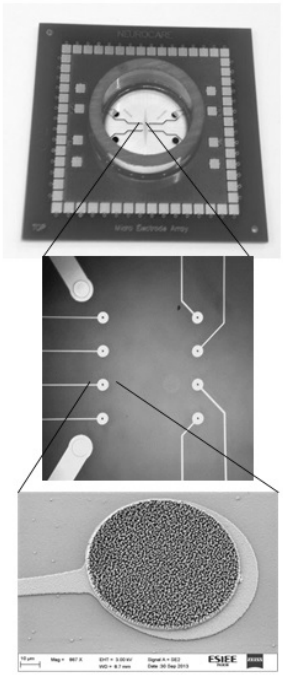

Fig. 2. MEAs packaging. MEAs are fabricated on a glass chip (SEM pictures showing the electrodes on glass) that is assembled on a printed circuit board, compatible with the data acquisition system from MultiChannelSystems (MCS).

3 Conclusion

Micro-electrodes made of the CNTs/BDD composite offer higher surface areas, an increased double capacitance layer, lower impedance and noise in comparison with the BDD ones. Such MEAs are thus promising for in vitro and in vivo studies.

Acknowledgement

The authors would like to thank the French National Research Agency for their financial support through the MEDINAS project as well as the European Community's Seventh Framework Programme (FP7) under grant agreement n° 280433 (NEUROCARE project).

References

[1] R. Kiran, L. Rousseau, G. Lissorgues, E. Scorsone, A. Bongrain, B. Yvert, S. Picaud, P. Mailley, and P. Bergonzo. Multichannel Boron Doped Nanocrystalline Diamond Ultramicroelectrode Arrays: Design, Fabrication and Characterization. Sensors, 2012, 12(6): 7682–7700.

[2] C. Hébert, J-P. Mazellier, E. Scorsone, M. Mermoux, P. Bergonzo. Boosting electrochemical properties of nanocrystalline diamond electrode using a vertically-aligned carbon nanotube scaffold. Carbon, 2014, 71: 27–33

New Developments on the Fabrication of High Density and Low Density Diamond-Based MEA

A. Battiato[1,2,4], E. Bernardi[1,2,4], V. Carabelli[3,4], E. Carbone[3,4], S. Gosso[3,4], P. Olivero[1,2,4], A. Pasquarelli[5], F. Picollo[2,1,4*]

1 Physics Department and NIS Inter-departmental Centre, University of Torino, via P. Giuria 1, 10125 Torino, Italy
2 INFN section of Torino, via P. Giuria 1, 10125 Torino, Italy
3 Department of Drug Science and Technology and NIS Inter-departmental Centre ,University of Torino, Corso Raffaello 30, 10125 Torino, Italy
4 Consorzio Nazionale Inter-universitario per le Scienze fisiche della Materia (CNISM), Section of Torino
5 Institute of Electron Devices and Circuits, Ulm University, 89069 Ulm, Germany
* Corresponding author. E-mail address: picollo@to.infn.it

Abstract

In the present work we report about the development of our activity on diamond modification devoted to Multi Electrode Arrays realization. High energy (MeV) ion implantation has been used to obtain biosensors having different configuration with the employment of suitable masks and techniques. Our diamond-based devices are developed for amperometric measurements and chromaffin cells were chosen as first target of analysis. The investigation of the mechanisms involved in the catecholamine (adrenaline) secretion is in fact crucial in neuroscience research in order to achieve a better understanding of the signal transmission among neurons.

1 Diamond microfabrication

The development of a diamond-based device has the aim of addressing to different extents, which are not met by conventional biomaterials (silicon, metals and metals oxides, polymers), robustness and reproducibility in performance over repeated bio-sensing cycles, bio-compatibility and long term stability for *in vitro* measurements.

Our three-dimensional lithographic technique (Deep Ion Beam Lithography – DIBL) in diamond is based on the combination of ion beams with energy of the order of MeVs with other advanced lithographic techniques based on laser beams and ion beams with energy of the order of keVs (Focused Ion Beam – FIB). The innovative fabrication scheme allows to modify diamond properties tuning the conductivity and the chemical reactivity of this material.

The biosensors are fabricated implanting He^+ ions (energy range: 0.8 – 2 MeV) on high-purity monocrystalline CVD (Chemical Vapour Deposition) diamond samples. Suitably aligned metal masks and variable-thickness contact masks were employed to define "highly damaged" regions, i.e. converted from sp_3 diamond bonds to sp_2 graphitic-like bonds, with emerging end-points with micrometric resolution.

The damage profile of the above-mentioned ions in the diamond lattice is reported in Fig.1, as derived from the SRIM-2008.04 Monte Carlo Simulation code by setting a displacement energy value of 50 eV. The damage profile is derived by assuming a simple linear dependence of the defect density from the implantation fluence, i.e. ignoring complex non-linear processes such as self-annealing and defect-defect interaction. In such a drastically simplified approach it is nonetheless possible to have a satisfactory estimation of the thickness of the buried graphitized layer which is formed upon thermal annealing, by setting a "graphitization" threshold for the vacancy density of ~$9 \cdot 10^{22}$ cm^{-3} [1], as shown in Fig.1.

After diamond implantation, a thermal annealing at 900 °C for 2 hours was performed in order to convert the damaged region into graphite.

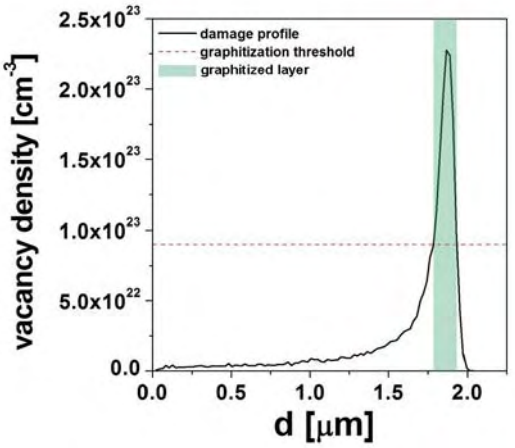

Fig. 1. Damage density profile (black continuous line) for a 1.1 MeV He^+ implantation at a fluence of $1 \cdot 10^{17}$ cm^{-2}. The graphitization threshold is reported in the red dashed line. The graphitized layer formed upon thermal annealing is highlighted in the green box.

This fabrication process provides buried highly conductive graphitic micro-channels (resistivity ~1 mΩ·cm) embedded in a highly insulating (resistivity ~10^{14} Ω·m) and chemically inert diamond matrix, whose emerging zones act in the central area as multiple bio-sensing electrodes for cellular *in vitro* record-

ings and at the chip peripheral provide contacts for chip bonding.

2 Devices configuration

DIBL technique is extremely versatile, has a scalable approach and allows the realization of different geometries of the devices for different sensing goals.

2.1 Low density MEA

The diamond implantation is obtained using a broad (spot size up to several mm^2) and uniform ion beam. Free-standing masks are employed to define the geometry of the graphitic paths. They were realized on aluminium thin film by means of metal ablation using an high power pulsed laser. Emerging end-points were obtained suitably aligning the mask over variable thickness metal deposition [2]. This approach allows to obtain a 16-channel multi-cell setup (Fig.2), where a culture of chromaffin cells can be directly grown over the surface of the device.

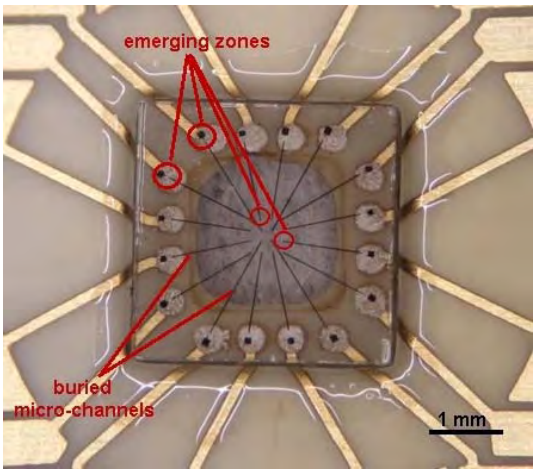

Fig. 2. Bottom-view image of low density diamond-based biosensor: 16-channel multi-cells setup having the following graphitic paths dimensions: ~30 µm wide, ~1 mm long and electrodes dimensions: ~30 µm × ~5 µm is shown. Buried regions and emerging zones, where the signal is collected, have been highlighted.

2.2 High density MEA

In such configuration thin metal films (< 5 µm) are directly deposited over diamond surface and subsequently microfabricated by means of FIB milling in order to obtain variable thickness masks. This strategy allows to define a more resolved geometry of the graphitic structures: a high density 16-channel single-cell setup was realized (Fig.3), where all the implanted paths are emerging inside a 20×20 μm^2 area (typical chromaffin cell dimensions), thus giving the possibility to study in detail the single-cell secretion of catecholamines.

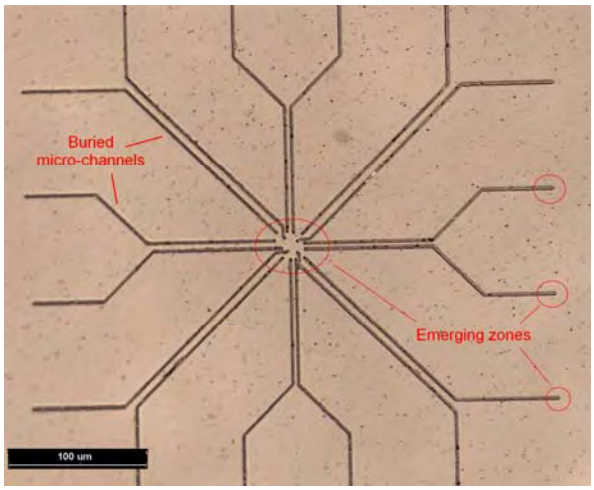

Fig. 3. Image of high density diamond-based biosensor: 16-channel single-cell setup having the following graphitic paths dimensions: ~3 µm wide, ~400 µm long and electrodes dimensions: ~3 µm × ~3 µm is shown. Buried regions and emerging zones, where the signal is collected, have been highlighted.

3 Conclusions

DIBL has been shown to be a scalable and versatile technique for diamond-based biosensors realization. Future activities will be focused on the amperometric measurements of chromaffin cells exocytosis.

Acknowledgement

The authors wish to thank Ottavio Giuliano for the kind technical support.

This work is supported by the following ongoing projects: FIRB “Futuro in Ricerca 2010” (CUP code: D11J11000450001) funded by MIUR; “A.Di.N-Tech.” (CUP code: D15E13000130003), “Linea 1A - ORTO11RRT5” projects funded by the University of Torino and “Compagnia di San Paolo”; “MicroDiBi” project funded by “BioPMed” and Regione Piemonte and “DiNaMo” (project n° 157660) by National Institute of Nuclear Physics.

References

[1] Olivero P., Rubanov S., Reichart P., Gibson B. C., Huntington S. T., Rabeau J. R., Greentree A. D., Salzman J., Moore D., Jamieson D. N., Prawer S., (2006). Characterization of three-dimensional microstructures in single crystal diamond, *Diamond and Related Materials*, 15, 1614 -1621

[2] Picollo F., Gosso S., Vittone E., Pasquarelli A., Carbone E., Olivero P., Carabelli V., (2013). A new diamond biosensor with integrated graphitic microchannels for detecting quantal exocytic events from chromaffin cells. *Advanced Materials*, 25, 4696–700

[3] Picollo F., Gatto Monticon D., Olivero P., Fairchild B. A., Rubanov S., Prawer S., Vittone E., (2012). Fabrication and electrical characterization of three-dimensional graphitic microchannels in single crystal diamond. *New Journal of Physics* 14, 053011.

Graphene and Silicon-Nanowire Field Effect Transistors for Neuronal Interfacing

Farida Veliev[1], Anne Briancon-Marjolet[2], Mireille Albrieux[3], Dipankar Kalita [1], Antoine Bourrier[1], Zheng Han[1], Vincent Bouchiat[1], Cécile Delacour[1*]

1Institut Néel, Grenoble France
2 Laboratoire HP2, UJF-INSERM U1042, Grenoble, France
3 Grenoble Institut des Neurosciences, Inserm, Univ. Joseph Fourier, Grenoble, France
* Corresponding author. E-mail address: cecile.delacour@grenoble.cnrs.fr

Abstract

Due to their high sensitivity and strong coupling to the cell membrane Graphene and Silicon Nanowire Field Effect Transistors (SiNW-FETs) are considered to be powerful devices for interfacing electrogenic cells. At Institut Néel we study the interface of both materials to E16 mouse embryonic primary hippocampal neurons in terms of cell growth, electrical recording/stimulation and future applications. Here we present the capabilities of solution-gated Graphene and SiNW-FETs and in-vitro recording of action potentials from cultured neurons.

1 Introduction

Recently bioelectric interfacing of brain regions and single neurons has become an exciting and growing field of research. Several research groups have already reported successful electrical recording from cultured neurons [1, 2] and cardiomyocyte cells [3] using SiNW-FETs. However, following the propagation of neural signals through mature networks remains challenging. Graphene has also been shown to be a promising material for neuron culturing [4-6] and successfully used for recording electrical signals from cardiomyocyte cells [7, 8], hinting at the feasibility of graphene-neuron-interface and its possible applications for neural prostheses.

2 Methods

2.1 Device fabrication and characterization

Arrays of 100nm wide and 7µm long SiNW-FETs were realized by a top down approach using standard lithography techniques and reactive ion etching. CVD grown single layer graphene sheet was transferred on Si-SiO2 substrate. Arrays of 40µm wide graphene stripes with varying length were etched in oxygen plasma using a photoresist mask. Source/Drain contacts were realized by Ti/Au and further passivated using photoresist S1818.

Both devices were characterized in terms of gate effect and sensitivity to rapid potential changes. The measurements were carried out in cell culture medium. A voltage sweep or a rapid small voltage pulse (1ms, 5-100mV) was applied to the medium through a Pt-electrode in order to modulate the carrier density and thus the device conductance.

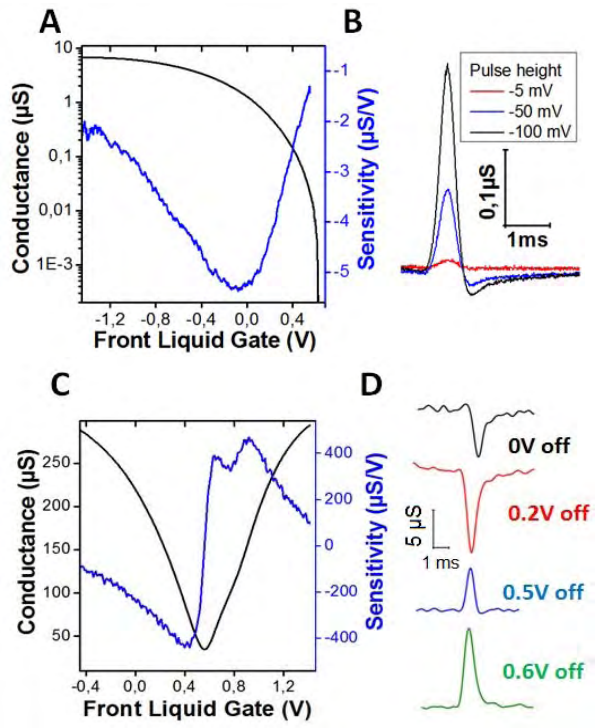

Fig.1: Gate effect on SiNW and G-FETs recorded in cell culture medium. (A) Conductance of SiNW-FET as function of front liquid gate measured at a polarisation voltage of 250 mV. **(B)** Detection of potential spikes using SiNW-FET: a 1 ms long Gaussian voltage pulse with varying amplitude was applied to the cell culture medium through a Pt-electrode at a polarisation voltage of 100 mV. **(C)** Conductance of G-FET as function of front liquid gate measured at a polarisation voltage of 10 mV. (D) Detection of potential spikes using G-FET: a 1 ms long 50 mV high Gaussian voltage pulse with varying offset was applied to the cell culture medium through a Pt-electrode at a polarisation voltage of 10 mV. The signal amplitude could be tuned by varying the liquid gate offset. The sign of the detected signal is inverted by transition from n- to p-branch.

It has been shown, that SiNW-FETs have a very high signal-to-noise ratio and on/off ratio of 10^4 with sensitivity of 5.5µS/V. Graphene-FETs (G-FETs) also show a clear response to the potential changes with higher sensitivity up to 0.4mS/V. The

conductance signal amplitude of G-FETs could be tuned by varying the liquid gate offset. Figure 1 shows the gate effect and the detection of 1ms long 5 to 100mV high Gaussian voltage pulses in cell culture medium.

2.2 Neuron Culture

Hippocampal neurons were dissociated as previously described [9] from E16.5 mouse embryos. The cell suspension was transferred to sterilized poly-L-lysine covered chip surfaces. Neurons were then incubated at 37°C with 5% CO2 for periods of 19-21 days.

3 Results

The hippocampal neuron cells could be grown up to maturation stage on both SiNW- and G-FETs. High resolution Ca^{2+} imaging as well as immunofluorescent (IF) microscopy were both used to investigate the maturation and the connectivity of cells, showing the presence of Ca^{2+} channels and a high density of synapses around the dendrites and soma (Fig.2A, B).

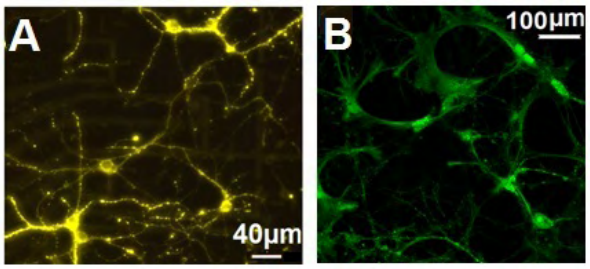

Fig.2: (A) IF microscopy image of synapsin staining, 21DIV. **(B)** High resolution Ca2+ imaging using fluo4-labeling, 19DIV.

In-vitro electrical measurements of signal from random neuron cultures were carried out showing neuro-sensing ability of both devices (Fig.3A, B).

In conclusion it has been shown, that SiNW- and G-FETs are promising devices for neuron interfacing due to their excellent sensitivity and subcellular resolution and high stability respectively with living cells. For further investigation of neural activity these measurements will be performed on patterned neural networks combined with electrical stimulation.

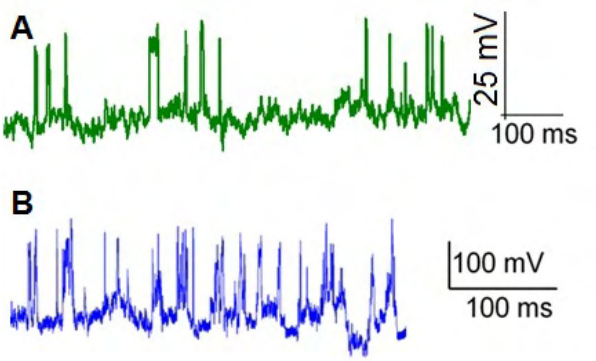

Fig.3: In-vitro measurements on SiNW- and G-FETs (A) In-vitro electrical measurement of signal from cultured neurons using G-FET, 21DIV. **(D)** In-vitro electrical measurement of signal from cultured neurons using SiNW-FET, 19DIV.

Acknowledgements

We thank C. Villard for support in electrical measurements and cell culture, E. André for parylene deposition and T. Crozes (NanoFab) for micro and nanofabrication.

References

[1] A. Stett, B. Müller, P. Fromherz (1997): Two-way silicon-neuron interface by electrical induction. *Phys. Rev. E, **55**, 1779-1782.*

[2] F. Patolsky, B. Timko, G. Yu, Y. Fang, A. Greytak, G. Zheng, C. Lieber (2006): Detection, stimulation, and inhibition of neuronal signals with high-density nanowire transistor arrays. *Science, **313**, 1100-1104.*

[3] *J. F. Eschermann, R. Stockmann, M. Hueske, X. Thang Vu, S. Ingebrandt, A. Offenhäusser (2009): Action potentials of HL-1 cells recorded with silicon Nanowire transistors. Appl. Phys. Lett. E, **95**, 083703.*

[4] A. Benadali, L. Hess, M. Seifert, V. Forster, AF Stephan, J. Garrido, S. Picaud (2013): Purified neurons can survive on peptide-free graphene layers. *Adv. Healthcare Matter,* DOI: 10.1002/adhm.201200347

[5] M. Lorenzoni, F. Brandi, S. Dante, A. Giugni, B. Torre (2013): Simple and effective graphene laser processing for neuron patterning application. *Scientific Reports, 3:1954,* DOI: 10.1038/srep01954

[6] SY Park, J. Park, SH Sim (2011): Enhanced differentiation of human neural stem cells into neurons on graphene. *Adv Matter, **23**, H263-H267.*

[7] L. Hess, M. Jansen, V. Maybeck, M. Hauf, M. Seifert, M. Schutzmann, I. Sahrp, A. Offenhäusser, J. Garrida (2011): Graphene transistors for bioelectronics: Graphene transistor arrays for recording action potentials from electrogenenic cells. *Adv. Matter, **23**, 5045-5049.*

[8] T. Cohen-Karni, Q. Qing, Q. Li, Y. Fang, C. Lieber (2010): Graphene and Nanowire transistors for cellular interfaces and electrical recording. *Nano Lett., **10**, 1098-1102.*

[9] Kaech, S., & Banker, G. (2006). Culturing hippocampal neurons. *Nature protocols, 1(5), 2406-2415.*

MEA Technology

Advances in Fabrication and Instrumentation

A CMOS-based Microelectrode Array System for Stimulation and Recording in Neural Preparations In Vitro

Takashi Tateno[1*]

1 Graduate School of Information Science and Technology, Hokkaido University, Sapporo, Japan
* Corresponding author. E-mail address: tateno@ist.hokudai.ac.jp

Abstract
In this report, we describe the system integration of a CMOS chip that is capable of both stimulation and recording of neurons or neural tissues to investigate electrical signal propagation within cellular networks in vitro. The overall system consisted of three major subunits; a 5.0 mm × 5.0 mm CMOS chip, a reconfigurable logic device (field-programmable gate array, FPGA), and PC software. To test the system, microelectrode arrays (MEAs) were used to extracellularly measure activity of cultured rat cortical neurons and mouse cortical slices. The MEA had 64 bidirectional (stimulation and recording) electrodes. In addition, the CMOS chip was equipped with dedicated analog filters and amplification stages and a stimulation buffer. Signals from the electrodes were sampled at 15.6 kHz with 16-bit resolution. The measured input-referred circuitry noise was 10.1 μV root mean square (10 Hz to 100 kHz), which allowed reliable detection of neural signals ranging from several millivolts down to approximately 60 μV_{pp}. Experiments involving the stimulation of neurons with several spatio-temporal patterns and the recording of the triggered activity were carried out. An advantage over current microelectrode arrays, as demonstrated by our experiments, includes the ability to stimulate (voltage stimulation, 5-bit resolution) spatio-temporal patterns in arbitrary subsets of electrodes. Furthermore, the fast stimulation reset mechanism allowed us to record neuronal signals from a stimulating electrode around 5 ms after stimulation.

1 Introduction

Microelectrode arrays (MEAs) allow researchers to stimulate and record electrical signals at the single-cell level, and thus have become an indispensable tool in the study of neural networks properties such as network formation, network dynamics and signal processing. An advantage of MEAs is that they can be arranged in planar structures using microfabrication technology, allowing for the investigation not only of neuronal cultures and brain slices in vitro, but also of animal tissues in vivo. Several recent studies also reported on the system integration of a CMOS chip that is capable of both recording and stimulation of neurons or neural tissues [1]. However, the frequency range of recording signals was not easily adjustable for specific targets, including action potentials and local field potentials. In addition, stimulation in typical MEA systems has been strictly limited to simple pulse patterns and few electrodes. In this study, we report on the system integration of a CMOS chip that is capable of both stimulation and recording of neurons or neural tissues, permitting investigation of electrical signal propagation within cellular networks in vitro.

2 Materials and methods

The total system includes three major components: (1) the application-specific integrated circuit (ASIC) chip, (2) the field programmable gate array (FPGA) board for chip evaluation, and (3) the PC (Fig. 1). In the ASIC chip, each of the 64 readout channels includes amplification and filter stages. The gain and filter settings of the stages can be programed digitally. Sixteen channels are then multiplexed and buffered by one amplifier in the next stage, followed by an analog-to-digital converter (ADC) working at 16.5 kHz to provide 16-bit resolution in the FPGA board. The data are subsequently transferred into a data processing unit in the FPGA. In contrast, the digital interfaces (DIs) in the chip decode commands that are used to define the parameters of signal amplitude and bias settings as well as the stimulation control parameters. The on-chip system includes 64 stimulation buffers and 5-bit DACs. The command decoder in the DI allows for specific DAC selection and configures the buffer in voltage mode. Each channel is also equipped with a stimulation artifact suppressor, which reduces the dead time of the system after each stimulation pulse.

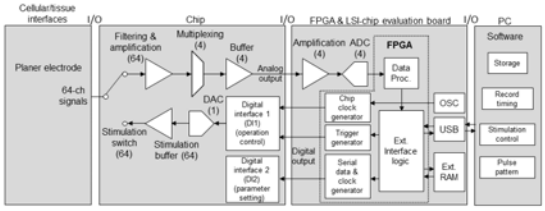

Fig. 1. Block diagram of the CMOS-based MEA system.

To test the properties of the system, commercially available MEAs (MED-P210A and MED-P515A, Alpha MED Scientific, Japan) were used to extracellularly measure activity of rat cultured cortical neurons [2] and mouse cortical slices [3].

3 Results

The midband gain of the on-chip bandpass filter was selectable via the DIs from one of four gains, measured to be 26.2, 29.6, 31.8, and 39.4 dB. The tunable upper corner frequencies of the lowpass filter were 0.80, 1.9, 3.9, 5.5, and 8.3 kHz (Fig. 2A), and the lower corner frequencies of the highpass filter were 3.1, 8.1, 28.6, and 101 Hz (Fig. 2B). The input-referred noise was 10.1 μVrms (10 Hz–100 kHz) at a gain of 31.8 dB. This is comparable to the thermal noise of the platinum electrodes in physiological saline solution, which was measured to be 6.19 μVrms for 50 μm × 50 μm electrodes in a band between 10 Hz and 100 kHz. The total noise in the measurements was dominated by the background activity of the neuronal culture, which was on the order of 20–40 μVrms in a dense culture. The measured power consumption of the chip was relatively high at 167 mW at 3.7 V because of stimulation for bipolar voltage pulses (1.0–2.5 V).

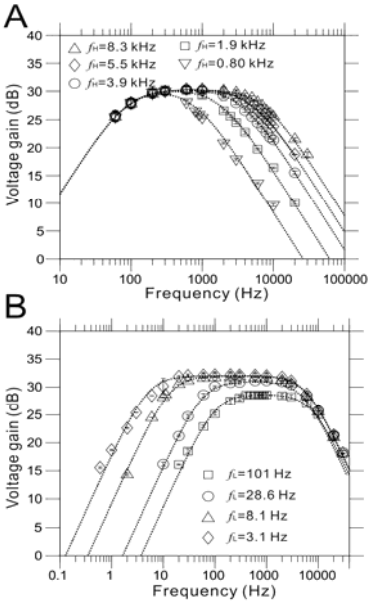

Fig. 2. Filter properties of the ASIC chip. A, Upper corner frequencies (f_H) of the lowpass filter. B, Lower corner frequencies (f_L) of the highpass filter.

Neural signal recordings from rat cultured cortical neurons were also performed with MEAs after 37 days in vitro. Action potentials could be successively identified based on the recording (Fig. 3A). Using the same system, local field potentials in a mouse cortical slice were recorded from over 20 MEA channels (Fig. 3B) when a bipolar pulse of 1.0 V was applied to a single site (Ch. 29).

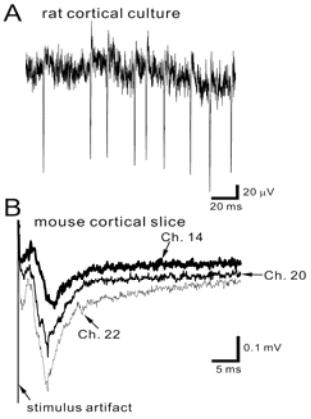

Fig. 3. Extracellular recording of neural signals. A, Spontaneous activity of rat cultured cortical neurons. B, Evoked activity of a mouse cortical slice (Chs. 14, 20, and 22) when a bipolar short pulse (125-μs pulse width) was applied to a single electrode (Ch. 29).

4 Conclusion

We describe an ASIC system designed for electrical stimulation of neural tissue using MEAs. Our design is intended for applications in systems requiring simultaneous stimulation and recording of signals from various types of neural tissue, both in vitro and in vivo. The developed ASIC comprises 64 independent stimulation channels capable of generating almost arbitrarily defined bipolar voltage pulses below the amplitude of 2.5 V with 5-bit resolution. Each channel is also equipped with a stimulation artifact suppressor controlled in real time, which reduces the dead time of the system after each stimulation pulse.

Acknowledgements

This work was supported by the Funding Program for Next Generation World-Leading Researchers (NEXT program). The author would like to thank to Dr. Jun Nishikawa.

References

[1] Hafizovic S, Heer F, Ugniwenko T, Frey U, Blau A, Ziegler C, Hierlemann A (2007): A CMOS-based microelectrode array for interaction with neuronal cultures. *J Neurosci Meth, 164(1), 93-106.*

[2] Jimbo Y, Kasai N, Torimitsu K, Tateno T, Robinson HP. (2003): A system for MEA-based multisite stimulation. *IEEE Trans Biomed Eng, 50(2), 241-248.*

[3] Tateno T, Harsch, A. Robinson H. P. C (2004): Threshold firing frequency–current relationships of neurons in rat somatosensory cortex: type 1 and type 2 dynamics. *J Neurophysiol, 92(4), 2283-2294.*

A Novell LabVIEW™ based Multi-Channel Closed-Loop Stimulator

Christiane Thielemann*, Maike Stern, Christoph Nick and Robert Bestel

1 University of Applied Sciences Aschaffenburg, BioMEMS lab, Germany
* Corresponding author. E-mail address: Christiane.thielemann@h-ab.de

Abstract
Understanding learning, memory and the control of motor functions are still great challenges in neuroscience. In-vitro cell cultures have been helpful to study neural networks on a small scale. In this context closed-loop stimulation is a powerful tool to fully, bi-directionally interact with such an in-vitro neural network. We present an easy-to-use, modifiable, open and inexpensive system for the recording and electrical stimulation with microelectrode arrays based on *National Instruments*® Software and Hardware components.

1 Background

Microelectrode Arrays (MEA) are a widely used tool for studying cardiac and neural activity. While recording of spontaneous activity can be used to evaluate the effects of drugs or radiation [1], electrical stimulation is essential to fully interact with an in-vitro network. Thus, for a bi-directional interface, a closed loop stimulation set up is desirable, which enables recording, online-data processing and electrical stimulation [2]. We herein present an easy accessible, open, and expandable closed-loop stimulator for up to 32 electrodes, based on the programming software LabVIEW™. This system enables on one hand recording and processing of neural signals and on the other hand elaborated electrical stimulation. Further and very important for closed loop systems, it features the interaction between these separated tasks, hence allowing the development of complex experiment designs.

2 Methods

For the system design we set the following constraints, which define the hard- and software characteristics:

- microelectrode array with 60 electrodes
- min. 5 kS/s sampling rate
- ± 0,8 V peak to peak pulse for stimulation [3]
- 400 µs – 600 µs stimulating pulse duration [3]
- independent output channels.

The system consists of a recording and a stimulation stage, which are built into a CompactDAQ USB Chassis as depicted in Figure 1. The recording stage is composed of an amplifier (MEA1060-inv, Multichannel Systems®, Reutlingen, Germany) connected to two National Instruments (NI®) measurement modules (NI9205), providing a total sample rate of 250 kS/s for 32 analogue recording channels each. Hence, considering the 60 electrodes of the microelec-

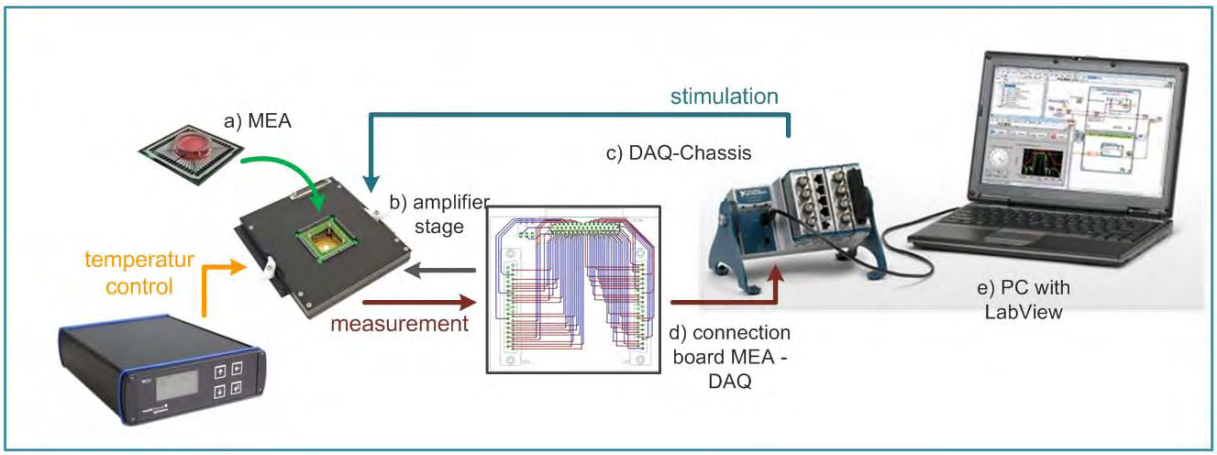

Fig. 1: Closed-loop system overview. a) Cell networks are cultivated on a MEA chip. b) The electrodes of the chip are connected to an amplifier stage [Multichannel Systems®]. c) A DAQ chassis with two NI measurement modules and two stimulation modules serves as hardware-software interface. Electrodes can be addressed individually and the 32 stimulation channels can cover multiple stimulation patterns. d) A connection board allows the data transfer between MEA and DAQ boards and at the same time supplies the amplifier stage with voltage. e) The user interface of the closed-loop system is implemented in LabVIEW™.

trode array and the overall sample rate of both modules (500 kS/s), recordings can be performed at a sampling rate of up to 8.2 kHz with a resolution of 16 bit. The lower resolution limit of the system can be improved from 96.0 µV down to 4.0 µV by adjusting the input voltage range.

The two stimulation modules (NI9264) consist of 32 analogue channels with a voltage range of ± 10 V and a maximum update rate of 25 kS/s for each channel. Electrodes to be stimulated can be freely chosen as the stimulation channels are plugged into the Multichannel Systems amplifier stage. Therefore different areas of the microelectrode array can be stimulated simultaneously further allowing the development of elaborated time and space dependent stimulation protocols. Moreover, even high-frequency stimulations at frequencies in the range of 5 – 10 kHz can be conducted [4].

The interface of the closed-loop system is implemented in LabVIEW™. On one panel of the graphical user interface the current data measurement is shown, while the stimulation parameters can be set or adjusted on a separate stimulation panel. Basic signal processing like spike detection is performed in real time by a threshold based algorithm. Thresholds are calculated, based on the standard deviation (SD) of a recorded data subset with a length of 1ms containing solely background noise. The derived SD value of the standard deviation is multiplied by an adjustable factor, which is set to 3 by default. Once the signal crosses this calculated value, the minimum of the spike is stored as a spike-timestamp [5].

Since executable files can be generated from LabVIEW™, the application program can be run by any PC without a LabVIEW™ licence, making the system very flexible and mobile.

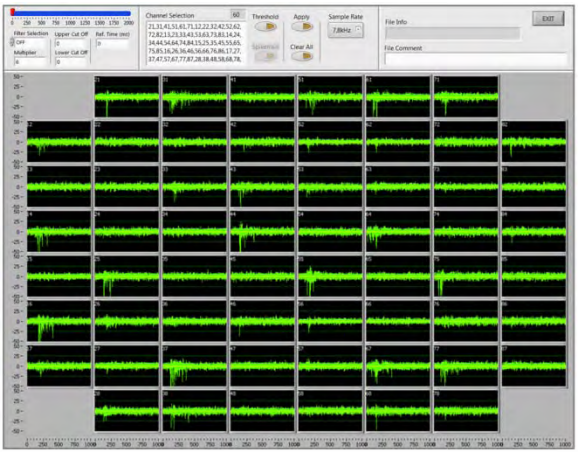

Fig. 2: LabVIEW™ based measurement interface of the closed-loop system. Measurements are displayed for every electrode individually. The upper panel offers various settings, e.g. filter and channel selection as well as different sample rates.

3 Conclusion and Outlook

A variable, mobile LabVIEW™ based multichannel Closed-Loop Stimulator has been developed and tested. Sampling rates of up to 8.2 kHz with 60 channels and stimulations with up to 25 kHz at 32 channels are possible. By fusing the different subtasks, stimulation, recording, and signal processing into a single interface, our setup allows more complex and elaborated experiments as compared to common stand-alone devices. Furthermore the system is composed of portable units, which will allow for easy transfer between collaborating labs.

Acknowledgement

C.N. is grateful to the German National Academic Foundation (Studienstiftung des deutschen Volkes) for supporting his research.

References

[1] Daus, A.W. et al. (2011): Electromagnetic exposure of scaffold-free three-dimensional cell culture systems. *Bioelectromagnetics 5(32)*

[2] Rolston, J.D. et al. (2009): A low-cost multielectrode system for data acquisition enabling real-time closed-loop processing with rapid recovery from stimulation artifacts. *Frontiers in Neuroengineering 2(12)*

[3] Wagenaar, D.A. et al. (2004): Effective Parameters for stimulation of dissociated cultures using multi-electrode arrays. *Journal of Neuroscience Methods 138*

[4] Dura, B. et al. (2012): High-Frequency Electrical Stimulation of Cardiac Cells and Application of Artifact Reduction. *IEEE Transactions on Biomedical Engineering, Volume 59(5)*

[5] Nick, C. and Bestel, R. and Steger, F. and Thielemann, C. (2013): Spike Detection, Sorting and Propagation of Cell Signals Recorded with Extracellular Microelectrodes *IEEE EMBS, Short Papers No. 3081*

An Automated Method for Characterizing Electrode properties of High-Density Microelectrode Arrays

Vijay Viswam[1], David Jäckel[1], Marco Ballini[1], Jan Müller[1], Milos Radivojevic[1], Urs Frey[2], Felix Franke[1], Andreas Hierlemann[1]

1. ETH Zürich, Bio Engineering Laboratory, D-BSSE, CH-4058 Basel, Switzerland
2. RIKEN Quantitative Biology Center, Kobe, Japan
* Corresponding author. E-mail address: vijay.viswam@bsse.ethz.ch

Abstract

Here we report on an efficient automated method for characterizing electrode properties on a high-density microelectrode array. The method can be used to check the homogeneity of Pt-black deposition on the array by screening the impedance response of each electrode.

1 Introduction

Novel in vitro high-density microelectrode array (HD-MEA) systems incorporate up to several thousand electrodes in highly dense arrangements on a single chip. Characterizing the properties of each electrode of a HD-MEA system is a difficult but important task for many experiments. Here, we present a method for estimating the electrode size and uniformity of impedance in a CMOS-based planar HD-MEA.

2 Methods

Fig.1 shows the equivalent circuit of a metal electrode and recording channel interface in our existing CMOS-based HD-MEA [1]. Our system consists of 11'011 microelectrodes, 126 on-chip readout channels and on-chip analog-to-digital converters for digitizing the signals. The impedance of the electrode (Z_e) reduces the known input impedance (Z_{in}) of the Low-Noise Amplifier (LNA) and thus affects the gain response of the readout channel. By carefully measuring the amplitude response of each channel we can estimate the electrode impedance at certain frequencies.

Alternating voltage at the amplitude of 1mV (V_{stim}) peak-to-peak was applied to a buffer solution through the Reference Electrode (RE) of the HD-MEA, using a DS360 Ultra-Low Distortion Function Generator. The measurements were performed in phosphate-buffered saline solution (PBS) which has similar electrical properties as a physiological solution. Since the MEA can only acquire signals from 126 electrodes simultaneously, 91 electrode configurations were used, covering all electrodes on the array. Each configuration was recorded for 1 second, and the entire electrode array was scanned within 5 minutes. The acquired signals were demodulated in Matlab to extract the input-referred signal amplitude (V_{meas}) at 1 kHz. We can estimate the impedance of the electrode using the following equation:

$$Z_e = Z_{in}\,[V_{stim}/\,V_{meas} - 1]\;;\; Z_{in} = 41.8M\Omega@1kHz$$

The procedure can be repeated at different frequencies.

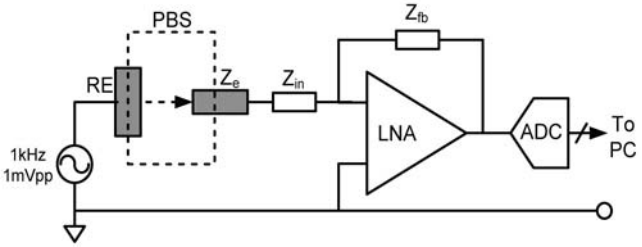

Fig. 1. Equivalent circuit of metal-electrode recording interface

3 Results

For testing this method, we fabricated a HD-MEA with 4 different electrode sizes, as shown in *Fig.2.A*. The signal attenuation (V_{meas}/V_{stim}) is displayed in *Fig.2.B*; from the plot a clear distinction of electrode size can be made. *Fig.2.C* shows the 2-D impedance plot of the entire electrode array, with same electrode size of 8.2x5.8µm^2. Pt-black has been deposited on each of the microelectrodes except for a few. The impedance has been attained from the signal attenuation of each electrode. From Figure 2C one can clearly identify electrodes, for which the deposition was not successful. *Fig.2.D* shows the optical image of such an electrode. *Figs.2.E-F* shows the homogeneity of Pt-black deposition.

4 Conclusion

We presented a method, which allows to identify electrodes with different electrode sizes and to estimate individual electrode impedances on HD-MEAs.

Acknowledgements

This work was supported by the ERC Advanced Grant "NeuroCMOS" under contract number AdG 267351. M. Radivojevic received funding support from the Swiss National Foundation through an Ambizione Grant (PZ00P3_132245)

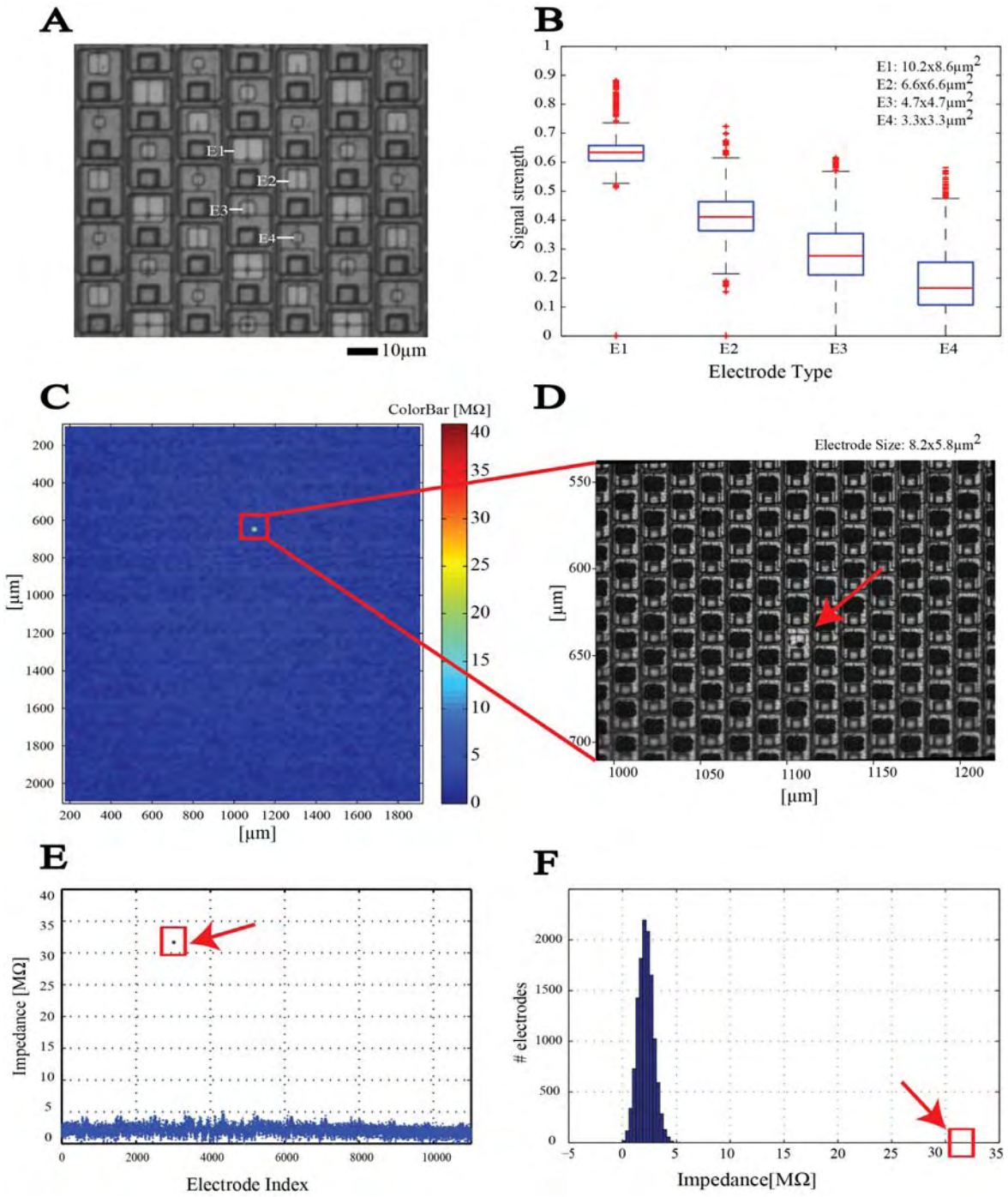

Fig. 2. Signal response and impedance of micro electrodes. A) Optical image of the MEA having different electrode sizes. B) Signal attenuation of electrodes having different electrode sizes. C) Impedance distribution plot of the high-density electrode array. D) Zoomed optical image of an electrode without Pt-black. E) Impedance of 11'011 Pt-black deposited electrodes. F) Impedance distribution of electrodes. The red boxes in Figs. 2E and F mark data of electrodes without Pt-black.

References

[1] U. Frey, J. Sedivy, F. Heer, R. Pedron, M. Ballini, J. Mueller, D. Bakkum, S. Hafizovic, F. D. Faraci, F. Greve, K.-U. Kirstein, and A. Hierlemann, "Switch-matrix-based high-density microelectrode array in CMOS technology", *IEEE Journal of Solid-State Circuits*, no.2, pp. 467–482, 2010

3D Electrodes for In-Cell Recording: Electrogenic Cell Membrane Deformation and Seal Resistance Estimation

Francesca Santoro[1], Jan Schnitker[1], Sabrina Ullmann[1], Andreas Offenhäusser[1*]

1 *CS-8/PGI-8 Institute of Bioelectronics, Forschungszentrum Jülich, Germany*
* Corresponding author. Email address: a.offenhaeusser@fz-juelich.de

Abstract
Planar Multi Electrode Arrays (MEAs) have been recently modified with 3D nano and microstructures in order to improve thecell-device coupling. These new approaches aimed to increase the seal resistance of the cell-electrode electrical equivalent circuit. Here, we present a study for investigating the interface between electrogenic cells (HL-1 cells and neurons) with nanocylinders and nanocylinders with a mushroom-shaped cap. We also present an estimation of the seal resistance considering different cell membrane cleft thicknesses.

1 Background

The development of multi electrode arrays (MEAs) towards 3D structures have shown great progress regarding signal recording and stimulation of electrogenic cells (1). We contributed to these advancements by showing the possibility to simultaneously guide cardiomyocytes and record action potentials with mushroom-shaped 3D nanoelectrodes (2). Such 3D nanoelectrode MEAs greatly improved the coupling between cells and MEAs and, moreover, they extend the concept of extracellular to in-cell recording/stimulation. Our aim is to predict an optimal design for a 3D nanoelectrode for in-cell recording towards an intracellular non-invasive nanoelectrode depending on the type of electrogenic cell which has to be studied. In our investigation, we also took into account the position of the engulfment-like event (3). We performed scanning electron microscopy/focused ion beam sectioning to estimate the membrane cleft and the deformation as response to the studied 3D nanostructures.

2 Methods

We carried out a study to understand how the shape (nanocylinders with and without mushroom-shaped caps) and size (nanometers range) of 3D nanoelectrodes affect the response of cardiomyocytes-like cells and primary neurons. In particular, we investigated the interface at the nanoscale regime by using fluorescence microscopy and scanning electron microscopy/focused ion beam sectioning (SEM/FIB) (4). We fabricated 3D nanocylinders with and without cap ranging from 300 nm up to 800 nm in diameter and 300 nm up to 1000 nm in height.

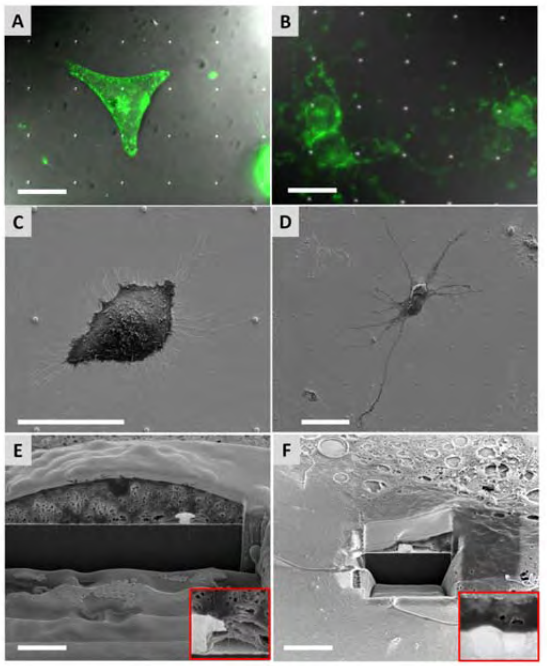

Fig. 1. Electrogenic cells on 3D nanostructures: A) HL-1 cell labelled with WGA; B) cortical neuron labelled with WGA; C) SEM micrograph of a HL-1 cell fixed on a 3D nanocylinder with cap; D) cortical neuron fixed on a 3D nanocylinder; E) FIB cross section of C); F) FIB cross section of D). Scale bars A-D: 20 µm, E: 3 µm, F: 4 µm.

First, we fluorescently labeled the cell membrane of HL-1 cells (after 3 DIV) and primary cortical neurons (after 4 DIV) with Wheat Germ Agglutinin (Life Technologies) in a 1:500 dilution in PBS incubated for 15 minutes (Fig. 1 A-B). Then, we fixed the cells with 3.2% glutaraldehyde, dehydrated them with 10% up to 100% ethanol and, finally, we dried the samples by performing critical point drying (CPD).

Subsequently, we observed the cells by SEM (Fig. 1 C-D). The cells engulfing a 3D nanostructure were cut in a transversal section by FIB (Fig. 1 E-F). Our aim is to predict an optimal design for a 3D nanoelectrode for in-cell recording

toward an intracellular non-invasive nanoelectrode depending on the type of electrogenic cell, which has to be studied.

3 Results

We found that primary neurons form a tent-like conformation in presence of 3D nanocylinders while they wrap around 3D nanocylinders with cap (data not shown). These results are comparable with evidence we have previously shown for a biomechanical study performed on HL-1 cells (3).

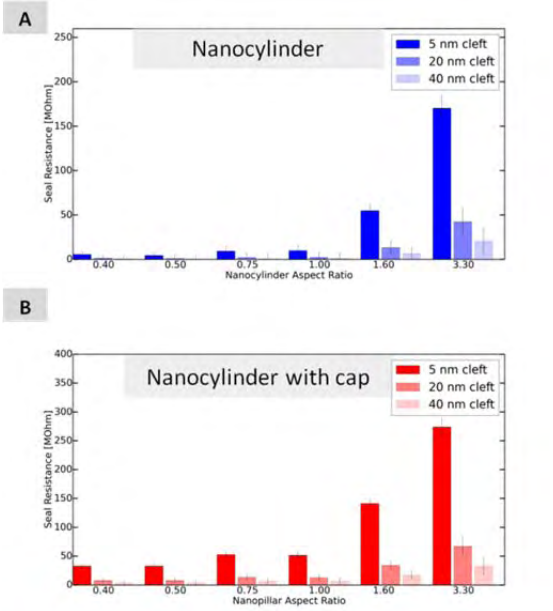

Fig. 2. Seal resistance estimation: A) seal resistance calculated for cells adhering on nanocylinders; B) seal resistance calculated for cells adhering on nanocylinders with caps.

In addition, we estimated the seal resistance for 3D nanocylinders with and without caps considering different cleft dimensions, ranging from 5 nm up to 40 nm according to the model showed by Fendyur et al. (5). Moreover, we considered the aspect ratio of the nanocylinder stalk as the ratio between the height and the diameter. We found that cylinders with cap promote a seal resistance up to 270 M□ when the cleft between the cell and the electrode is 5 nm. In contrast to the nanocylinder scenario where the seal real is maximum about 160 M□ fat the smallest cleft thickness.

4 Conclusion

We found that the cell membrane deforms in different ways when the 3D nanoelectrodes have different geometries. We assume that the cap plays an essential role while promoting an engulfment-like event in electrogenic cells. In particular, we studied the response of a cell line (Hl-1 cells) and primary cells (cortical neurons). Finally, according to our results, we estimated the electrical seal resistance in order to conclude which of the studied structures are most suitable for an optimal cell coupling on top of the MEA.

References

[1] Spira ME, Hai A. Multi-electrode array technologies for neuroscience and cardiology. Nat Nanotechnol. 2013 Feb;8(2):83–94.

[2] Santoro F, Schnitker J, Panaitov G, Offenhäusser A. On Chip Guidance and Recording of Cardiomyocytes with 3D Mushroom-Shaped Electrodes. Nano Lett. 2013 Nov 13;13(11):5379–84.

[3] Santoro F, Dasgupta S, Schnitker,Jan, Auth,Thorsten, Neumann,Elmar, Panaitov,Gregor, et al. Interfacing electrogenic cells with 3D nanoelectrodes: do position, shape and size matter. Manuscr Revis.

[4] Santoro F, Neumann E, Panaitov G, Offenhäusser A. FIB section of cell–electrode interface: An approach for reducing curtaining effects. Microelectron Eng. 2014 Jul 25;124:17–21.

[5] Fendyur A, Mazurski N, Shappir J, Spira ME. Formation of Essential Ultrastructural Interface between Cultured Hippocampal Cells and Gold Mushroom-Shaped MEA-Toward 'IN-CELL' Recordings from Vertebrate Neurons. Front Neuroengineering [Internet]. 2011 Dec 8 [cited 2013 Nov 10];4. Available from: http://www.ncbi.nlm.nih.gov/pmc/articles/PMC3233721/

A Benchtop Device for Prolonged Experiments with Microelectrode Arrays

Regalia Giulia[1*], Achilli Silvia[1], Biffi Emilia[2], Menegon Andrea[3], Ferrigno Giancarlo[1], Pedrocchi Alessandra[1]

1 Electronics, Information and Bioengineering Department, Politecnico di Milano, Milan, Italy
2 Bioengineering Laboratory, Scientific Institute IRCCS Eugenio Medea, Bosisio Parini, Italy
3 Advanced Light and Electron Microscopy Bio-Imaging Centre, San Raffaele Scientific Institute, Milan, Italy
* Corresponding author. E-mail address: giulia.regalia@polimi.it

Abstract
The stabilization of environmental conditions at the experimental setup is a mandatory requirement to permit recordings with Microelectrode Arrays lasting more than a couple of hours. In this work we present the preliminary validation of a device engineered to control the environmental conditions during benchtop MEA experiments. The device is based on a Polymethyl-Methacrylate closed chamber which houses multiple neuronal cultures on MEAs, connected to a custom air heating and humidification control system and a thermostat. Custom multichannel boards connected to a commercial data acquisition system (Multi Channel Systems GmbH) were integrated inside the chamber. Preliminary tests to validate the effectiveness of the device showed that it allows to keep hippocampal networks viable outside the incubator and constantly monitor their electrical activity over days. Studies of networks development and neuropharmacological dose-response experiments are example of applications which can benefit from the proposed device.

1 Background/Aims

When performing prolonged experiments with neuronal cultures grown on Microelectrode Arrays, a mandatory requirement is to keep cells functionally unperturbed by external conditions. A possible approach is to perform recordings inside an incubator [1], with limits to accessibility and handiness to use. Proposed benchtop setups are in general temporary solutions [2], do not allow investigations for prolonged periods without activity alterations up to decline [3] or require a stable and sterile perfusion setup to maintain cells viable [4]. Our group proposes the utilization of a compact, closed climate-controlled chamber which stabilizes environmental conditions (temperature, humidity and CO2) on the lab bench [5,6]. Here we describe an improved prototype of the system and demonstrate the effectiveness of the whole experimental apparatus performing recordings from hippocampal dissociated cultures.

2 Methods / Statistics

The device consists of a 22x22x6 cm Polymethyl-Methacrylate chamber housing four MEA chips, connected to environmental control systems and a MEA acquisition system. The desired temperature results from the combined action of heating water flowing in a jacket around the chamber (circulating bath and temperature controller, Lauda GmbH), warmed air injected in the chamber (150 ml/min) and a warmed top plate (3W). A high level of humidity (RH>95%) is obtained bubbling air inside a bottle filled with water, with temperature regulated by the RH reading from a miniaturized sensor in the chamber (Sensirion Inc.). The CO_2 is maintained to 5% by the use of a 5% CO_2 gas mixture and monitored by an infra-red sensor (Gas Sensing Solution Ltd). MEA signals are collected by custom pre-amplifiers inside the chamber and external filter-amplifiers (gain:1100, bandwidth:300Hz-3kHz) and acquired by a commercial device (Multichannel Systems GmbH). The internal boards are sealed to avoid damaged due to the high RH% level. Hippocampal cultures on 60 channel MEAs (Multichannel Systems) were positioned in the chamber between the second and the third week in vitro and monitored thereafter for periods ranging from 12 hours to several days in a row. If necessary, the medium exchange was performed from outside with PTFE tubes (330µl every 48h) (ALA-MEA-MEM-PL caps, MultiChannel Systems). Spikes were detected by comparison with a threshold (-5*standard deviation of noise), updated every 12 hours, and analysed with McRack (Multichannel Systems).

3 Results

The maintenance of adequate environmental conditions in the chamber allowed to monitor the spontaneous behaviour of neuronal networks, i.e. not influenced by unforeseen environmental fluctuations. Figure 1 reports a 60 hours snapshot of activity (13-14 DIV), where an activity alteration following the culture medium change (i.e., an induced perturbation to network activity) is clearly visible.

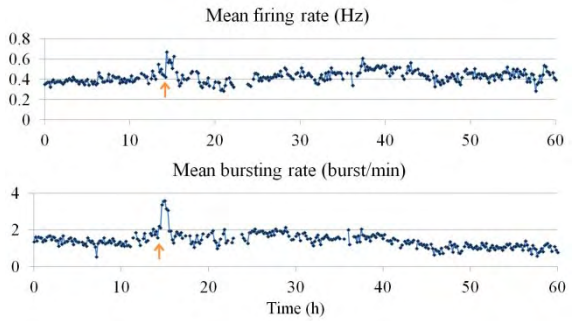

Fig. 1. Mean firing rate (Hz) and mean burst rate (burst/min) profiles exhibited by an hippocampal culture recorded in the climate-controlled chamber. It is shown that the spontaneous activity is perturbed by the medium change procedure (orange arrow).

Figure 2 reports raster plots showing the occurrence of spiking activity and the mean firing rate exhibited by a culture maintained in the setup for six days (15-20 DIV). Differences over time reflecting the maturation of the network (i.e., re-organization of patterns of synchronous activity) were observed.

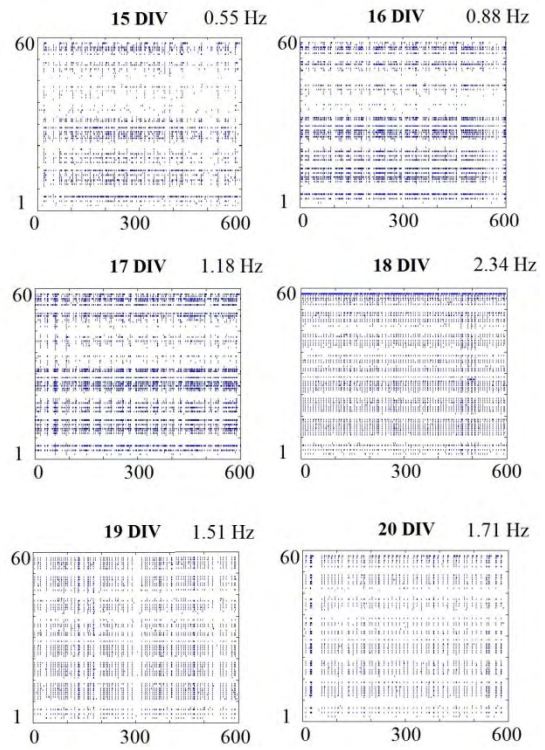

Fig. 2. Raster plots showing the occurrence of spiking activity in the same hippocampal culture maintained in the controlled environmental chamber over different days *in vitro* (DIVs). Each panel represents the activity of 60 channels over a 10 minute snapshot and was extracted every 24 hours of recordings. The mean firing rate (Hz) is reported in the top right corner of each raster plot.

4 Conclusion/Summary

The chamber presented here constitutes an effective experimental platform to obtain environmental stability during MEA experiments lasting more than few hours. We presented here preliminary data demonstrating that it allows to follow the evolution of cultured networks activity over days. The possibility to maintain cultures on MEAs in a controlled environment and constantly connected to the recording stage avoids any stress to cells, differently from repeated short-term recordings, which imposes to move cells from the incubator to the recording stage repeatedly over the culturing period [7]. Applications such as maturation studies, functional degeneration or effects of chronic neuropharmacological treatments are examples of experiments which can benefit from this device.

Acknowledgement

We thank Alembic facility for its support and Dr. De Ceglia for the dissection of hippocampi. We are very grateful to Karl-Heinz Boven, Andreas Grall and all the people from Multi Channel Systems GmbH who supported us in the production of custom printed circuit boards.

References

[1] Lignani G. et al (2013). Long-term optical stimulation of channel rhodopsin-expressing neurons to study network plasticity. *Front Molecular Neuroscience*, 6(22).
[2] Novellino A. et al (2011). Development of micro-electrode array based tests for neurotoxicity: assessment of interlaboratory reproducibility with neuroactive chemicals, *Front. Neuroeng*, 4(4).
[3] Potter S.M. and DeMarse T. (2001). A new approach to neural cell culture for long-term studies. *J Neurosci Methods*, 110, 17-24.
[4] Martiniuc A.V. et al. (2012). Tracking the evolution of neural network activity in uninterrupted long-term MEA recordings. *Proceedings of MEAMeeting 2012*, Reutlingen.
[5] Biffi E. et al. (2012). A novel environmental chamber for neuronal network multisite recordings. *Biotechnol Bioeng*, 109, 2553-2566.
[6] Regalia G. et al. (2013). An experimental platform aimed at long lasting electrophysiological multichannel recordings of neuronal cultures. *Proceed of the 5th International Joint Conference on Computational Intelligence*, doi: 10.5220/0004659005510557, 2013.
[7] E. Biffi, G. Regalia, et al. (2013). The influence of neuronal density and maturation on network activity of hippocampal cell cultures: a methodological study. *Plos One.* 8(12).

Development of a Stand-alone Integrated MEA Biochip System for Chronic Recordings

Paolo De Pasquale[1,2]; Antonin Sandoz [1]; Igor Charvet [1]; Philippe Passeraub [1]; Michela Chiappalone [2]; Luc Stoppini [1]

1 Hepia, HES-SO Geneva, Switzerland;
2 Istituto Italiano di Tecnologia (IIT), Genova, Italy
* Corresponding author. E-mail address: michela.chiappalone@iit.it; luc.stoppini@hesge.ch

Abstract
Stand-alone integrated MEA system were developed and tested to investigate the effect of toxic compounds on network neural activities during chronic recordings. The system, consisting of specifically designed MEA aim to receive microfluidic organic substances and to communicate using wireless technology with the computer device. The system has been tested with several types of 2D and 3D neuronal cultures. The electrophysiological data are processed by NeuroSpy, a modify version of SpyCode. The software developed is able to analyze the basal activity, drug and stimulation evoked response.

1 Background

"Cell biochips" containing engineered tissue interconnected by a microfluidic network allows the control of microfluidic flows for dynamic cultures by continuously feeding of nutrients and waste removal. Thus, these types of systems can enhance functionality of cells by mimicking the tissue architecture complexities when compared to in vitro analysis, but at the same time present a more rapid and simple process when compared to in vivo testing procedures. To date, one of the most promising tools for neuropharmacological functional tests is the Micro-Electrode Array (MEA). MEAs have been applied to study multiple aspects of electrically excitable cells and to explore the pharmacological and toxicological effects of numerous compounds on spontaneous activity of electrogenic cells (A. Novellino, T. J. Shafer et al. 2011). As a complementary tool to standard MEA platforms, we are developing a novel stand-alone system able to acquire, stimulate and feed the cultures. This new approach will keep the cultures inside the incubator providing a useful tool for chronic long-term recordings, with the possibility to continuously submit exposure to drugs or chemicals.

2 Methods and Statistics

We have developed a small-volume in vitro system in which neural cells/tissues can be cultivated in four separate porous membrane microchambers. These are connected by microchannels with the presence of a MEA in each well (Fig. 1). Each MEA, in this configuration, is composed by 8 recording electrodes plus two additional electrodes which can be used for electrically stimulating the cultures through the STG4002 stimulator (MCS). Electrophysiological activities recorded from the 4 integrated MEAs are transmitted through the Wireless System W32 (developed for in vivo applications by Multi Channel Systems, Reutlingen, Germany) and adapted to this particular in vitro application.
The wireless headstage is directly linked to the chip and integrated into the main body of the system. A specific micro-peristaltic pump, developed in order to feed the culture during the incubating period, is controlled by a dedicated software to operate it via Bluetooth or wireless mode.
We developed a modified version of the Spycode software (Bologna et al. 2010), called NeuroSpy (Fig. 2), to perform the analysis of electrophysiological data of neuronal cultures, acquired by MEAs. NeuroSpy allows performing basic and high precision offline analyses . Moreover, the software is able to perform a specific type of analysis aim to study the behaviour of the 2D or 3D neural cultures, as a result of both chemical and electrical stimulation.

Fig. 1. Complete system: MEA chip, wifi system, perfusion pump.

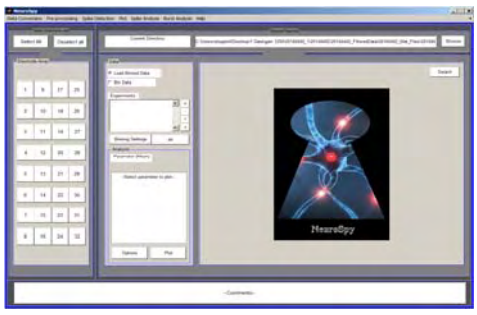

Fig. 2. Analysis software: Neurospy interface.

3 Results

In the first series of experiments, we could record the electrophysiological signals from several types of cells, with the aim at testing the system performance.

Basically, the behaviour of the system has been studied with 2D and 3D cells structure, derived from human sphere stem cells, rat brain cortex, rat hippocampus slices and dissociated cells.

Fig.3 shows a *network burst activity*, recorded from a 3D neural network (derived from H9 or iPs stem cells), through the *raw data* and a *raster plot*. Fig.4 Shows the *Mean Firing Rate* and the *Mean Bursting Rate* from dissociating cells from rat brain cortex. Fig.5 shows the *ISI histogram* relative to the same experiment of Fig.4 and Fig.5.

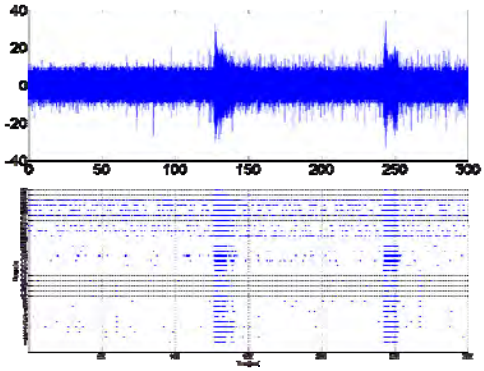

Fig. 3. Electrophysiological activity from a representative experiment of a neural network derived from H9 cells. *Top panel*, raw data recorded from one electrode. *Bottom panel*, raster plot depicting the activity from the 32 channels of the array.

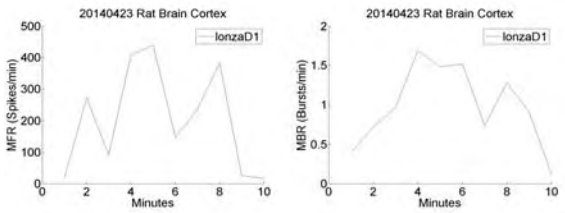

Fig. 4. MFR and MBR from a representative experiment of a neural network derived from rat brain cortex. *Left panel*, Mean Firing Rate (spikes/sec). *Right panel*, Mean Bursting Rate (Bursts/Min).

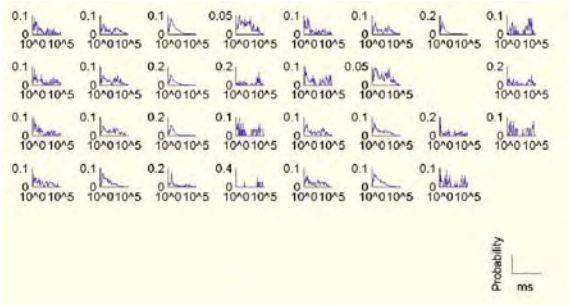

Fig. 5. ISI histogram from a representative experiment of a neural network derived from rat brain cortex

4 Conclusion

These human surrogate integrated Biochips will enable the determination of toxicological profiles of new drug candidates. In addition, the developed system will provide scientists with alternative ways to test more thoroughly new drugs or chemicals. It will also help to understand the process that causes an organism to react and adapt when exposed to drugs over a long timescales.

Moreover, the system will provide scientists with a new independent device able to reduce contaminations factors, due to interactions between the organic components and external agents, thanks to the feeding, recording and stimulating remote wireless control. Scientists will be able to monitor the culture since the first day in vitro, without the risk of expose them to an excessive stress due to the behaviours changing.

Statement of financial support: Supported by the HES-SO, CTI/KTI and the SCAHT.

References

[1] Tieng V, Stoppini L, Villy S, Fathi M, Dubois-Dauphin M, Krause KH. Engineering of Midbrain Organoids Containing Long-Lived Dopaminergic Neurons. Stem Cells Dev. 2014 Apr 3.

[2] Kern I, Xu R, Julien S, Suter DM, Preynat-Seauve O, Baquié M, Poncet A, Combescure C, Stoppini L, Thriel CV, Krause KH. Embryonic stem cell-based screen for small molecules: cluster analysis reveals four response patterns in developing neural cells. Curr Med Chem. 2013;20(5):710-23.

[3] Krug AK, et al. A. Human embryonic stemcell-derived test systems for developmental neurotoxicity: a transcriptomics approach. Arch Toxicol. 2013 Jan; 87(1):123-43. doi: 10.1007/s00204-012-0967-3. Epub 2012 Nov 21.

[4] Sundstrom L, Biggs T, Laskowski A, Stoppini L. OrganDots--an organotypic 3D tissue culture platform for drug development. Expert Opin Drug Discov. 2012 Jun;7(6):525-34. doi: 10.1517/17460441.2012.686488. Epub 2012 May 19.

[5] Bologna, L. L.; Pasquale, V.; Garofalo, M.; Gandolfo, M.; Baljon, P. L.; Maccione, A.; Martinoia, S. and Chiappalone, M.Investigating neuronal activity by SPYCODE multichannel data analayze.Neural Networks, 23 (6): 685-697, 2010.

[6] Chiappalone, M., Novellino, A., Vajda, I., Vato, A., Martinoia, S. & van Pelt, J. (2005) Burst detection algorithms for the analysis of spatio-temporal patterns in cortical networks of neurons. Neuro-computing, 65-66, 653-662.

[7] A. Novellino, Bibiana Scelfo, T. Palosaari, A. Price, Tomasz Sobanski, T. J. Shafer, A. F. M. Johnstone, G. W. Gross, A. Gramowski, O. Schroeder, K. Jügelt, M. Chiappalone, F. Benfenati, S. Martinoia, M. T. Tedesco, E. Defranchi, P. D'Angelo and M. Whelan. (2011) Development of micro-electrode array based tests for neurotoxicity: assessment of interlaboratory reproducibility with neuroactive chemicals. Front. Neuroeng., 27 April 2011

3D Multi Electrode Arrays

Martin Baca[1*], Heike Bartsch[2], Tom Porzig[2], Adam Williamson[1], Andreas Schober[1]

1 FG Nanobiosystemtechnik, Technische Universität Ilmenau (TUI), Germany
2 FG Elektroniktechnologie, Technische Universität Ilmenau (TUI), Germany
* Corresponding author. E-mail address: martin.bacca@tu-ilmenau.de

Abstract
Neurobiological concepts derived from measurements provided by the current generation of MEA technology have so far lacked the complexity of actual high-level neurobiological systems. Two key advances are needed to improve our understanding of such systems: *in vivo* 3D-neuronal cell cultures (including multiple types of neural cells), and 3D MEA systems for measuring this 3D-cultures [1][2][3]. We have constructed an in vitro measurement system for exactly such 3D-neuronal cell cultures. The principal cultures to be investigated with this system will be neural cells derived from human stem cells.

1 Requirements

Neurobiological concepts derived from measurements provided by the current generation of MEA technology have so far lacked the complexity of actual high-level neurobiological systems. Two key advances are needed to improve our understanding of such systems: in vivo 3D-neuronal cell cultures (including multiple types of neural cells), and 3D MEA systems for measuring this 3D-cultures [1][2][3].

Two major technical specifications have been taken into account for the 3D-MEA design:

1.Culture Thickness - The standard method of measuring the electroactivity of cell cultures and slices is the use of a 2D-MEA beneath the culture with a typical electrode diameter of 30-100 µm and a typical distance between electrodes of 100 µm. However, the typical thickness of a 3D culture can exceed a few hundred micrometers. Clearly for better 3D spatial and temporal resolution of cultures, one would ideally use a 3D-MEA capable of reaching at least a few hundred micrometers into the cultures.

2. Incubator Compatibility - For measuring standard electroactivity in 2D, cultures are grown on the 2D MEA itself. The MEA on which the cells are growing is moved from the incubator to the amplifier system each time a measurement is desired. The culture is enclosed in a housing to prevent contamination. Standard commercially available 3D-MEA systems use sets of prongs inserted into a 3D culture from above. This requires the removal of the housing lid, making placement of the culture back into the incubator impossible and also disregards the cellular damage caused to the 3D culture during MEA insertion. The ideal situation for 3D cultures is a 3D-MEA which is compatible with the incubator conditions.

2 MEA design and manufacturing

The above mentioned requirements call for smart multilayer and packaging technology. Low temperature cofired ceramics (LTCC) are chosen as material system for the MEA design because those ceramics enable complex multilayer assemblies and feature excellent temperature and solvent stability. In our case we decided to use Green Tape ™ 951 form DuPont Nemours. The compatibility of the material and available metallisation with cell cultures was already proven [5].

An LTCC multilayer board with gold electrodes is the base of the 3D MEA. **Fehler! Verweisquelle konnte nicht gefunden werden.** depicts a schematic cross section of the assembly. LTCC vias (material DP 5738 from DuPont) serve as electrodes in cell contact. They are interconnected via the buried wiring and a 90° solder contact with printed gold pads (material DP 5742 from DuPont). The layout of these gold pads is designed to fit the MEA2100-System for in vitro recording from Multi Channel Systems and enable thus a comparable data processing to established 2D MEAs

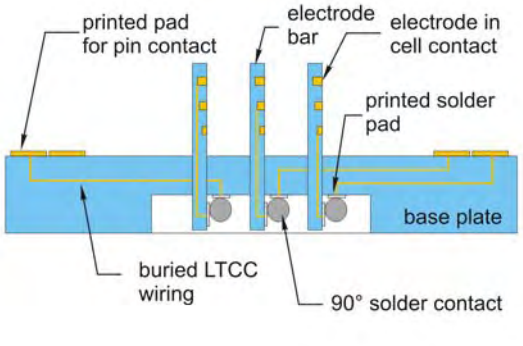

Fig. 1. Schematic cross section of the LTCC assembly

Slots with dimensions of 450 µm are laser cut into the base plate for the assembly of three finger electrode bars, which carry 3 electrode fingers with 3 gold

contacts each. These bars are manufactured separately using LTCC technology. The outer contour of the fingers is laser cut.

There exist no reliable data for useful electrode pitches and dimensions applied to 3D cultures so far. Hence, two different finger electrode layouts were manufactured, one with small fingers and one with tall fingers. Their dimensions and electrode pitches are presented in Fig. 2. The fingers have a thickness of 400 µm and the diameter of the gold electrodes in cell contact is 85 µm. In addition to the 3D electrodes on the fingers each MEA is equipped with 3x10 2D electrodes, which are situated in the near vicinity of the bars and one 2D reference electrode

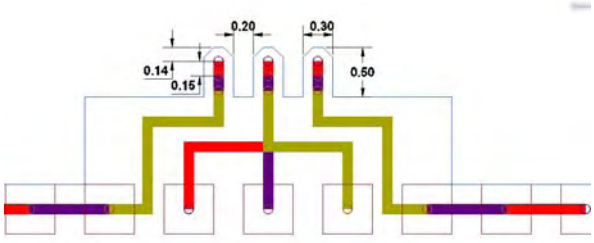

a)

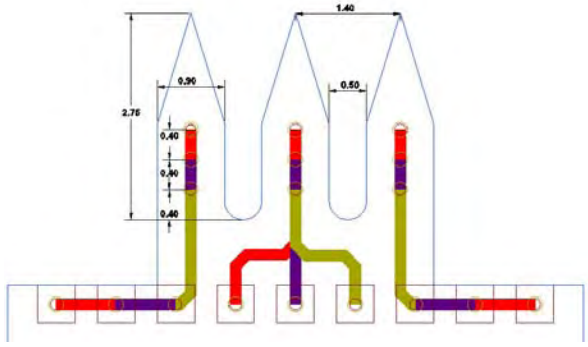

b)

Fig. 2. Finger dimension for both types

After the finger assembly the MEA is equipped with a ring, which serves as a culture chamber. The ring consists of fused silica and it is bonded on the LTCC surface using silicone adhesive (LOCTITE® SI 5366™). **Fehler! Verweisquelle konnte nicht gefunden werden.** depicts a complete MEA with tall fingers and details of both LTCC electrode fingers. In a next step the MEAs are prepared for the use with cell medium.

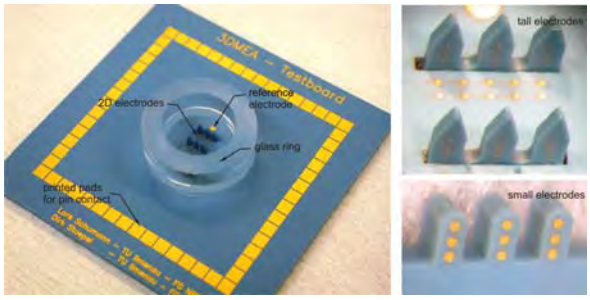

Fig. 3 MEA with cell culture ring and finger types

3 Conclusion

Future work will now increase the number of sensors from 9 per microtower up to 80. Due to the small signal amplitude the amplification should be as close as possible to the sensor. An ASIC (Application Specific Integrated Circuit) has been designed which is able to manage 8 sensors per finger, and 10 fingers per microtower. An arbitrary number of ASIC amplified microtowers can be placed in parallel. Additionally a version of the MEA presented here, with a transparent base plate is in production, to include imaging with electrophysiological measurement of 3D-cultes [4].

Acknowledgement

This research has been supported by the 3DNeuroN project in the European Union's Seventh Framework Programme, Future and Emerging Technologies, grant agreement n°296590.

References

[1] http://www.3dneuron.eu/
[2] Klefenz F, Williamson A (2013): Modeling the formation process of grouping stimuli sets through cortical columns and microcircuits to feature neurons, Computational Intelligence and Neuroscience Volume 2013, Article ID 290358, 10 pages http://dx.doi.org/10.1155/2013/290358
[3] Husar P, Laqua D, Fischer M, Lilienthal, K, Hampl, J, Fernekorn U, Schober A (2010): Hybrid three-dimensional sensor array, in particular for measuring electrogenic cell assemblies, and measuring assembly. DE 10 2010 000 565.7 // PCT/EP2011/052638
[4] Just T, Husar P (2014) Amplifier ASIC for multichannel and real 3D-MEA
[5] Bartsch de Torres H, Rensch C, Fischer M, Schober A, Hoffmann M, Müller J (2009). Thick film flow sensor for biological microsystems. *Sensors and Actuators A: Physical*, 160, 109-115 http://dx.doi.org/10.1016/j.sna.2010.04.010

The Influence of Medium Conductivity on Cellular Impedance Measurements with Field-Effect Transistor Arrays

Felix Hempel, Nathalie Bernhard, Jessica Ka-Yan Law, Anna Susloparova, Dieter Koppenhöfer, Xuan-Thang Vu and Sven Ingebrandt*

Department of Informatics & Microsystem Technology, University of Applied Sciences Kaiserslautern, Zweibruecken, Germany
* Corresponding author. E-mail address: sven.ingebrandt@fh-kl.de

Abstract
In the present study the influence of measurement media with different conductivities on cell impedance measurements was investigated. HEK 293 cells were cultured on the field-effect transistor surfaces and their transistor transfer function was measured in different buffer solutions. Changing the conductivities of the measurement buffers is strongly influencing the measured spectra. By fitting the data to an established model, the change of the seal resistance and the membrane capacitance due to the conductivity of the media can be calculated. The derived cell-related data advance our understanding in cell-transistor interface modelling.

1 Introduction

Impedance spectroscopy with field-effect transistors (FETs) has been used for several biosensing applications, including DNA detection [1] and cell-substrate adhesion studies [2]. Unlike the commercially available Electric Cell-Substrate Impedance Sensing (ECIS) system, our FETs have smaller sensor sizes, which enable the detection of single cell-substrate adhesion events. With our in house-fabricated system we specialized in such single cell impedance measurements [3], [4] and the interpretation of the measured data [5]. The essential, cell-related parameters for our sensing platform are the membrane capacitance (C_M), which reflects the morphology of the attached cell and the seal resistance (R_{seal}), which represents the adhesion strength between cell and transistor gate. The seal resistance should scale with the conductivity of the solution [5] resulting in a stronger electronic coupling between cell and transistor gate.

In this study we conducted experiments to validate our model for cell impedance measurements and to study the influence of the conductivity of the solutions on the transistor-transfer function (TTF). Data fitting can be performed to optimize cell impedance measurements with FET devices by providing values of R_{seal} and C_M for different experimental configurations using an electrically equivalent circuit (EEC). The EEC mainly uses the well-known point-contact model for FET devices in contact with adherent cells [5].

2 Methods

HEK 293 cells were cultured on our FET devices (gate width: 8 µm and length: 5 µm) without additional coating. The devices were fabricated similar to the protocol described in a previous publication [6]. The electronic readout was performed with our TTF amplifier. A 10 mV signal with a frequency ranging from 1 Hz to 1 MHz was applied to the Ag/AgCl pseudo reference electrode to measure the TTF spectra. The measurement solutions were prepared as following:

- Sodium containing buffer: NaCl 135mM, $CaCl_2$ 1.8 mM, $MgCl_2$ 1 mM with a conductivity of 25.8 mS/cm.
- Sodium free buffer: KCl 5mM, $CaCl_2$ 1.8 mM, $MgCl_2$ 1 mM with a conductivity of 2.21 mS/cm.

Both solutions were adjusted to pH 7.4 and to the same osmolarity of 340 mOsm/kg by adding glucose.

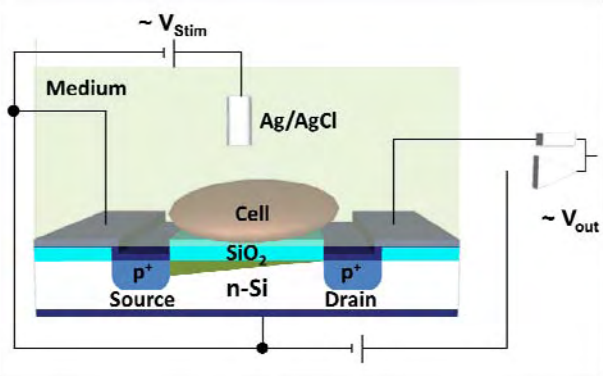

Fig. 1. Schematic of a cell-covered field-effect transistor to explain the configuration for transistor-transfer function measurements [5].

3 Results

The TTF measurements were performed with cell-covered gates and with cell-free gates, after trypsinization. The FETs were characterized before each measurement and operated in a working point with highest transconductance value (g_m). In this configuration the sodium-containing solution mimics

the standard culture medium, while the sodium-free solution drastically reduces the conductivity. The measurements of the transfer function show significant differences for cell-covered and cell-free gates, for both measurement solutions (Fig. 1).

A drop of the transfer function can be observed when cells are adherent on top of the transistor gate (Fig. 2). The same result can be seen when the bathing solution was changed to the sodium-free solution. The graphs show that the drop in transfer function for sodium-containing solution generally happens at higher frequencies. This drop is shifted to lower frequencies for the sodium-free solution, where the drop can be seen at 10 kHz already.

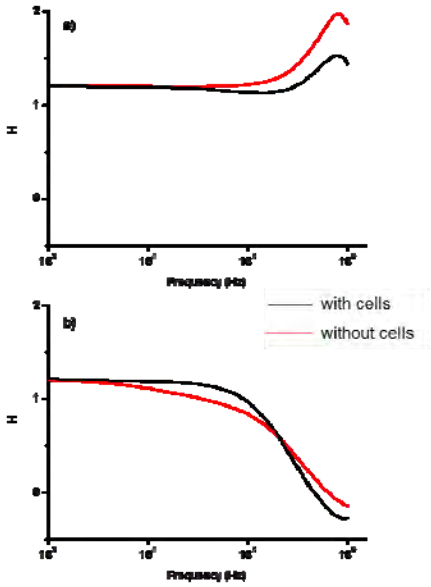

Fig. 2. Transfer function measurements with a) sodium containing buffer and b) in sodium-free buffer.

By fitting the data of the measurements the values of R_{seal} and C_M can be obtained [5]. Figure 3 shows an exemplary measurement with the fitted curve for the adherent cells. The data were fitted such that R_{seal} and the resistance of the reference electrode (R_{el}) change with changing conductivity of the solution. Following values resulted for the sodium-containing buffer R_{seal}: $1.34 \cdot 10^6$, C_M: $1.86 \cdot 10^{-12}$ and R_{el}: $1.5 \cdot 10^3$ and for the sodium-free buffer R_{seal}: $1.47 \cdot 10^7$, C_M: $1.72 \cdot 10^{-12}$ and R_{el}: $1.9 \cdot 10^3$. The fitted curves show an increase of R_{seal} by by one order of magnitude when changing to measurement buffers with lower conductivity.

4 Conclusion

The seal resistance is a crucial factor for cell-substrate adhesion measurements with FETs. We observed clear differences in measured impedance signals with different conductivity of the measurement medium. By fitting the data we are able to determine the relations between measurement medium and cell adhesion spectra of our system.

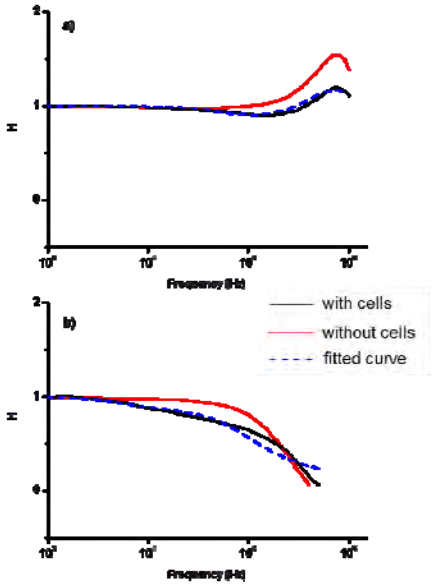

Fig. 3. Fitted curves for a) sodium containing buffer and b) in sodium-free buffer.

Acknowledgements

This work was supported by the Federal Ministry of Education and Research in Germany under projects 17008X10 and 17042X11.

References

[1] S. Ingebrandt, Y. Han, F. Nakamura, A. Poghossian, M. J. Schöning, and A. Offenhäusser (2007), Label-free detection of single nucleotide polymorphisms utilizing the differential transfer function of field-effect transistors, *Biosensors and Bioelectronics* 22, 2834–2840.

[2] S. Schäfer, S. Eick, B. Hofmann, T. Dufaux, R. Stockmann, G. Wrobel, A. Offenhäusser, and S. Ingebrandt (2009), Time-dependent observation of individual cellular binding events to field-effect transistors, *Biosensors and Bioelectronics*, 24, 1201–1208.

[3] A. Susloparova, D. Koppenhöfer, X. T. Vu, M. Weil, and S. Ingebrandt (2013), Impedance spectroscopy with field-effect transistor arrays for the analysis of anti-cancer drug action on individual cells, *Biosensors and Bioelectronics*, 40, 50–56.

[4] D. Koppenhöfer, A. Susloparova, D. Docter, R. H. Stauber, and S. Ingebrandt (2013), Monitoring nanoparticle induced cell death in H441 cells using field-effect transistors, *Biosensors and Bioelectronics*, 40, 89–95.

[5] A. Susloparova, D. Koppenhöfer, J. K. Y. Law, X. T. Vu, and S. Ingebrandt, Electrical Cell-substrate Impedance Sensing with field-effect transistors is able to unravel cellular adhesion and detachment processes on a single cell level, *submitted*.

[6] A. Offenhäusser, C. Sprössler, M. Matsuzawa, and W. Knoll (1997), Field-effect transistor array for monitoring electrical activity from mammalian neurons in culture, *Biosensors and Bioelectronics*, 12,819–826.

Organic Field-Effect Transistor Arrays as a Possible Low-Cost Alternative for In-Vitro Monitoring of Different Cell Cultures

Lotta Emilia Delle[1], Anna Susloparova[1], Xuan Thang Vu[1,2], Olga Fominov[1], Felix Hempel[1], Jessica Ka-Yan Law[1], Sven Ingebrandt[1*]

1 Department of Informatics & Microsystem Technology, University of Applied Sciences Kaiserslautern, Zweibruecken (Germany)
2 Present address: Department of Physics IA, RWTH Aachen University, Aachen (Germany)
* Corresponding author. E-mail address: sven.ingebrandt@fh-kl.de

Abstract
In this work micro-scale, organic field-effect transistor (OFET) devices based on polymeric semiconductor materials as an active channel are presented and used to study the cell-substrate adhesion by impedance spectroscopy and to record extracellular signals from cardiac myocyte cultures. As an organic semiconductor poly(3,4-ethylenedioxythiophene) doped with poly(styrene sulfonate) (PEDOT:PSS) was used. The electronic bandwidth of the micro-scale devices is mainly limited by the channel length and the carrier mobility in the material. In order to improve this performance a fabrication process for nano-sized OFET devices was developed with the aim to compare the nano-scale devices to their micro-scale counterparts.

1 Introduction

Biosensors based on silicon field-effect devices offer a wide range of possible applications. Main advantages as high sensitivity to changes in the surface potential and a possible miniaturization in size favor the detection of biomolecules [1], enzymatic activities [2] and cellular signals [3]. Disadvantages are high production costs and the typically opaque substrates, which interfere with standard cell culture microscopy. Devices based on organic polymers provide a cheap and transparent alternative. The conductive polymer PEDOT:PSS is a common material for applications in chemical and biological sensing [4].

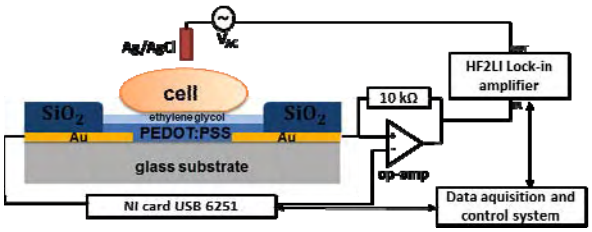

Fig. 1. Schematics of the OFET device cross-section and of the measurement setup [6].

In the present work the fabrication process of organic field-effect transistor (OFET) devices based on PEDOT:PSS is presented. In order to increase the electrical perfomance of the devices, gold interdigitated electrodes were used as a transistor gate for cell adhesion studies. The measurements show a significant difference between cell-covered and cell-free transistor gates, when sensors are read out in the so-called transistor transfer function (TTF) method typically used in our studies [5,6,7]. The TTF spectrum represents the combined bandwidth limiting effect of reference electrode, electrolyte solution, attached cell, transistor and first amplifier stage. The frequency dependent response of the attached cell to an ac voltage can be used to extract the characteristics of the attached cell (Fig. 1).

2 Materials and Methods

The OFET devices used in this study were fabricated on glass substrates. Micro-sized gold interdigitated source and drain electrodes (IDEs) were fabricated by a lift-off process on glass substrates and PEDOT:PSS was used as an active layer.

Nano-sized interdigitated electrodes (IDE) with spacings of 5 or 10 µm between electrode fingers were fabricated by nanoimprint lithography in combination with optical lithography for the source and drain contacts of the OFETs. After electrical passivation of the gold contact lines, the IDE areas were opened and used as electric contact to the polymer layer. The PEDOT:PSS solution was inkjet-printed by means of a material printer (Dimatix Material Printer 2831, Fujifilm Inc., USA). After printing, ethylene glycol was spin-coated and devices were subsequently annealed. The use of ethylene glycol leads to an increase in conductivity improving the carrier mobility and the electronic performance of the devices [8]. Most importantly annealing enhances the durability of PEDOT:PSS in aqueous media enabling long-term cell cultures. Chips were connected to a carrier via wire bonding and encapsulated for cell culture. HEK293 cells were cultured for adhesion assays and HL1 cardiac cells for electrical recordings of action potentials under standard conditions on the OFET arrays.

3 Results and Discussion

The micro-sized OFET devices were developed with the objective to investigate Electric Cell-Substrate Impedance (ECIS) [9] or to record electrical activity from cardiac myocytes [10]. For the ECIS assays HEK293 were cultured on the OFET devices and after 2 days in vitro (DIV) TTF spectra with cells and after cell removal using trypsin were compared (Fig. 2). For recording from cardiac myocyte cultures, HL1 cells were cultured and electrical activity was monitored after 2-3 DIV. Changes in impedance spectra were clearly monitored in case of the ECIS assays. In order to confirm that the measured effect is influenced by the attachment of the cells to the transistor surface and not by the degradation of the device, control measurements were performed. For the electrical recordings from cardiac myocyte cultures the bandwidth of the micro-scale devices is still too narrow so that only slow components of the extracellular signal shapes were visible (Fig. 3). Nevertheless, first action potentials were recorded demonstrating the general possibility to apply such devices for cell culture monitoring.

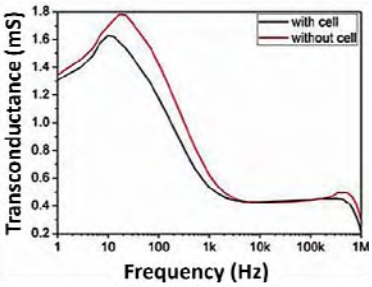

Fig. 2. ECIS assays with OFET devices. In general, the bandwidth of the micro-scale devices is too narrow to enable high-performance extracellular recordings. However, differences of cell-adhered to cell-detached situation are clearly visible.

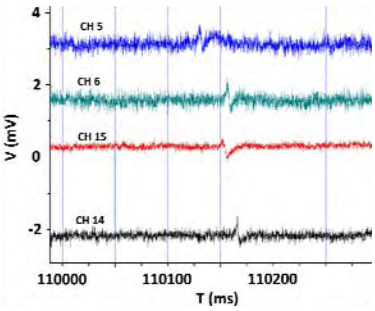

Fig. 3: Recording of action potentials from beating HL1 cell cultures after 3 DIV. Four channels were selected out of the 16-channel OFET array. Due to the limited bandwidth of the micro-scale OFETs, only slow frequency components of the field-potentials are visible.

To optimize the performance of the OFET devices, nano-sized IDE gate structures were fabricated (Fig. 4) by nanoimprint lithography in order to characterize them in terms of sensitivity and bandwidth compared to the micro-sized OFET devices.

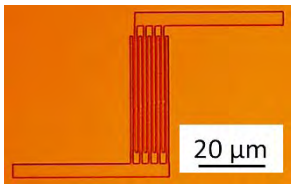

Fig. 4. Nano-sized IDE imprinted in an intermediate polymer stamp.

4 Conclusion

In this study, we demonstrate a straightforward fabrication process for OFETs suitable for different in vitro assays. It can be stated that the OFET devices can be used to analyze cell adhesion. Bandwidth of micro-scale OFETs is wide enough to record slow components of action potentials from cardiac myocyte cultures. The performance is influenced by the channel length of the devices, which can further be downscaled by fabrication with nanoimprint lithography. In general, OFETs offer a low-cost alternative to the already commercialized ECIS systems based on gold electrodes and eventually as single-use alternative to the silicon-based FET arrays for action potential detection.

References

[1] Ingebrandt S., Yeung C.K., Krause M., Offenhäuser A. (2007). Label-free detection of single nucleotide polymorphisms utilizing the differential transfer function of field-effect transistors. *Biosens. Bioelectron.*, 22, 2834–2840

[2] Katz E., Willner I. (2003). Probing Biomolecular Interactions at Conductive and Semiconductive Surfaces by Impedance Spectroscopy: Routes to Impedimetric Immunosensors, DNA-Sensors and Enzyme Biosensors. *Electroanalysis*, 15, 913–947

[3] Ingebrandt S., Yeung C.K., Krause M., Offenhäusser A. (2001). Cardiomyocyte-transistor-hybrids for sensor application. *Biosens. Bioelectron.*, 16, 565 – 570

[4] Khodagholy D., Rivnay J., Sessolo M., Gurfinkel M., Leleux P., Jimison L. H., Stavrinidou E., Herve T., Sanaur S., Owens R. M., and Malliaras G. G. (2013). High transconductance organic electrochemical transistors. *Nat. Commun.*, 4, 2133

[5] Schäfer S., Eick S., Hofmann B., Dufaux T., Stockmann R., Wrobel G., Offenhäusser A., Ingebrandt S. (2009). Time-dependent observation of individual cellular binding events to field-effect transistors. *Biosens. Bioelectron.*, 24, 1201-1208

[6] Susloparova A., Koppenhöfer D., Vu X.T., Weil M., Ingebrandt S. (2013). Impedance spectroscopy with field-effect transistor arrays for the analysis of anti-cancer drug action on individual cells. *Bios. Bioelectron.*, 40, 50-56

[7] Koppenhöfer D., Susloparova A., Docter D., Stauber R.H., Ingebrandt S. (2013). Monitoring nanoparticle induced cell death in H441 cells using field-effect transistors. *Bios. Bioelectron.*, 40, 89-95

[8] Yamashita M., Otani C., Shimizu M., Okuzaki H. (2011). Effect of solvent on carrier transport in poly(3,4-ethylenedioxythiophene)/poly(4-styrenesulfonate) studied by terahertz and infrared-ultraviolet spectroscopy. *Appl. Phys. Lett.*, 99, 143307

[9] Giaever I. and Keese C. R. (1993). A morphological biosensor for mammalian cells. *Nature*, 366, 591–592

[10] Stett A., Egert U., Guenther E., Hofmann F., Meyer T., Nisch W., and Haemmerle H. (2003). Biological application of microelectrode arrays in drug discovery and basic research. *Anal. Bioanal. Chem.*, 377, 486–495

Oriented Cortical Networks in Polydimethylsiloxane Microchannel Scaffolds for Recordings from Network Modules and Individual Connections

Rouhollah Habibey[1*], Asiyeh Golabchi[1], Anilkrishna Konduri[1], Marina Nanni[1], Francesco Difato[1], Axel Blau[1]

1 Fondazione Istituto Italiano di Tecnologia (IIT), Dept. of Neuroscience and Brain Technologies (NBT), Via Morego 30, 16163, Genoa, Italy, www.iit.it * Corresponding author. E-mail address: *rouhollah.habibey@iit.it*

Abstract

Compartmentalized PDMS devices are used for producing cortical or hippocampal networks with defined connections of neurites growing through microchannels. Using miniaturized PDMS microchannel devices, we generated two-compartment cortical networks with unidirectional connectivity. The two network modules and their interconnecting axons were accessible for extracellular recording and optical observation or manipulation. Seeding different types of neurons in each compartment may help in understanding the functional properties of oriented networks similar to *in vivo* models.

1 Introduction

Separate modules of small neuronal networks can be connected by chemical patterning and physical confinements through one or more neurite bundles to examine how sub-networks of neurons interact with each other [1]. Others have previously demonstrated that oriented connectivity between two networks can be created on microelectrode array (MEAs) by sequential seeding of neurons in two PDMS wells connected by microchannels [2]. However, the size of the wells made it almost impossible to record from all parts of each network. Here, we present a new miniaturized and thin PDMS tile for decreasing the network size, thereby making network modules and axons available for recording and optical observation or manipulation. The device is compatible with commercial MEAs and the design can easily be adapted to different electrode configurations.

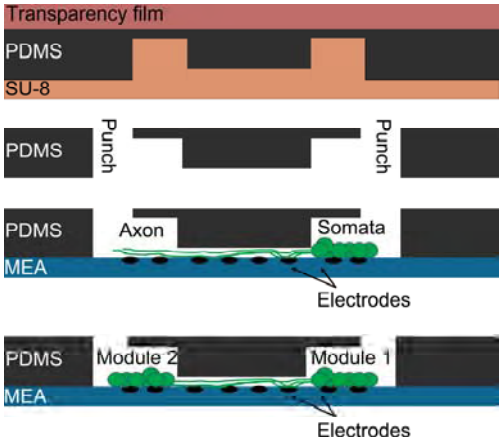

Fig. 1. Fabrication of the PDMS microchannel tile (A-B) and seeding of cortical neurons (C-D). A) Molding of the PDMS device from an SU-8 template, B) punching out of big reservoirs, C) device alignment on a MEA and seeding of the first network module, D) seeding of the second module.

2 Methods

2.1 PDMS device fabrication

The fine PDMS structures were molded by soft-lithography on SU-8 templates, including two small reservoirs for cell somata, which were connected by eight channels (widths: 30 µm, heights: 7 µm, lengths: 800 µm) (Fig .1). PDMS pre-polymer and catalyst were mixed (10:1), poured on the SU-8 master and a thin film of plastic foil placed on the surface to reduce the overall device thickness to < 200 µm. Big seeding reservoirs were punched on the two far edges of each small reservoir (Fig .2).

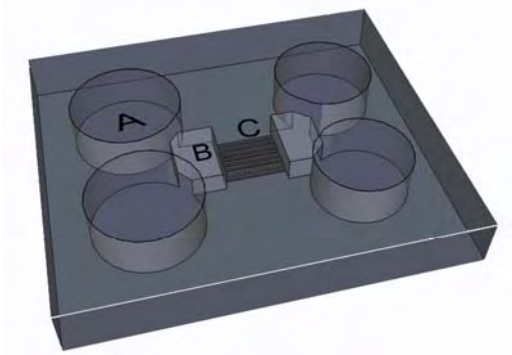

Fig. 2. PDMS microdevice with 4 big (A) and 2 small (B) reservoirs which are connected through 8 microchannels (C; h=7 µm, w=30 µm, l=800 µm). The capacity of each big reservoir (r = 1 mm) is equal to 0.628 µl, each small reservoir (h=100 µm, w=2000 µm, l=1400 µm) is equal to 0.28 µl.

2.2 Cell culture in microchannel tiles

Cured PDMS tiles were baked for 12h at 100 ^{o}C to crosslink any remaining oligomers. MEAs (electrode diameters = 30 µm, pitch = 200 µm) were coated with 0.1 mg/ml poly-D-lysine (PDL) and 0.05 mg/ml laminin after aligning the PDMS microchannels over the electrodes. Two rows of electrodes were located in

each reservoir while the rest of the electrodes were recording from microchannels (4 electrodes in each microchannel; Fig .1). After adding 1.5 ml cell culture medium (Neurobasal (NBM), B27 2%, Glutamax 1%, penicillin/streptomycin 1%) to each MEA and overnight incubation (5% CO_2, 37 ^oC, 95% RH), the medium was drained and rat cortical neurons were added through the supporting reservoirs (3 µl, 8000 cell/µl). A second neural network module was formed by adding new cells to the opposite compartment after 14 days *in vitro* (DIV) (Fig.3).

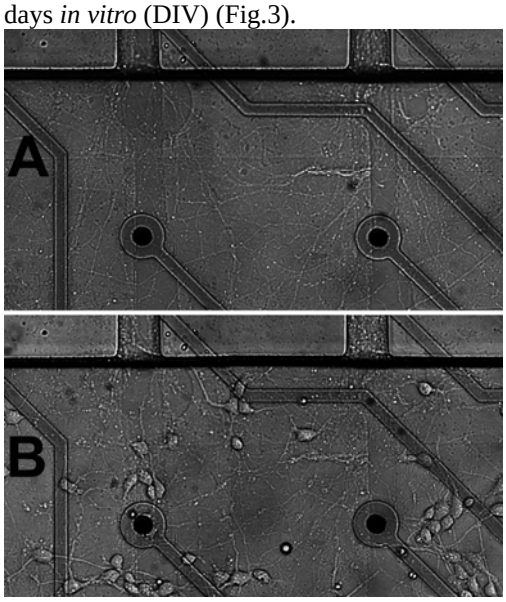

Fig. 3. Before and after seeding the cells in the second module. A) Axons from the first module had reached the second reservoir at 14 DIV before seeding the new cells. B) 3 DIV after adding new cells to the second reservoir, these started to get in contact with axons from neurons in the first reservoir (17 DIV). Electrode pitches are 200 µm.

3 Results

Adding cells through the open reservoirs automatically let them enter into the small reservoir and settle there. The small reservoirs produced almost closed chambers for small network formation on top of the electrodes. Cells were distributed homogenously in the small reservoirs with a maximum number of 2240 cells per module (reservoir). Neurites grew into the microchannels after 3 DIV and reached the opposite reservoir after 10 DIV. Freshly prepared cortical neurons were added after 14 DIV into the counterpart reservoir (Fig.3). Because of its thinness, the device was sufficiently transparent to track axonal growth and network formation by bright field or phase contrast up-right or inverted microscopy (Fig.4).

Fig. 4. Growing axons inside the microchannel at 10 DIV. Electrode pitch: 200 µm.

In spite of the small network sizes (≃ 2500 cells per reservoir), normal activity and amplified signals could be recorded from reservoirs and microchannels (250 µV and 1.2 mV, respectively; Fig.5). The first signals from axons inside the microchannels were recorded after 8 DIV, while no activity could be recorded from the first cortical module in the first reservoir. Only after 13 DIV, first signals could be recorded from the first cortical module. Signals from the second cortical module in the opposite reservoir could be recorded already after 6 DIV after plating (first module was 20 DIV). It seems that the presence of axons from the first module accelerates the differentiation and activity onset in the second module.

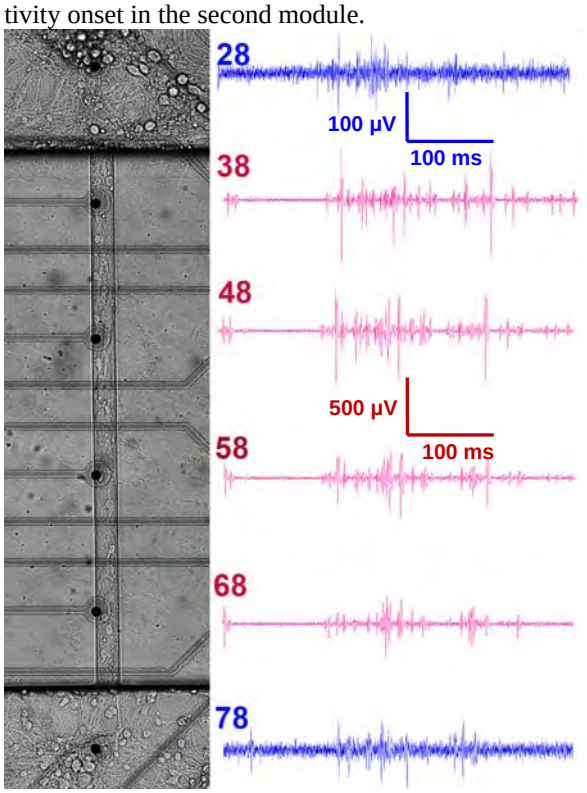

Fig. 5. An example of activity between two cortical modules and one of their connecting channels. Electrode 28 records from module 1, electrode 78 records from module 2 and electrodes 38, 48, 58 and 68 record from connecting axons. Recording window = 500 ms. Signal amplitudes on electrodes 28 and 78 are ≃ 250 µV. Maximum signal amplitudes on electrodes 38, 48, 58 and 68 are ≃ 1500 µV. Recording and microscopy pictures were prepared from the culture at 25 DIV (first module) and 9 DIV (second module).

Acknowledgement

We thank the Fondazione Istituto Italiano di Tecnologia for intramural funds in support of all parts of this study.

References

[1] Shein Idelson M, Ben-Jacob E, Hanein Y. (2010): Innate synchronous oscillations in freely-organized small neuronal circuits. PLoS One 5(12):e14443

[2] Pan L, Alagapan S, Franca E, Brewer GJ, Wheeler BC. (2011): Propagation of action potential activity in a predefined microtunnel neural network. J Neural Eng. 8(4):046031.

A Microfluidic Device for Selective Positioning of Invertebrate Neurons

Katharina Krumpholz[1*/**], Akram El Hasni[2*], Andreas Neuhof[1], Rudolf Degen[1], Uwe Schnakenberg[2], Peter Bräunig[1], Katrin Bui-Göbbels[1]

1 RWTH Aachen University, Institute of Biology II, 52074 Aachen (Germany)
2 RWTH Aachen University, Institute of Materials in Electrical Engineering (IWE 1), 52074 Aachen (Germany)
* Authors contributed equally
** Corresponding author. E-mail address: krumpholz@bio2.rwth-aachen.de

Abstract
We present microfluidic devices for selective positioning of locust and pond snail neurons. Fluid flows containing the neurons were generated by a syringe pump. The influence of different channel geometries as well as differences in flow rates were investigated to achieve appropriate conditions for handling the neurons gently and achieve efficiency in positioning.

1 Background /Aims

We are interested in the construction and investigation of small defined neuronal networks to gain detailed insight in network activity. Our aim is the control of neuronal activity inside the network and the unambiguous assignment of signals to individual cells. This becomes possible if every cell of the network grows on just one electrode of a MEA surface. In this context the use of invertebrate neurons provides the advantage that - in contrast to vertebrate cells - they can be cultured at extremely low cell density (Fig.1). Furthermore many neurons of invertebrates are very large. So they cover individual electrodes completely resulting in a better signal to noise ratio. The construction of such networks requires the positioning of neurons on the electrode surfaces, but positioning of cells onto single electrodes by manual handling without stressing them is still a problem.

In our project directed positioning should be achieved by a closed hydrodynamically working microfluidic device. Our far goal is the development of a cost-efficient, automatic biohybrid system. A combination of microfluidic device and MEA shall enable the selective positioning of individual neurons on the electrodes and the long term electrophysiological characterisation of single neurons as well as their interactions in the network.

2 Methods

2.1 Animal dissection

Insect (*Locusta migratoria*) and molluscan (*Lymnaea stagnalis*) neurons were extracted from thoracic ganglia and from the central ganglionic ring respectively, and affiliated in particular media (*Locusta*: modified Leibovitz L-15 cell culture medium [1]; *Lymnaea*: modified L-15 defined medium (DM) [2].

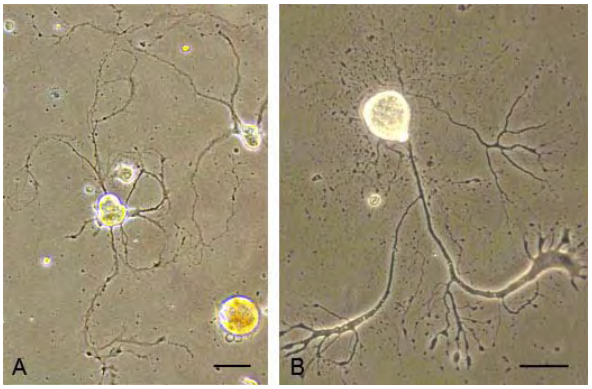

Fig. 1. Cultured neurons at low density sprouting numerous neurites. **A**: *Lymnaea* neurons. Scale bar: 50µm **B**: *Locusta* neuron. Scale bar: 20µm

2.2 Microfluidic devices

The microfluidic devices were fabricated in polydimethylsiloxane (PDMS) on glass using standard soft lithography and O_2 plasma bonding techniques.

Design variations of the cell trap device are shown schematically in Figure 2A/B. A fluid stream of defined velocity generated by a syringe pump, containing the pre-processed neurons, was guided into the device. The system is based on the principle of differential fluidic resistance. The fluid tends to flow along the path of least fluidic resistance. Here the meandering main channel has a higher fluidic resistance than the small transverse channels, which causes a higher flow rate through the transverse channels. This principle leads to a guiding of the neurons into the depressions upstream the transverse channels (Fig. 2A), where they can adhere.

The cell trap design shown in Figure 2A and 3A has the advantage that the integration of a MEA can be achieved most easily. Other design channel geometries and trap arrangements are improvements with respect to optimized flow proportions between main and transverse channel to increase efficiency of cell trapping. An example is shown in Fig. 2B and 3B.

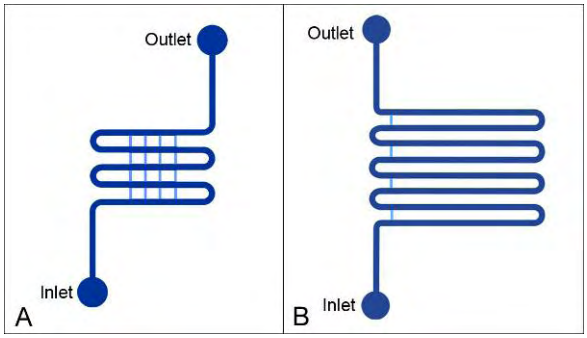

Fig. 2. Schematics of microfluidic cell traps. **A/B**: Meandering microchannel systems (dark blue) with transverse channels (light blue) for trapping neurons.

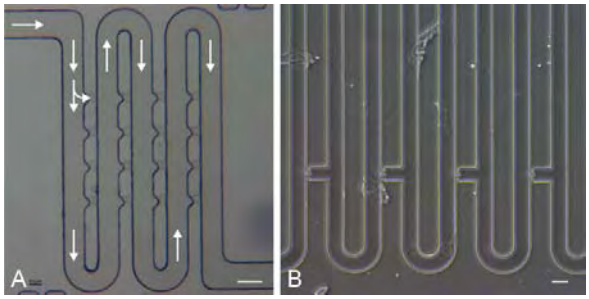

Fig. 3. Photographs of microfluidic cell traps. **A:** Device with 16 semi-circular trapping depressions and funnel shaped transverse channels. The white arrows indicate the direction of the fluid stream. **B:** Cut-out of device with four square trapping depressions in every other main channel section. Scale bars: 50µm

3 Results

The functionality of the cell traps with respect to different parameter variations like channel heights and widths as well as different flow rates was tested. Therefor we used polystyrene beads (Fig. 4A), *Locusta* and *Lymnaea* neurons.

It was possible to position invertebrate neurons in the depressions of the microfluidic cell trap devices (Fig. 4B). It turned out that very slow flow rates for the neurons (1 µl/min) are necessary otherwise the cells would simply become squeezed through the transverse channels because they deform quite readily. Channel widths wider than 75µm do not lead to an adequate deflection of the neurons when passing the depressions. Also the height of the transverse channel as well as the shape of the depression are important for trapping success. The transverse channels should be of the same height as the main channel otherwise the flow rate through the transverse channels would not be strong enough to deflect the cells. In addition, deeper trapping depressions prevent the neurons from coming adrift.

Preliminary results show that we are able to culture neurons in the closed microfluidic devices over a period of several days where they build numerous neurites (Fig.4C).

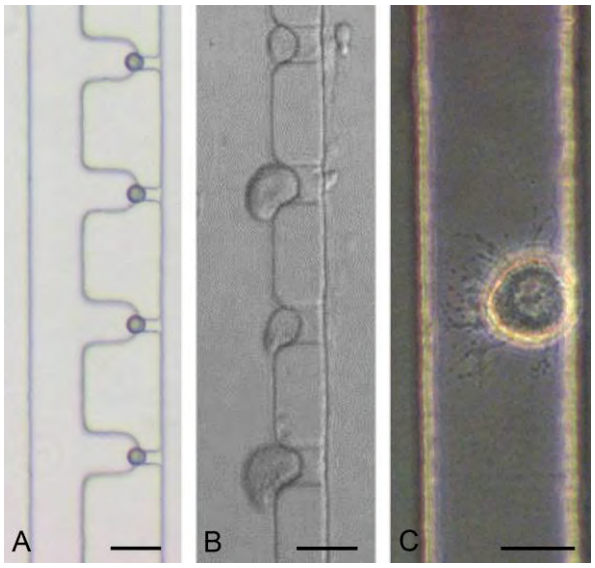

Fig. 4.A: Captured Polystyrene beads. Scale bar: 50µm **B**: Captured *Locusta* neurons. Scale bar: 50µm **C**: Cultured *Locusta* neuron in a microfluidic channel with numerous neurites. Scale bar: 25µm

4 Conclusion/Summary

Our tests show that the cell trap is suitable in capturing individual cells.

We observed that the successful use of the devices predominantly depends on the channel geometry as well as on the fluid velocity.

In general it turned out that beads tolerate parameter variations in channel sizes and flow rates much better than neurons. Our results indicate that neurons react sensitively to the shear stress they are subjected to. We observed that the neurons were deformed in the trapping depressions by the pressure of the stream. This effect was not described previously with cells of different cell lines [3].

So far the microfluidic devices represent a promising approach to handle the problem of positioning neurons selectively on electrodes on a MEA surface.

References

[1] Ridgway, R. L. (1991): Nerve Growth Factor (NGF) Induces Sprouting of Specific Neurons of the Snail, Lymnaea stagnalis. J. Neurobiol., 22, 377-390.
[2] Göbbels, K. (2010): Neuronal cell growth on iridium oxide. Biomaterials, 25, 1055-1067
[3] Frimat, J.-P. (2011): A microfluidic array with cellular valving for single cell co-culture. *Lab on a Chip*, 11, 231-237

Amplifier ASIC for Real 3D-Multichannel-MEA

Thomas Just[1*], Peter Husar[1]

1 Technische Universität Ilmenau, Germany
* Corresponding author. E-mail address: thomas.just@tu-ilmenau.de

Abstract
In this paper we will show the first results of a multichannel amplifier for 3D-MEAs with 800 capacitive sensors. One chip has included two amplification stages and sample-and-hold gate which will acquire the value of every sensor at the same time. 10 ASICs will be parallelized to read out in summary the 800 capacitive sensors of the 3D-MEA. The first simulation show a generated action potential of a spiking cell and the integrated signal at the output for further offline analyses.

1 Aims

For standard measurements of neuronal cell activity commercial 2D-MEAs are used. To get information in the third dimension it is necessary cultivate cells in additional layers. A 2D-MEA records only the activity on the bottom layer. To get signals from cells of the higher layers we will build towers with sensors. Because of the signal properties and the high number of sensors an ASIC will amplify, filter and multiplex the signals.

2 Methods

2.1 Concept of 3D-MEA

Standard MEAs are having sensor arrays on a two dimensional plate. To crow up into the third dimension sensors have to be placed on micro towers (Fig. 1). Every tower has 8 sensors, 10 towers per shape and one 3D-MEA will have 10 shapes (max. 800 sensors). Due to the small signal amplitude [1] the amplifier should be as near as possible at the sensor. The chip is designed to work as signal amplifier and stimulator simultaneously at 80 bidirectional channels on one shape.

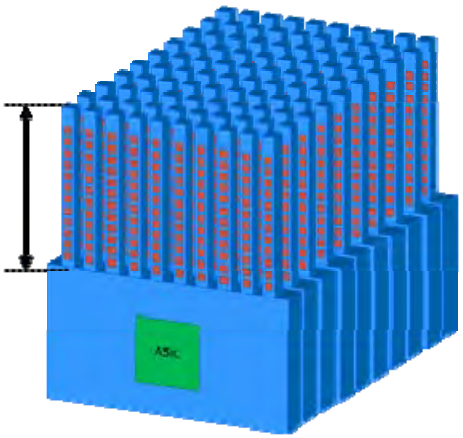

Fig. 1. Tower design; 8 sensors per finger, 10 fingers per shape, 10 shape build one 3D-MEA (in summary 800 sensors).

2.2 Concept of the ASIC

Every chip can synchronize itself with each other. The ASIC can be configured by the SPI interface, however, it can work autonomously by default settings.

Fig. 3 shows the equivalent network of neuron, sensor and amplifier. The cell produces potentials of about 100 mV across the membrane, the extracellular potential amounts only up to -80 µV – 40 µV [2]. The most signal power lies in the frequency range from 100 Hz to 10 kHz [3]. The activity of the cells is captured through the sensors capacity into the chip. 80 input signals are pre-amplified and filtered with low noise amplifiers. In the next step the signals are sampled in 160 sample-and-hold units which realize the snapshot function (reading from 80 sensors at one time and saving 80 samples from last timestamp). Several internal MUXs provide the signals to 4 output channels. The chip has a maximal amplification of 1000.

3 Results

Fig. 4 shows the simulated signal at the sensor (b) which was evoked by the intracellular signal (a). At the output we will get an inverted amplified signal for further analysis.

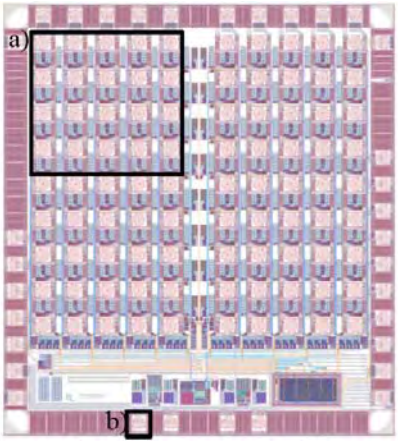

Fig. 2. ASIC-Layout. a) first amplification stage, b) output

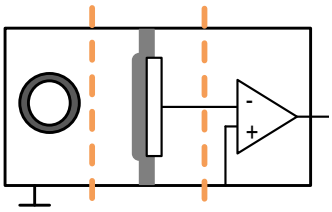

Fig. 3. Equivalent circuit diagram. Extracellular (blue), capacitive sensor (red), amplifier (green)

a)

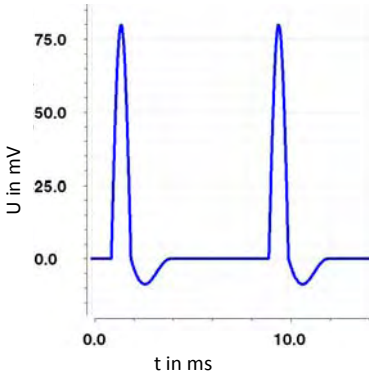

b)

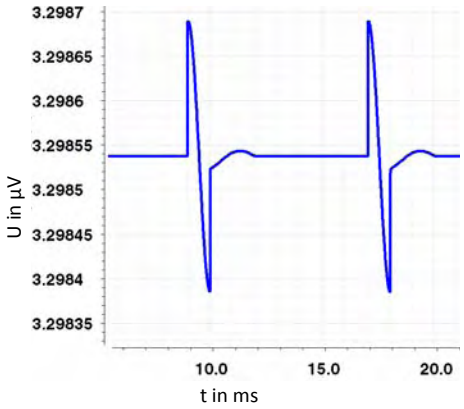

c)

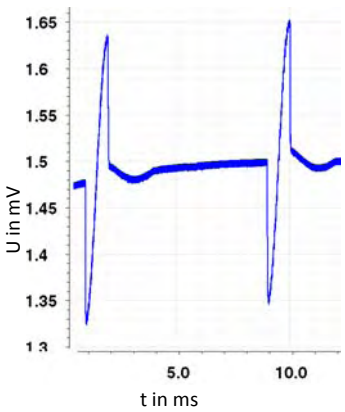

Fig. 4. Simulations; a) intracellular, b) extracellular, c) output of the ASIC

4 Summary

To get more information about 3D cell structures a novel kind of 3D-MEAs was developed. Additionally an ASIC was produced which will amplify measured cell activity as near as possible to the sensor. In this paper the concept of an amplifier ASIC for 3D-MEAs and first tests of the simulation results was shown.

Acknowledgement

This research has been supported by the 3DNeuroN project in the European Union's Seventh Framework Programme, Future and Emerging Technologies, grant agreement n°296590.

We will also thank the Institut für Mikroelektronik- und Mechatronik-Systeme (IMMS, Erfurt) for producing the ASIC.

References

[1] Silbernagl, S.; Despopoulos, A.: Taschenatlas Physiologie. Thieme Verlag.
[2] Carter M. (2010): Guide to research techniques in neuroscience. Academic Press, 1-376.
[3] Just T. et al (2013): Spike Sorting Algorithm for Multichannel MEA Recordings Based on Cross Correlation. Biomedizinische Technik/Biomedical Engineering (Biomed Eng)

Simultaneous Electrical Investigation of Isolated Neurites Using a Neurite-Isolation Device as Neurite Regeneration Model

Johann K. Mika[1], Karin Schwarz[2], Heinz Wanzenböck[1*], Petra Scholze[2], Emmerich Bertagnolli[1]

1 Institute of Solid State Electronics, Vienna University of Technology, Vienna, Austria
2 Center for Brain Research, Medical University of Vienna, Vienna, Austria
* Corresponding author. E-mail address: heinz.wanzenboeck@tuwien.ac.at

Abstract

The understanding of how neurites are guided to each other plays an important role in neurobiology inter alia in regrowth and repair of disconnected nerve cells. In the last decades several neurotrophic factors were identified to promote neurite out-growth and guidance to target links. While the effects of neurotrophins on the molecular properties of neurites are quite well examined, the impact on the electrical functioning was nearly neglected due to the limited possibility for simultaneous recordings with patch clamp technique. Microelectrode Arrays offer a method to overcome this limitation but do not guarantee for a small electrode to neurite distance.

In order to investigate the influence of neurotrophins on the electrical activity of growing neurites we developed a device that separates the neurites from the whole culture and provide microelectrodes near them. Our approach consists of a microfluidic device aligned on top of a multielectrode array. This setup enables the simultaneous recording of neuronal activity of growing neurites through microchannels and optical investigation of the whole growing cell population at the same time. The proof-of-concept was demonstrated with the growth of sympathetic neurons from the superior cervical ganglion of P5 WT mice responding to different levels of nerve growth factor (NGF), one of the most well-studied neurotrophic factors.

Due to the microchannels which act as guidance tubes for neurites the device is capable to act as neurite regeneration model. The approach to combine the guidance tubes with a multielectrode array further helps to verify the effect of neurite growth promoters on metabolical and electrical characteristics. It also enables a universal applicable device for future studies where neurites and somata need to be treated independently of each other.

1 Introduction

The guidance and reconnection of disconnected nerve cells of the central and peripheral nervous system to a target link is currently a strong research topic in neurobiology. In the last decades, several neurotrophins were identified as proteins which induce the survival, development, and function of neurons [1]. In detail, they also promote neurite out-growth and guidance to target cells [2]. While the effects of neurotrophins on the growth rate and molecular properties were quite well examined in the past, the impact on the electrical functioning of a whole network of neurons was nearly neglected due to the limitation of patch clamp technology. The development of multielectrode arrays by Thomas et al. 1972 [1] and finally the rise of this technology enabled neurobiologists to record nerve signals from a whole culture simultaneously.

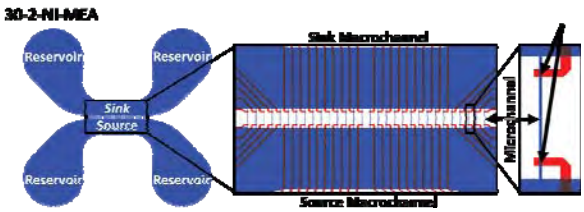

Fig. 1. Schematic drawing of the 30-2-Neurite Isolation-MEA. The NI-part consists of 4 supply reservoirs and a sink and source macrochannel (left, blue). The cells will be seeded either in the source or in both macrochannels. The 30 microchannels (blue) allow only neurites to enter whereas 2 electrodes per channel enable electrical activity recordings of the neurite.

While MEAs broke through the limitation of few electrodes, they did not guarantee a small, defined contact zone between electrode and neurite. To overcome this issue and to investigate electrical signals of multiple neurites our approach consists of a microfluidic neurite-isolation (NI-) device aligned on top of a multielectrode array. Figure 1 shows a schematic view of our device.

This setup enables the simultaneous recording of neuronal activity of growing neurites through microchannels and optical investigation of the whole growing cell population at the same time. We

demonstrated the proof-of-concept with neurons from the superior cervical ganglion of P5 WT mice responding to different levels of nerve growth factor (NGF).

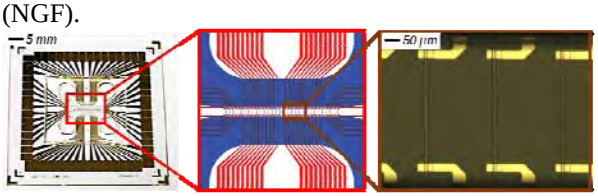

Fig. 2. Neurite-Isolation MEA with a closer look on the inner microelectrode-microchannel area.

2 Material and Methods

The NI-MEA device is composed of two components, the neurite-isolation device (NI-device, upper part) and a custom designed multielectrode array (MEA, lower part). The NI-device consists of two culture chambers (source and sink) with reservoirs at their ends as cell inlets and media supply. Source and sink chambers are connected together by 30 microchannels (diameter < 10 µm) which act as physical barriers for neuronal somata allowing only neurites to enter. The MEA with its electrodes is precisely aligned within the microchannels so that each microchannel is equipped with two microelectrodes (electrode material either gold or ITO with TiN coating). Figure 2 shows a produced NI-MEA and a closer look on the microchannel/microelectrode area.

Cells of the superior cervical ganglion of P5 WT mice were loaded into the source chamber via the cylindrical reservoirs. The cells were grown in NI-MEAs with different nerve growth factor concentrations for 14 days. Electrical measurements on days 4, 7 and 14 using a BC1060 recording setup (MultiChannelSystems, Reutlingen, Germany) were taken. The data was then analyzed using a developed MATLAB program using a combination of threshold analysis and principal component analysis [4].

After 14 days the cells were fixed and stained using different antibodies to acquire parameters like cell distribution, neurite growth and type. The data was also compared with the images captured regularly after each electrical measurement.

3 Results

The optical and electrical results were correlated and the overall results analyzed. Electrical activity maps showed different patterns in accordance to chemical stimulation of the growing cells.

The optical transparency of the NI-MEA allowed tracing cultures by optical light microscopy as well as fluorescence microscopy using immunocytochemistry (Figure 3).

As proof-of-concept and also to show the sensitivity of the device different nerve growth factor gradients in the macrochannels were analyzed (Figure 4). A degree of consistence between the ingrowth of neurites into microchannels and electrical activity was determined with 93.6%.

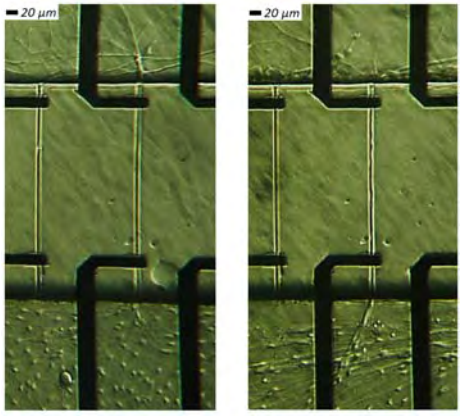

Fig. 3. Optical light microscopy of the same area (DIV 7 and 10).

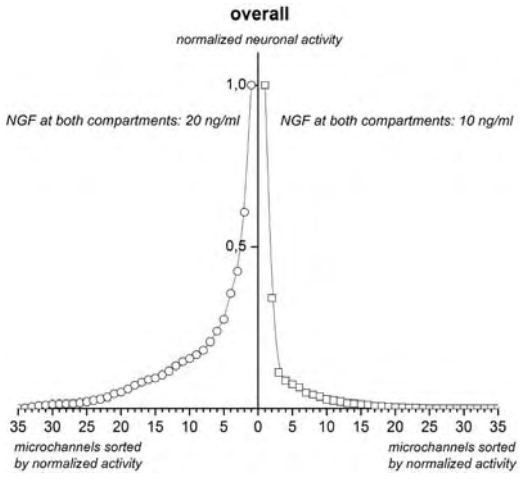

Fig. 4. Different concentrations of neurite growth factor result in different recorded electrical activity.

4 Conclusion and Discussion

We designed a new microfluidic-microelectrode device that combines a neurite isolation device with a MEA. This platform for (re-)generating neurites enables both microscopic observations of and electrophysiological recordings from neurites. The proof of concept of the device was shown by recording spontaneous as well as nicotine-induced electrical activity of mouse sympathetic neurons for two weeks with two different concentrations of NGF.

References

[1] Bradbury EJ & McMahon SB. (2006). Spinal cord repair strategies: why do they work? *Nature reviews Neuroscience* 7, 644-653.

[2] Sofroniew M.V., Howe C.L. & Mobley W.C. (2001). Nerve growth factor signaling, neuroprotection, and neural repair. *Annu Rev Neurosci* 24, 1217-1281.

[3] Thomas C.A., Springer P.A., Loeb G.W., Berwald-Netter Y., Okun L.M. (1972) A miniature microelectrode array to monitor the bioelectric activity of cultured cells. *Exp Cell Res*, 74: 61–66

[4] Schuller P (2014) Investigation of Neuronal Activity recorded with Multi-Electrode Arrays using Principal Component Analysis. *9th International. Meeting on Substrate-Integrated Microelectrode Arrays*, Reutlingen, Germany.

Ultra-Low Cost Arrays of Printed Carbon Electrodes for Extracellular Recordings

Jan Schnitker[1], Alexey Yakushenko[1], Francesca Santoro[1], Fabian Brings[1], Bernhard Wolfrum[1], Andreas Offenhäusser[1]

1 ICS-8/PGI-8 Institute of Bioelectronics, Forschungszentrum Jülich, Germany
* Corresponding author. Email address: a.offenhaeusser@fz-juelich.de

Abstract
Multielectrode arrays are a commonly used tool in neuroscience for the investigation of cellular networks and their communications processes by recording extracellular signals. In particular, advanced MEAs featuring 3D electrode can achieve very high signal noise ratios and a high durability for extracellular recordings. The fabrication of MEAs requires typically a cleanroom environment and uses expensive materials for the fabrication process. We investigated a new approach based on printed carbon. We fabricated by hand printed carbon electrode MEAs in very few and steps and used extremely cost-efficient materials for the fabrication. These printed carbon chips were successfully used for extracellular recordings from cardiomyocyte-like cells showing a high signal-noise ratio.

1 Background

Modern chip-based electrophysiological investigations can rely on a variety of different chip types ranging from planar metal microelectrodes to 3D nanoelectrodes [1]. These biosensor devices can feature excellent cell-chip coupling for recording and stimulation of electrogenic cells. Moreover, they can reach subcellular spatial resolution. They require elaborated fabrication methods such as cleanroom facilities and, therefore, are expensive and potentially labor intense in fabrication. It is not only for high-throughput oriented applications such as drug-screening very desirable to have ultra-low cost devices which are even disposable. We demonstrated the successful use of individual printed carbon electrodes for neurotransmitter release measurements [2]. We extended this ultra-low cost fabrication approach to carbon-based multi electrodes arrays (MEAs) and applied them for extracellular recordings from electrogenic cells. Arrays of such printed carbon electrodes can be manufactured in very few simple steps.

2 Methods

We applied different kinds of carbon pastes, commercially available as well as self-synthetized inks on flexible polymer substrates and rigid glass surfaces. Then, we covered them with Polydimethylsiloxane (PDMS, Sylgard 184, Dow Corning). The electrode apertures were manually pinched with a needle. The fabrication process was completed with the connection of the electrode feedlines to a carrier adapting to the electronic socket of the amplifier system for later readout. The surface of a commercial and self-synthesized ink is shown in Fig 1 showing large differences in roughness.

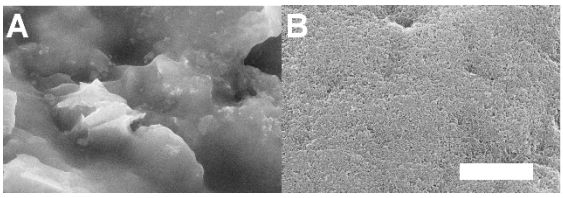

Fig. 1. SEM micrographs of two printed carbon inks with **(A)** commercial ink with high roughness, **(B)** self-synthesized ink with smooth surface
(scale bar 5 µm).

A fabricated 6 channels MEA with different sized electrode the stripes on printed carbon is shown in Fig. 2. We fabricated printed carbon electrodes on three different substrates: glass, polyimide (Kapton ™, Dupont) and polyethylene terephthalate (PET, Dupont).

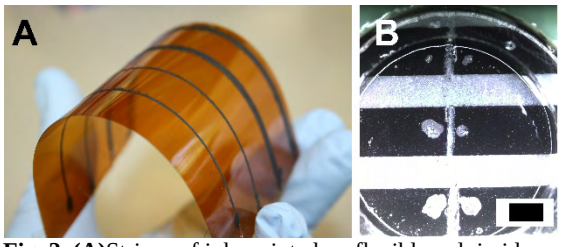

Fig. 2. (A) Stripes of inks printed on flexible polyimide subsrtate, **(B)** six stripes of printed carbon with 6 different sized electrodes on a encapsulated MEA (scale bar 1 mm).

3 Results

We cultured cardiomyocyte-like cells (HL-1) on the chips and measured the electrical activity after 3 DIV with a self-developed low-noise amplifier system. An example trace of an extracellular voltage recording is shown in Fig. 3. The extracellular recording exhibits a low

background noise-level and a high signal-to-noise ratio, comparable to the recording quality of e.g. Au or Pt-MEAs produced by means of standard cleanroom fabrication (data not shown).

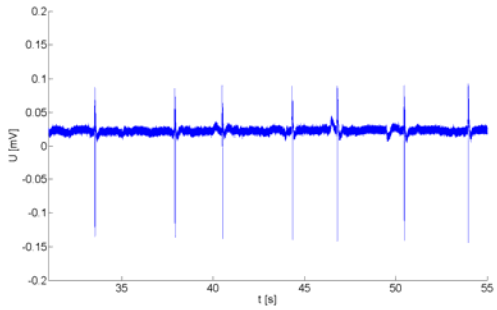

Fig. 3. Extracellular recording of action potentials with printed carbon electrodes from HL-1 cells.

4 Conclusion

We demonstrated a novel fabrication method for printed carbon electrode MEAs which can be used for extracellular voltage recordings. The printed carbon electrodes have shown a similar performance in terms signal-noise ratio compared to typical recordings metal-based multi electrode arrays in the regime of few hundred microvolts. The manufacturing process of the disposable printed carbon chips employs very cheap commercial or homemade carbon pastes for the electrodes and PDMS as passivation material. This keeps the overall fabrication costs extremely low. Printed carbon electrodes can be applied for a wide range of applications in chip-based life-sciences ranging from amperometric measurements to extracellular voltage recordings of action potentials.

References

[1] Spira ME, Hai A. Multi-electrode array technologies for neuroscience and cardiology. Nat. Nanotechnol. 2013 Feb;8(2):83–94.

[2] Yakushenko A., Schnitker J., B. Wolfrum. Printed Carbon Microelectrodes for Electrochemical Detection of Single Vesicle Release from PC12 Cells. Analytical Chemistry. 2012 May 15;84 (10):4613–4617.

Stimulation Artifact Suppression Techniques for High-Density Microelectrode Arrays

A.Shadmani[1], J. Müller[1], P. Livi[1], M. Ballini[1], Y Chen[1], A. Hierlemann[1]

1 ETH Zürich, Department of Biosystems Science and Engineering, Basel, Switzerland

Abstract

Stimulation protocols used with Microelectrode arrays (MEAs) cause residual charges and artifacts on the stimulation electrodes or on the immediately neighboring electrodes. Here, we report on two techniques that help to suppress the generated artifacts on the neighboring electrodes of the stimulation site. The first technique is to disconnect the electrodes from the recording channels during stimulation. The second technique includes to measure and then store the respective resting potential values of the electrodes and to then restore those potentials on the electrodes after stimulation.

1 Background/Aims

The possibility to stimulate individual neurons is an essential requirement to answer many questions in neuroscience. Electrical stimulation is required for triggering action potentials and analyzing neuronal network dynamics or investigating neuronal plasticity. It is important to have the possibility to investigate the neuronal activity immediately after stimulation pulses in close vicinity to the stimulation sites. Therefore, efforts have been undertaken, e.g. [1], to enable recording from the same electrode that has been used for stimulation. These efforts mainly focus on removing of the residual stimulation signal, i.e., stimulation artifact on the stimulation electrode to have it ready for immediate recording after stimulation. While this is an interesting solution for low-density MEAs, high-density MEAs allow for achieving high-resolution recordings without the need to acquire the signal on the stimulation electrode by simply using the recordings from the closely spaced neighboring electrodes.

Since the gain of recording circuits in the high density MEA is high, and the distance between the electrodes is small, a stimulation signal will affect the recording circuits of the surrounding electrodes and potentially prohibits recording for a few seconds before those channel circuits get back to their operating state.

2 Methods/Statistics

One solution to suppress the artifacts is to disconnect the neighboring electrodes from the recording circuits during the stimulation phase and then immediately reconnect them once the stimulation has been performed. The second solution is to measure and store the resting potential of the neighboring electrodes before stimulation, and then keep the electrodes at this stored potential during stimulation. Immediately after stimulation the potential application is stopped, and the electrodes will be available to record neural activities.

3 Results

Fig. 1a, shows a set of electrodes on the high-density MEA, configured for stimulation (red) and recording (blue) with a gain of 512. Fig. 1b shows the stimulation signal and the resulting artifact on the neighboring recording channel. It takes about 2 seconds to get back to the operating state. Fig. 2 shows the schematic and measurement results of the circuit used for the disconnection technique. In this case, the recording channel is ready for recording around 1 ms after stimulation. Fig. 3 shows the schematic and measurement results of a test circuit fabricated in 0.18 µm CMOS technology, which can apply the initially measured potential of the recording electrode during the stimulation phase. This circuit is connected to a CMOS-based high-density microelectrode array (HD-MEA), featuring 26,400 electrodes at 17.5 µm pitch, 1024 recording channels, and 32 stimulation units for bidirectional communication with electrogenic cells [2,3]. In this case the recording channel will be ready to record in less than 1 ms after the stimulation pulse.

4 Conclusion/Summary

Two techniques were presented for suppressing the stimulation artifacts on neighboring electrodes of the stimulation site. Both techniques show a significant improvement for suppressing the artifacts. The recording channel disconnection technique does not require any additional circuitry.

Acknowledgement

This work was supported by the Advanced ERC Grant “NeuroCMOS” under contract number AdG 267351. Amir Shadmani received individual support through the Marie Curie Research Training Network “EngCaBra” (grant agreement no. 264417)

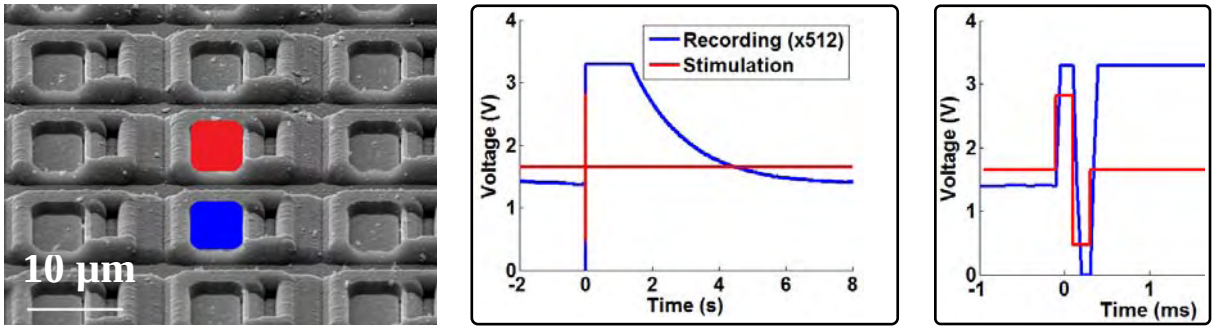

(a) **(b)** **(c)**

Fig. 1.. **(a)** Pt-microelectrodes, 17.5 µm pitch (red: stimulation electrode, blue: recording electrode), **(b)** Stimulation and recording voltages without artifact suppression (recording amplification is 512 times), **(c)** Zoom-in around stimulation pulse

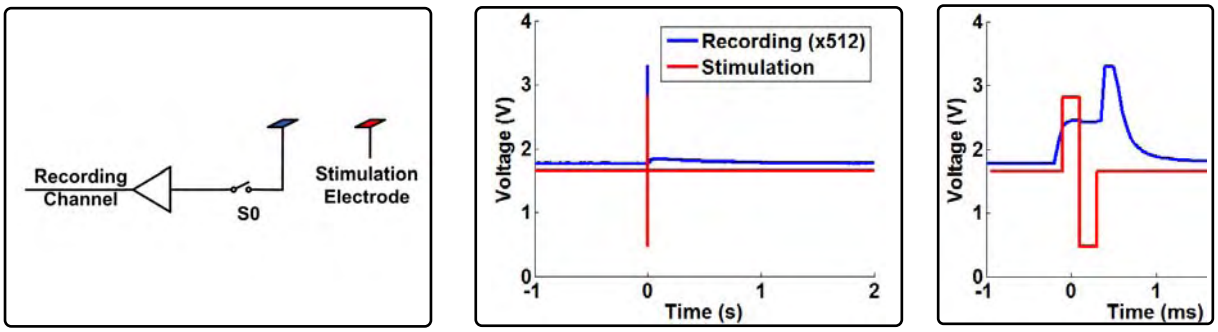

(a) **(b)** **(c)**

Fig. 2. (a) Circuit schematic for stimulation artifact suppression by using the recording channel disconnection technique. **(b)** Improved stimulation artifact by using this technique. **(c)** Zoom-in around stimulation pulse

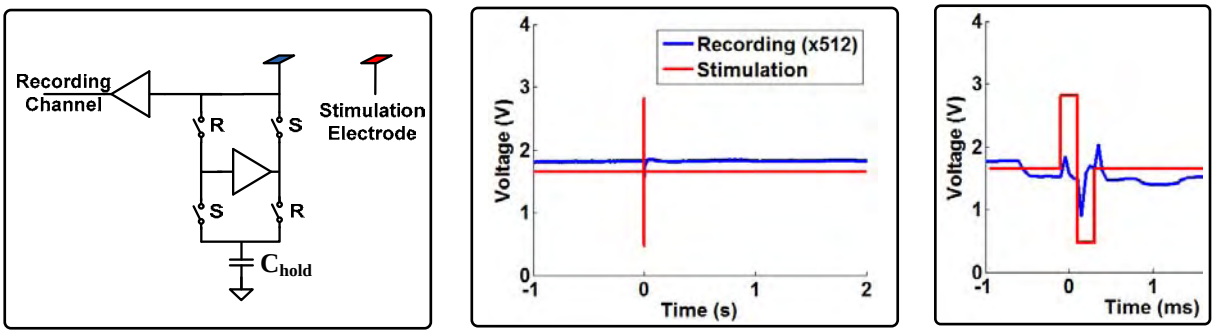

(a) **(b)** **(c)**

Fig. 3. (a) Simplified circuit schematic for stimulation artifact suppression using the technique of first storing the electrode potential to C_{hold}, then maintaining this potential during the stimulation phase, **(b)** Improved stimulation artifact by using this technique, **(c)** Zoom-in around the stimulation pulse

References

[1] E. A. Brown et al., Stimulation Artifact Elimination in a Multi-Electrode System, *IEEE Transactions on Biomedical Circuits and Systems*, Vol. 2, No. 1, March 2008

[2] M. Ballini, A 1024-Channel CMOS Microelectrode-Array System with 26’400 Electrodes for In-vitro Recording and Stimulation of Electro-active Cells In-vitro, *VLSI Symposium 2013*, Kobe Japan, 2013.

[3] J. Müller et al., Conferring Flexibility and Reconfigurability to a 26'400 Microelectrode CMOS Array for High Throughput Neural Recordings", in *Proc. Transducers ’13*, Barcelona, Spain, pp. 744-747, 2013.

Large-Area, High-Density Arrays of Micro-Needles for Acute Slice Electrophysiology

D.E. Gunning[1*], P. Hottowy[2*], W. Dabrowski[2], A. Sher[3], J.M. Beggs[4], C.J. Kenney[5], D.A. Young[1], A.M. Litke[3] and K. Mathieson[1]

1 Institute of Photonics, SUPA, University of Strathclyde, Glasgow, UK
2 AGH University of Science and Technology, Krakow, Poland
3 SCIPP, University of California Santa Cruz, Santa Cruz, California, USA
4 Biocomplexity Institute, Indiana University, Bloomington, Indiana, USA
5 SLAC National Accelerator Laboratory, Menlo Park, California, USA
* Corresponding author. E-mail address: deborah.gunning@strath.ac.uk

Abstract

This paper introduces a highly dense, large-area array of micro-needles developed specifically for in vitro, acute slice electrophysiology. The array incorporates 512 needles with 60 μm inter-needle spacing. Each needle measures up to 250 μm in height and at the tip has a small (5-10 μm diameter) conducting platinum electrode. The electrode impedance is measured to be ~300 kΩ at 1 kHz and the system noise is ~7 μV allowing action potentials to be recorded from individual neurons. The needles can penetrate in to neural tissue and with the potential to record from hundreds of neurons simultaneously, this technology will be used in high-resolution connectivity studies of local networks of neurons in acute slices.

1 Introduction

For many years, the use of planar microelectrode arrays has been a widely adopted electrophysiological approach to studying connected neural activity. Whilst these types of arrays work very well to record the simultaneous activity of hundreds of neurons in both retina and culture [1,2,3], it is widely accepted that, as a consequence of the planar nature of the electrodes, their usefulness in vitro is limited to studying neurons on the surface of a tissue preparation. For the study of acute slices, where the surface neurons and their connections can be damaged by the slicing procedure, arrays of 3-d microelectrodes address this limitation by penetrating in to the slice to bypass the damaged surface layer and record from the intact interior volume of the slice [4,5,6,7].

Here, the fabrication and electrical characterization of a large-area, high-density array of micro-needles is presented. The array is fabricated in silicon and incorporates 512 needles with a needle density of 256 needles/mm^2. The needles can measure up to 250 μm in height and at the tip of each is a small, 5-10 μm diameter platinum electrode. The device has been electrically characterized to show that the platinum electrode impedance at 1 kHz is ~300 kΩ and the complete readout system operates with an RMS noise of ~7 μV.

The array covers an area of 1 x 2 mm^2 allowing the connectivity of neurons between cortical layers and multiple cortical columns in the mouse brain to be recorded simultaneously. The small electrode size combined with low impedance enables single-cell resolution recordings with an excellent signal to noise ratio (~15:1).

2 Method

Each micro-needle array is a 32 x 32 mm^2 chip, four of which are fabricated on to a 100 mm diameter silicon wafer using a novel sequence of semiconductor fabrication techniques. The process relies on the high-aspect ratio etch capability of the Bosch process and the conformality of a tungsten film deposited by low pressure CVD. In Figure 1, the major fabrication steps of a single needle are illustrated.

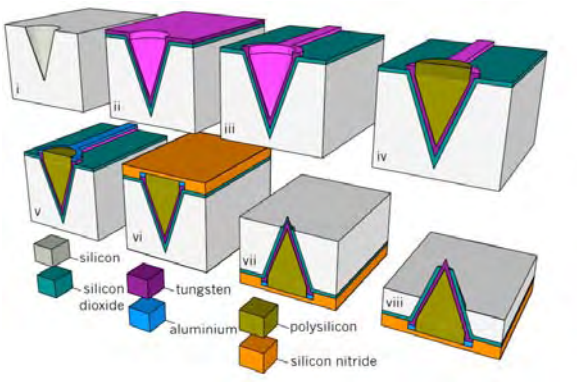

Fig. 1. A schematic of the main steps in the micro-needle array fabrication process. The fabrication of a single micro-needle is illustrated. The needles (etched hole, silicon dioxide passivation, metallization and polysilicon filler) are 'embedded' in to the silicon (i-vi) and in the final process steps, the silicon is removed to expose the array of needles and the silicon dioxide insulation is removed from the tips of the needles to expose a tungsten electrode (vii-viii) which is subsequently electroplated with platinum black.

The fabrication process for the 512-channel micro-needle array has been adapted from that described in [7] for the fabrication of a 61-channel micro-needle array. The most significant modifications include using an SF_6/Ar etch chemistry for the high-resolution

(2 μm minimum feature size) tungsten readout pattern (to improve the etch selectivity to photoresist). Also the deep silicon etch (step viii of Figure 1) has been optimised to use a combination of the Bosch process and wet chemical (TMAH) etching to expose the micro-needles. This results in a faster and more anisotropic silicon etch. The completed chip is wire-bonded in to a 512-channel system of low-noise pre- and post-amplification readout circuitry [8].

3 Results

An array of 512 micro-needles was successfully fabricated and electrically characterized. A 100% of needles were shown to be mechanically viable (no broken needles) across an array. The platinum electrode impedance was measured to be ~300 kΩ at 1 kHz, a suitable value to allow recordings of neuronal action potentials (duration ~1 ms).

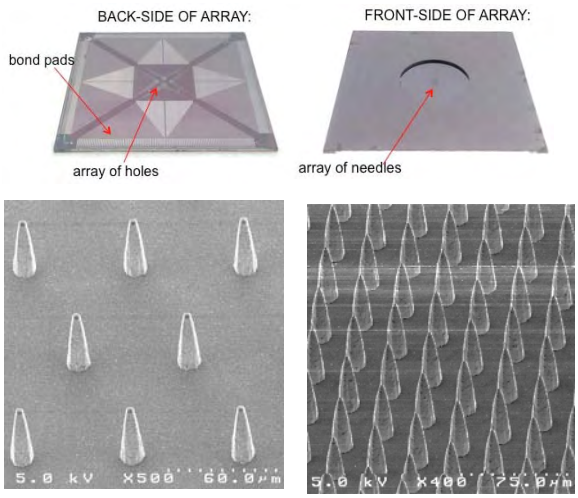

Fig. 2. (top) Photo of front- and back-side of a 512-channel micro-needle array showing tungsten readout wires leading to aluminium bond pads. (bottom left) SEM image of ~75 μm tall 60 μm spaced micro-needles. (bottom right) SEM image of ~75 μm tall 30 μm spaced micro-needles.

The readout system operates with ~7 μV RMS noise, making biological recordings with an excellent signal to noise ratio (15:1) possible. Images of the front- and back-side of an individual chip and SEMs of the micro-needles spaced at 60 and 30 μm (i.e. respective densities of 256 and 512 needles/mm^2) are shown in Figure 2.

4 Conclusions

A 512-channel micro-needle array with a needle density of 256 needles/mm^2 was successfully fabricated to have dimensions suitable for a large-area, high-resolution study of connectivity in local neural networks. The small, low-impedance platinum recordings enable recordings of action potentials from individual neurons. The designed fabrication process is robust and versatile, lending itself to future arrays with longer needles, multiple needle lengths across a single array, higher densities and larger area coverage. Ultimately, this innovative new technology could allow neuroscientists to look, with unprecedented detail, at the connected electrical behaviour of neural circuits in vitro.

Acknowledgement

The work was funded by RAEng fellowship EP/H044639/1 (DEG), NSF grants IIS-0904413, PHY-0750525 (AML) and IIS-0904912 (JMB), the Pew Charitable Trust's Scholarship in the Biomedical Sciences (AS) and Polish Ministry of Science and Higher Education grants (WD, PH). The device fabrication was done at the SNF, Stanford University, the JWNC, University of Glasgow and microfabrication labs at the Queen's University, Belfast and the University of Strathclyde.

References

[1] Field G.D. et al (2010). Functional connectivity in the retina at the resolution of photoreceptors. *Nature*, 467, 673-677.
[2] Jimbo Y. and Kawana A. (1992). Electrical stimulation and recording from cultured neurons using a planar electrode array. *Bioelectrochem. Bioenergy*, 29, 193-204.
[3] Tang A. et al (2008). A maximum entropy model applied to spatial and temporal correlations from cortical networks in vitro. *J. Neurosci*., 28, 505.
[4] Nordhausen C.T., Rousche P.J. and Normann R.A. (1994). Optimising recording capabilities of the Utah intracortical electrode array. *Exp. Brain Res.*, 637, 27-36.
[5] Charvet G. et al (2010). BioMEA: A versatile high-density 3D microelectrode array system using integrated electronics. *Biosens. Bioelectron.*, 25, 1889-1896.
[6] Heuschkel M.O. et al (2002). A three-dimension multi-electrode arrays for multi-site stimulation and recording in acute brain slices. *J. Neurosci. Methods*, 114, 135-148.
[7] Gunning et al (2013). Dense arrays of micro-needles for recording and electrical stimulation of neural acute brain slices. *J. Neural Eng*., 10, 016007 (11pp)
[8] Litke A.M. et al (2004) What does the eye tell the brain?: Development of a system for the large-scale recording of retinal output activity. *IEEE Trans. On Nucl. Science*, 51(4), 1434-1440.

A Hybrid Multi Optrode Electrode Array for Optogenetics

Luis Hoffman[1], Alexandru Andrei[1], Robert Puers[1,2], George Gielen[1,2], Dries Braeken[1]*

1 Imec, Leuven, Belgium
2 ESAT, KULeuven, Leuven, Belgium
* Corresponding author. E-mail address: dbraeken@imec.be

Abstract
Today, optogenetic tools play an important role in the unraveling of neuronal circuits in the brain. Here, we present a novel hybrid multi optrode electrode array (MOEA) for optogenetic applications *in vitro*. The MOEA comprises of an arrangement of 64 titanium nitride electrodes and 64 optical outputs distributed over two different wavelengths (470 nm and 590 nm); both functionalities are integrated monolithically into a silicon substrate using CMOS compatible technology. This enables the device to optically stimulate a single cell and simultaenously record its electrical activity.

1 Background

Optogenetics has emerged as an invaluable tool to study brain connectivity by optically controlling well-defined events in living cells. To ensure continuous progress in this field, new tools with improved capabilities should be developed. Such devices are ideally cheaper, offer better reproducibility and feature multiple independent optical outputs. Additionally, full integration of optical stimulation of different wavelengths combined with electrical recording would increase the degrees of freedom of experimental design in optogenetics.

2 The proposed device

MOEA

The presented in vitro device contains 64 TiN electrodes and 64 optical outputs, located closely together to allow for optical stimulation and recording of the same cell. The electrodes are 30 µm in diameter and the optical outputs are approximately 6 by 20 µm in size, which resembles the area of a single cell (see **Fehler! Verweisquelle konnte nicht gefunden werden.**). Light is carried from external sources (light emitting diodes or lasers) into silicon nitride waveguides by optical input gratings. Two different grating designs were incorporated; one is capable of coupling light of 470 nm into one set of waveguides and the other of 590 nm in another set of waveguides. At the electrode/optrode site, the light is extracted from the waveguides perpendicular to the electrode plane by optical output couplers (see Fig 2).

Fabrication

The device is fabricated in imec's clean room facilities. It is manufactured on silicon wafers using a CMOS compatible process and combines two well-established techniques: one used for the fabrication of neural probes and the other for the creation of optical interconnects in telecommunication systems. All this ensures that the resulting devices are highly reproducible, reliable and scalable.

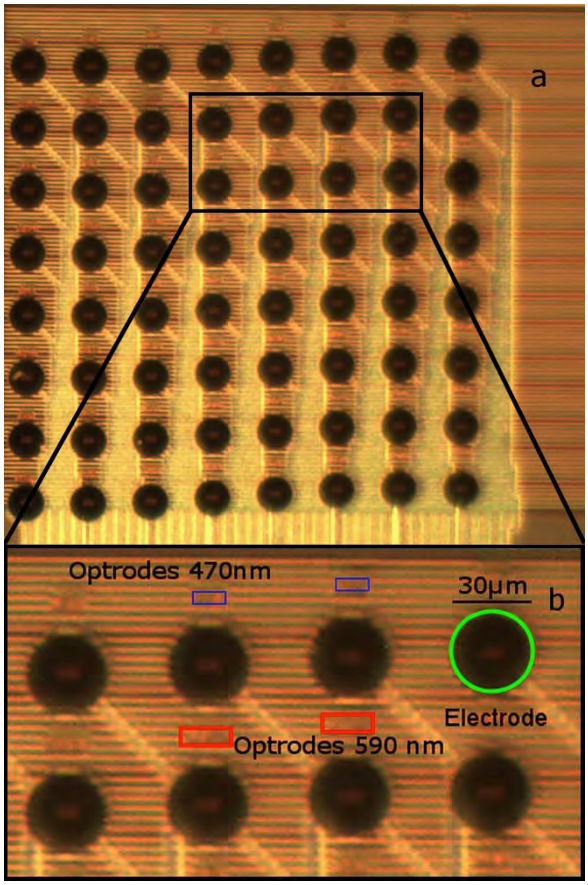

Fig. 1. (a) Complete view of the MOEA. (b) Detail section where the different components are highlighted

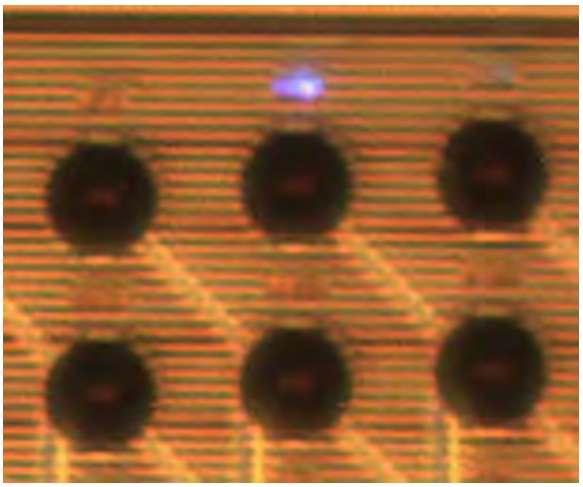

Fig. 2. Blue light (470 nm) out-coupled from a waveguide at a grating site.

3 Results

The optical outputs were tested using light coupled in by a miniature laser diode with a wavelength of 470 nm. The optical power density (OPD) was measured using an off-the-shelf optical power meter. The smallest OPD measured on a single grating out-coupler, which is in direct contact with the cells, was 70 mW/mm²: more than sufficient to activate commonly used optogenetic ion channels (ranging from 1 – 20 mW/mm²).

4 Conclusion

This novel hybrid multi optrode electrode array will stimulate progress in optogenetic applications by allowing for multi-wavelength stimulation and subsequent recording of the same cell.

Acknowledgements

Funding was provided by the IWT (grant 110068). The authors would like to thank Olga Krylychkina, Katrien Mols and Marleen Welkenhuysen.

Image Processing Based Quantitative Analysis of MEA Cultured Neurons

João Fernando Mari[1,2], José Hiroki Saito[2,3], Amanda Ferreira Neves[5], Celina Monteiro da Cruz Lotufo[4], João-Batista Destro-Filho[4*] Alberto Pasquarelli[6]

1 Universidade Federal de Viçosa – Campus Rio Paranaíba – Brazil
2 Department of Computer Science – Federal University of São Carlos – Brazil
3 Faculty of Campo Limpo Paulista – Brazil
4 Federal University of Uberlândia – Campus Santa Mônica – Brazil
5 Department of Structural and Functional Biology – University of Campinas – Brazil
6 University of Ulm – Germany
* Corresponding author. E-mail address: jbdestrof@yahoo.com.br

Abstract
In this work we propose image processing methods that enable quantitative studies on MEA cultured neurons by means of fluorescence microscopy. The neurons are segmented from the fluorescence channel images and the positioning of microelectrodes is obtained from the transmitted light channel images. The proposed method is applied to images from dissociated cultures of rat dorsal root ganglion (DRG) neurons. Our method efficiently identifies the neurons and microelectrodes in the images. The quantitative analysis results in information about the state of the culture, such as neuron's morphology and spatial distribution. Microelectrodes positioning enables to describe the interface between neurons and microelectrodes and improve the analysis of the electrophysiological signals recorded by MEA.

1 Backround

Microelectrode Arrays (MEAs) allow studying the distributed patterns of electrical activities in dissociated cultures of brain tissues, composed by neurons and glia [1]. Fluorescence microscopy imaging allows monitoring the cell morphology and even the cell culture topology, it still permits to investigate the relation between cell and electrode, critical to recording a good-quality signal [2]. The objective of this work is to perform quantitative analyses about DRG neurons cultured in MEA from confocal fluorescence microscopy images.

2 Methods

Culture Preparation and Image Acquisition: The cell cultures were performed using dorsal root ganglia (DRG) taken from male Wistar rats. The rats were anesthetized with CO2 and sacrificed by decapitation in accordance with the IASP and approved by the local Ethic Committee of Animal Experiments (CEUA/UFU). Dissociated cells were then plated on 60-channel MEAs (30 μm diameter, 200 μm spacing; Multichannel Systems). Cells were incubated with $DiBAC_4(3)$, and then imaged using an inverted fluorescence laser scanning confocal microscopy (Zeiss LSM 510 META). Volumetric 3D images were acquired in two channels, a fluorescence channel and a transmitted light one. Images were acquired in 3D to enable other studies, such as [3]. This work only considers 2D analysis, and maximum and minimum intensity project tions are applied over fluorescence and transmitted light channels in order to build 2D images.

Microelectrodes identification: We pre-process the projected image by a median filter to reduce the noise and by a botton-hat transform to suppress the background and to highlight the microelectrodes. The circular Hough transform [4] is then applied to automatically detect the microelectrodes.

Neurons segmentation: The median filter is applied in order to reduce the noise and top-hat transform is applied to suppress the background and to highlight the neurons.

After the pre-processing step, we tile the image into 8x8 small images, and apply Otsu thresholding algorithm to segment each gray level tile. The area opening operation is applied to eliminate the connected components and morphological reconstruction is applied to fill holes inside the objects. We apply the morphological closing in order to smooth the object borders.

Marker based Watershed transform is then applied to separate under segmented cells. Inner distance transform and extended maxima transform are applied to obtain markers for each neuron [5]. The skeleton by influence zone (SKIZ) of the binary image is considered as a marker for the image background. The objects and background markers are imposed as regional minima over a topographic surface defined by the morphological gradient of the binary image.

After watershed transform it is still possible to observe a large number of segmentation errors, mainly artifacts. We propose a simple classification step to

remove most of these objects based on three shape features: area, roundness, and eccentricity.

Quantitative Analysis: Remaining errors are interactively corrected and the segmented neurons, with the information about microelectrodes positioning, are employed to obtain quantitative measures, such as: number of cells; perimeter, area, diameter, roundness and eccentricity of the cells; distances between each pair of cells and distances between cells and microelectrodes.

Neurons in the image are then classified according to its diameter as: small neurons (≤ 20); intermediate neurons (≤ 40 μm); and large neuron (> 40 μm). Neurons located inside the microelectrode recording area are classified in accordance with the distances between neurons and the microelectrodes as: potentially connected (≤ 30 μm); neighboring (≤ 60 μm); and distant from microelectrodes (< 100 μm). Other neurons are considered outside any microelectrode recording area.

3 Results

The methods were applied over the top-right MEA quadrant of a confocal microscopy image. Fig. 1(a) shows the automatically identified microelectrodes, (b) the automatically segmented neurons. In this experiment 88% of the neurons had been correctly segmented by the method. Fig. 1(c) shows the neurons classified in accordance with the diameter and distance to the microelectrodes after remaining error interactive correction. Charts in Fig. 2 show diameter (a) and distance (b) based neuron classifications.

4 Conclusion

Microelectrode identification and neurons segmentation methods show to be capable to identify most of the microelectrode and the neurons. The measurements enable to obtain important information about the neuronal culture that can be used for the study and interpretation of the electrophysiological signal recorded by MEA. The neuron measurements, such as area, diameter, and distribution, are related to the soma membrane, and give the microelectrode recording probability. The distances between neurons and microelectrodes provide a tool for studies regarding to the relationship between the neuron electrophysiological activity and the signal recorded by the MEA system [5].

Acknowledgement

We thank Genoa Univ. and Multi Channel Systems Inc., DE, for providing us with MEA devices, and Mariane Silva and Prof. M.E. Beletti (Histology Dept. – UFU) for technical support.

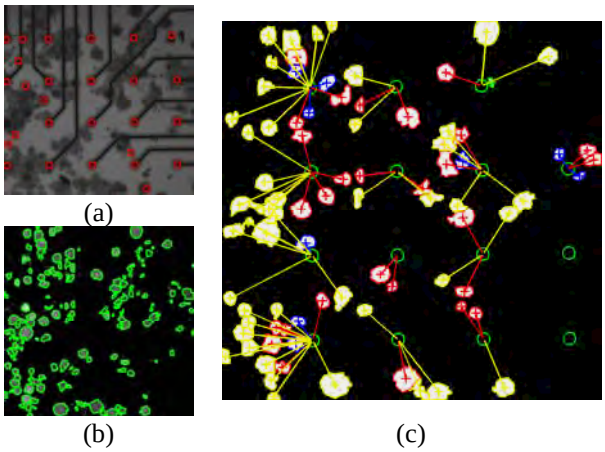

Fig. 1. (a) Automated Microelectrode Identification. (b) Automated Neuron Segmentation. (c) Neurons classified in accordance to the distance to the nearest microelectrode.

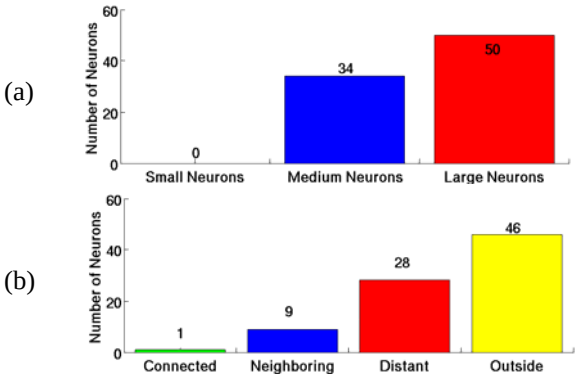

Fig. 2. Quantitative analysis results. (a) Diameter based neurons classification and (b) distance to the nearest microelectrode neurons classifications.

References

[1] Potter, S.M. (2001). Distributed processing in cultured neuronal networks. In: Nicolelis, M.A.L. (Ed) Progress in Brain Research, 130, 49-62.

[2] Van Pelt, J., Wolters, P.S., Corner, M.A., Rutten, W.L., Ramakers, G.J. (2004). Long-term characterization of firing dynamics of spontaneous bursts in cultured neural networks. IEEE T. Bio-Med Eng., 51(11), 2051-2062.

[3] Mari, J.F., Neves A. F., Saito, J.H., Lotufo, C.M.C., Destro-Filho, J.B., Oliveira, A.A.B. (2012). Three-dimensional quantitative analysis of the dorsal-root-ganglia neuron-electrode interface. Proc. MEA Meeting 2012, 43-44.

[4] Peng T, Balijepalli A, Gupta SK, LeBrun T (2007) Algorithms for On-Line Monitoring of Micro Spheres in an Optical Tweezers-Based Assembly Cell. J. Comput. Inf. Sci. Eng. 7:330–338.

[5] Ross J (2008) Microstimulation and multicellular analysis: A neural interfacing system for spatiotemporal stimulation. Georgia Institute of Technology, USA.

MEA Technology

Culture Techniques

Long-Term Cultivation and Recording from Organotypic Brain Slices on High-density Micro-electrode Arrays

Wei Gong[1]*, David Jäckel[1], Jan Müller[1], Michele Fiscella[1], Milos Radivojevic[1], Douglas Bakkum[1], Felix Franke[1], Frederic Knoflach[2], Beat Gähwiler[3], Branka Roscic[1], Thomas Russell[1], Andreas Hierlemann[1]

1 Bio Engineering Laboratory, D-BSSE, ETH Zürich, Basel, Switzerland
2 F. Hoffmann-La Roche, Basel, Switzerland
3 University of Zürich, Brain Research Institute, Zürich, Switzerland
* Corresponding author. E-mail address: wei.gong@bsse.ethz.ch

Abstract
Organotypic brain slices are a standard preparation in neuroscience research. Here we present a method to study hippocampal neuronal networks in vitro by cultivating the respective slices directly on top of high-density multi-electrode array (HD-MEA) chips for more than 30 days. Directly cultivating brain slices on the HD-MEA chips provides close neuron-to-electrode contacts and the possibility to maintain a register of cell identities, with respect to the electrode locations and recorded activity, over weeks. Moreover, very thin cell layers can be obtained in later stages of the cultivation procedure. The high resolution of the HD-MEA chips, with over 10,000 electrodes, allows for single cell resolution signal acquisition and mapping of the network activities.

1 Introduction

This project aims at cultivating hippocampal slices on high-density multi-electrode array (HD-MEA) chips for long-term extracellular electrophysiology recordings. Organotypic brain slices constitute a preparation in between dissociated cell cultures and *in vivo* electrophysiological experiments with respect to the representation of brain-like morphology. Organotypic brain slice cultures preserve the local neuronal network architectures, cell-to-cell connections, and characteristics of the original neuronal network. Long-term brain slice cultivation allows for studying network development and dynamics. The culturing of organotypic brain slices directly on HD-MEAs preserves, to a large extent, the slice morphology and enables to precisely allocate the cells in close vicinity to the underlying electrodes. Spontaneous neuronal activity can be assessed at any time point, and the slice becomes very thin at an advanced stage of cultivation. The latter property, combined with the HD-MEA chips, containing over 11’000 electrodes, allows for obtaining an overview of network activities at single-cell resolution thanks to easier spike sorting. The brain slice cultivation method presented here relies on the Gähwiler method [1]. Slice cultures on HD-MEAs have been maintained for over 30 days, while daily recordings have been conducted.

2 Material and Methods

Newborn mice (C57Bl/6 mouse, age post natal day 6) were sacrificed for brain slice preparation. 8 sagittal hippocampal slices (300 µm thickness) were obtained per mouse and affixed to HD-MEA chips with chicken plasma and thrombin. The slice cultures on the HD-MEAs were maintained in custom culturing chambers that allowed for air exchange. The culturing chambers were continuously rotated, inside an incubator with stable temperature (36°C), gas atmosphere composition (5% CO2), and humidity (100%).

HD-MEAs featuring 11’011 platinum electrodes were used for slice recordings [2, 3], 126 recording channels can be simultaneously used for readout. Sequences of 147 high-density block configurations were used to record from the whole electrode array area with overlaps. The recordings were performed daily inside an incubator under defined and sustained culturing conditions.

The slice culture recordings were analyzed and yielded activity maps displaying varying spike amplitudes. Single-neuron activity was extracted by manual inspection of multichannel spike waveforms based on the principle component analysis (PCA) spike sorting (UltraMegaSort 2000, Hill D, 2011).

3 Results

Organotypic hippocampus slices have been directly cultivated on HD-MEA chips for over 30 days.

Hippocampus CA3 neuronal network activities and single cell footprints have been extracted during the cultivation period (Fig.1).

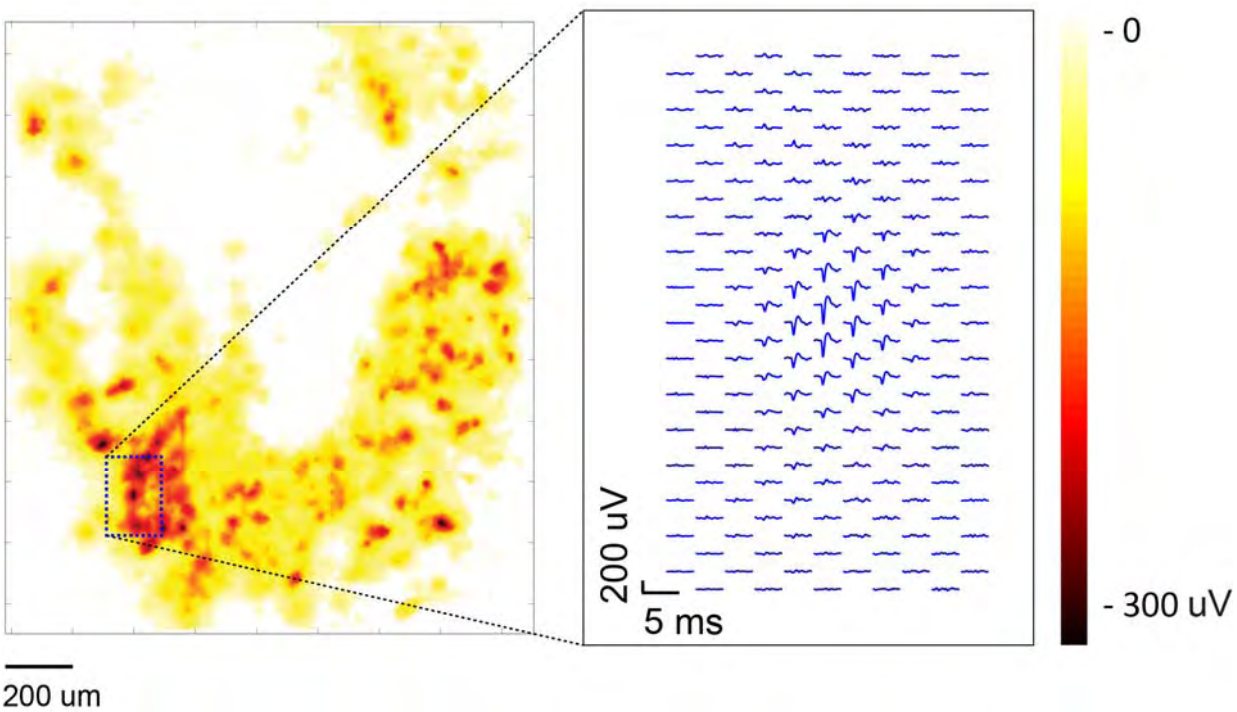

Fig. 1. Activity map of one hippocampal CA3 slice culture after 10 days in vitro (DIV 10, left panel). The spike amplitudes are indicated by the color bar. The box region indicates the whole MEA array surface. The spike-triggered average spatial distribution (footprints) of one neuron is shown in the right panel

4 Conclusions

The method presented here provides an opportunity to follow single-neuron activities and related network dynamics in slices over extended time periods, while the relative positions of the preparation and electrodes remain stable.

Acknowledgement

This work was supported by the ERC Advanced Grant "NeuroCMOS" under contract number AdG 267351. Wei Gong received individual funding through the EU Marie Curie Initial Training Networks (ITN) EngCaBra. Contract number 2010-264417.

References

[1] Gähwiler BH. 1981 Organotypic monolayer cultures of nervous tissue. J Neurosci Methods. 1981 Dec; 4(4):329-42.

[2] Frey U, Egert U, Heer F, Hafizovic S, Hierlemann A. 2009, Microelectronic system for high-resolution mapping of extracellular electric fields applied to brain slices. Biosens Bioelectron. 2009 Mar 15;24(7):2191-8.

[3] Frey, U., Sedivy, J. , Heer, F. , Pedron, R. , Ballini, M. , Mueller, J. , Bakkum, D. , Hafizovic, S. , Faraci, F.D. , Greve, F. , Kirstein, K.-U. , Hierlemann A., 2010, Switch-Matrix-Based High-Density Microelectrode Array in CMOS Technology. IEEE Journal of Solid-State Circuits. 45, 467-482.

Four-Layer Closed-Loop Neuronal Networks

Gregory J. Brewer[1*], Liangbin Pan[2], Sankaraleengam Alagapan[2], Eric Franca[2], Thomas DeMarse[2], Bruce C. Wheeler[2]

1 University of California Irvine, USA
2 University of Florida, Gainesville, FL USA
*Corresponding author. E-mail address: GJBrewer@uci.edu

Abstract
Our knowledge of the collection of interconnected networks in the brain would benefit from a greater understanding of the computational ability of these networks and their information transfer principles. To better understand the self-assembly of neuron networks and their communication, we created a four-compartment interconnected MEMS device over an electrode array and seeded it with live rat cortical neurons to be able to monitor electrical activity between sub-networks. We used tapered microtunnels to direct activity in a sequential direction around a four- compartment loop. During the spontaneous formation and propagation of bursts along this closed loop system one of the four chambers tended to dominate initiation of these events. We discuss potential mechanisms for this phenomenon. This type of design will facilitate construction of models for communication within and between subregions of the brain to decode information transfer

1 Background / Aims

The brain is now widely appreciated as a collection of interconnected networks, but our understanding of the computational ability of these networks and their information transfer principles are poorly understood. To better understand the self-assembly of neuron networks and their communication we created a four-compartment interconnected device over an electrode array and seeded it with live neurons to be able to monitor electrical activity between sub-networks.

2 Methods

A four-chambered device was constructed in PDMS with microtunnel connections between the chambers. The 51 microtunnels that interconnected each chamber were tapered from widths of 10 to 3 um wide to guide the direction of axon growth. This design was intended to promote a unidirectional closed-loop system of interconnected chambers where activity propagates along this loop. Each device was positioned onto the surface of a planar electrode array. Neurons from rat cortical hemispheres were seeded into each chamber (3000 cells/mm^2 per chamber). After 3 weeks in culture, neural activity (spiking) was recorded to determine whether activity propagated in a preferred direction around the loop.

3 Results

Four well devices, each containing a small population of cortical neurons, quickly extended neurites into the tunnels. However, due to differences in the size of the opening at each end of the tunnel (i.e., the taper) the direction of growth was biased. Neurites located on the wall of the chambers with large 10 um tunnel entrances quickly extended into those openings and eventually filled the tunnels between chambers. Neurites that originated near tunnel entrances with the small 3 um opening were less likely to enter the tunnels. Because of this bias, connectivity tended to extend from chamber to chamber in a unidirectional pattern that formed a closed loop. The effect was apparent in the pattern of spontaneous bursting that emerged and propagated between chambers (Fig. 1). First, the timing of these bursts indicated unidirectional propagation of activity in a sequential order around the loop reflecting the unidirectional bias in connectivity. Second, while any of the four chambers could initiate a burst, one of the four chambers tended to dominate. Bursts evoked by electrical stimulation in each compartment propagated in the same unidirectional manner, demonstrating preference for a closed, one-way loop.

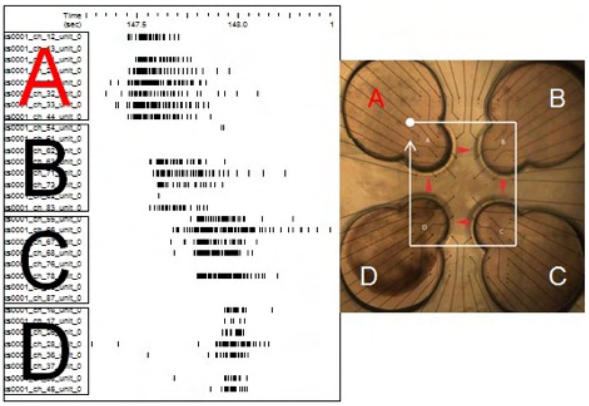

Fig. 1. A burst of spiking activity recorded in sub-network A appeared to propagate sequentially to compartments B, C and D to form a closed loop with delays of 70-500 ms between subnetworks

4 Conclusion/Summary

Tapered microtunnels were effective in directing activity in a sequential direction around a four- compartment loop. During the spontaneous formation and propagation of bursts along this closed loop system one of the four chambers tended to dominate initiation of these events. We discuss potential mechanisms for this phenomenon. This type of design will facilitate construction of models for communication within and between subregions of the brain to decode information transfer.

Acknowledgement

We thank NIH for their support (R01 NS052233).

.

3D Neural Networks Coupled to Planar Microtransducer Arrays: An Innovative In-Vitro Experimental Model for Investigating Network Dynamics

Monica Frega[1], Mariateresa Tedesco[1], Paolo Massobrio[1], Mattia Pesce[2], Sergio Martinoia[1*]

1 Neuroengineering and Bio-nano Technology Group (NBT), Department of Informatics Bioengineering Robotics and System Engineering, University of Genova, Genova Italy
2 Department of Neuroscience and Brain Technologies, Italian Institute of Technology (IIT), Genova Italy
* Corresponding author. E-mail address: sergio.martinoia@unige.it

Abstract
Despite the extensive use of in-vitro models for neuroscientific investigations, all studies on cultured cells devoted to elucidate neurophysiological mechanisms and computational properties, are based on 2D neuronal networks. In this work, we present a new experimental paradigm constituted by 3D hippocampal networks coupled to Micro-Electrode Arrays (MEAs). We show how the features of the recorded network dynamics differ from the corresponding 2D network model suggesting new avenues for the use of such 3D models for studies or for the development of bio-hybrid microsystems for in-vivo neural repair.

1 Introduction

Large networks of cultured neurons chronically coupled to micro-transducer arrays are nowadays considered a valid experimental model for studying basic neurophysiological mechanisms governing the formation and conservation of neuronal cell assemblies. Despite the extensive use of such in-vitro models, studies on cultured cells devoted to network electrophysiology are still exclusively based on 2D neuronal networks. In recent years, scientists have used different methods in attempts to create 3D neuronal cultures [1]. It has shown that cells cultured in a 3D environment better represent in-vivo behaviour than cellular populations cultured in a monolayer [2]. However, no attempt has been made to collectively record the electrophysiological activity of such 3D neuronal networks. In this work, we present a novel experimental model in which 3D networks are coupled to MEAs to form a structurally and functionally connected 3D neural network. The introduction of this new in-vitro model systems will complement and further exploit the possibility offered by in-vitro model system for studying network dynamics and for addressing specific issue such as the relationships between structure and functions.

2 Methods

2.1 Cell culture and MEA setup

Dissociated neuronal cultures are obtained from hippocampus of embryonic rats (E18) and plated onto 60-channels MEAs (Multi Channel Systems - MCS, Reutlingen, Germany). In order to construct a 3D neuronal network that resembles in-vivo conditions, we took inspiration from the Pautot's method [3]. 3D neuronal networks are constructed by seeding neurons onto a scaffold constituted by micrometric glass beads on which they are able to grow. The resulting 3D structure is composed on average by 5 layers of micro-beads and cells obtaining a physically connected 3D neuronal network with a cell density of about 80'000 cells/mm^3. The developed set-up allowed us to record the network activity from planar MEAs. Additionally, we were able to deliver an electrical stimulation both from the bottom and from the top layers (in the latter case, by using a conventional tungsten electrode).

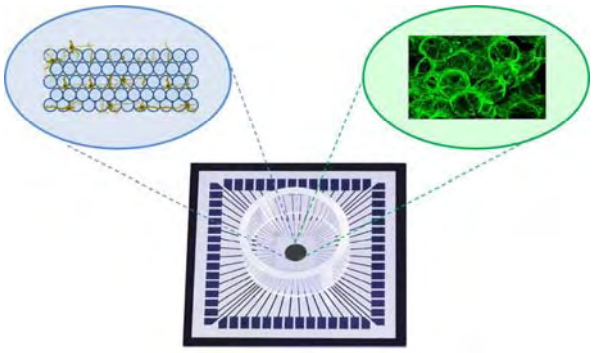

Fig. 1. Multi-layers of microbeads and neurons confined by a PDMS structure onto the active area of the MEA (blue shaded circle) and extensive encapsulation by neuritic processes (exposed to Map-2) around the micro-beads (green shaded circle).

3 Results

3.1 Spontaneous activity characterization

Spontaneous activities of 2D (n=28) and 3D (n=39) neuronal networks were recorded after four weeks in culture by means of TiN 60 channels MEAs. Figure 2a shows a raster plot of the spontaneous activ-

ity of a representative experiment performed on a 2D hippocampal culture. We can observe a quasi-synchronous activity and network dynamics composed mainly of network bursts. Similarly, Figure 2b shows a raster plot of the spontaneous activity of a representative experiment of a 3D network. It can be observed that the signature of the network dynamics presents a wider repertoire of activities with less global synchrony and more pronounced spiking at a single channel-neuron level.

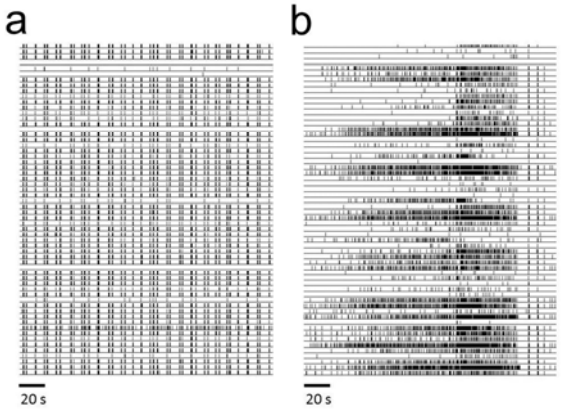

Fig. 2. 3 min of spontaneous activity of **a.** 2D neuronal network and **b.** 3D neuronal network.

The previous observations were quantified by evaluating the percentage of random spikes (i.e., the fraction of spikes outside bursts) in all the performed experiments. 2D network displays a low value of percentage of random spikes (15.9 ± 2% (mean ± standard error of the mean)), while 3D neuronal networks show a significant higher level of random spiking (33.8 ± 3 %; P-value =10-4, Mann-Whitney U-test). Even if network bursting remains a common signature for both preparations, the shift from 2D to 3D does also affect the bursting behavior. In 2D neuronal networks, the number of detected network bursts is high, the network burst duration seams similar for all the detected network burst. On the contrary, in 3D neuronal network we observed that the number of network bursts is lower and their duration is more variable.

To examine the level of synchronization of the network activity, the cross-correlation (CC) function was evaluated for the 2D and 3D neuronal networks. CC function for 2D networks underlines the high level of correlation among all the recording channels. On the contrary, 3D neuronal networks exhibits a low level of correlation among the active channels in the random spike activity region; within the burst activity region, instead, the level of correlation among channels is high.

To demonstrate whether the layers are effectively connected, we studied the propagation of the signal. In 2D neuronal network, the propagation of the signal is continuous, the signal starts from one source and propagates rapidly and in a continuous way in all the network. The estimated speed of propagation computed for all the experiment is 42 ± 3.5 mm/s. In 3D neuronal network, the signal that starts from one site propagates slowly in the network in a discontinuous way.

3.2 Stimulus-evoked activity characterization

To further prove that the layers are functionally connected, we performed experiments by delivering electrical stimulating from the bottom and top layers. To quantify and compare the neuronal network responses to electrical stimulation we evaluated the percentage of Post-Stimulus Time Histogram (PSTH) area generated after electrical stimulation in different time windows. The response to stimulation of 2D networks is relatively fast as about 90% of the PSTH area is reached within the first 500 ms. 3D neuronal networks stimulated from the bottom layer exhibit a similar response to stimulation within all the time windows: we could observe a fast response (35% of PSTH area reached within the first 100 ms) and a slow response (among 30% of the response to stimulation is detected between 1s and 2s). In the case of 3D networks stimulated from the top layer, the fast response was practically not detected (only about 10% of PSTH area is within the first 500 ms) suggesting that no direct pathways are present. The responses generated from this type of stimulation are slow as about 90% of PSTH area is reached between 500 ms and 2 s.

4 Conclusion

The obtained results demonstrate that we constructed a physically connected 3D neuronal network that exhibits a much richer repertoire of activity that cannot be found in uniform (i.e., non-patterned) 2D neuronal networks. This electrophysiological activity resembles more the one detected in in-vivo measurements in freely behaving rats [4].

References

[1] Cullen, D. K., Wolf, J. A., Vernekar, V. N., Vukasinovic, J. and LaPlaca, M. C. (2011). Neural tissue engineering and biohybridized microsystems for neurobiological investigation in vitro. *Crit. Rev. Biomed. Eng*. 39, 201-240.

[2] Irons H. R., Cullen, D. K., Shapiro, N. P., Lambert, N. A., Lee, R. H. and LaPlaca, M. C. (2008).Three-dimensional neural constructs: a novel platform for neurophysiological investigation. *J Neural Eng*, 5, 333-41.

[3] Pautot, S., Wyart, C., and Isacoff, E. Y. (2008). Colloid-guided assembly of oriented 3D neuronal networks. *Nature Methods*, 5, 735-740.

[4] Leinekugel, X., Khazipov, R., Cannon, R., Hirase, H., Ben-Ari, Y. and Buzsaki, G. (2002). Correlated bursts of activity in the neonatal hippocampus in vivo. *Science*, 296, 2049-2052.

Directed Neuronal Networks on Multi-Electrode Arrays

László Demkó[1*], Csaba Forró[1], Harald Dermutz[1], János Vörös[1]

1 Laboratory of Biosensors and Bioelectronics, Institute for Biomedical Engineering, ETH Zurich, CH-8092, Switzerland
* Corresponding author. E-mail address: demko@biomed.ee.ethz.ch

Abstract
The use of cultured neuronal networks as a model for their in vivo counterparts allows researchers to study the central nervous system, especially the brain, in a controlled environment. Specific neuronal connectivity patterns in the brain are implicated to play a role in the perception, processing and storage of information, so the building of small neuronal networks with controlled topology is a promising approach to investigate the basic circuits of the nervous system. The present work focuses on the different techniques developed in our group to realize small neuronal networks with well-defined topology, directly on MEA chips.

1 Aims

One of the grand challenges of this century is to learn how our brain functions. Despite of the vast amount of technical possibilities we still have very little insight (and especially consensus) into e.g. how memory is stored. One reason for this might be that our current knowledge in neurosciences mostly derives from single cell technologies such as patch clamping, or system level studies (e.g. MRI). Multi-electrode arrays (MEA) try to fill in this gap by providing information about neural slices and cultures, however, even though several attempts have been made to build more controlled neuron networks (microcontact printing, microfluidics, etc.) there is still no reliable technology that could provide well-defined *in vitro* networks with oriented connections on MEA chips. Due to the lack of such “study networks”, the field is forced to perform experiments on highly complex systems which makes a complete understanding of the fundamental aspects very difficult.

2 Methods

In this work we demonstrate different methods to realize small neuronal networks on MEA chips in a controlled and reproducible manner. The type, number, position of the neurons, as well as the connections and their directionalities can be defined and kept under control by combining PDMS sheets and electrically driven axonal outgrowth. The role of the PDMS sheets are multifold: first they provide control over the seeding concentration and cell positions, then they confine neurite outgrowth into the predefined directions and make closed compartments for improved electrical recordings.

3 Results

We demonstrate the applicability of the developed methods on MEA chips with different electrode arrangements. The results show the proof of concept by realizing directed connections between rat hippocampal neurons sitting on neighbouring electrodes, and the analysis of the resulted neuronal activity from the measured extracellular signals.

4 Summary

By creating reproducible neuronal networks with well-defined topology, our vision is to bridge the gap between micro and macro, the molecular or few cell level and whole brain experiments. With the results, we aim to provide insights into the role of neuronal and synaptic properties such as synapse development, plasticity and connectivity, and extract the algorithms that support information processing and neurocomputation in brain tissue.

Acknowledgement
This research has been supported by the 3DNeuroN project in the European Union's Seventh Framework Programme, Future and Emerging Technologies, grant agreement n°296590.

Human Pluripotent Stem Cell Derived Neural Cells Obtained Either Using Adherent or Neurosphere Based Differentiation Have Ability to Form Spontaneously Active Neuronal Networks

Tiina Joki[1*], Pauliina Salonen[2], Tarja Toimela[2], Riikka Äänismaa[1], Timo Ylikomi[2], Susanna Narkilahti[1]

1 NeuroGroup, BioMediTech, University of Tampere, Tampere, Finland
2 Finnish Centre for Alternative Methods (FICAM), University of Tampere, Tampere, Finland
* Corresponding author. E-mail address: tiina.joki@uta.fi

Abstract
Human pluripotent stem cells derived neural cells are considered to be a promising tool for both basic research and clinically orientated purposes. The ability to from functional interconnected networks is innate to neurons *in vivo*. Thus it is important that this ability is also retained *in vitro* differentiated neurons. In this work we used two types of human stem cell derived neural cultures, differentiated using either adherent or suspension based method, to study their emerging neuronal network properties. According to our results, both culture types were able to maturate into functional neuronal networks within the similar time frame.

1 Background / Aims

Neural differentiation of hPSCs is mainly performed using two growth factor based technics a) suspension culture of floating cell aggregates (embryoid bodies or neurospheres) or b) adherent culture as a cell monolayer or combination of both [1, 2]. Both methodologies have their lacks and advantages. Suspension methods require longer differentiation times and produce more heterogeneous cell populations containing also glial cells. More laborious adherent methods are faster and produce more homogenous neural stem cell populations which can be further used for creation of neural precursor cell banks.

In the brain, the main function of neurons is to transmit and process electrical signals. When the neural differentiation is performed *in vitro*, it is important to show that the produced neuronal networks are able to form *in vivo*-like electrophysiological properties. The micro electrode array (MEA) is an ideal tool for long term follow up studies of network level functionality. Although the MEA technology has been available for many decades [3, 4], only few articles about hPSC derived neurons on MEAs exist [5–12]. Previously, suspension method has been shown to produce active neuronal networks [8–12].

The aim of this work was to study whether commercially available neural precursor cells differentiated via adherent method have similar ability to form spontaneously active neuronal networks compared to suspension method.

2 Methods / Statistics

Cells used in this experiment were:
1) Group1: hNP1 (ArunA Biomedical, Inc. Athens, GA, USA), commercial neural precursors manufactured from human embryonic stem cell (hESC) line WA09 using an adherent method
2) Group2: Regea 08/023 hESC line derived neural cells, differentiated using a suspension based method

The hNP1 neural precursors (LOT: 7003-001, p0) were maintained according to manufacturer's instructions and for experiments maturated according to the published protocol [13]. The hESCs (Regea 08/023) were differentiated into neural cells according to previously published method [2] and used for experiments at 8 week differentiation point as previously described [8].

Cell maturation was studied with immunocytochemistry and with network level spontaneous activity measurements using 6-well MEAs (MultiChannel Systems GmbH, MCS, Reutlingen, Germany) with in-house build silicone cell culture chambers [12]. The electrophysiological MEA measurements were performed in BioMediTech's electrophysiology laboratory after culturing cells 22, 28, 31 and 35 days *in vitro* (DIV) on MEA dishes (parallel samples: hNP1 n=18 and Regea 08/023 n= 12). Spike detection was performed online with MC_Rack (MCS), spikes and bursts were analyzed using Neuroexplorer (NEX Technologies, AL, USA) and previously published burst detection algorithm [11] for MATLAB (MathWorks, MA, USA). Immunocytochemical studies were performed at DIV 28 with cell plated on 48 well culture plates (Nunc, NY, USA) according previously published protocol [2]. Statistical analysis was performed with GraphPad Prism 5 (GraphPad Software, Inc. CA, USA) using Kruskal-Wallis test followed by Dunn's multiple comparison test (post hoc test).

3 Results

According to immunocytochemical analysis, both groups were positive for neuronal and astrocytic markers after differentiation and maturation. The hNP1 and Regea 08/023 cultures contained MAP-2 positive neurons. Both studied groups were also posi-

tive for GFAP, an astrocytic marker, however, the morphology of GFAP+ cells was very different between the cultures (representative image, Fig.1).

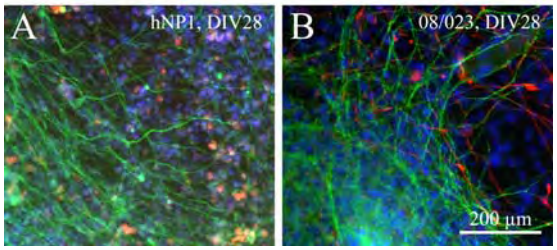

Fig. 1. Immunocytochemical staining of hNP1 derived (A) and Regea 08/023 derived (B) neuronal networks. Staining with neural markers MAP-2 (green, neurons) and GFAP (red, astrocytes) and nuclear staining with DAPI (blue).

Both groups were able to form neuronal networks that expressed spontaneous activity on MEA (Fig. 2 A, B).

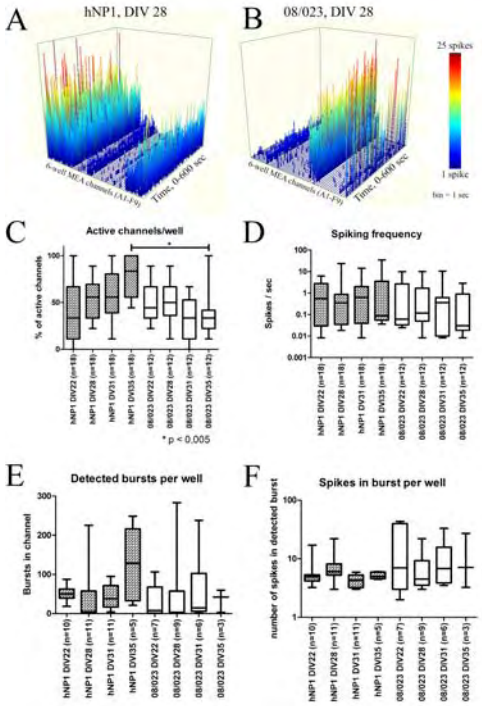

Fig. 2. Representative 3D plot of spontaneous activity during 10 min measurement of one hNP1 MEA (A) and one Regea 08/023 MEA (B). The percentage of active channels compared to all channels (C), spiking frequency, spikes per second (D), the amount of detected bursts per well (E), and the average amount of spikes in bursts (F). n= amount of parallel wells, in D and C (active channel: more than 5 spikes per measurement) and E and F, n = active wells defined by burst detection algorithm [11].

The activity developed from single spikes into training and even bursting during the 5 weeks of culturing as previously described for hESC derived neuronal cultures [8]. Although the amount of active channel was increasing in time in hNP1 networks and decreasing in 08/023 networks, the spiking frequency was unchanged between cultures (Fig. 2 C, D). The burst analysis suggested differences in burst behavior but no statistically significant differences were found (Fig 2 E, F). Synchronous activity was seen in both groups (Fig. 3.)

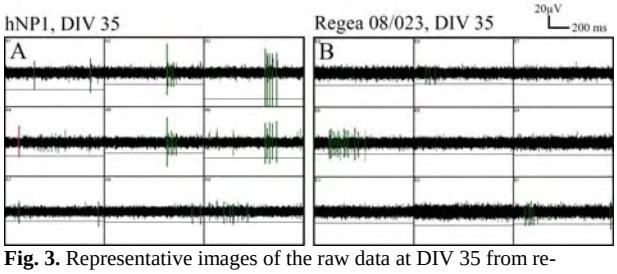

Fig. 3. Representative images of the raw data at DIV 35 from recordings showing synchronous electrical activity of the hNP1 derived (A) and Regea 08/023 derived (B) neuronal networks.

4 Conclusion/Summary

Here we show that neural cultures derived from hPSCs either using adherent or suspension based method have the ability to form functional neuronal networks. The activity development was similar between the two studied groups and also comparable to earlier studies [8–12]. However, for verifying the effect of different differentiation methods, larger experimental set-up is required.

Acknowledgement

We acknowledge for financial support: Academy of Finland (SpareBrain project, 139345), Finnish Funding Agency for Innovation (Human Spare Parts project), The Pirkanmaan Reginal Fund, and FPDP-T.

References

[1] Dhara, S. K., & Stice, S. L. (2008). Neural differentiation of human embryonic stem cells. *Journal of cellular biochemistry*, *105*(3), 633–40. doi:10.1002/jcb.21891

[2] Lappalainen, R., Salomäki, M., Ylä-Outinen, Heikkilä, T., Hyttinen, J., Pihlajamäki, H., … Narkilahti, S. (2010). Similarly derived and cultured hESC lines show variation in their developmental potential towards neuronal cells in long-term culture. *Regen. Med. (2010)*, *5*(5), 749–762. Retrieved from http://www.futuremedicine.com/doi/abs/10.2217/rme.10.58

[3] Pine, J. (1980). Recording action potentials from cultured neurons with extracellular microcircuit electrodes. *J Neurosci Methods*, *2*(1), 19–31. Retrieved from http://www.ncbi.nlm.nih.gov/entrez/query.fcgi?cmd=Retrieve&db=PubMed&dopt=Citation&list_uids=7329089

[4] Gross, G. W., Rieske, E., Kreutzberg, G. W., & Meyer, A. (1977). A new fixed-array multi-microelectrode system designed for long-term monitoring of extracellular single unit neuronal activity in vitro. *Neurosci Lett*, *6*(2-3), 101–105. Retrieved from http://www.ncbi.nlm.nih.gov/entrez/query.fcgi?cmd=Retrieve&db=PubMed&dopt=Citation&list_uids=19605037

[5] Odawara, a, Saitoh, Y., Alhebshi, a H., Gotoh, M., & Suzuki, I. (2014). Long-term electrophysiological activity and pharmacological response of a human induced pluripotent stem cell-derived neuron and astrocyte co-culture. *Biochemical and biophysical research communications*, *443*(4), 1176–81. doi:10.1016/j.bbrc.2013.12.142

[6] Gonzalez, R., Garitaonandia, I., Abramihina, T., Wambua, G. K., Ostrowska, A., Brock, M., … Semechkin, R. a. (2013). Deriving dopaminergic neurons for clinical use. A practical approach. *Scientific reports*, *3*, 1463. doi:10.1038/srep01463

[7] Muratore, C. R., Rice, H. C., Srikanth, P., Callahan, D. G., Shin, T., Benjamin, L. N. P., … Young-Pearse, T. L. (2014). The familial Alzheimer's disease APPV717I mutation alters APP processing and Tau expression in iPSC-derived neurons. *Human molecular genetics*. doi:10.1093/hmg/ddu064

[8] Heikkilä, T. J., Ylä-Outinen, L., Tanskanen, J. M., Lappalainen, R. S., Skottman, H., Suuronen, R., … Narkilahti, S. (2009). Human embryonic stem cell-derived neuronal cells form spontaneously active neuronal networks in vitro. *Exp Neurol*, *218*(1), 109–116. Retrieved from http://www.ncbi.nlm.nih.gov/entrez/query.fcgi?cmd=Retrieve&db=PubMed&dopt=Citation&list_uids=19393237

[9] Ylä-Outinen, L., Heikkilä, J., Skottman, H., Suuronen, R., Äänismaa, R., & Narkilahti, S. (2010). Human cell-based micro electrode array platform for studying neurotoxicity. *Front Neuroeng*, *3*(pii: 111).

[10] Mäkinen, M., Joki, T., Ylä-Outinen, L., Skottman, H., Narkilahti, S., & Äänismaa, R. (2013). Fluorescent probes as a tool for cell population tracking in spontaneously active neural networks derived from human pluripotent stem cells. *Journal of Neuroscience Methods*, *215*, 88–96. doi:10.1016/j.jneumeth.2013.02.019

[11] Kapucu, F. E., Tanskanen, J. M. A., Mikkonen, J. E., Ylä-Outinen, L., Narkilahti, S., & Hyttinen, J. A. K. (2012). Burst analysis tool for developing neuronal networks exhibiting highly varying action potential dynamics. *Frontiers in Computational Neuroscience*. doi:10.3389/fncom.2012.00038

[12] Kreutzer, J., Ylä-Outinen, L., Kärnä, P., Kaarela, T., Mikkonen, J. E., Skottman, H., … Kallio, P. (2012). Structured PDMS Chambers for Enhanced Human Neuronal Cell Activity on MEA Platforms. *Journal of Bionic Engineering*, *9*, 1–10. Retrieved from http://www.ncbi.nlm.nih.gov/entrez/query.fcgi?cmd=Retrieve&db=PubMed&dopt=Citation&list_uids=19243222

[13] Young, a, Machacek, D. W., Dhara, S. K., Macleish, P. R., Benveniste, M., Dodla, M. C., … Stice, S. L. (2011). Ion channels and ionotropic receptors in human embryonic stem cell derived neural progenitors. *Neuroscience*, *192*, 793–805. doi:10.1016/j.neuroscience.2011.04.039

Design and Fabrication of a Second-Generation Perfusion Cap for Enhanced Optical Access and Manipulation of Cell Cultures

Anil Krishna Konduri[1], Dirk Saalfrank[2], Rouhollah Habibey[1], Asiyeh Golabchi[1], Marina Nanni[1], Axel Blau[1*]

1. Dept. of Neuroscience and Brain Technologies (NBT), the Italian Institute of Technology (IIT), Via Morego 30, 16163 Genoa, Italy, www.iit.it
2. Dept. of Informatics and Microsystem Technology, University of Applied Sciences Kaiserslautern, 66482 Zweibrücken, Germany, www.fh-kl.de
*Corresponding author: anilkrishna.konduri@iit.it

Abstract
This work describes a novel neural cell culture perfusion system compatible with a commercial multielectrode array (MEA) recording setup. A controlled and continuous flow of cell culture medium and the long-term monitoring of cell physiology are two advantages of perfusion systems. However, both can be significantly disturbed by air bubble entry through the external tubing. This study targeted at the improvement of the internal perfusion cap design to not only trap and guide bubbles to the medium outlet, but improve its overall tightness and suitability for short-working distance microscopy. For the latter reason, we integrated a glass cover slip window at the bottom of the PDMS perfusion cap to improve the optical clarity and an internal wall groove for guiding air bubbles. The flow and leakage properties of this cap design were compared to a cap featuring a PDMS membrane instead of a glass coverslip.

1 Introduction

Perfusion systems made of PDMS have been widely used in cell culture-based studies. They show advantages over traditional cell culture containers *i.e.* by offering the possibility of mimicking an *in vivo* environment. Control over continuous medium flow through micro tubes could be useful for extending long-term survival on MEAs previously shown for static cultures [1] [2]. Long-term cell culture is useful in many case studies, like continuous time-lapse imaging and extracellular electrophysiology at ambient conditions [3].

PDMS is an advantageous polymer for various cell culture applications because of its transparency, gas permeability, bio-compatibility and flexibility. However, some of these features could be considered as a disadvantage for a PDMS perfusion system. For instance, the flexibility of a PDMS cap could lead to leakage and air bubble formation, which are problematic for optical imaging and culture viability in long-term electrophysiology studies on MEAs [3].

We designed a second-generation perfusion cap, which can be easily fabricated using a PDMS scaffold with an integrated PDMS/glass coverslip window. It has the advantages of (1) having a higher resistance against pumping pressure fluctuations, (2) featuring mechanical stability paired with high transparency for optical imaging, and (3) including a bubble trap guidance mechanism towards the medium outlet. It can be fabricated either by additive manufacturing (3D printing) or replica-molding and its implementation is low-cost.

2 Materials & Methods

2.1 Perfusion cap fabrication

We present a perfusion concept based on a replica-molding strategy from a 3D-printed acrylonitrile butadiene styrene (ABS) moulding template, which consisted of three removable parts (Fig.1 A). Their combination determined the height as well as the outer and inner diameters of the PDMS cap. The two-part PDMS material (Sylgard 184, Dow Corning) was mixed in the ratio of 10:1 (v/v), and, after degassing, was poured into the assembled moulding template and cured at 85 °C for 30 min (Fig. 1 B). Two holes (Ø 1.2 mm) were centered at opposite sides of the upper edge (Fig 1. C) [2]. They served as holders for polytetrafluorethylene (PTFE) inlet and outlet tubes. Each cap consumed 6-7 ml of the PDMS precursor mix.

Perfusion cap templates were designed (Creo CAD, PTC) to fit the 30 mm standard outer diameter (OD) of commercially available MEA rings.

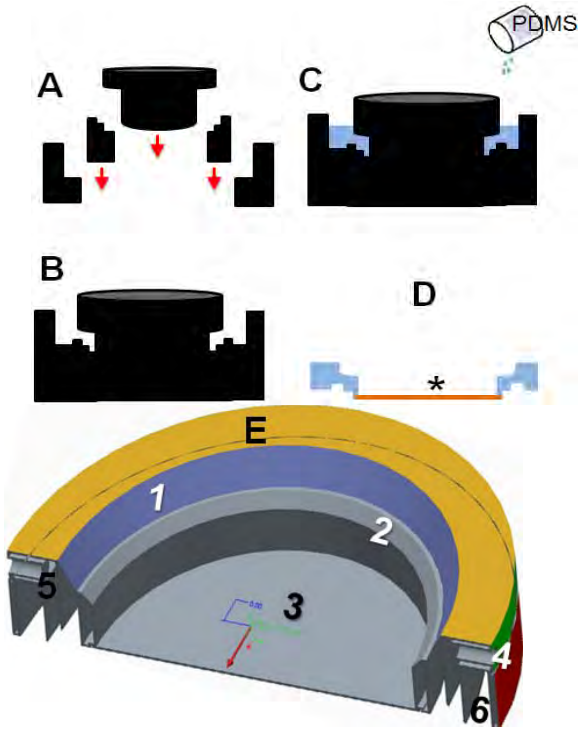

Fig.1 . Perfusion cap assembly. Overview of the cap production out of PDMS: (A) Template components, (B) assembled template, (C) molding PDMS perfusion cap from template, (D) cross-section of PDMS perfusion cap with a glass coverslip or PDMS window (*), (E) 3D cross-section of an experimental PDMS perfusion cap design currently being under production. (1. Slope for microscope objective movement, 2. groove for laser dissection objective movement, 3. glass coverslip/PDMS membrane, 4. space for tubing, 5. groove for bubble trap/guidance mechanism, 6. double-walled jacket)

3 Results

Two types of PDMS caps have been developed and compared, namely a PDMS perfusion cap with the central window composed of a PDMS membrane (number 3 in Fig 1. D) and a cap with a glass coverslip instead of the PDMS membrane. Both types of the caps were made from the same template (Fig.1 A). The glass slide was bonded with PDMS to the perfusion cap. Resistance to pump-induced fluctuations in the fluid flow and bubble trapping was compared for these two caps.

3.1 Fluctuation tolerance test

The tolerance of each cap against deformation was tested by monitoring the fluid pressure created by a stepper motor-driven syringe pump (flow rate: 20 µl/day). In both prototypes we observed that the cap with the glass coverslip was more stable to deformation. The cap made with PDMS showed signs of leakage between the glass ring and the perfusion cap, while the PDMS cap with the glass cover slip showed a homogenous fluid distribution without leakage (Fig.2).

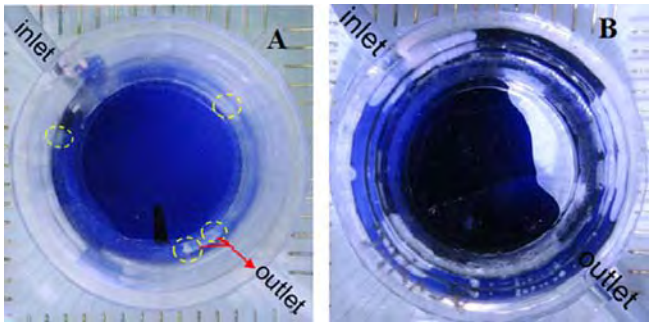

Fig.2. Fluctuation tolerance test in two types of perfusion caps. (A) PDMS cap with glass coverslip and desired fluid flow, (B) PDMS cap with PDMS window, which showed leakage of fluid.

3.2 Bubble guidance mechanism

Air may penetrate the cap or tubing and enter the device. In the presented PDMS cap, bubbles were trapped in a groove (number 5 in Fig. 1E) at a minimum flow rate of 20 µl/day. Due to the continuous fluid flow, the bubbles tended to move slowly toward the outlet (Fig. 2A). This prevented them from accumulating underneath the central window thereby causing subsequent image distortion during long-term imaging. A minimum flow rate of 20 µl/day was sufficient for guiding bubbles to the outlet.

4 Conclusions

The second generation PDMS perfusion cap with a glass cover slip window minimized fluid related problems and leackage. In addition, the device successfully guided bubbles toward the outlet. The glass coverslip window and bubble guidance will be useful in improving the optical visibility of samples in a perfusion system.

Acknowledgement

This work was supported by intramural funds at the Italian Institute of Technology.

References

[1] Blau A., Neumann T., Ziegler C., Benfenati F. (2009) Replicamolded poly(dimethylsiloxane) culture vessel lids attenuate osmotic drift in long-term cell culturing, *J. Biosci., 34, 59-69.*

[2] Potter, S.M., DeMarse. T.B. (2001) "A new approach to neural cell culture for long term studies." *J. Neurosci Methods 110: 17-24.*

[3] Saalfrank D., Vasile Martiniuc A., Konduri AK., Habibey R., Golabchi A., Latifi Sh., Knoll A., Ingebrandt S., and BlauA; Incubator-independent cell culture perfusion platform for continuous long-term electrophysiology and time-lapse imaging reveals fluctuations in neural network activity and local architecture over the months *paper submitted.*

Primary and Stem-Cell Derived Cardiac Myocyte Cultures

Combined MEA Recording and Ca-Ratiometry in hiPSC-Derived Cardiomyocytes for Cardiac Safety Assessment

Georg Rast

Abteilung Drug Discovery Support
Boehringer Ingelheim Pharma GmbH & Co. KG
Birkendorfer Straße 65
D-88397 Biberach an der Riss
georg.rast@boehringer-ingelheim.com

Abstract
Multi-Electrode arrays (MEA) enable the recording of multiple field potentials from various electrically active surfaces. This presentation focuses on the acquisition of ECG-like signals from two-dimensional cultures of human induced pluripotent stem cell (hiPSC)-derived cardiomyocytes in combination with Fura-based Ca-ratiometry. Fura-2 is a Ca-sensitive dye which is used to record intracellular Ca levels with medium temporal resolution. The nine well, 256 channel MEA platform provided by Multichannel Systems was extended to accommodate nine independent fiber optic channels for composite Ca transient recording from the cell population in each well. The wells were equipped with an individual perfusion for sequential and escalating application of test compound or solvent (control). Experiments were designed in a way that on each nine well chip, three wells treated with solvent control can be tested against six wells treated with test compound at up to five concentrations.
Profiling of reference compounds demonstrates that the combination of the read-out parameters from field potential and Ca transient analysis enables a detailed characterization of the pharmacology of the respective compound. In particular, inhibition of ion channels, intracellular calcium handling, and changes in cAMP may be detected.
Furthermore, specific physiological properties of the cells in use may be characterized. In the present case using hiPSC-derived cardiomyocytes, it was found that they deviate substantially from primary cells. An in-depth analysis of the base-line properties of the cellular systems used is essential for the interpretation of potential compound effects.

Human Stem-Cell Derived Neuronal Cell Based In Vitro Platforms for Neurotoxicity and Disease Modelling

Susanna Narkilahti[1*]

1 NeuroGroup, BioMediTech, University of Tampere, Tampere, Finland
* Corresponding author. E-mail address: susanna.narkilahti@uta.fi

Abstract
Human pluripotent stem cells and their neuronal and glial derivatives have raised high hopes in the field of regenerative medicine. Furthermore, these cells are useful in the fields of human development studies, disease modelling, drug screening, and neurotoxicology. Currently, most of the analyses are based on *in vitro* and *in vivo* animal models or cells. Moreover, most of the neurotoxicological analyses are based on molecular biology end point analyses which do not take into account the cell type specific functionality at all. For neurons, their most crucial characteristic is the electrical signalling. The most optimal method to measure and monitor the electrical functionality of neuronal networks *in vitro* is the microelectrode array (MEA) setup. This method has been implemented by both academic research parties and industry for neurotoxicological screening to some extent using both animal and human derived neurons. Due to their close resemblance to the brains of developing human foetuses, human pluripotent stem cells derived neuronal cultures in MEA platform offer unique tool to study the aspects of neurotoxicity in humans and to model certain diseases. However, many aspects of these kinds of in vitro models still require optimization. The several aspects of model optimization will be discussed in this presentation.

1 Background

The discovery on human embryonic stem cells (hESC) in 1998 [1] opened a door for totally new area for both clinical treatment development and for in vitro research. It was hoped that these cells, able to differentiate into every cell type in human body (excluding placental structures), would provide source of making needed cells types in great amounts. And surely, it is possible for example to make various types on neurons and glial cells from hESCs in vitro [2]. Even though the first great expectation of utilizing hESC derivatives was in regenerative medicine, it was acknowledged that these cells would be beneficial also in other areas in vitro such as in drug development and screening, neurotoxicological analysis and in the developmental studies of human brain.

As hESC possesses ethical challenges, the discovery of human induced pluripotent stem cells (hIPSC) in 2007 [3] has broaden up the use of these human pluripotent stem cells (hPSC = hESC + hiPSC) for multiple purposes as hiPSCs can be produced from any individual. One of the greatest advantages of hiPSC is that when producing them from a patient bearing disease with genetic background it is possible to create particular cells in a laboratory dish that should have the same defect than the patient. It has already been shown making hiPSC derived neurons from patients with neurological diseases bearing genetic background is possible [4]. Thus, hiPSC derivatives have brought up new areas such as development of particular disease models and development of personalized medicine strategies where hPSC can further benefit us.

2 Methods and results

2.1 Neural differentiation and characterization of human pluripotent stem cells

After 2005 we have developed a relative simple cell suspension differentiation method for hPSCs [2]. With this method, we have tested the neuronal differentiation capacity of 15 hESC and 13 hiPSC lines derived and produced with different methods, obtained either from research laboratories or commercially. We have showed that all of these hiPSC lines can be differentiated into neuronal cells but there is a relatively huge line, but not origin, depended variation in the efficiency [2, 5, unpublished data]. The neuronal characteristics were studied in gene and protein expression levels (RT-PCR, qRT-PCR, immunocytochemistry, flow cytometry). Importantly, all produced neuronal cultures were able to form spontaneously functional neuronal networks when studied using micro electrode arrays (MEA, Multichannel Systems, MCS, Germany) in a setting developed by us [6]. The development of spontaneous activity and maturation was depended on the initial neuronal differentiation capacity of a particular hiPSC line.

In next step, we have taken both hESC and hiPSC lines which have good neuronal differentiation capacity into more detailed analysis to see if there are differences between neuronal properties. This is an ongoing

work. Preliminary results suggest that both electrophysiological properties of single neurons (patch clamp) and neuronal networks are very similar between cells derived either from hESCs of hiPSCs.

2.2 MEA measurements of hPSC derived neuronal networks

The MEA environment differs from cell culture plastic or glass were neuronal cells are typically cultured and thus it does not provide optimal culturing conditions. Also, as the electrodes on MEA's are embedded in the middle of the MEA chamber it is challenging to get the neurons grow on that area and not surrounding areas. To optimize the MEA culturing environment, we developed a silicone chamber that restricts the culturing area only to the area of electrodes in MEA [7]. This has provided us a way to be more successful with neuronal culturing in MEA's and also resulted in direct cost saving as less coating materials and cells are needed per MEA.

The hPSC derived neuronal networks represent developmentally the earliest types of networks existing. It is not known yet how far these networks can be maturated and thus what developmental stage they mimic in vivo (fetal, childhood or adult human neuronal networks). It is, however, quite clear that when comparing functional properties of hPSC and primary rodent neuronal networks in vitro, there are differences in network characteristics (maturation time, activity parameters, level of synchronous activity, ect.). Therefore, we developed an algorithm to analyse bursts in these highly variable hPSC derived neuronal networks [8].

One of the application areas of hPSC derived neurons is neurotoxicology. Thus, we tested if hPSC derived functional neuronal networks could be used for this purpose. We showed that methyl mercury, a known neurotoxicant, influences functionality of these networks in concentration level that does not cause visible toxic effects when measured with standard molecular biology methods [9].

The disease modelling in vitro has become very active research area especially after the discovery of hiPSC cells. In case neurological disorders, it is quite obvious that development of models were the functional properties of the created neuronal networks can be measured are needed. This reply both in developing disease models bearing genetic background or more general, for example, injury related models. In order to develop this area further we tested how the human cerebrospinal fluid affects functionality of neuronal networks [10]. As part of development of in vitro models certain type of platforms with additional features may be needed including culturing of mixed cell populations, restrictions between different cells areas or cell parts ect. This may also lead to need to design different kinds of MEA electrode arrays with different patterns. As part of developing our own in vitro models, we have tested different electrode materials and manufacturing process in order to made in-house MEA's [11, 12].

3 Discussion and conclusions

Human pluripotent stem cells derived neurons provide us tool to develop many application areas such as neurotoxicological screening and disease modelling. As the main function of neurons is to create functional neuronal networks, those networks should be used as principle component in the developed platforms. Thus, MEA provides basis for these platform development. There are, however, many aspects that need to take into account:

1) Although there are hundreds of hESC and hiPSC lines available today they do not differentiate similarly towards neurons. In addition, there are multiple differentiation methods resulting in different neuronal amounts and neuronal subtypes. Further, as hiPSC are modified cells from the beginning there may be some abnormalities or changes in the derived neuronal networks. Thus, one needs to think carefully what kind of hPSC line to use for production of the neuronal networks for particular use.

2) MEA measurements are feasible to conduct with hPSC derived neuronal networks. Those contain, however, relatively big network to network variations and differ from rodent primary neuronal networks that are more or less the standard for neurotoxicological screening today. Thus, there should be standardization of producing these hPSC derived neuronal networks and also more detailed characterization in multiple levels.

3) The development of MEA technology to the HTP systems will of course to help to tackle the variation seen in functional properties as sample sizes can be increased. That does not remove the need to analyse the properties of hPSC derived neuronal networks more carefully and compare those to the rodent primary neuronal networks. On the other hand, as the differentiation methods are optimized further that can result in more homogenous neuronal networks.

4) The disease modelling may require more complicated in vitro platforms. In these platforms both structural components and cellular composition of that particular brain area may need to be recapitulated as well as possible. Whether that leads even to 3D in vitro models remains to be seen. Of course that would add on requirements also for used MEA technology.

Acknowledgement

I like to thank previous and present persons in NeuroGroup, BioMediTech for all of their hard work and commitment. These studies have been funded by Academy of Finland (SpareBrain project, 139345), Finnish Funding Agency for Innovation (Human Spare Parts project) and FP7 Future and Emerging Technologies 3DNeuroN project (296590).

References

[1] Thomson, J. A., Itskovitz-Eldor, J., Shapiro, S. S., Waknitz, M. A., Swiergiel, J. J., Marshall, V. S., and Jones, J. M. (1998). Embryonic stem cell lines derived from human blastocysts. Science *282*, 1145-1147.

[2] Lappalainen, R. S., Salomäki, M., Ylä-Outinen, L., Heikkilä, T. J., Hyttinen, J. A., Pihlajamäki, H., Suuronen, R., Skottman, H. and Narkilahti, S. (2010). Similarly derived and cultured hESC lines show variation in their developmental potential towards neuronal cells in long-term culture. Regen Med. 5, 749-762.

[3] Takahashi, K., Okita, K., Nakagawa, M. and Yamanaka, S. (2007). Induction of pluripotent stem cells from fibroblast cultures. Nat Protoc. 2, 3081-3089.

[4] Han S.S˙, Williams L.A., Eggan K.C. (2011) Constructing and deconstructing stem cell models of neurological disease. Neuron 70, 226;70(4):626-644.

[5] Toivonen S., Ojala M., Hyysalo A., Ilmarinen T., Rajala K., Pekkanen-Mattila M., Äänismaa R., Lundin K., Palgi J., Weltner J., Trokovic R., Silvennoinen O., Skottman H., Narkilahti S., Aalto-Setälä K., Otonkoski T. (2013) Comparative analysis of targeted differentiation of human induced pluripotent stem cells (hiPSCs) and human embryonic stem cells reveals variability associated with incomplete transgene silencing in retrovirally derived hiPSC lines. Stem Cells Transl Med. 2(2)83-93.

[6] Heikkilä, T. J., Ylä-Outinen, L., Tanskanen, J. M., Lappalainen, R. S., Skottman, H., Suuronen, R., Mikkonen, J. E., Hyttinen, J. A. and Narkilahti, S. (2009). Human embryonic stem cell-derived neuronal cells form spontaneously active neuronal networks in vitro. Exp Neurol. 218, 109-116.

[7] Kreutzer, J., Ylä-Outinen, L., Kärnä, P., Kaarela, T., Mikkonen, J. E., Skottman, H., et al. (2012). Structured PDMS Chambers for Enhanced Human Neuronal Cell Activity on MEA Platforms. *Journal of Bionic Engineering*, *9*, 1–10

[8] Kapucu F.E., Tanskanen J.M.A., Mikkonen J.E., Ylä-Outinen L., Narkilahti S., Hyttinen J.A.K. (2012) Burst analysis tool for developing neuronal networks exhibiting highly varying action potential dynamics. Front Comput Neurosci. 6:38

[9] Ylä-Outinen L., Heikkilä J., Skottman H., Suuronen R., Äänismaa R., Narkilahti S (2010) Human cell-based micro electrode array platform for studying neurotoxicity. Frontiers in Neuroengineering 3(111):1-9

[10] Kiiski H., Äänismaa R., Ylä-Outinen L., Aho A., Yli-Hankala A., Bendel S., Skottman H., Kreutzer J., Kallio P., Tenhunen J., Narkilahti S. (2012) Human cerebrospinal fluid promotes glial differentiation of human embryonic stem cell-derived neural cells but does not prevent spontaneous activity in pre-existing neuronal networks. Biol Open. May 13;2(6):605-612.

[11] Ryynänen T., Ylä-Outinen L., Narkilahti S., Tanskanen J.M.A., Hyttinen J., Hämäläinen J., Leskelä M., Lekkala J. (2012) ALD IrOx Thin Film as Microelectrode Coating in Stem Cell Application. Journal of Vacuum Science and Technology A 30(4), Jul-Aug, 2012.

[12] Ryynänen T., Kujala V., Ylä-Outinen L., Korhonen I., Tanskanen J., Aalto-Setälä K., Hyttinen J., Kerkelä E., Narkilahti S., Lekkala J. (2011) All-Titanium Microelectrode Array for Field Potential Measurements from Neurons and Cardiomyocytes - a Feasibility Study. Micromachines 2, 394-409

Comparative Assessment of Different Types of Human Stem Cell Derived Cardiomyocytes for Predictive Electrophysiological Safety Screening Using Microelectrode Arrays (MEA)

Udo Kraushaar[1*], Dietmar Hess[3], Hua Rong Lu[2], David Gallacher[2] & Elke Guenther[1]

1 NMI Natural and Medical Sciences Institute, Reutlingen, Germany
2 Janssen Pharmaceutica NV, Beerse, Belgium
3 NMI-TT GmbH, Reutlingen, Germany
*corresponding author. Email adress: udo.kraushaar@nmi.de

The need for new strategies in preclinical compound testing is intensively debated by the pharmaceutical industry. In this respect, cardiomyocytes generated from human stem cells (hSCs) are regarded as a promising source to develop meaningful in vitro test models of adverse cardiovascular effects, including electrophysiological safety screening. Our study is the first to compare the pharmacological profile between different types of hSCs by means of MEA recordings and to relate it to existing electrophysiological preclinical cardiac safety models.

Commercially available human embryonic or induced pluripotent stem-cell derived cardiomyocytes (hiPSCs, hESCs) from three providers were electrophysiologically validated against ten compounds with different modes of action. Spontaneous field action potentials (fAP) were recorded from the cells directly seeded on the recording electrodes of 6-well MEAs.

Compound effects comprised changes of the initial phase of the fAP (Na^+ component), fAP duration as well as changes of the spontaneous beating frequency and regularity. For most of the reference compounds, all cell types investigated expressed the same alterations in the parameters analyzed in response to the compounds, but with different sensitivities. Comparison of our results with literature data from other preclinical cardiac safety models revealed in most but not all cases a good pharmacological correlation for all cell types tested.

Based on these findings, we conclude that hSC-derived cardiomyocytes in principle are a promising cell source for electrophysiological cardiac safety assays but still need to be improved towards the expression of a mature electrophysiological phenotype to avoid false-negative or -positive responses.

On-Chip Measuring of Drug-Induced Cardiac Action Potential Elongation of Single Cells with Patch Clamp Resolution

Danny Jans, Ben Huybrechts, Simon Schaerlaeken, Andim Stassen, Luis Hoffman, Jordi Cools, Geert Callewaert, Dries Braeken[1]

1 imec, Kapeldreef 75, 3001 Leuven, Belgium

Abstract

Drug development is hampered by the awareness of drug-induced cardiotoxicity resulting in the rejection of pharmaceutically active compounds. To a certain level cardiac malfunction can be understood from the electrical activity of single cardiac cells. In this study we present a novel assay applied on a multi-electrode array (MEA) built on top of complementary metal-oxide-semiconductor (CMOS) electrical circuitry to address the electrical activity of individual cardiac cells in a network. The electrodes (diameter ± 1 µm) are subcellular sized and allow for both electrical stimulation and recording. We used primary cultures of rat neonatal ventricular cardiac cells after 5 to 7 days of culture. Application of different doses of cisapride demonstrated the potential of the system to measure dose-dependent increases of the action potential duration (APD) of ventricular cardiac cells.

1 The Open-Cell State

Drug-induced cardiotoxicity of pharmaceutically active compounds is often recognized as an elongation of the QT segment in the electrocardiogram. Current in vitro tools fail either the versatility of using appropriate cell types or the ability to report detailed electrical activity. The *in vitro* screening system needs to involve the use of cardiac ventricular cells, since the APD of these cells coincides with the QT interval. Our CMOS-MEA presents the electrical activity of a single cardiac cell as individual spikes on a noise band with amplitudes of about 3 mV (SNR ± 100) (panels A, B). Electrical stimulation of the cell creates the so-called open-cell state shaping an electrical signal that displays the full time course of the action potential of the cardiac cell. The observed amplitudes range from 3 to 90 mV (SNR up to 300) (panels C, D). The open cell state is restricted in time and the recorded signal spontaneously returns to single spikes [1].

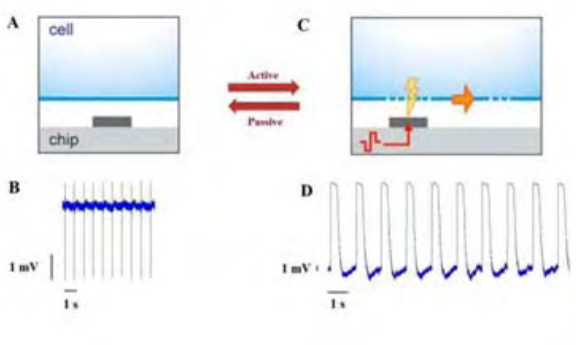

Fig. 1. The open-cell model. (A) Schematic depiction of a single cell (blue) on top of an electrode (grey). (B) Representative extracellular recording from a single cardiac cell. (C) Schematics of the cell upon electrical stimulation. (D) Representative recording of the cardiac electrical activity during the open-cell mode.

2 Dose-dependent drug-induced APD elongation

In this study, we evaluated the potential of the imec MEA in detecting drug-induced changes in APD. An open-cell assay was developed in which a cell was stimulated twice and the APDs of both situations were subtracted, resulting in a ΔAPD value. The first stimulation for each cell always occurred in the absence of the drug, whereas the second stimulation was performed both in the absence and in the presence of increasing concentrations of cisapride, a drug known to prolong the APD. In the absence of the drug, ΔAPD amounted 1.9 ± 1.2 ms. With increasing concentrations of cisapride, i.e., 10, 100, and 1000 nM, ΔAPD

increased to 33.5 ± 4.4, 53.6 ± 4.0 and 78.4 ± 5.6 ms, respectively (n = 30). Figure 2 shows the dose-dependent relationship between ΔAPD and the drug concentration.

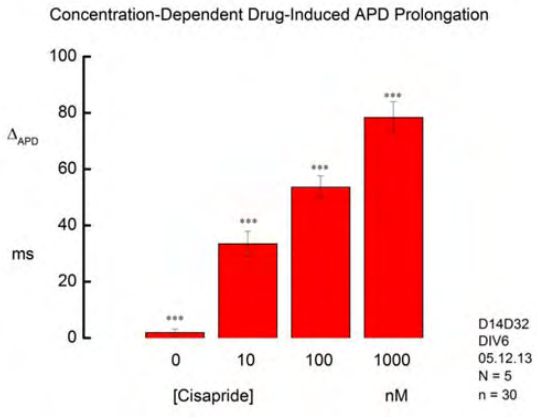

Fig. 2. Quantitative data of the effect of increasing concentrations of cisapride on ΔAPD. See text for explanation.

In conclusion, the imec CMOS-MEA shows to be a powerful tool for detailed analysis of the electrical activity of single cardiac cells and demonstrates potential to drastically improve predictability and accuracy of future drug screening assays.

References

[1] Braeken D, Jans D, Huys R, Stassen A, Collaert N, Hoffman L, Eberle W, Peumans P, Callewaert G. (2012). Open-cell recording of action potentials using active electrode arrays. *Lab Chip.7;12(21):4397-4402*.

Pharmacological Response of a Human Induced Pluripotent Stem Cell-Derived Neuron and Astrocyte Co-Culture

Aoi Odawara[1,3], Masao Gotoh[1], Ikuro Suzuki[2*]

1 School of Bioscience and Biotechnology, Tokyo University of Technology, 1404-1Katakura, Hachioji, Tokyo
2 Department of Electronics and Intelligent Systems, Tohoku Institute of Technology, Japan
3 Japan Society for the Promotion of Science, Tokyo, Japan
* Corresponding author. E-mail address: i-suzuki@tohtech.ac.jp, s.ikurou@gmail.com

Abstract
Human induced pluripotent stem cell (hiPSC)-derived neurons may be effectively used for drug discovery and cell-based therapy. However, the immaturity of cultured human iPSC-derived neurons and the lack of established functional evaluation methods are problematic. We here used a multi-electrode array (MEA) system to investigate the effects of the co-culture of rat astrocytes with hiPSC-derived neurons. The co-culture facilitated the long-term culture of hiPSC-derived neurons for >3 months and long-term spontaneous firing activity was also observed. After >3 months of culture, we observed synapse transmission. Compared with rat neurons, hiPSC-derived neurons required longer time to mature functionally. Furthermore, addition of the synapse antagonists induced significant changes in the firing rate. In conclusion, we used a MEA system to demonstrate that the co-culture of hiPSC-derived neurons with rat astrocytes is an effective method for studying the function of human neuronal cells, which could be used for drug screening.

1 Introduction

Human induced pluripotent stem cells (hiPSCs) differentiation techniques and culture methods are important evaluation models and an alternative to animal testing for drug discovery screening, toxicity testing, and elucidating disease mechanisms [1-3]. Neuronal cells can be generated from hiPSCs, providing a very important alternative to studies of humans and model organisms, to facilitate a better understanding of the mechanisms of neurological diseases and identifying novel therapeutic avenues [4, 5]. However, hiPSC-derived neurons cultured using traditional two-dimensional culture methods lack adequate maturation, and evaluation methods focusing on the function of cultured hiPSC-derived neurons have not been established. Additionally, using glial cell humoral factor in cultured neuronal cells increases the number of living cells [6,7]. We previously demonstrated that achieving long-term single cell culture is possible by adding glial cell humoral factor to rat hippocampal neurons [8].

Here, we used the MEA system to investigate the functional effects of co-culturing rat astrocytes with hiPSC-derived neurons on their long-term spontaneous activity and drug responsiveness.[9]

2 Materials and Methods

2.1 Planal MEA chip

To evaluate the long-term culture of hiPSC-derived neurons, we used a planar MEA measurement system (Alpha Med Scientific, Japan). The MEA chips were produced on a glass slide, comprising 64 electrodes (50 × 50 μm) with 150-μm spacing in an 8 × 8 grid arrangement. Each recording terminal surface was coated with Pt/Pt-black to reduce impedance.

2.2 hiPSC-derived neurons

hiPSC-derived neurons [iCell neurons; CDI Inc., USA] were cultured on MEA chips. The MEA chips were coated with 0.05% polyethylenimine solution for 1 h at room temperature, washed four times with sterilized water, and left to dry overnight. Next, 5 μg/ml of laminin solution was added, and the chips were incubated at 37°C in a 5% CO_2 /95% air atmosphere. On the day that culture commenced, the laminin solution was removed and a φ3.4-mm glass ring was placed in the middle of the probes where the electrodes were located. The cells (90 μl) were seeded inside the rings (density, 1.3×10^6 cells/ml) and incubated for 1 h. Culture medium was applied around the rings and were removed carefully. The cultures were grown at 37°C in a 5% CO_2/95% air atmosphere.

2.3 Humoral factor derived from rat astrocytes and rat astrocyte co-culture

To evaluate the pharmacological response and long-term spontaneous activity characteristics, we tested iCell neurons in three different culture conditions: (i) conventional culture conditions using samples with neurobasal medium culture; (ii) conventional culture conditions with the addition of rat astrocyte-derived humoral factor; and (iii) with the addition of

rat astrocyte-derived humoral factor and rat astrocytes.

The rat astrocytes were seeded (density, 1×10^3 cells/MEA chip) and co-cultured with hiPSC-derived neurons. The humoral factor was obtained from the same culture medium used to produce the astrocytes.

2.4 Pharmacological tests

To investigate pharmacological effects, we administered synaptic antagonists to hiPSC-derived neuronal networks on the MEA chips. The GABAA receptor antagonist bicuculline (Sigma-Aldrich) and the AMPA/kainate receptor antagonist 6-cyano-7-nitroquinoxaline-2,3-dione (CNQX) (Sigma-Aldrich) were used at final concentrations of 10 μM and 30 μM in the medium, respectively. Spontaneous recordings were obtained for 60 min before treatment with bicuculline or CNQX and again after administration. A 10-min washout was performed in the medium prior to recordings. The cultures were kept in a CO2 incubator between the recordings and washouts. To avoid medium changes and waiting for the effects of drugs, firing analyses were performed during the last 10 min of the 60 min period after drug administration.

3 Result

We applied bicuculline and CNQX to the humoral factor/astrocytes co-cultured samples at 37 and 92 culture DIV, and we observed changes in the spontaneous activity. Figure 1 shows the change in the firing pattern. Bicuculline administration (10 μM) increased the firing frequency, whereas CNQX administration (30 μM) stopped the firing activity completely, although it was restored after washing the samples. Bicuculline administration increased the amplitude and the firing rate. We detected multiple different waveforms, which we attributed to an increase in the number of firing neurons. No significant differences were observed with the conventional culture samples (data not shown). Figure 1B shows the electrodes that detected signals and the firing frequency of the 64 electrodes. At 37 and 92 culture DIV, the number of electrodes that detected signals and the firing rate increased after bicuculline administration, whereas they decreased after CNQX administration, although the firing rate was restored after washing out the samples. After bicuculline administration, among the treated samples, we detected an increase in the number of electrodes with firing activity (four and 11 more electrodes at 37 and 92 culture DIV, respectively). The firing rate in treated samples increased 2.8- and 2.4-fold at 37 and 92 culture DIV, respectively (Fig. 1C). After CNQX administration, there was a 0.54- and 0.17-fold reduction in the firing rate at 37 and 92 culture DIV, respectively.

4 Summary

The firing rate increased greatly at 92 DIV, including the synchronized burst firing rate, after bicuculline administration, indicating that the cells were pharmacologically responsive and it also validated the long-term culture of the samples. After CNQX administration, we observed that the firing rate took a long period to recover to its original rate after washing the samples. The relationship between CNQX concentration and recovery time requires further investigation. In conclusion, we demonstrated that the coculture of hiPSC-derived neurons with rat astrocytes facilitated long-term culture and functional measurements were obtained. Moreover, we detected major responses after the addition of synapse antagonist drugs. Therefore, using a MED64 system as a measurement method during hiSPC co-culture with rat astrocytes may be beneficial for clarifying the functions of human neuronal circuits and for drug screening applications

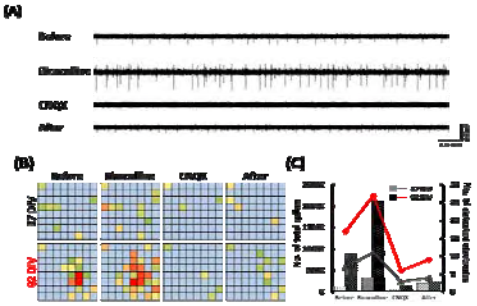

Figure 1. Effects of drugs in hiPSC-derived neurons with astrocyte co-culture

Acknowledgement

We thank Alpha Med Scientific company for collaborating in this research. This study was supported by the Japan Society for the Promotion of Science Grant Number 24700485 and by the Japan Science and Technology Agency Adaptable and Seamless Technology transfer Program (A-step) Grant Number AS251Z02961P.

References

[1] K. Takahashi, et al., Induction of pluripotent stem cells from adult human fibroblasts by defined factors, Cell 131 (2007) 861-872.
[2] M. Bellin, et al., Induced pluripotent stem cells: the new patient?, Nat Rev Mol Cell Biol 13 (2012) 713-726.
[3] A.B. Cherry, et al., Reprogrammed cells for disease modeling and regenerative medicine, Annu Rev Med 64 (2013) 277-290.
[4] M. Peitz, et al., Disease-specific iPS cell models in neuroscience, Curr Mol Med 13 (2013) 832-841.
[5] Y. Imaizumi, et al., Modeling human neurological disorders with induced pluripotent stem cells, J Neurochem (2013).
[6] I. Suzuki, et al., Detection of tetanus-induced effects in linearly lined-up micropatterned neuronal networks: application of a multi-electrode array chip combined with agarose microstructures, BBRC 356 (2007) 470-475.
[7] T. Fath, et al., Primary support cultures of hippocampal and substantia nigra neurons, Nat Protoc 4 (2009) 78-85.
[8] H.W. Muller, et al., A neurotrophic factor (NTF) released from primary glial cultures supports survival and fiber outgrowth of cultured hippocampal neurons, J Neurosci Res 8 (1982) 195-204.
[9] A.Odawara, et al., Long-term electrophysiological activity and pharmacological response in human induced pluripotent stem cell derived neuron and astrocyte co-culture, BBRC 443 (2014) 1176-1181.

Human Embryonic and Induced Pluripotent Stem Cells Form Functional Neuronal Networks in MEA

Ylä-Outinen Laura[1,*], Hannuksela Eija[1], Narkilahti Susanna[1]

1 NeuroGroup, BioMediTech, University of Tampere, Tampere, Finland
* Corresponding author. E-mail address: laura.yla-outinen@uta.fi

Abstract
Human pluripotent stem cell (hPSC) derived neuronal networks have large potential for creating human cell based *in vitro* platforms. Electrical signalling corresponding *in vivo* signalling in neuronal networks is one crucial parameter to evaluate the neuronality of the cells in networks. We show that both human embryonic stem cell (hESC) derived and human induced pluripotent stem cell (hiPSC) derived neuronal cells form functional networks on microelectrode array (MEA). Electrical activity development in hPSC derived neuronal networks show signal development from single spikes to bursting activity. Thus, those networks are potential cell material for MEA based *in vitro* platforms.

1 Backround / Aims

Human pluripotent stem cells (hPSC), including human embryonic stem cells (hESCs) and human induced pluripotent stem cells (hiPSCs), provide unique cell source for developing *in vitro* neuronal cell models for neurotoxicity, neural drug development as well as neurologic diseases [1-3]. Nevertheless, only little is known about the functionality and network formation of hPSC derived neuronal cells. The aim of our work was to use microelectrode array (MEA) technology to observe the functional development of both hiPSC and hESC derived neuronal networks.

2 Methods / Statistics

Both hiPSCs and hESCs were cultured and differentiated similarly. Shortly, hPSCs were cultured on top of feeder cell layer in colonies. Colonies were mechanically cut to aggregates and cultured as spheres in neuronal differentiation medium for 8 weeks. For MEA measurements, MEA dishes (60-6WellMEA 200/30, Multichannel Systems) with in-house designed silicone cell culture chamber (SpikeBooster, Fig. 1) [4] were used. Maturing neuronal networks were measured with 2100-MEA system (MCS) twice a week for 5 weeks. In addition, control networks were cultured in cell culture dish for gene expression and immunocytochemical analyses. Obtained MEA data was analysed using MATLAB (MathWorks, MA, USA) with in-house-built burst detection code [5] and with Neuroexplorer (NexTechnologies, AL, USA).

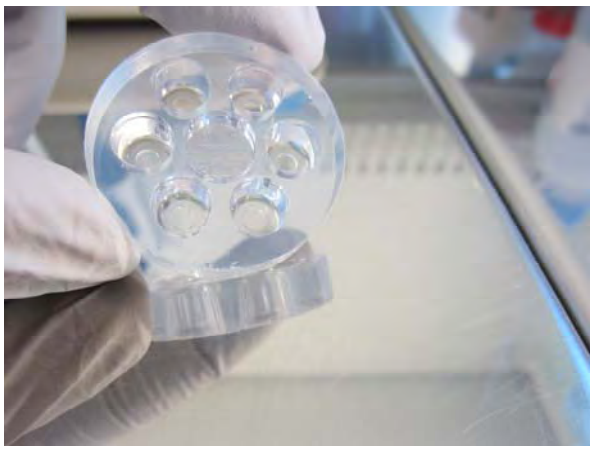

Fig. 1. SpikeBooster. Cell culture chamber designed for good cell attachment and fast network formation for 6-well MEA format.

3 Results

We detected the functional development that is typical for neuronal cultures in both hESC and hiPSC derived neuronal networks. First, single spiking activity occurred within first week on MEA, and thereafter the functionality matured into training activity, and even bursting (Fig. 2).

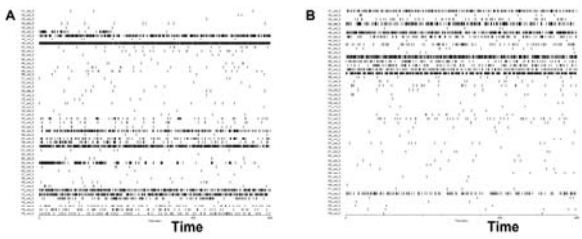

Fig. 2. A) Electrical signalling development from hESC derived neuronal networks in 4 weeks on MEA. B) Electrical signalling development from hiPSC derived neuronal networks in 4 weeks on MEA.

Moreover, both types of networks showed typical neuronal markers in gene expression and immunocytochemical analyses.

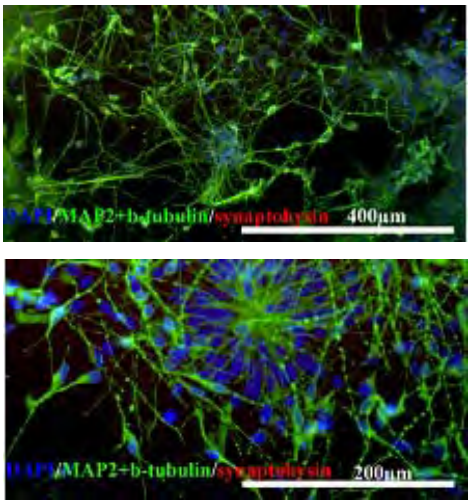

Fig. 3. A) Immunocytochemical analysis showed MAP-2 and beta-tubulin positive neuronal network (green) and synaptophysin (red) in hESC derived neuronal networks. B) Immunocytochemical analysis showed MAP-2 and beta-tubulin positive neuronal network (green) and synaptophysin (red) in hiPSC derived neuronal networks.

4 Conclusion/Summary

Neuronal cells differentiated from hESCs and hiPSCs form functional neuronal networks which further mature into even bursting networks. This shown functionality makes these cells potential starting material for different *in vitro* platforms.

Acknowledgement

We acknowledged the personnel of BioMediTech for support in stem cell culture and MEA technology. This work is funded by TEKES, Finnish Funding Agency for Technology and Innovations, Human Spare Part project.

References

[1] Johnstone, AF., Gross, GW., Weiss, DG., Schroeder, OH., Gramowski, A., Shafer, TJ. (2010). Microelectrode arrays: a physiologically based neurotoxicity testing platform for the 21st century. *Neurotoxicolog* 31(4):331-50.

[2] Ylä-Outinen, L., Heikkilä, J., Skottman, H., Suuronen, R., Äänismaa, R., & Narkilahti, S. (2010). Human cell-based micro electrode array platform for studying neurotoxicity. *Front Neuroeng*, *3*(pii: 111).

[3] Novellino, A., Scelfo, B., Palosaari, T., Price, A., Sobanski, T., Shafer, TJ., Johnstone, AF., Gross, GW., Gramowski, A., Schroeder, O., Jügelt, K., Chiappalone, M., Benfenati, F., Martinoia, S., Tedesco, MT., Defranchi, E., D'Angelo, P., Whelan, M. (2012). Development of micro-electrode array based tests for neurotoxicity: assessment of interlaboratory reproducibility with neuroactive chemicals. *Front Neuroeng*. 2011 Apr 27;4:4

[4] Kreutzer, J., Ylä-Outinen, L., Kärnä, P., Kaarela, T., Mikkonen, J. E., Skottman, H., Narkilahti, S., Kallio, P. (2012). Structured PDMS Chambers for Enhanced Human Neuronal Cell Activity on MEA Platforms. *Journal of Bionic Engineering*, *9*, 1–10.

[5] Kapucu, F. E., Tanskanen, J. M. A., Mikkonen, J. E., Ylä-Outinen, L., Narkilahti, S., Hyttinen, J. A. K. (2012). Burst analysis tool for developing neuronal networks exhibiting highly varying action potential dynamics. *Frontiers in Computational Neuroscience*. doi:10.3389/fncom.2012.00038

A Novel AFM-Based Technique for Measuring Coupled Phenomena in Cardiac Myocytes

Caluori Guido[1*], Andrade_Caicedo Henry [1,2], Tedesco Mariateresa[1], Raiteri Roberto[1]

1 Department of Informatics Bioengineering and Systems Engineering, Università di Genova, via Opera Pia 11, 16145 Genova
2 Centro de Bioingeniería; Universidad Pontificia Bolivariana; Circular 1 No. 73-76, Bloque 22C, Medellín, Colombia
* Corresponding author. E-mail address: s3837892@unige.it

Abstract
Excitation-contraction coupling (ECC) is the phenomenon through which cardiac myocytes convert electrical action potentials, via calcium ions handling, to a mechanical contraction. In parallel to ECC, cardiac muscle cells possess a feedback mechanism, to overcome environmental changes, which is called mechano-electrical feedback (MEF). Alterations of these phenomena are directly linked to occurrence of contractile dysfunction (pump/heart failure) or ventricular arrhythmias.
The main goal of this scientific work is to simultaneously monitor changes of different coupled phenomena in the cardiac mechano-electrical behavior at the subcellular level, combining different tools and experimental techniques: atomic force microscopy (AFM), microelectrode arrays (MEA), and fluorescence microscopy (calcium imaging).We also propose a novel method in which AFM nanoindentation is triggered with respect to the probed EFP with increasing delays at each electric event, thus providing an alternative, more powerful, approach in cardiomyocytes mechanical measurements.

1 Backround / Aims

Heart failure is a major pathological condition, which is associated with high mortality. It is directly caused by myocardium contractile dysfunction (pump failure) or ventricular arrhythmias. The phenomenon through which an electrical action potential is converted, via calcium ions handling, to a mechanical contraction goes under the name of excitation-contraction coupling (ECC) [1]. When environmental changes occur, an intracardiac chemical pathway provides adaptation of the cardiac ECC. Such biological control loop is known as mechano-electrical feedback (MEF). Alteration of the MEF has been linked to the occurrence of arrhythmias [2].

In the past decade, the use of the atomic force microscope (AFM) as a tool to study micro and nanomechanical properties of single cells has spread. The use of force spectroscopy techniques allows precise probing of the cell surface and underlying cytoskeleton [3]. Furthermore, AFM can operate in liquid environment; hence single cells can be probed in physiological conditions [4].

Microelectrode arrays (MEAs) is a well-accepted tool that enables the recording and the stimulation of cellular electrical activity, by means of extracellular field potential (EFP). They offer few advantages compared to other electrophysiological techniques, such as multiple experimental sites and long-time monitoring of the electrical behavior. Common cell types addressed by this technology are neurons, cardiac and skeletal muscle fibers [5].

Fluorescence techniques are widely used in cardiac research. Calcium fluorescence imaging allows direct visualization of Ca^{2+} fluxes through the cell membrane using specific fluorescent probes.

The main goal of this work is to simultaneously monitor changes of different components of the cardiac mechano-electric behavior at the subcellular level, namely elasticity, height, electrical activity, and intracellular calcium concentration. We also propose a novel method in which AFM nanoindentation is triggered with respect to the probed EFP with increasing delays at each electric event. This results in a series of time resolved measurements of the cell elasticity during the beating cycle [6], overcoming one of the main limitation of AFM measurement (e.g. low speed).

2 Methods / Statistics

2.1 Experimental setup

The experimental setup is based on a commercial AFM (AFM 5500, Agilent Technologies), mounted onto an optical inverted microscope (model IX70, Olympus) equipped for EPI-fluorescence microscopy. The cell culture is performed on commercial MEAs (60channels MEA, model ITO 200/30, Multichannel Systems). A custom-made sample holder houses the MEA device and provides heating and multi-site probing of bioelectrical signals. The signals pass through an amplification stage, supplied by a 64 channels, 1000-gain amplifier (FA64I, Multichannel Systems). AFM scanner vertical position and cantilever deflection are also recorded. All signals are acquired by a 64 channels DAQ board (NI PCI-6071E, National Instruments).

Calcium imaging is performed using fluorescent calcium green-emitting dyes (Oregon Green-BAPTA-AM/Fluo4-AM, Invitrogen). The images are recorded with a CMOS high-speed, high-sensitivity camera (Flash4, Hamamatsu Photonics)

To perform the triggered/delayed nanoindentation, a FPGA board (NI PCI-7830, National Instruments) is used. All the hardware is controlled by NI-LabVIEW customized softwares. The complete setup is schematically shown in Figure 1.

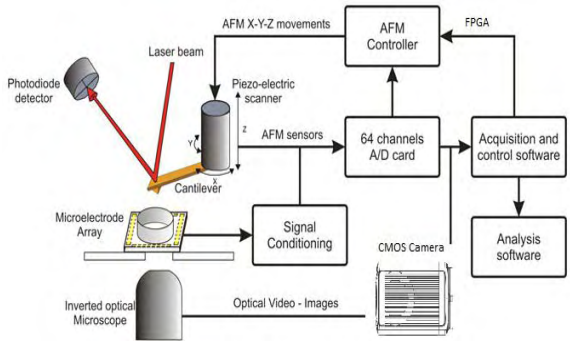

Fig. 1. Schematic representation of the combined setup for AFM-MEA-Calcium imaging measurements.

2.2 Experimental procedure

Embrionyc rat cardiomyocytes (16-19d days), cultured on MEA for four to seven days, are loaded with calcium sensitive fluorophore one hour before the experiment. EFP recording from microelectrodes are carried out together with optical inspection of the cell culture. A specific cell, sitting onto one microelectrode, which shows spontaneous electrical and beating activity, is selected. Simultaneous electrical and fluorescence imagining, together with AFM triggered/delayed nanoindentation are recorded and saved for off-line analysis.

3 Results

3.1 Results analysis

AFM "force-distance curves" are processed, according to the analysis proposed by Oliver and Pharr [7], to calculate elastic moduli at each delay from the last spontaneous extracellular AP peak measured at the targeted microelectrode [6]. The recorded EFP is also used to evaluate electrophysiology parameters (e.g. beating rate). Acquired fluorescence images are analyzed in terms of change of intensity, normalized with respect to the background (F/F0) in a selected region of the image corresponding to the cell area. All the analysis is performed with customized scripts in-MATLAB (Mathworks). An example of the recorded signals is shown in Figure 2

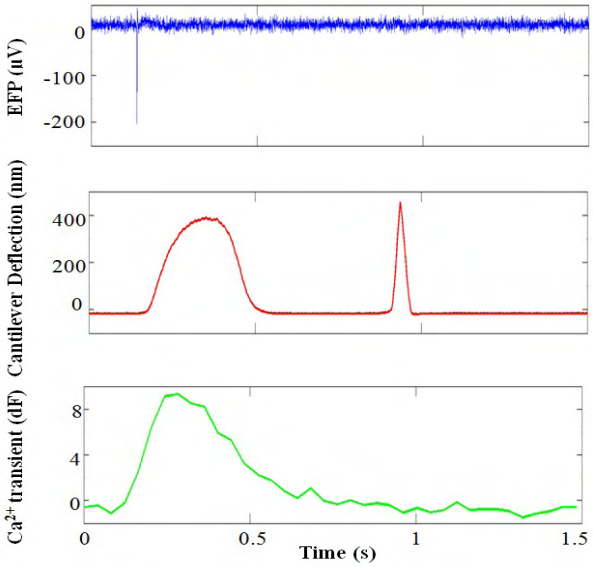

Fig. 2. Graphs of three signals recorded simultaneously during an experiment: MEA signal (top, blue), cantilever deflection (red, middle), intracellular calcium transient (bottom, green).

4 Conclusion/Summary

In vitro investigation of mechano-electrical behavior of cardiomyocytes can open new ways for detecting and predicting pathological conditions directly linked to the ECC alteration. The use of well-established techniques provides a solid support for the interpretation of data, and the exploitation of AFM sub-micrometric resolution allows us to treat the microelectrode array as a multisite sample which increases the throughput of experiments toward the validation of *in vitro* cardiac muscle cells models, and more efficient drug tests.

References

[1] D. M. Bers, "Excitation-contraction coupling," *Nature*, vol. 415, no.January, 2002.

[2] "Cardiac mechano-electric feedback: past, present, and prospect," *Progress in Biophysics & Molecular Biology 82 (2003) 3–9*, vol. 82, pp. 3–9, 2003.

[3] T. G. Kuznetsova, M. N. Starodubtseva, N. I. Yegorenkov, S. A. Chizhik, and R. I. Zhdanov, "Atomic force microscopy probing of cell elasticity," *Micron*, vol. 38, pp. 824–833, 2007.

[4] D. Kirmizis and S. Logothetidis, "Atomic force microscopy probing in the measurement of cell mechanics," International Jour nal of Nanomedicine, pp. 137–145, 2010.

[5] A. Stett, U. Egert, E. Guenther, F. Hofmann, T. Meyer, W. Nisch, and H. Haemmerle, "Biological application of microelectrode arrays in drug discovery and basic research.," Analytical and bioanalytical chemistry, vol. 377, no. 3, pp. 486–95

[6] J. F. S. Saenz Cogollo, M. Tedesco, S. Martinoia, and R. Raiteri, "A new integrated system combining atomic force microscopy and microelectrode array for measuring the mechanical properties of living cardiac myocytes," *Biomed Microdevices*, vol. DOI 10.100, 2011.

[7] W.C. Oliver, G.M. Pharr, "An improved technique for determining hardness and elastic modulus using load and displacement sending indentation experiments", *Journal of materials research*, 7(6), 1564–1582 (1992

Author Index

Author Index

Äänismaa R 342
Achilli S 306
Adagunodo MO 286
Agrawal H 83
Alagapan S 81, 337
Albrieux M 295
Alfaro Sáez A 200
Alhebshi A 127
Alloisio S 124, 131
Andrade Caicedo HH 358
Andrei A 330
Anisimova M 170
Arendt T 158
Asboth L 237
Asnaghi V 124
Averna A 216
Baca M 310
Baekelandt V 56
Baez C 212
Bakkum D 60, 147, 153, 160, 166, 176, 244, 335
Ballini M 244, 302, 326
Barrett J 64
Barth B 33
Bartsch H 310
Bartz-Schmidt KU 45
Battiato A 293
Becker B 76
Beckler M 129
Béduer A 278
Beggs J 328
Berdondini L 100, 208
Bergonzo P 266, 291
Bernardi E 293
Bernhard N 312
Bertagnolli E 133, 222, 322
Bertotti G 247
Bestel R 194, 300
Bhat N 255
Biffi E 306
Bikbaev A 214
Birbaumer N 29, 30
Bisio M 208, 216
Blanquie O 174
Blau A 181, 289, 316, 344
Bocos-Bintintan V 181
Boedecker J 76
Bogdan M 34
Bonfiglio A 242
Bonifazi P 216
Bosca A 208
Bouchiat V 295
Boucsein C 42
Bourrier A 295
Boven KH 42, 137, 247
Braeken D 162, 330, 352
Bräunig P 318
Brewer GJ 81, 83, 337
Briancon-Marjolet A 295
Brings F 324
Brossard J 51
Brown C 235
Brugger D 44
Bucher V 38
Buehler S 126
Bui-Göbbels K 318
Bullmann T 158
Burkhardt C 38, 272, 274, 280
Calderon N 116
Callewaert G 352
Caluori G 358
Capurro A 212
Carabelli V 284, 293
Carbone E 284, 293
Cesare P 287
Channappa L 41, 85
Charvet I 308
Chaudet L 64
Chaudhary U 29
Chee C 45
Chen CC 192
Chen Y 244, 326
Chew D 50
Chiantore M 124
Chiappalone M 208, 210, 216, 308
Cihova M 38
Conte Granado T 284

Cools J 352
Cosseddu P 242
Cottance M 291
Courtine G 233, 237
Dabrowski W 328
Daus AW 194
de la Paz F 198
de Pasquale P 308
de Weerd E 259
Defranchi E 131
Degen R 318
Degenaar P 64
Dehnke S 44
Delacour C 295
Delle L 314
DeMarse T 81, 337
Demko L 341
Dermutz H 341
Desai H 83
Destro-Filho JB 284, 332
Devesa I 118
Di Marco S 100
Difato F 216, 316
Dihné M 178
Dijkstra J 188
Dityatev A 114
Divoux JL 266
Dodel N 247
Doerr L 129
Dong N 64
Dragas J 185
Drews G 137
Dürr C 68
Eba I 50
Egert U 76
Eglen S 187
Ehlis AC 33
Ehnert C 135
Eickenscheidt M 41, 66, 78, 247
El Hasni A 318
Elsen G 178
Engleder E 133
Esir P 224
Exler A 133
Fallgatter AJ 33
Famm K 50
Fayuk D 120, 164, 168
Fernández E 198, 200
Ferrández-Vicente J 198, 200
Ferrandiz Huertas C 118
Ferreira Neves A 332
Ferrer-Montiel A 118
Ferrigno G 306
Fertig N 129
Fiscella M 74, 98, 102, 335
Flahaut E 278
Fominov O 314
Forró C 341
Franca E 81, 337
Franke F 74, 98, 102, 153, 160, 185, 302, 335
Frech S 122
Frega M 339
Frey U 88, 147, 153, 158, 160, 166, 244, 302
Fukayama O 206
Fukuda M 270
Füll Y 179
Gabor F 133
Gähwiler B 335
Gallacher D 351
Gallegos-Ayala G 29
Gao ZY 284
Garnham C 51
Garrido J 264
Gekeler F 45
George M 129
Gharabaghi A 47
Gielen GGE 330
Giese M 276
Gimsa J 126
Girard H 266
Giugliano M 56, 202
Giussani V 124
Gladkov A 226, 228
Gohara K 143, 170
Golabchi A 181, 289, 316, 344
Goldental A 149
Gong W 335
Goo YS 70
Gopal K 116
Gosso S 293
Gotoh M 127, 354

Gross G 109, 116, 156
Guenther E 137, 280, 351
Guex A 235
Guinot D 129
Gunning DE 328
Gutöhrlein K 274
Habibey R 181, 289, 316, 344
Hahnewald S 51
Han Z 295
Hanein Y 139
Hannuksela E 356
Hébert C 266, 291
Heidingsfelder S 251
Heikkilä J 168
Heine M 214
Helmhold F 66, 85
Hempel F 312, 314
Herrmann T 54, 68
Hess D 351
Hess L 264
Heuschkel M 212, 278, 282, 291
Hierlemann A 60, 74, 88, 98, 102, 147, 153, 160, 166, 176, 185, 190, 244, 302, 326, 335
Hight A 235
Hilgen G 100
Hirsch A 237
Hoffman L 330, 352
Holmes K 109
Holzer M 158
Homsy A 51
Hoshino T 206
Hoth M 251
Hottowy P 328
Husar P 320
Huybrechts B 352
Hyttinen J 204, 218
Hyung S 95, 103
Ingebrandt S 251, 312, 314
Isomura T 183
Ito D 143, 170
Ito H 230
Jäckel D 60, 153, 160, 185, 302, 335
Jackson TL 45
Jans D 352
Jedidi N 282
Jiko H 270
Jimbo Y 91, 112, 172, 183
Joki T 342
Jones I 60, 74, 98
Jones PD 287
Jügelt K 135
Jung H 62
Just T 320
Kalita D 295
Kang DH 95, 103
Kanter I 149
Kanzaki R 147, 166
Katso R 50
Kazantsev V 224, 226, 228
Kenney C 328
Keppner H 51
Kern D 272, 274
Kilb W 174
Kim J 70
Kleber C 280
Knoflach F 190, 335
Knoll A 181
Knott T 122
Konduri A 316, 344
Koppenhöfer D 312
Kotani K 91, 112, 172, 183
Kraushaar U 137, 280, 351
Kriebel M 68
Krippeit-Drews P 137
Krumpholz K 318
Kubon M 38
Lacour S 235, 237
Lai S 242
Laprell L 58
Larmagnac A 233, 286
Lassen D 122
Law J 251, 312, 314
le Feber J 188, 259
Ledee D 116
Lee D 235
Lee WW 70
Lekkala J 268
Lenk K 204, 218
Leondopulos S 81, 83
Lepina A 226, 228

Lerche H 178, 179
Lewandowska M 176
Li W 72
Link G 38
Lissorgues G 291
Litke A 328
Liu Y 179
Livi P 244, 326
Löffler H 179
Lorente V 198, 200
Lottner M 264
Lotufo C 332
Lu HR 351
Luhmann HJ 174
Luthi-Carter R 212
Mabuchi K 206
Maccione A 100
MacLaren R 45
Mahmud M 202
Mäkinen M 120, 168
Makohliso S 212, 282
Maljevic S 178, 179
Marconi E 51
Mari J 332
Marmari H 149
Martina M 280
Martinez V 286
Martiniuc A 181
Martinoia S 131, 196, 210, 220, 242, 339
Massobrio P 196, 220, 339
Mathieson K 328
Mathivanan S 118
Maybeck V 72
McLaughlin B 50
Melchionna T 51
Menegon A 306
Mer C 266
Micholt L 162
Mika J 133, 222, 322
Minev I 237
Mistrik P 51
Mita T 147, 166
Mitroshina E 114
Möller A 42, 247
Moon HJ 95, 103
Mukhina I 114, 224, 226, 228
Müller J 60, 74, 98, 102, 153, 244, 302, 326, 335
Müller-Dahlhaus F 32
Münch T 102
Musienko P 233
Musumeci G 56
Mutter M 102
Nam Y 62
Nanni M 289, 316, 344
Narkilahti S 120, 164, 168, 218, 268, 342, 348, 356
Neil M 64
Nemeth J 45
Neuhof A 318
Nick C 300
Nisch W 38
Nissen M 126
Novellino A 124, 131
Obien MEJ 88
Odawara A 127, 354
Offenhäusser A 72, 304, 324
Okawa S 166
Okujeni S 76
Olivero P 293
Paavilainen T 164, 168
Pajunen M 164, 168
Pan L 81, 337
Park JH 95, 103
Pasquale V 208, 310, 216
Pasquarelli A 284, 293, 332
Passeraub P 308
Pastore VP 196
Patel S 50
Pavlova N 237
Pedrocchi A 306
Peltola M 268
Perrone S 212
Pesce M 339
Piazza S 196
Picaud S 291
Picollo F 293
Pielka AM 135
Pimashkin A 114, 226, 228
Piret G 291
Pirino V 220
Podssun A 135

Poli D 196
Popov C 276
Porzig T 310
Postma W 259
Premoli I 32
Puers R 330
Pulizzi R 56, 202
Qu B 251
Radivojevic M 60, 74, 153, 160, 244, 302, 335
Raiteri R 358
Ramos-Murguialday A 29
Rao Bhaskar R 255
Rast G 347
Rayan A 214
Regalia G 306
Reinhard K 102
Reithmaier JP 276
Renaud P 235, 278
Riccomagno E 220
Riedmiller M 76
Roccio M 51
Roehler S 38, 272
Rosa F 179
Roscic B 335
Rosenstiel W 34
Rousseau L 291
Russell T 74, 153, 160, 335
Rutten W 259
Ryynänen T 268
Saalfrank D 344
Sachs H 45
Saito J 332
Sakai K 91, 172
Sakharnova T 114
Salonen P 342
Samba R 38, 54
Sandoz A 308
Santoro F 304, 324
SaseendranKumar S 76
Sauter-Starace F 266
Schaerlaeken S 352
Scheel O 122
Schnakenberg U 318
Schneider K 274
Schnitker J 72, 304, 324
Schober A 310
Scholze P 222, 322
Schönecker S 137
Schreiter M 247
Schröder O 135
Schuller P 222
Schwarz C 44
Schwarz K 322
Scorsone E 291
Sejer Wismer M 264
Senn P 51
Sernagor E 64, 100, 187
Shadmani A 326
Sher A 328
Shimba K 91, 172
Shin HJ 95, 103
Shirakawa K 270
Sikdar SK 255
Simonov A 224
Singh K 255
Sinning A 174
Sitaram R 29
Sivasubramaniapandian M 268
Smith D 109, 156
Smith LS 187
Soekadar SR 29, 30
Spanu A 242
Spüler M 34
Sridhar A 50
Stamm B 274
Stassen A 352
Stauffer F 286
Stelzle M 38, 287
Stengl M 276
Stern M 300
Stett A 38, 247, 272, 274
Stieler J 158
Stingl K 45
Stoelzle-Feix S 129
Stoppini L 308
Streit J 51
Stubbe M 126
Stutzki H 66
Succol F 289
Suh JKF 95, 103
Sumser M 58
Sun X 64
Susloparova A 312, 314
Suzuki I 127, 270, 354
Suzuki M 170

Takahashi H	147, 160, 166
Tanskanen JMA	204
Tateno T	298
Tedesco M	242, 339, 358
Thewes R	41, 78, 247
Thielemann C	194, 300
Thomas U	129
Tietz L	218
Tillack B	247
Tipney H	50
Toimela T	342
Trauner D	58
Treutlein T	158
Tscherter A	51
Uchida T	170
Ullmann S	304
van den Haute C	56
van Lier B	190
van Stiphout P	122
Vardi R	149
Varshney A	278
Vasilaki E	202
Vedunova M	114
Veliev F	295
Velychko D	78
Verma R	235
Viswam V	60, 302
Voeroes J	233, 286, 341
von Metzen R	38
Vornanen I	204
Voss A	135, 276
Vu XT	251, 312, 314
Wallach G	139
Walter A	34
Wandinger KP	178
Wanzenboeck H	133, 222, 322
Wei H	276
Weinmann M	38
Weir K	174
Wenger N	233
Weusthof M	259
Wheeler B	81, 83, 337
Widmer HR	51
Williamson A	310
Wimmer R	76
Wirth M	133
Witkowski M	30
Wolansky D	247
Wolf CJ	118
Wolfrum B	324
Wolking S	178
Wong D	45
Wrobel WG	43
Wülfing J	76
Yada Y	206
Yakushenko A	324
Ylä-Outinen L	120, 164, 218, 356
Ylikomi T	342
Yokoyama K	170
Yoshida L	112
Young D	328
Yvert B	291
Zakharov Y	114
Zanin M	124, 131
Zeck G	41, 54, 66, 68, 78, 85, 247
Zhou X	251
Ziemann U	32
Zrenner E	45

ISSN 2199-1596